MICROCOPY RESOLUTION TEST CHART

NATIONAL BUREAU OF STANDARDS-1963-A

SECURITY CLASSIFICATION OF THIS PAGE *(When Data Entered)*

REPORT DOCUMENTATION PAGE		READ INSTRUCTIONS BEFORE COMPLETING FORM
1. REPORT NUMBER AFOSR-TR- 84-0977	2. GOVT ACCESSION NO.	3. RECIPIENT'S CATALOG NUMBER
4. TITLE *(and Subtitle)* TUNABLE MICROWAVE TRANSVERSAL FILTERS		5. TYPE OF REPORT & PERIOD COVERED Annual Technical Report 8-1-82 - 7-31-84
		6. PERFORMING ORG. REPORT NUMBER
AUTHOR(s) J. M. Owens R. L. Carter		8. CONTRACT OR GRANT NUMBER(s) AFOSR 80-0264
PERFORMING ORGANIZATION NAME AND ADDRESS Department of Electrical Engineering University of Texas at Arlington Arlington, Texas 76019		10. PROGRAM ELEMENT, PROJECT, TASK AREA & WORK UNIT NUMBERS 61102F 2306, B2
CONTROLLING OFFICE NAME AND ADDRESS Air Force Office of Scientific Research Building 410 Bolling AFB, D.C. 20332		12. REPORT DATE 1 May 1984
		13. NUMBER OF PAGES
MONITORING AGENCY NAME & ADDRESS*(If different from Controlling Office)*		15. SECURITY CLASS. *(of this report)* UNCLASSIFIED
		15a. DECLASSIFICATION/DOWNGRADING SCHEDULE

16. DISTRIBUTION STATEMENT *(of this Report)*

Approved for public release; distribution unlimited.

17. DISTRIBUTION STATEMENT *(of the abstract entered in Block 20, if different from Report)*

18. SUPPLEMENTARY NOTES

19. KEY WORDS *(Continue on reverse side if necessary and identify by block number)*

DTIC
ELECTE
DEC 7 1984
S D
D

20. ABSTRACT *(Continue on reverse side if necessary and identify by block number)*

See attachment

DD FORM 1 JAN 73 1473

84 11 27 006

SECURITY CLASSIFICATION OF THIS PAGE *(When Data Entered)*

20. Abstract

This final report for the third year of contract AFOSR-80-0264 summarizes the results of a fundamental investigation of a viable technological realization of this goal through magnetostatic waves MSW propagating at microwave frequency in magnetically biased, liquid phase epitaxial films of yttrium iron garnet (YIG) grown on gadolinium gallium garnet (GGG). This technology has a number of advantages; low loss (greater than 30db/usec at xband), tunable by bias field to any center frequency (1-20GHz), long wavelengths (10-100 micrometers at any frequency), and finally a well understood and characterized wave phenomena (MSW) is utilized. The necessary non-recursive transversal filtering is achieved through multi-element transducer and/or the interaction of the MSW with periodic structures in or on the YIG film.

This report summarizes the work accomplished in the last year toward achieving MSW transversal filtering. First studies of MSSW (Magnetostatic Surface Wave) transducers composed of periodic arrays of narrow shorted microstrips are summarized. These studies develop an empirical (experimentally derived) 3 port model for this type of transducer. Next, studies of a variable time delay device based on a cascaded MSSW forward wave line and an MSBVW backward wave delay line, are presented. Finally, studies of MSSW resonators and resonators oscillators are summarized.

Accession For	
NTIS GRA&I	X
DTIC TAB	☐
Unannounced	☐
Justification	
By	
Distribution/	
Availability Codes	
Dist	Avail and/or Special
A/1	

TABLE OF CONTENTS

1.0 INTRODUCTION AND SUMMARY

A military need exists for a microwave solid state device technology with a complementary analog signal processing capabilities to that developed over the past ten years in surface acoustic waves (SAW) technology. In this technology, non-recursive transversal filters have been realized through either interdigital transducers and/or periodic reflective arrays defined on the piezoelectric substrates in which the surface acoustic waves are propagated. Utilizing this technology simple delay lines, complex matched filters, high Q resonators and chirp filters, have been realized in the VHF, UHF frequency range. Unfortunately, the extension of this technology to the microwave region (f>1 GHz) has been difficult. At these frequencies the surface acoustic wave length is less than 1μm making fabrication difficult and the propagation loss becomes excessive (>100db/ usec at 10 GHz.)

This final report for the third year of contract AFOSR 80-0264 summarizes the results of a fundamental investigation of a viable technological realization of this goal through magnetostatic waves MSW propagating at microwave frequency in magnetically biased, liquid phase epitaxial films of yttrium iron garnet (YIG) grown on gadolinium gallium garnet (GGG). This technology has a number of advantages; low loss (>30db/ usec at xband), tunable by bias field to any center frequency (1-20GHz), long wavelengths (10-100μm at any frequency), and finally a well understood and characterized wave phenomena (MSW) is utilized. The necessary non-recursive transversal filtering is achieved through multi-element transducer and/or the interaction of the MSW with periodic structures in or on the YIG film.

1

This report summarizes the work accomplished in the last year toward achieving MSW transversal filtering. First studies of MSSW (Magnetostatic Surface Wave) transducers composed of periodic arrays of narrow shorted microstrips are summarized. These studies develop an empirical (experimentally derived) 3 port model for this type of transducer. Next, studies of a variable time delay device based on a cascaded MSSW forward wave line and an MSBVW backward wave delay line, are presented. Finally, studies of MSSW resonators and resonators oscillators are summarized.

2.0 THREE-PORT SCATTERING PARAMETER MODELING FOR MSSW ARRAY TRANSDUCERS

This research presents work accomplished to model Magnetostatic Surface Wave Array Transducers. This work starts by deriving a 3-port scattering parameter model by use of several previous models. The derivation is presented in two parts, namely the wave ports and the electric ports. The results are shown for single and multiple bar arrays along with the equivalent experimental results. The data given by the derived model will show that this model is only good for up to two bar arrays. Next an empirical (experimentally derived) 3-port model will be investigated. The layout of several devices which were used to measure the 3-port scattering parameters for

the empirical model will be shown. These devices include a single bar five micrometer wide measuring transducer on each side of the array being measured. Error correcting factors are presented for each of the S-parameters measured. The results from the empirical model will show that this is a very good model for magnetostatic surface wave array transducers.

CHAPTER II

2.1 THEORETICAL 3-PORT MODEL

2.1.1 Introduction

This section outlines the steps in the development of a theoretical 3-port scattering parameter model for MSSW transducers. A computer program has been developed based on this model. Limitations of the model will be discussed as well as recommendations for further work.

2.1.2 Derivation and Development

Any linear n-port electrical network may be analyzed in several ways. Convenience usually dictates which method is used. For example, if the network operates open circuited, impedance parameters are best, but if it is operated shorted circuited, admittance parameters are best. Now, when the network operates under matched load conditions, scattering parameters are usually used. Scattering parameters form a transformation between variables which are linear combinations of voltages and currents in a network. They are very convenient for problems which involve insertion loss and matching networks. [7]

The scattering parameters for MSSW have been derived using techniques similar to those of Hasnain [6] for MSFVW or Smith [8] for SAW. Because Wu's [5] impedance model based on the Poynting vector is used in deriving the S-parameters, a power normalization was chosen. The 3-port model has two wave ports and one electric port as shown in Figure 2.1. Since MSSW is anisotropic and is characterized by two surface waves traveling on the two ferrite surfaces in opposite directions, the forward wave will be defined as, "the wave traveling from port 1 to port 2". A Transmission line model for MSW derived by Snapka [9] will be used to find wave port S-parameters. This model consists of forward and reverse wave transmission and reflection coefficients which can be easily derived using Kirchoff's laws for voltage and current. The electric port S-parameters will be found from Wu's impedance model.

2.1.3 The Wave Port S-parameters

For the wave ports the transmission matrix becomes:

$$
\begin{bmatrix} V_o \\ I_o \end{bmatrix} = \begin{bmatrix} A & B \\ C & D \end{bmatrix} \begin{bmatrix} V_i \\ I_i \end{bmatrix}
$$

$$
= \frac{1}{z_F + z_R} \begin{bmatrix} \left(z_F e^{-F} + z_R e^{-R} \right) & \left(z_R z_F (e^{-F} - e^{-R}) \right) \\ \left(e^{-F} - e^{-R} \right) & \left(z_F e^{-R} + z_R e^{-F} \right) \end{bmatrix} \begin{bmatrix} V_i \\ I_i \end{bmatrix} \quad (2.1)
$$
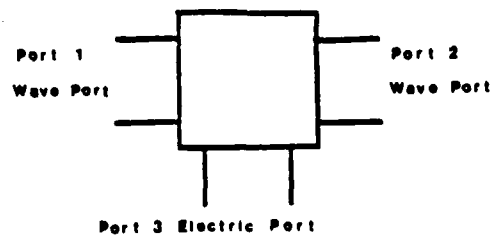
Figure 2.1: Three Port Model
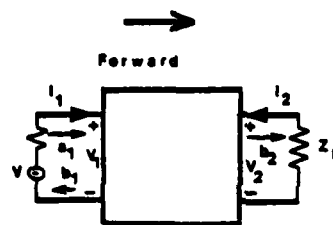
Figure 2.2a: Conditions for Finding S_{11} and S_{21}
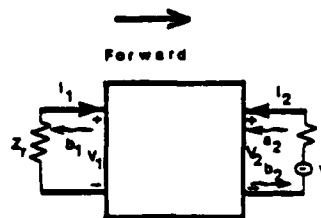
Figure 2.2b: Conditions for Finding S_{12} and S_{22}

7

where Z_F and Z_R are the forward and reverse wave impedance and $\int_F$ and $\int_R$ are forward and reverse propagation constants. If an open circuited microstrip is assumed as wave loading, we can calculate S_{11}, S_{12}, S_{21} and S_{22}. By match terminating port 2 in its' characteristic impedance and exciting port 1 (see Figure 2.2a), we can calculate S_{11} and S_{21}.

Where:

$$S_{11} = \frac{b_1}{a_1} \qquad (2.2)$$

$$S_{21} = \frac{b_2}{a_1} \qquad (2.3)$$

$$V_1 = a_1\sqrt{Z_F} + b_1\sqrt{Z_R} \qquad (2.4)$$

$$I_1 = \frac{a_1}{\sqrt{Z_F}} - \frac{b_1}{\sqrt{Z_R}} \qquad (2.5)$$

$$V_2 = b_2\sqrt{Z_F} - I_2 = \frac{b_2}{\sqrt{Z_F}} \qquad (2.6)$$

And:

$$S_{11} = \frac{A - Z_F C - D + B/Z_F}{B - Z_R A - Z_F D + Z_F Z_R C} \qquad (2.7)$$

$$S_{21} = \frac{(BC - AD)(Z_F + Z_R)}{Z_R Z_F C - Z_F D + B - Z_R A} \qquad (2.8)$$

Then by inverting the transmission matrix, matching terminating port 1, and exciting port 2 (see Figure 2.2b.) S_{12} and S_{22} can be found:

$$S_{12} = \frac{b_1}{a_2} \qquad (2.9)$$

$$S_{22} = \frac{b_2}{a_2} \qquad (2.10)$$

$$V_2 = a_2\sqrt{Z_R} + b_2\sqrt{Z_F} \qquad (2.11)$$

$$-I_2 = \frac{b_2}{\sqrt{Z_F}} - \frac{a_2}{\sqrt{Z_R}} \qquad (2.12)$$

$$V_1 = b_1\sqrt{Z_R} \qquad (2.13)$$

$$I_1 = \frac{-b_1}{\sqrt{Z_R}} \qquad (2.14)$$

And:

$$S_{12} = \frac{-(Z_F + Z_R)}{Z_F Z_R C - Z_R A - Z_F D + B} \qquad (2.15)$$

9

$$S_{22} = \frac{D + B/Z_R - Z_R C - A}{Z_F Z_R C - Z_R A - Z_F D + B} \qquad (2.16)$$

I_2 was chosen to flow in the opposite direction of its' definition for cascading purposes.

2.1.4 Electric Port S-parameters

The electric port S-parameters were derived by assuming the wave ports were match terminated (see Figure 2.3) and that the electric port is also matched by adjusting the thickness of the microstrip. Adjusting the thickness of the microstrip allows one to find the value of conductor resistance that will give intrinsically better coupling, hence a better match to the driving electromagnetic field. [4] To derive the electric port S-parameters, Wu's impedance model was used (see Figure 2.4.). Wu calculated the equivalent circuit impedances by use of the Poynting vector. In his model, Rm_1, Xm_1, Rm_2, and Xm_2 are the equivalent forward wave resistance, forward wave reactance, reverse wave resistance, and reverse wave reactance respectively of the MSSW. R_c and X_c are due to the conduction loss in the microstrip. With ports 1 and 2 matched, where R_2 is the source resistance, the electric port parameters are found.
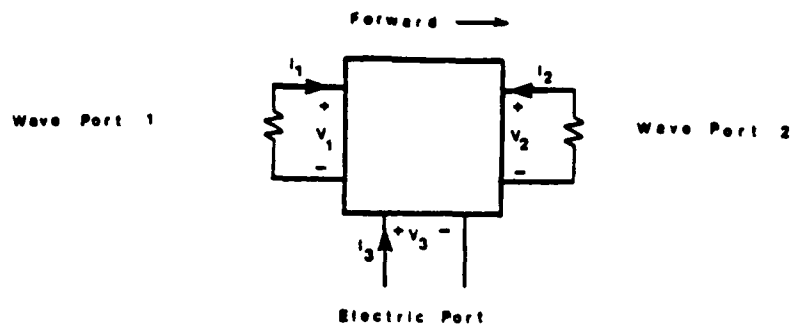
Figure 2.3: Three Port Model with Matched Wave Ports
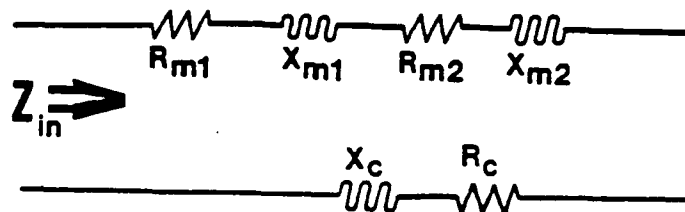
Figure 2.4: Wu Equivalent Circuit Model for MSSW
Microstrip Transducer

$$S_{33} = \frac{b_3}{a_3} \qquad (2.17)$$

$$S_{13} = \frac{b_1}{a_3} \qquad (2.18)$$

$$S_{23} = \frac{b_2}{a_3} \qquad (2.19)$$

$$V_3 = a_3 \sqrt{R_s} + b_3 \sqrt{R_s} \qquad (2.20)$$

$$I_3 = \frac{a_3}{\sqrt{R_s}} - \frac{b_3}{\sqrt{R_s}} \qquad (2.21)$$

$$V_2 = b_2 \sqrt{Z_F} \qquad (2.22)$$

$$-I_2 = b_2 / \sqrt{Z_F} \qquad (2.23)$$

$$V_1 = b_1 \sqrt{Z_R} \qquad (2.24)$$

$$I_1 = b_1 / \sqrt{Z_R} \qquad (2.25)$$

And:

$$S_{33} = \frac{Z_{in} - R_s}{Z_{in} + R_s} \qquad (2.26)$$

$$S_{13} = \frac{2 \sqrt{(R_s / Z_R)} Z_{in}}{R_s + Z_{in}} \star \frac{V_1}{V_3} \qquad (2.27)$$

$$S_{23} = \frac{2\sqrt{(R_s/Z_F)}Z_{in}}{R_s + Z_{in}} * \frac{V_2}{V_3} \qquad (2.28)$$

If MSSW power radiated in the slab is equated to the electrical power dissipated in the lumped radiation resistance we find:

$$\frac{|V_1|^2}{2|Z_R|^2} * Re(Z_R) = \frac{|V_3|^2}{2|Z_{in}|^2} * R_{m2} \qquad (2.29)$$

$$\frac{|V_2|^2}{2|Z_F|^2} * Re(Z_F) = \frac{|V_3|^2}{2|Z_{in}|^2} * R_{m1} \qquad (2.30)$$

Where:

$$\frac{|V_1|}{|V_3|} = \frac{|Z_R|}{|Z_{in}|} \sqrt{\frac{R_{m2}}{Re(Z_R)}} \qquad (2.31)$$

$$\frac{|V_2|}{|V_3|} = \frac{|Z_F|}{|Z_{in}|} \sqrt{\frac{R_{m1}}{Re(Z_F)}} \qquad (2.32)$$

And:

$$\left[\frac{V_1}{V_3}\right] = Arctan\left[\frac{Im\left[\dfrac{R_{m2}}{Z_{in}}\right]}{Re\left[\dfrac{R_{m2}}{Z_{in}}\right]}\right] \qquad (2.33)$$

13

$$\left[\frac{V_2}{V_3}\right] = \text{Arctan} \left[\frac{\text{Im}\left[\frac{R_{m1}}{Z_{in}}\right]}{\text{Re}\left[\frac{R_{m1}}{Z_{in}}\right]}\right] \qquad (2.34)$$

At present there is no direct way to find S_{31} or S_{32} (wave port to electric port) so we assume $S_{23} = S_{31}$ and $S_{32} = S_{13}$. The only justification for this assumption is that S_{23} and S_{31} are both forward waves and S_{32} and S_{13} are both reverse waves. However, there is a difference in the coupling in that S_{23} and S_{13} represent electromagnetic to magnetostatic coupling and S_{32} and S_{31} represent magnetostatic to electromagnetic coupling. Having all the S-parameters, we next convert them to Y-parameters. The conversion to Y-parameters is done by assuming the S-parameters are terminated in the characteristic impedance of the unmetalized region. Since the conversion from S- to Y-parameters is straight forward, it will not be shown here. [6] Finally, cascading of the Y-parameters was done in order to model arrays and achieve the overall response of the coupling from the input transducer array to the YIG and then to the output transducer array (see Figure 2.5). These equations were also straight forward since all they involved was writing a system of equations and solving by Laplace's expansion. These equations from the S-parameters on down to the response function were derived
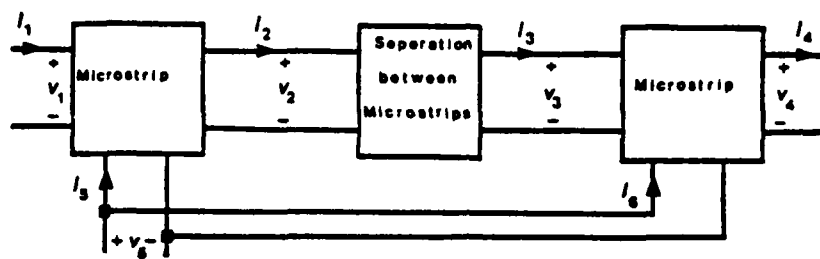
14

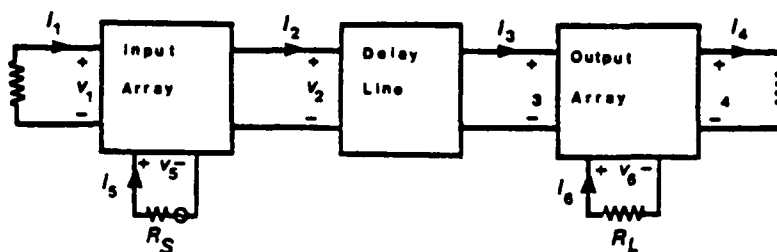Figure 2.5a: Cascading of Microstrips to Form Arrays

Figure 2.5b: Cascading of Arrays to Compute
Overall Response

15

and programmed in Fortran on an IBM 4341 and are shown in Appendix 1. The dispersion relationship for MSSW utilized is that of Brinlee. [10]

2.1.5 Results and Problems Encountered

The simplest case of a single bar 50 micrometers wide transducer was first tried. The computer program appeared to yield the correct frequency response as that found from experiment (see Figures 2.6a and 2.6b). Then cascaded microstrips both 2- and 4-bar arrays were tried and the program did not yield the correct frequency response. Figures 2.7 and 2.8 show the experimental and theoretical frequency response of a 2-bar and 4-bar transducer array pairs. The frequency responses of these devices had gain at some frequencies which is not physically possible for passive devices. Conservation of energy was then considered and the squared magnitudes were output by the program. Conservation of energy for a lossless 3-port says:

$$|S_{11}|^2 + |S_{31}|^2 + |S_{21}|^2 = 1 \qquad (2.35)$$

$$|S_{2\angle}|^2 + |S_{12}|^2 + |S_{32}|^2 = 1 \qquad (2.36)$$

$$|S_{33}|^2 + |S_{13}|^2 + |S_{23}|^2 = 1 \qquad (2.37)$$

Figure 2.6a: Theoretical Frequency Response for Single Bar 50um Transducer

Figure 2.6b: Experimental Frequency Response for Single Bar 50um Transducer

17

Figure 2.7a: Theoretical Frequency Response for 2-Bar
50um Transducer

Figure 2.7b: Experimental Frequency Response for 2-Bar
50um Transducer

18
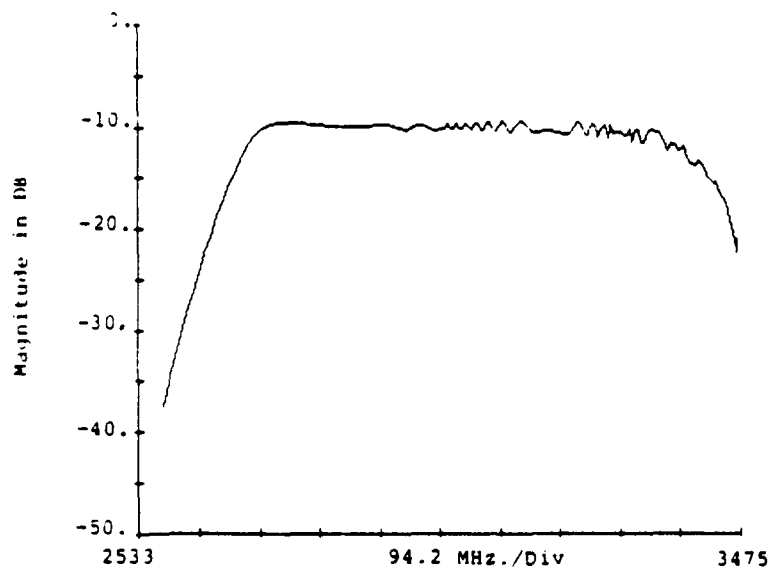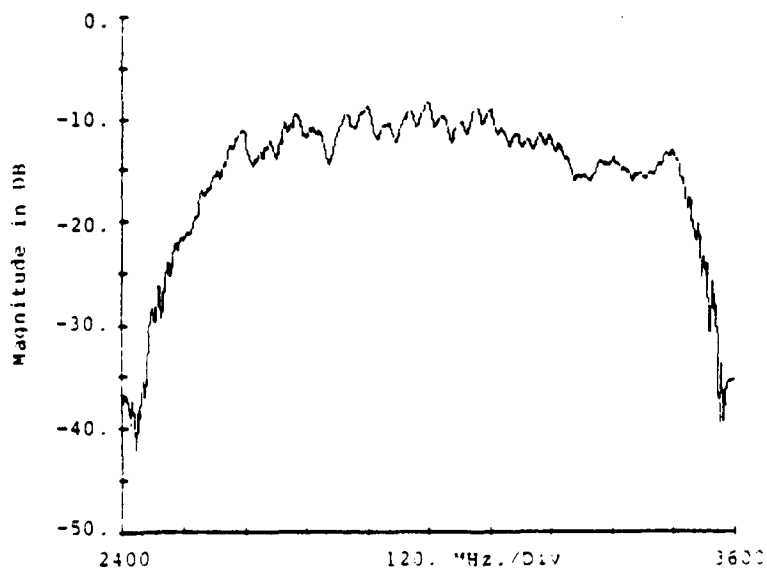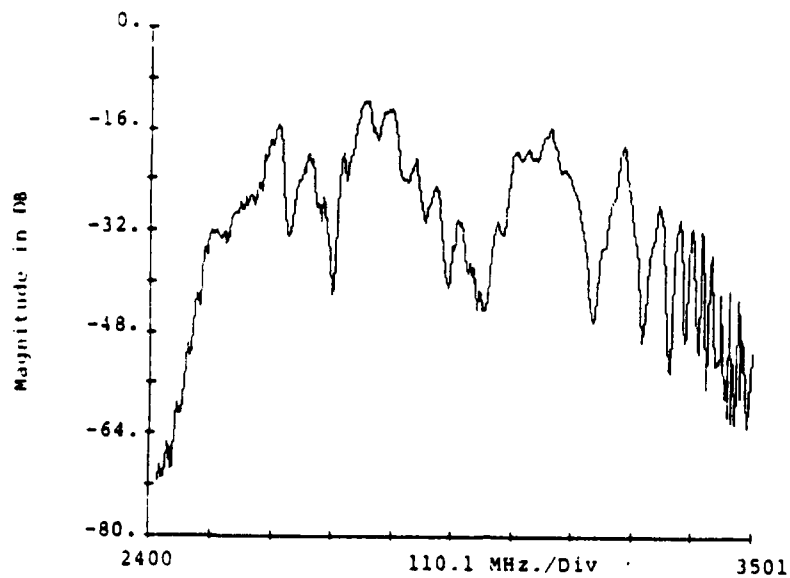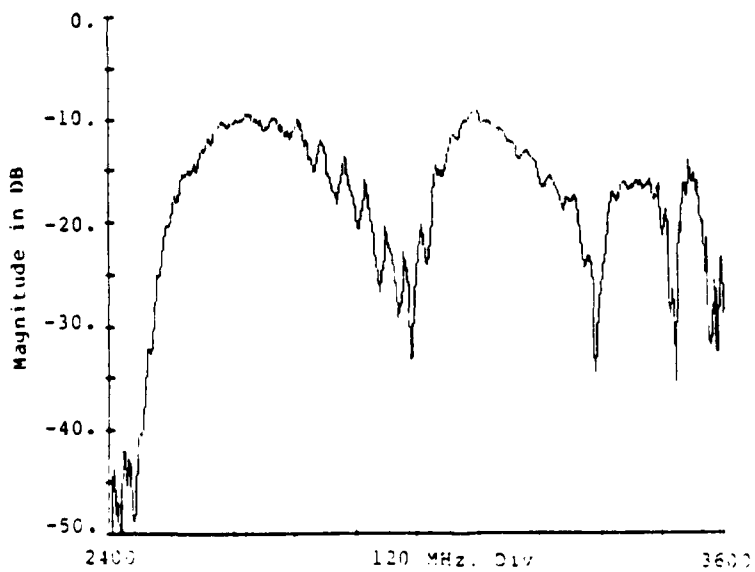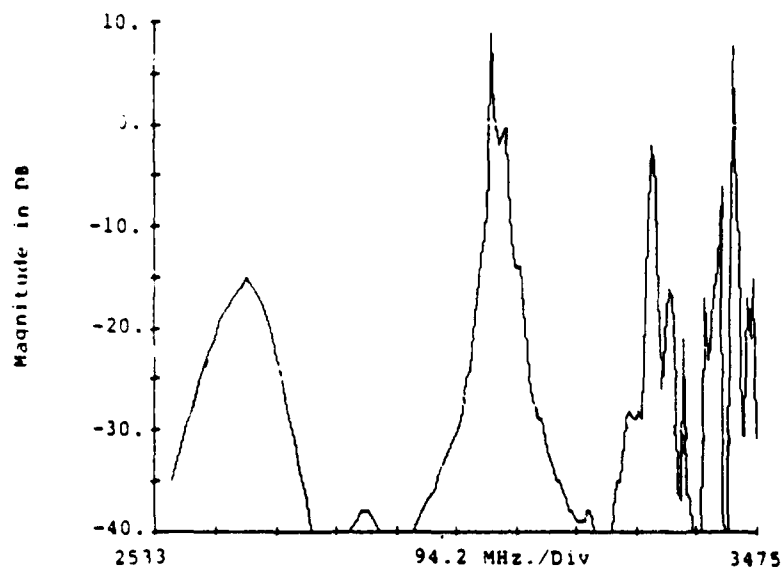
Figure 2.8a: Theoretical Frequency Response for 4-Bar
50um Transducer
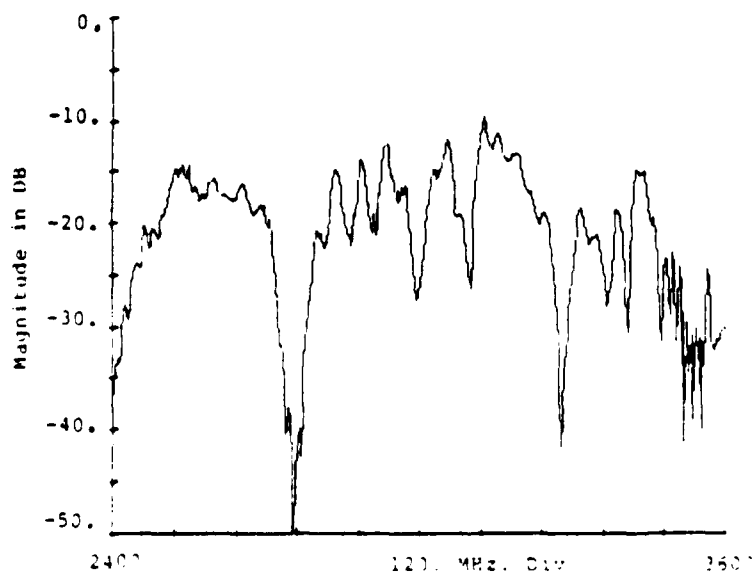
Figure 2.8b: Experimental Frequency Response for 4-Bar
50um Transducer

19

Since this is not the lossless case, the sum of the squared magnitudes should be less than one. As things turned out, all the squared magnitudes were indeed less than one but the sums were not. The first two equations 2.35 and 2.36 were violated while equation 2.37 was not because it came directly from Wu's impedance model derived from the Poynting vector. The equations 2.35 and 2.36 were violated because they came from the open circuited microstrip transmission line model. The transmission line model behaves very much like an ideal transmission line in that $S_{11} = S_{22} = 0$ and $S_{21} = S_{12}$. From a physical point of view this is not possible since there must be some coupling to the electric port. Some other approaches were tried in order to overcome these problems including forcing equations 2.35 and 2.36 to obey conservation of energy by adjusting the magnitude of S_{12} and S_{21} while leaving the phase alone. This was done by allowing equation 2.37 to set the total energy and then solving for the new magnitudes. After all this was done, gain still existed at certain frequencies. The Y-parameters were then converted to Z-parameters and some Z-parameters had negative real parts. The problem seems to be in the phase of the S-parameters or Y-parameters. The possibility of the computer not handling the complex numbers right exists, however the real problem is believed to be in

finding accurate values for S_{31} and S_{32}. The final
solution will be to make Poynting vector calculations for
a loaded microstrip and "that" solution is still pending
at this time. Since solving the loaded microstrip problem
is very difficult, in the following chapters an empirical
approach will be tried. A device structure will be
developed and made in order to measure the S-parameters of
a transducer array.

CHAPTER III

2.2 DEVICE DESIGN AND MANUFACTURE

2.2.1 Introduction

The simplest and easist built transducer for
conversion of electromagnetic to magnetostatic energy is
one that has the microstrip fabricated on a dielectric
substrate with the ferrite flipped over on it. All
transducer designs will be based on this flipped
configuration as shown in Figure 2.9. Efficient
conversion of energy is obtained when the length of the
microstrip is small compared to the electromagnetic
wavelength, and when the width is small compared to the
magnetostatic wavelength. If a microstrip is excited by a
current and the ferrite is biased by a magnetic field, two
magnetostatic waves are launched by the microstrip in
opposite directions perpendicular to the axis of the
microstrip (Figure 2.10).

2.2.2 Device Design

The transducer design for measuring the 3-port S-
parameters of a microstrip transducer array is very
straight forward. Two measuring single microstrip
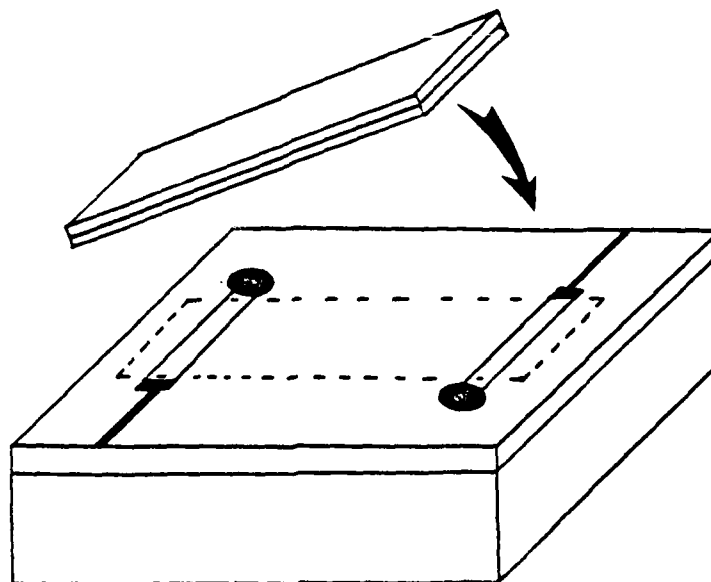transducers are placed symmetrically on both sides of the

22

Figure 2.9: Magnetostatic Delay-Line Utilizing Flipped Configuration

Directions of Propagation

$\otimes$
H
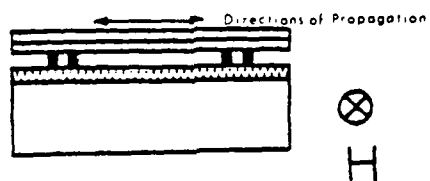
Figure 2.10: Bias Field Direction for Magnetostatic Surface Wave Propagation

23

microstrip transducer array to be measured. The single microstrip transducers are placed at a distance greater than that of a magnetostatic wavelength, and at the same time, not equal to any integer multiple of a quarter of that same wavelength. All total sixteen different devices were made including single, two, four, and eight bar microstrip arrays with widths of five, ten, twenty, and fifty micrometers. The measuring microstrip transducer width was chosen as five micrometers because it was the narrowest line that could be fabricated consistently. Narrower transducers should have a tendency to be more decoupled from the microstrip transducer array under measurement.

In the single and two bar microstrip arrays, the measuring transducers were 2200 micrometers or seven and one-third magnetostatic wavelengths away from the array; while in the four and eight bar arrays, the measuring transducers were 1600 micrometers away or five and one-third wavelengths. These distances were chosen to meet the constraints of the above and for ease of fabrication. The center-to-center spacing of the input and output arrays was chosen to be one centimeter for convenience, and the microstrip length was three millimeters or one-tenth of an electromagnetic wavelength. The transmission lines connecting all transducer arrays to the outside

world were 50 Ohms for measurement purposes. Fiqure 2.11 shows the layout of a typical device. All of the devices were then fabricated and tested.

2.2.3 Device Fabrication

After the transducer desiqn was completed, fabrication of the devices was next. Special care had to be taken in making these devices since lengthy five micrometer wide lines are not easy to achieve with a single reduction photographic process. A Haag-Streit Bern coordinatograph was used to cut masks for each device. This coordinatograph could cut all lines except the five micrometer wide lines because its' resolution is about ten micrometers. To replace the five micrometer lines, fine copper wire of the appropriate width was used. This wire was straightened and fixed to the mask by tape at the ends and clear silicon grease in the middle. Each mask was shot with a 25.4 to 1 reduction camera where focusing was tried prior to the reduction process, but was abandoned since it could only be achieved over a small region of the mask. The lack of a good focus caused many problems which were overcome by under-developing the photographic reduction by about fifty percent. The reductions of each mask were carefully examined for problems. Each line was checked for uniformity, width, and spacing with a Lietz microscope. An actual
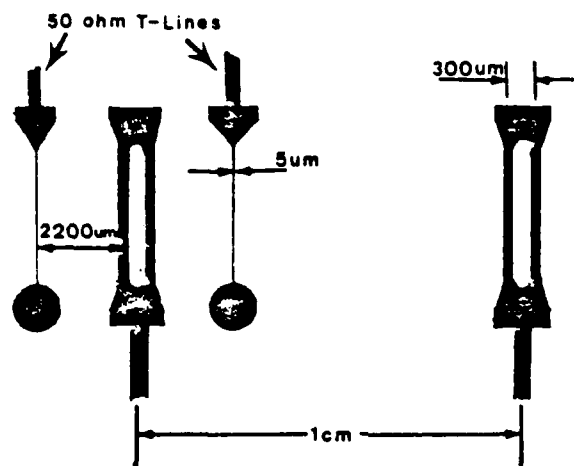
25

Figure 2.11 Transducer Layout
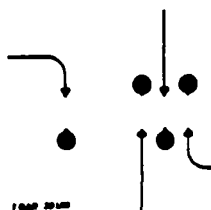
Figure 2.12 Reproduction of a Reduced Mask

reproduction of a reduced mask can be seen in Figure 2.12 After the photo-reduction process came the photo-resist process.

KTI positive photo-resist with a viscosity of 90 centistokes @25° C was spun onto a substrate at 5000 rpm for 40 sec. yielding a thickness of about 3 micrometers. The photo-resist was then prebaked for about 15 minutes at 70° C. After the prebake, the substrates were exposed with a Colbilt CA-400 mask aligner. The exposure time depended on the quality of each mask. The substrates were then post baked overnight for a hard bake to prevent widing of the lines in the up-plating process. The 10 mil. alumina substrates have about 100 Angstroms of chrome and about 700 Angstroms of gold evaporated on both sides. Before the evaporation process, the substrates were cleaned with a one to one solution of sulfuric acid and hydrogen peroxide and baked dry. After the substrates were cleaned and dried, they were placed in the evaporation system and futher dried with the substrate heater.

The up-plating process consisted of Englehard ECF-63 noncyanide gold plating solution, a hot plate stirrer, and an HP model 721A power supply. The substrates (the cathode) were clamped in parallel each with a alligator clip in series with a 1K Ohm resistor. A circular platinum

electrode was submerged in the plating solution and served as the anode. The solution required that no glass be used so a nalgene beaker served as the container for the solution and the electrodes (see Figure 2.13) The solution was first filtered thru a Gelman syringe filter and then heated to 45-50° C. A current of 10 ma per substrate for 30 min. yielded about 3 micrometers of gold. A problem was encountered with the up-plating, in that, the gold was not sticking very well. This problem was thought to be caused by unclean substrates and was resolved by reversing the current for about 1 minute before beginning the up-plating process and every 10 minutes thereafter. When the up-plating was complete, the solution was refiltered back into the original container and the hard baked photo-resist was stripped off with a one-to-one solution of sulfuric acid and hydrogen peroxide. The substrates were etched in a premixed solution of 125 grams of KI, 40 grams of I_2, and 500 milliliters of water to remove the excess gold and then etched in another premixed solution of 50 grams of NaOH, 40 grams of $K_3Fe(CN)_6$, and 180 milliliters of water to remove the chrome. After careful examination under a microscope for correct width and line continuity, the substrates were mounted on an aluminum block and tested.
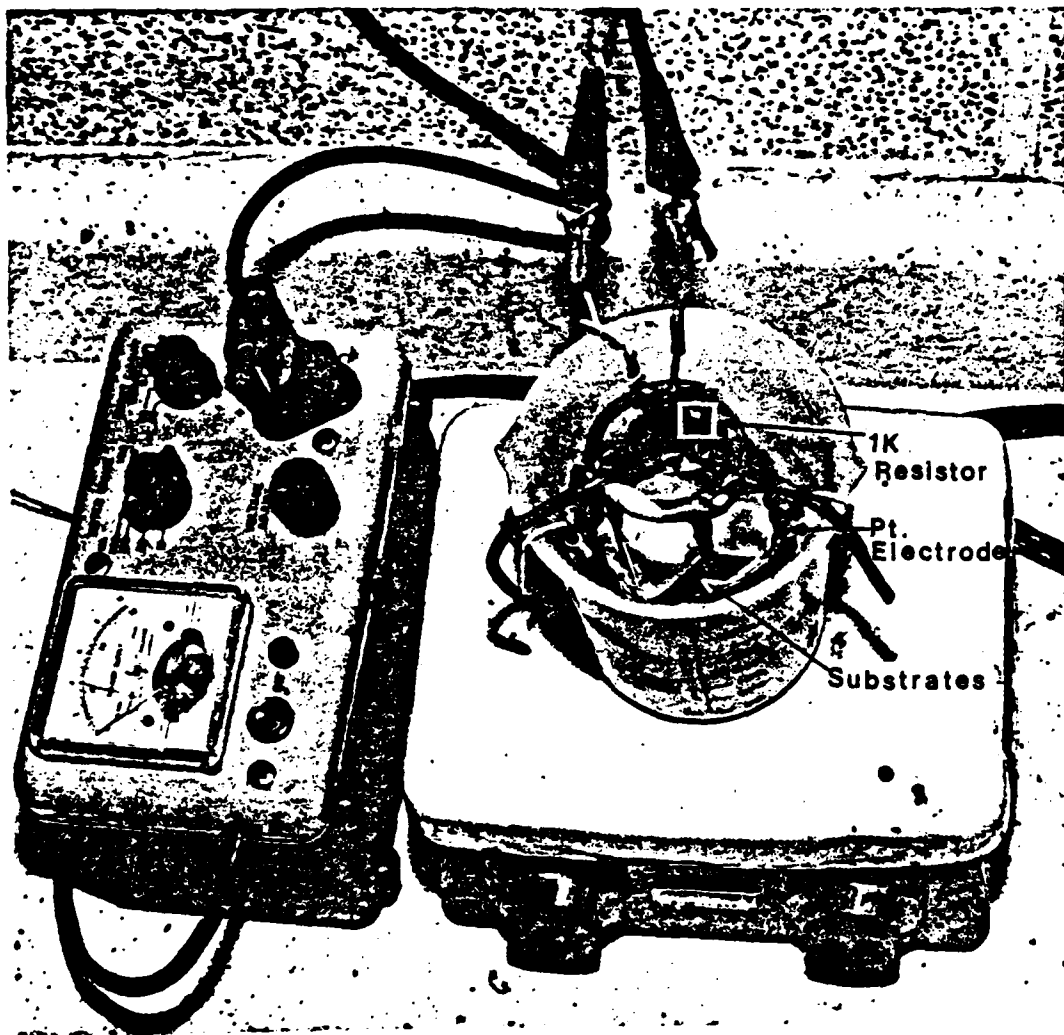
Figure 2.13   Gold Up-Plating Set-Up

2.2.4 Measurement Techniques

The 3-port S-parameters represented by equation 3.1 are to be measured.

$$
\begin{bmatrix} b_1 \\ b_2 \\ b_3 \end{bmatrix} = \begin{bmatrix} S_{11} & S_{12} & S_{13} \\ S_{21} & S_{22} & S_{23} \\ S_{31} & S_{32} & S_{33} \end{bmatrix} \begin{bmatrix} a_1 \\ a_2 \\ a_3 \end{bmatrix}
\tag{3.1}
$$

Previous mathmatical models [6] assumed that the two wave ports (Fig. 2.14) were match terminated making the reflections coefficents zero. Since all indications from the measurements show that this condition holds, and because the wave port reflection coefficients are very hard to measure, S_{11} and S_{22} will be assumed equal to zero. The validity of this assumption as well as other assumptions will be examined later. S-parameters are similar to Y- and Z-parameters in that in order to measure these parameters, one must set something equal to zero. For example, to measure S_{31}, a_2 and a_3 must be zero. Consequentially, the ratio of b_3 to a_1 will be S_{31}. Since excitation of a microstrip in the presence of a magnetically biased ferrite launches waves in two directions, one must develop techniques for eliminating the other wave in order to measure the S-parameters. Due to the fact that the reverse wave is more difficult to couple to, it generally contains much less power than the

analyzer, which has the ability to measure reflection and transmission coefficients directly.

2.2.5 Conclusion

This chapter showed how each device was made and measured. All the measurements taken were stored on cassett tape and later transferred to an IBM 4341 computer and stored on disk. The following chapter studies this data and examines an empirical model derived from it.

CHAPTER IV

2.3 EMPIRICAL 3-PORT MODEL

2.3.1 Introduction

Measuring S-parameters of a transducer with a similar transducer at microwave frequencies introduces errors. These errors can be corrected by introducing correction factors. The errors result from transducer conversion loss, the propagation path between the measuring transducer and the transducer array being measured, and the transmission line between the network analyzer reference plane and the transducer reference plane. These correction factors will be derived and the resulting measurements will be corrected and placed in the S-parameter model derived in Chapter 2.

2.3.2 Correction Factors

The transducer conversion loss is assumed to be a real constant loss and is accounted for by adding the assumed values of 5 dB per transducer for forward wave coupling and 10 dB for reverse wave coupling. The phase difference between the reference planes was measured with the network analyzer by taking an equivalent section of transmission line and shorting the end. The measured
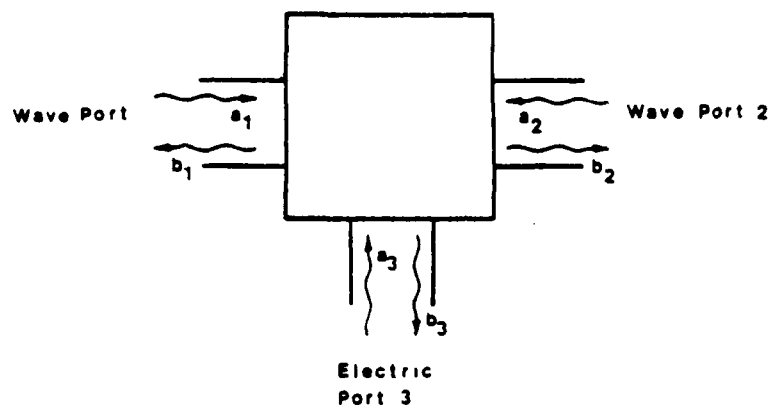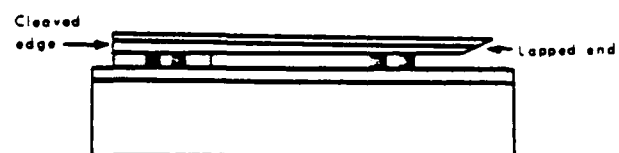
Figure 2.14 Three Port Model

Figure 2.15 Techniques for Measurements

forward wave, therefore a_2 can be neglected in the measurement of S_{21}, S_{23}, S_{31}, and S_{33}. However, in measuring the reverse wave S-parameters, S_{12}, S_{32}, and S_{13}, a_1 cannot be neglected. This problem can be eliminated by cleaving the ferrite crystal at one end and placing the cleaved edge directly on the transmitting transducer as shown in Figure 2.15 This forces all the energy in one direction eliminating any wave that might propagate in the other direction. To kill secondary reflected waves created by unterminated transducers, 50 Ohm loads were connected to each transducer not currently being used.

Another problem associated with measuring the S-parameters is ripple in the passband due to reflections from the ends of the ferrite crystal. This problem was partially solved by terminating the end of the crystal not cleaved. The termination was achieved by lapping the end at about a 1° angle as shown in Figure 2.15 Terminating the ends by lapping works exceptionally well because the thinner the ferrite crystal the longer the delay associated with the magnetostatic wave. Therefore, any wave traveling to the end is attenuated before it has time to be reflected back. The results of lapping are very good as can been seen from Figure 2.16 All measurements were taken with a Hewlett-Packard 8409 automatic network

34
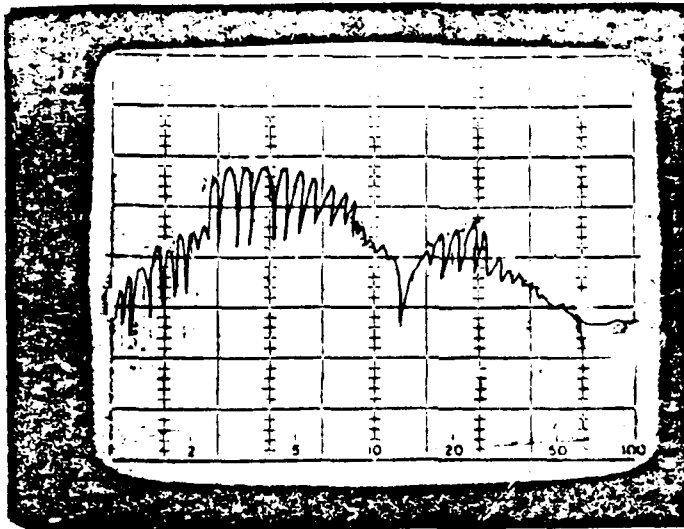
Figure 2.16   Unlapped Crystal Response
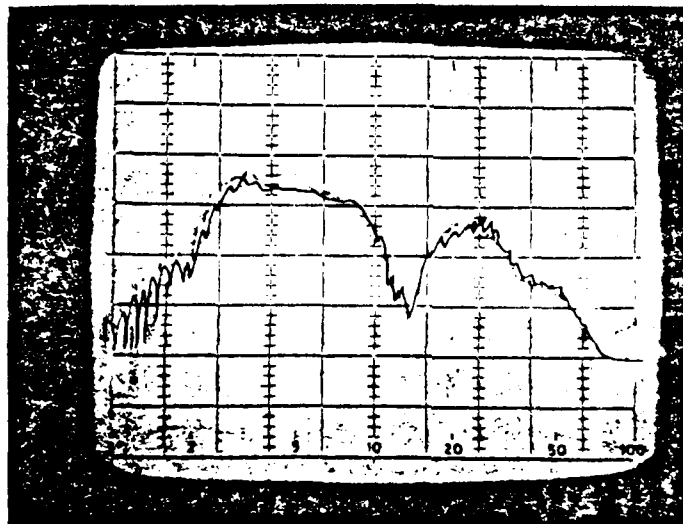
Figure 2.17   Lapped Crystal Response

angle was subtracted from 180° and the result divided by two, yielding the correct electrical length of the transmission line. The propagation path error was corrected by solving the dispersion relation for the propagation constant and assuming exponential propagation. The propagation correction factors were derived as follows: (refer to Fig. 2.14)

for S_{21}:

$$S_{21m} = \frac{b_{2m}}{a_{1m}} = \frac{b_{2c}\exp(-\int_f d)}{a_{1c}\exp(+\int_f d)} = S_{21c}\exp(-2\int_f d) \quad (4.1)$$

therefore,

$$S_{21c} = S_{21m}\exp(+2\int_f d) \quad (4.2)$$

for S_{12}:

$$S_{12m} = \frac{b_{1m}}{a_{2m}} = \frac{b_{1c}\exp(-\int_r d)}{a_{2c}\exp(+\int_r d)} = S_{12c}\exp(-2\int_r d) \quad (4.3)$$

therefore,

$$S_{12c} = S_{12m}\exp(+2\int_r d) \quad (4.4)$$

for S_{31}:

$$S_{31m} = \frac{b_{3m}}{a_{1m}} = \frac{b_{3c}}{a_{1c}\exp(+\int_f d)} = S_{31c}\exp(-\int_f d) \quad (4.5)$$

therefore,

$$S_{31c} = S_{31m}\exp(+\hat{\int}_f d) \qquad (4.6)$$

for S_{13}:

$$S_{13m} = \frac{b_{1m}}{a_{3m}} = \frac{b_{1c}\exp(-\int_r d)}{a_{3c}} = S_{13c}\exp(-\int_r d) \qquad (4.7)$$

therefore,

$$S_{13c} = S_{13m}\exp(+\int_r d) \qquad (4.8)$$

for S_{32}:

$$S_{32m} = \frac{b_{3m}}{a_{2m}} = \frac{b_{3c}\exp(-\int_r d)}{a_{2c}} = S_{32c}\exp(-\int_r d) \qquad (4.9)$$

therefore,

$$S_{32c} = S_{32m}\exp(+\int_r d) \qquad (4.10)$$

for S_{23}:

$$S_{23m} = \frac{b_{2m}}{a_{3m}} = \frac{b_{2c}}{a_{3c}\exp(+\int_f d)} = S_{23c}\exp(-\int_f d) \qquad (4.11)$$

therefore,

$$S_{23c} = S_{23m}\exp(+\int_f d) \qquad (4.12)$$

where the subscripts "m", "c", "f", and "r" represent the measured and corrected S-parameters, and the forward and reverse waves respectively.

The final S-parameters with all the corrections made are as follows:

$$S_{11}=0 \qquad\qquad (4.13)$$

$$S_{22}=0 \qquad\qquad (4.14)$$

$$S_{12}= (\ S_{12m} +20\ dB)*\exp(2\ \gamma_r d)*\exp[j(\underline{/S}_{12m}+$$
$$(180-\theta_1)/2 + (180-\theta_2)/2)] \qquad (4.15)$$

$$S_{21}= (\ S_{21m} +10\ dB)*\exp(2\ \gamma_f d)*\exp[j(\underline{/S}_{21m}+$$
$$(180-\theta_1)/2 + (180-\theta_2)/2)] \qquad (4.16)$$

$$S_{13}= (\ S_{13m} +10\ dB)*\exp(\gamma_r d)*\exp[j(\underline{/S}_{13m}+$$
$$(180-\theta_1)/2 + (180-\theta_3)/2)] \qquad (4.17)$$

$$S_{31}= (\ S_{31m} +5\ dB)*\exp(\gamma_f d)*\exp[j(\underline{/S}_{31m}+$$
$$(180-\theta_1)/2 + (180-\theta_3)/2)] \qquad (4.18)$$

$$S_{23}= (\ S_{23m} +5\ dB)*\exp(\gamma_f d)*\exp[j(\underline{/S}_{23m}+$$
$$(180-\theta_2)/2 + (180-\theta_3)/2)] \qquad (4.19)$$

$$S_{32}= (\ S_{32m} +10\ dB)*\exp(\gamma_r d)*\exp[j(\underline{/S}_{32m}+$$
$$(180-\theta_2)/2 + (180-\theta_3)/2)] \qquad (4.20)$$

$$S_{33}= S_{33}\ \exp[j(\underline{/S}_{33m} + (180-\theta_3))] \qquad (4.21)$$

These equations were programmed into an IBM 4341 computer, where the data had been previously stored.

2.3.3 The Measurement System

The Hewlett-Packard 8409 Automatic Network Analyzer provides reliable accurate measurements of a 2-port network. Control of the network analyzer was done by using an HP-9845B Desk Top Computer together with an Accuracy Enhancement Program. The Accuracy Enhancement Program was written by Hewlett-Packard and has the ability to automatically measure the reflection and transmission coefficients over any frequency range from 100 MHz. to 18 GHz. and then take the measured data and correct it using either an 8-term or 12-term error model. All measurements taken for this thesis used the 12-term error model. Before any measurements were made, the system had to be calibrated. The Accuracy Enhancement Program provides a calibration routine which sets the reference magnitude levels and the phase reference plane using shorts, opens, and loads. Since the device being measured is a 3-port device, a multi-port measurement system would be more appropriate. Such systems have been developed but not available for these measurements. The limitations of the 2-port system was not easily overcome. Each time a measurement was taken, special care had to be used in lining up the magnetically tunable passband. For all

measurements, the frequency span was from 2.4 to 3.6 GHz.
with the passband centered at 3 GHz. The data was stored
on tape after each measurement and later transferred to
the IBM for processing. The device under test was placed
on a galvanometer for proper alignment in a Varian 9-inch
magnet.

2.3.4 Measured and Corrected Results

The first measurements were on a single microstrip,
50 micrometer wide transducer. The results are shown in
Figure 2.18 (Note the similarity in S_{31}, S_{23} and S_{13},
S_{32}.) When these results were transferred to the IBM, S_{31}
was set equal to S_{23}; and S_{13} was set equal to S_{32} to
simplify the alignment problems.

The following pages are the measured results of
several selected devices. Only a few devices were chosen
due to the large amount of data. This data is included in
Figures 2.18 thru 2.52 As one will note, there is a small
problem with alignment of the measurements. This problem
is due to reversing the magnetic field and is somewhat
overcome by shifting the frequency of the measured data
before using it in the model. Figures 2.53 thru 2.87 shows
the corrected data of the devices shown in Figures 2.18
thru 2.52 As one can see from comparing the corrected
results to the measured results, only the angle has
actually changed. The only change in magnitude that can

Figure 2.18 Measured S_{11} for 1-Bar 50 um Transducer

41

Figure 2.19 Measured S_{13} for 1-Bar 50 um Transducer

42
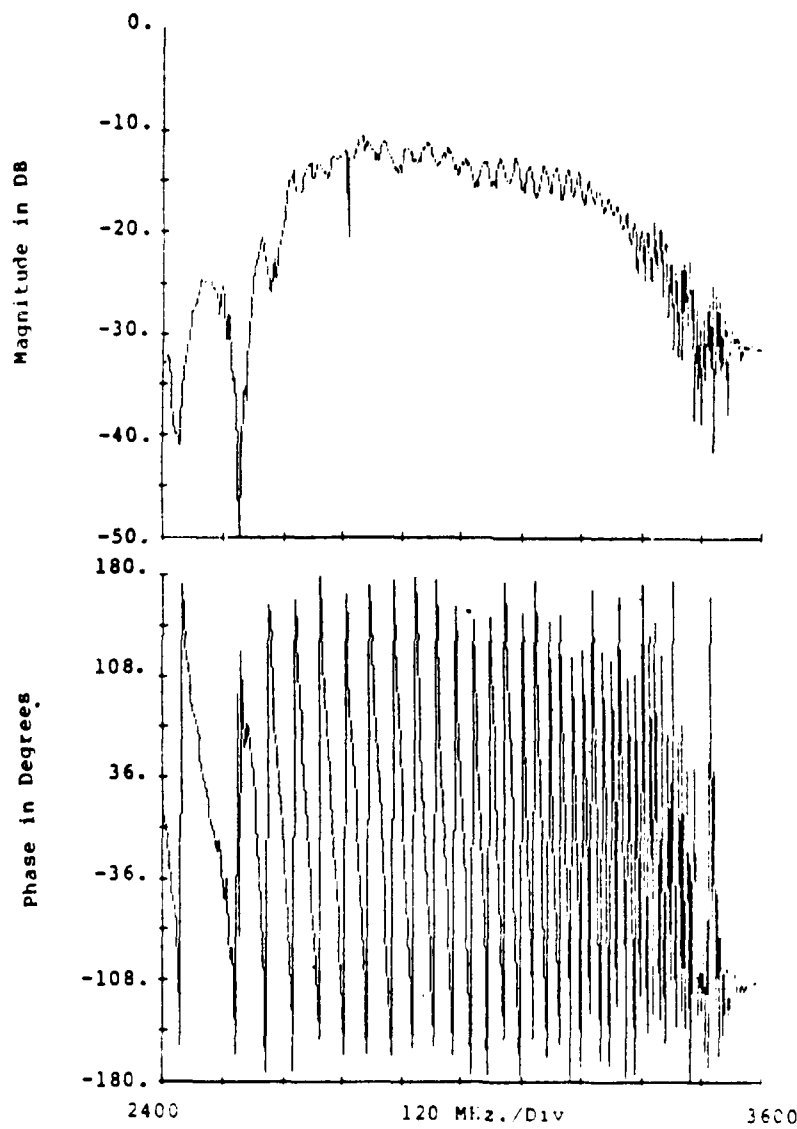
Figure 2.20: Measured S_{21} for 1-Bar 50 um Transducer

43

Figure 2.21: Measured S₁₁ for 1-Bar 50 um Transducer

44
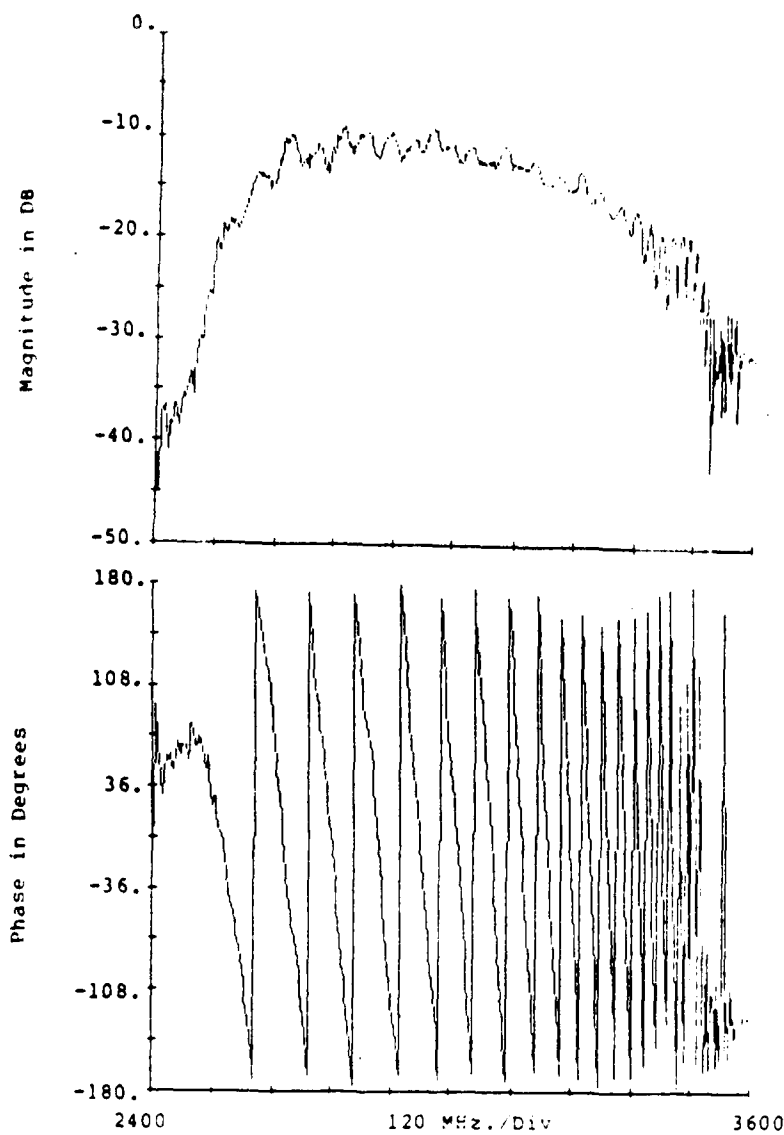
Figure 2.22: Measured S_{31} for 1-Bar 50 um Transducer
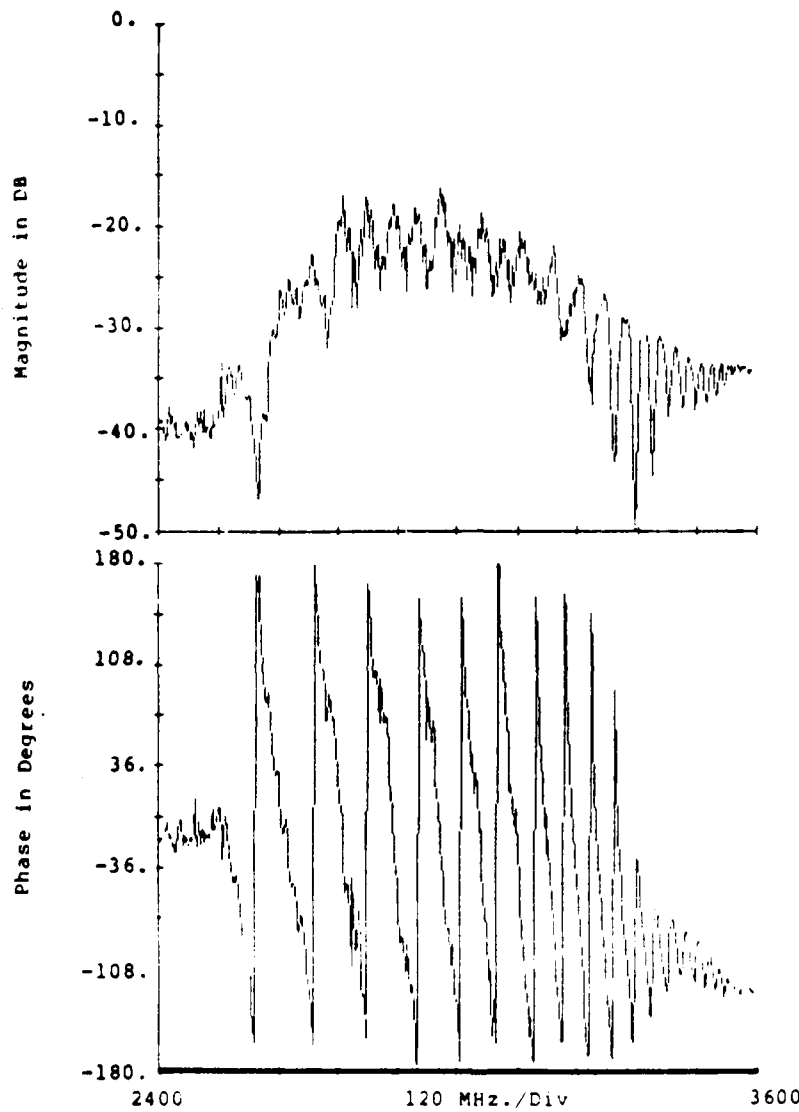
Figure 2.23: Measured S_{12} for 1-Bar 50 um Transducer

46
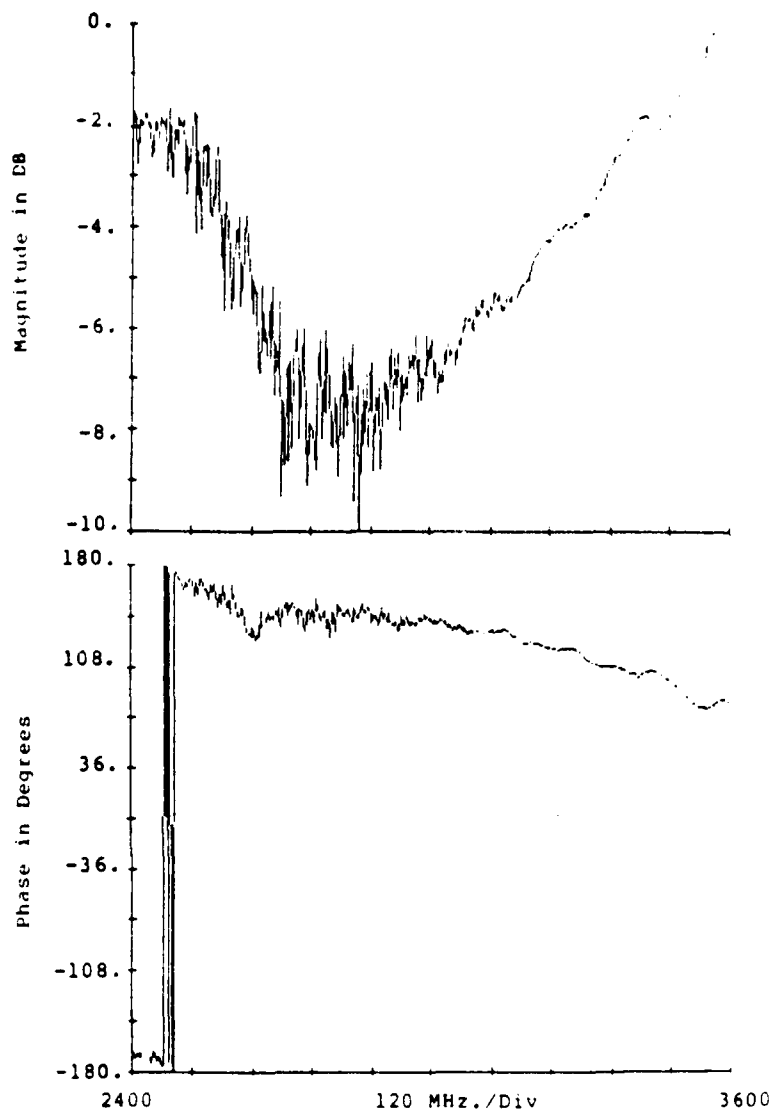
Figure 2.24: Measured S_{33} for 1-Bar 50 um Transducer

47
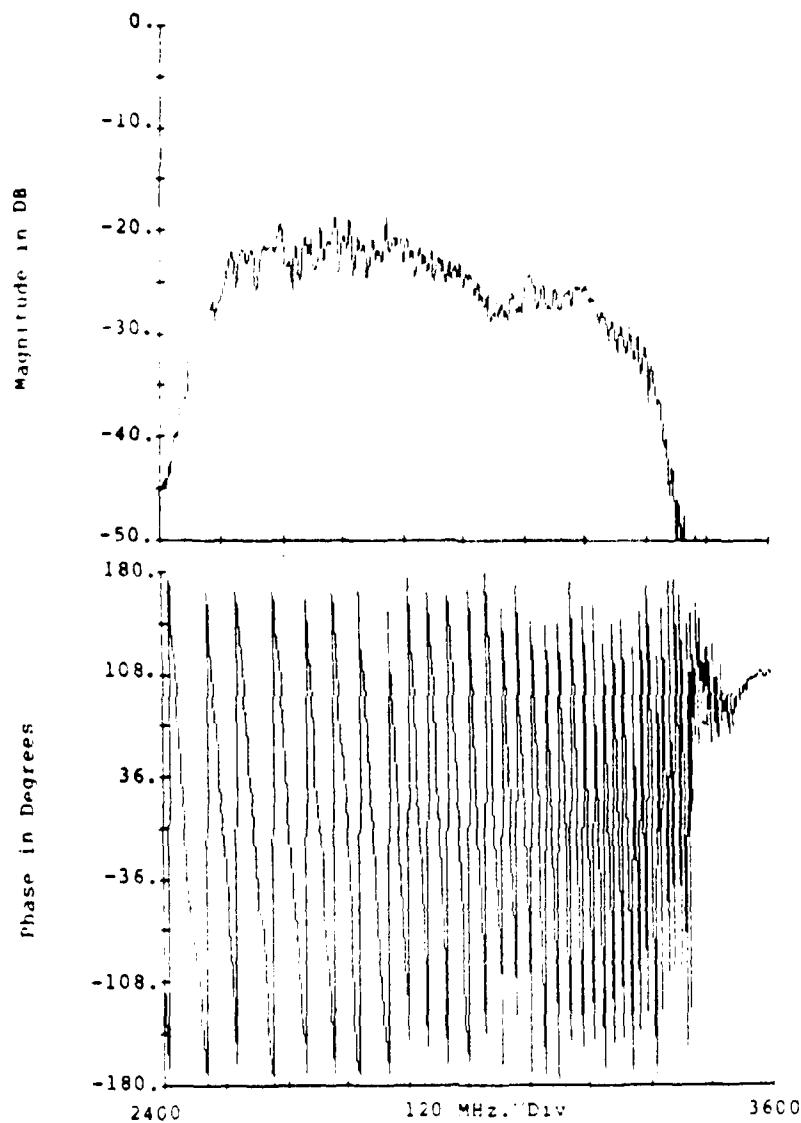
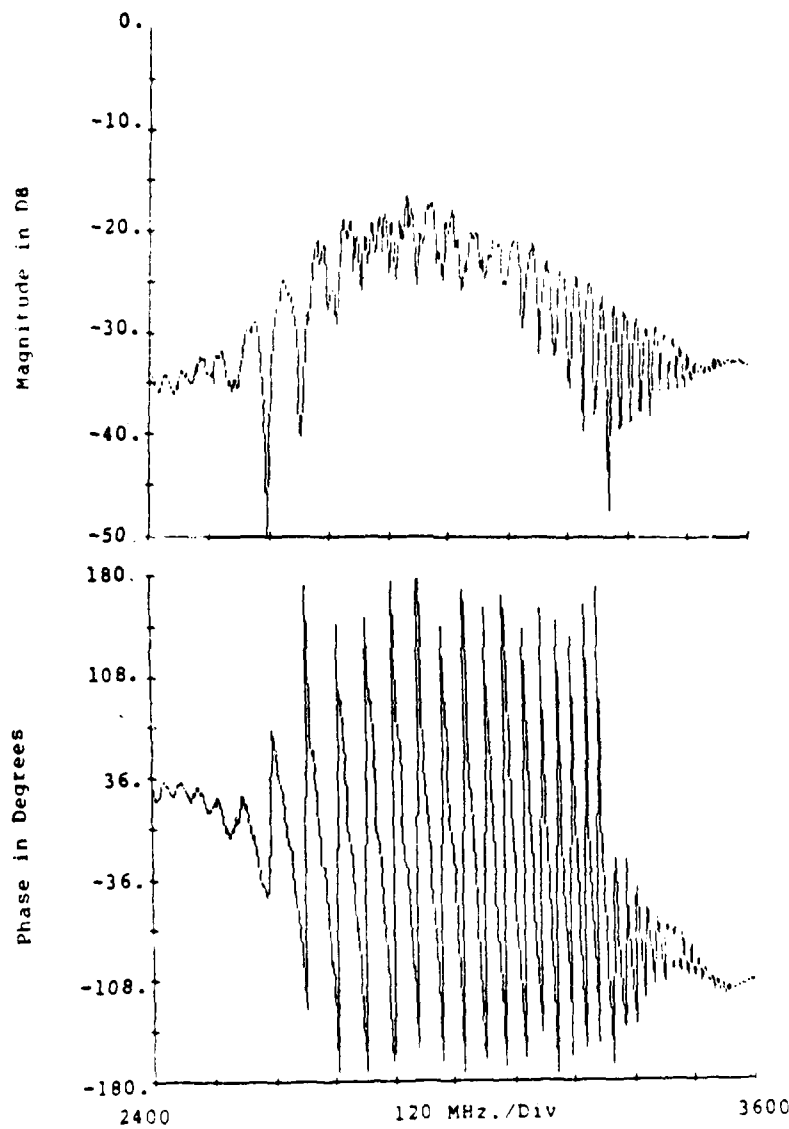Figure 2.25: Measured S_{12} for 1-Bar 10 um Transducer

48
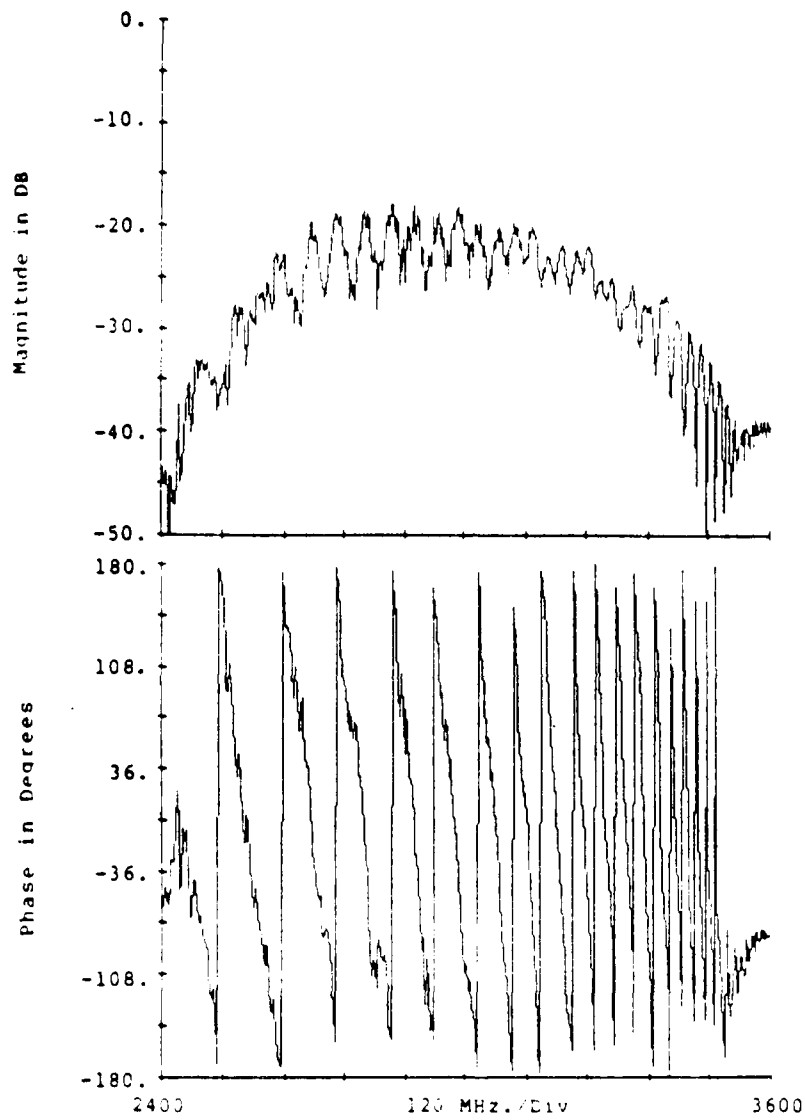
Figure 2.26: Measured S_{13} for 1-Bar 10 μm Transducer
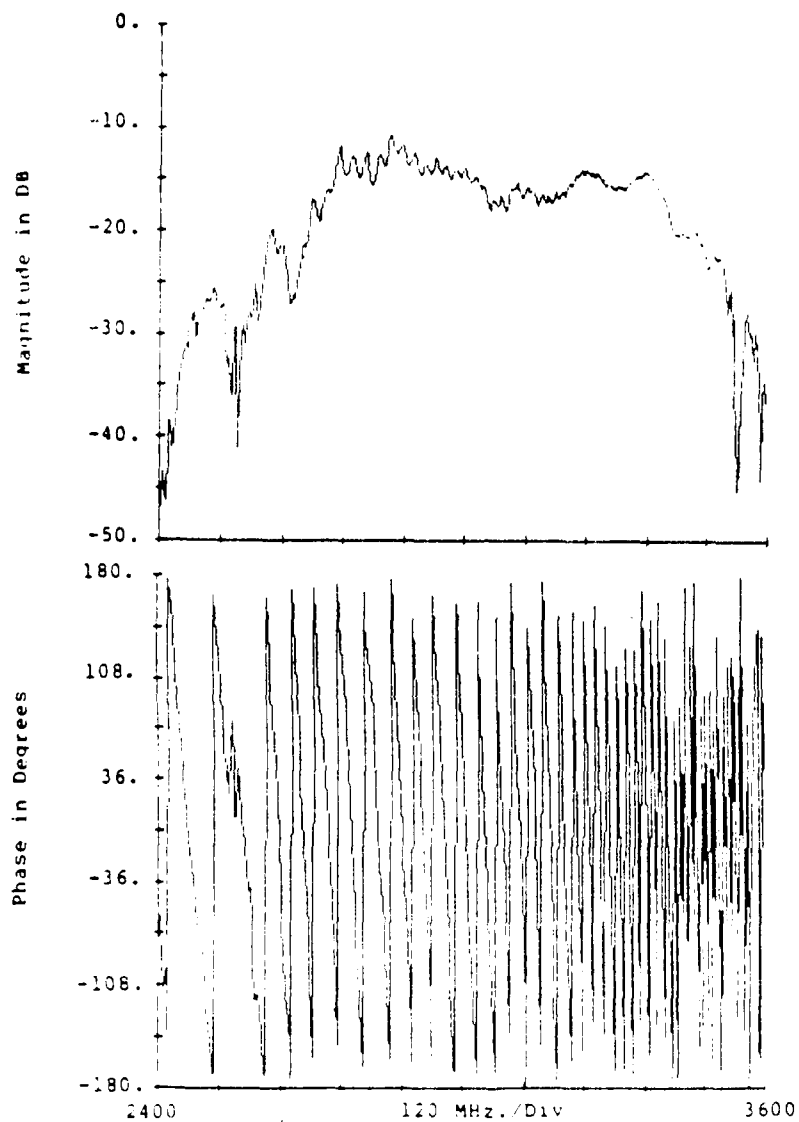
Figure 2.27: Measured S_{21} for 1-Bar 10 um Transducer
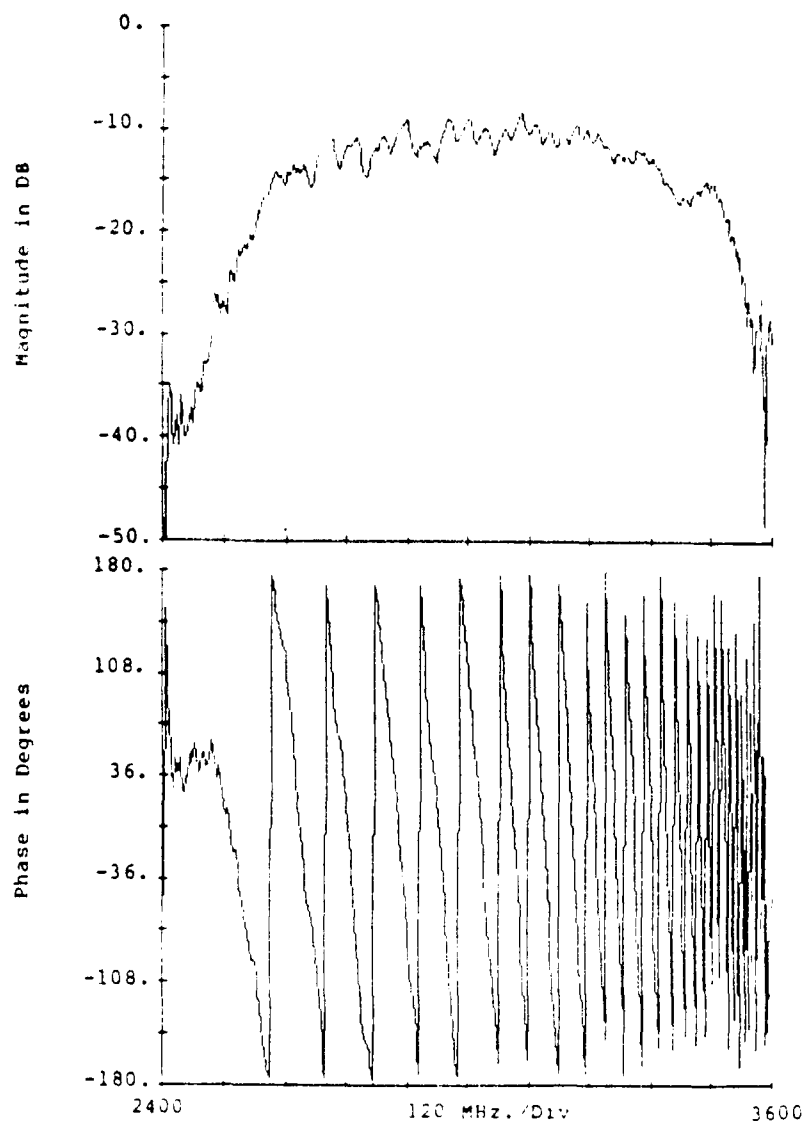
Figure 2.28: Measured S_{22} for 1-Bar 10 um Transducer
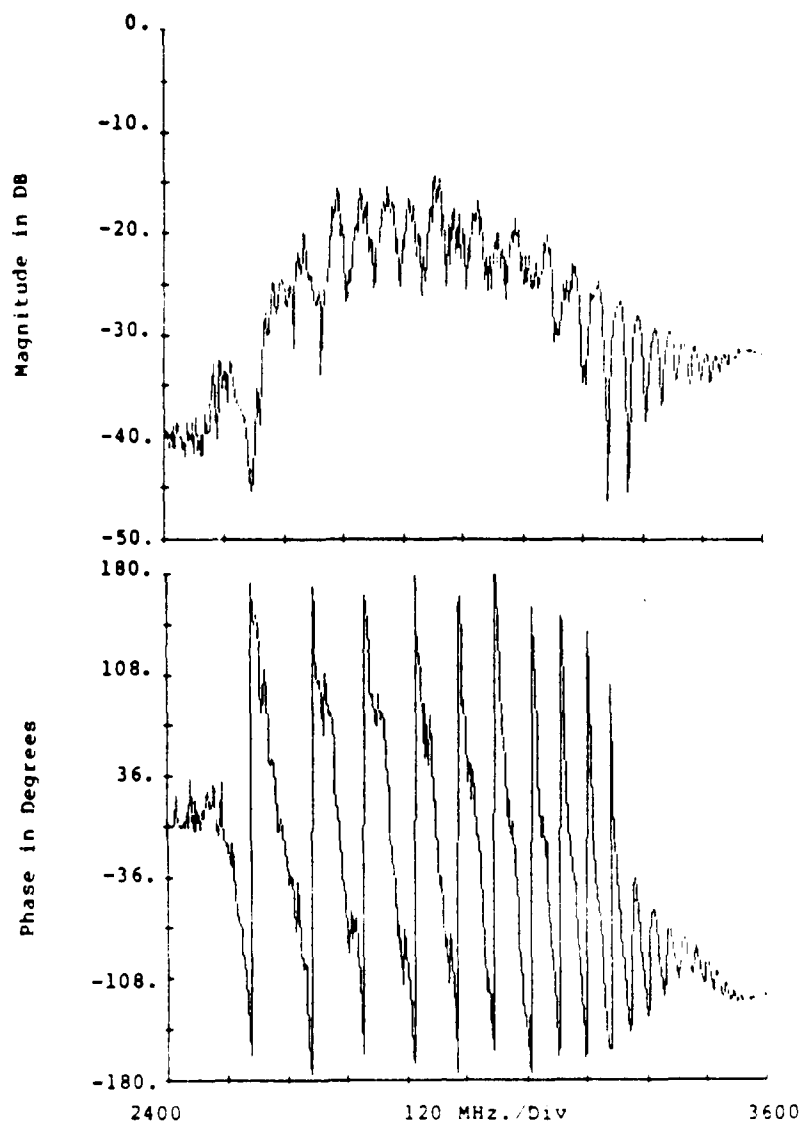
51
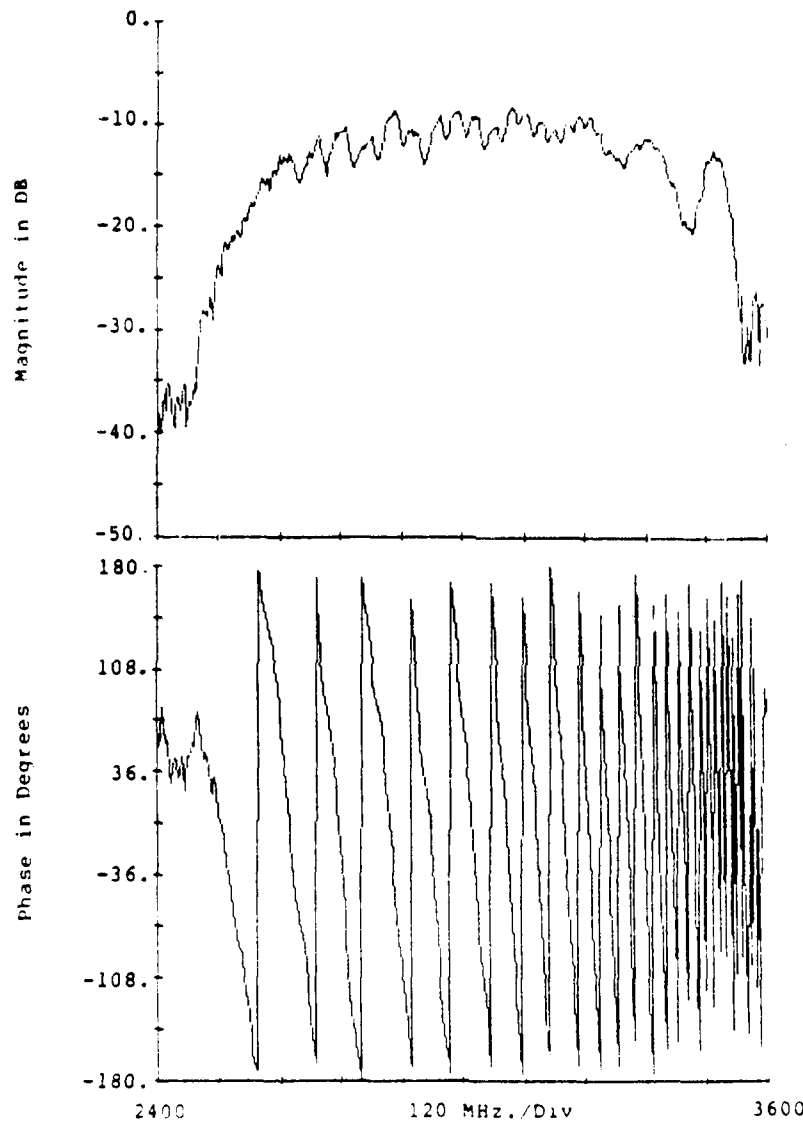
Figure 2.29: Measured S_{31} for 1-Bar 10 um Transducer
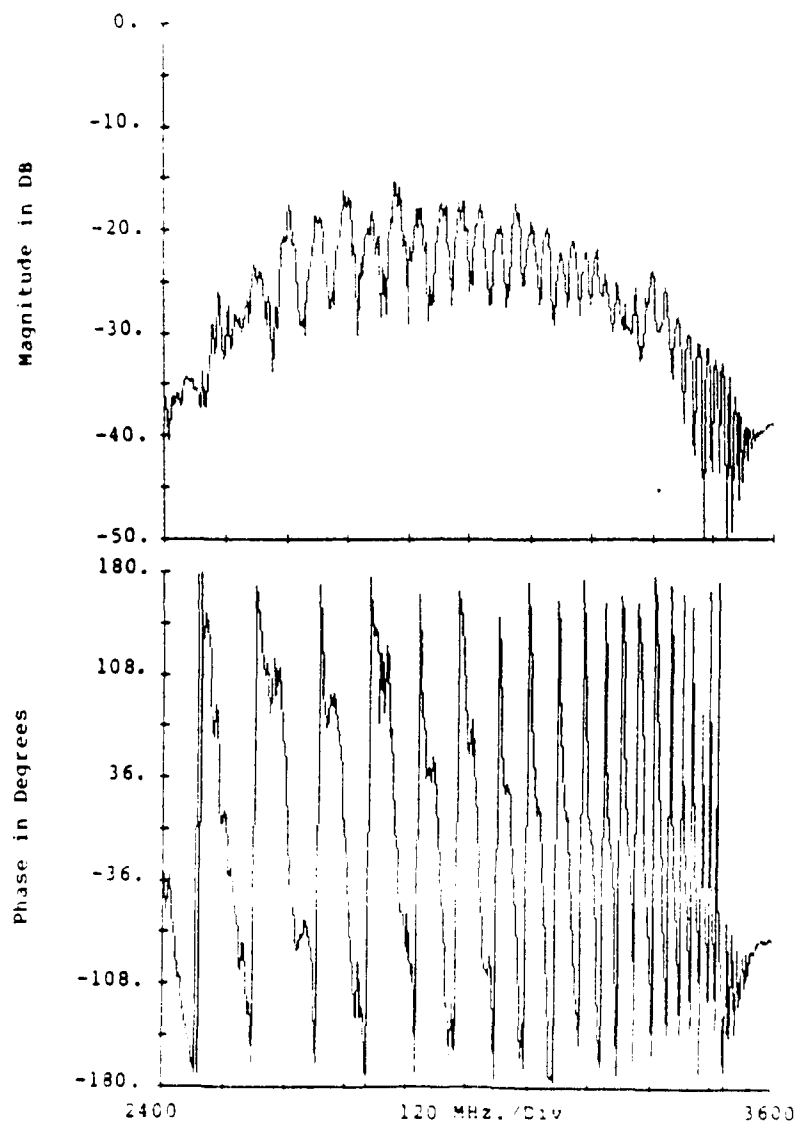
Figure 2.30: Measured S_{33} for 1-Bar 10 um Transducer
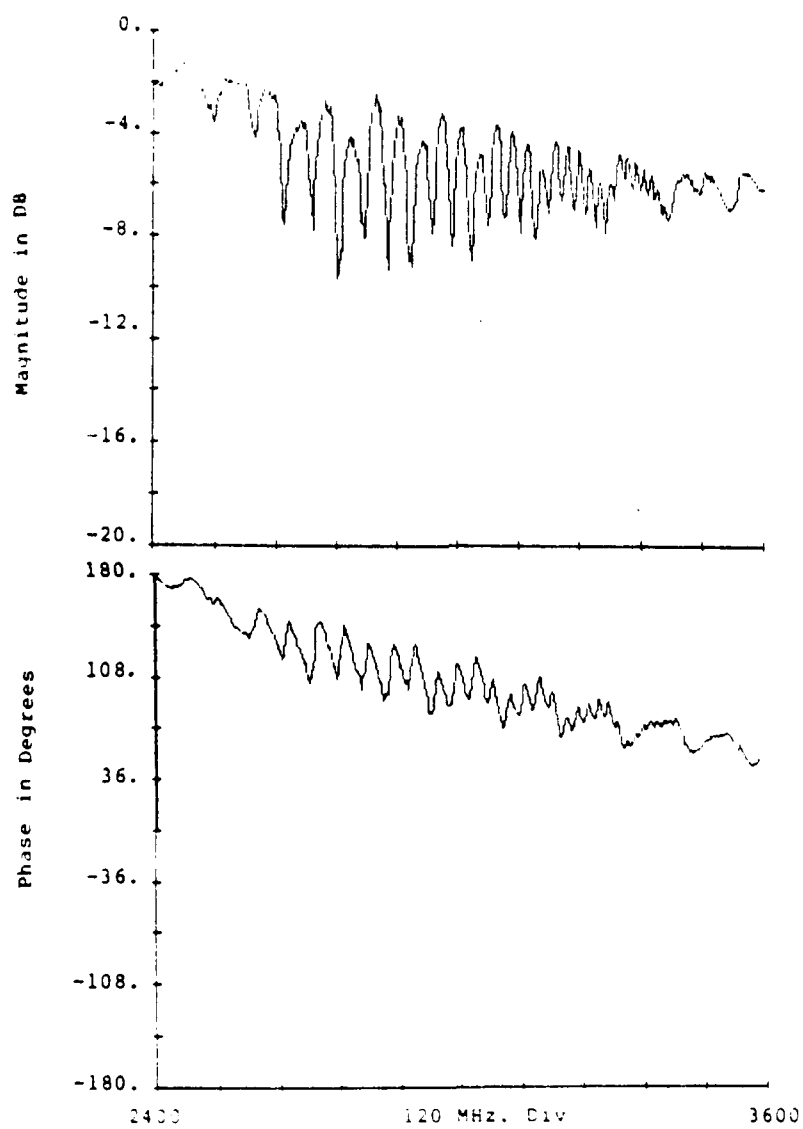
Figure 2.31: Measured S_{33} for 1-Bar 10 um Transducer
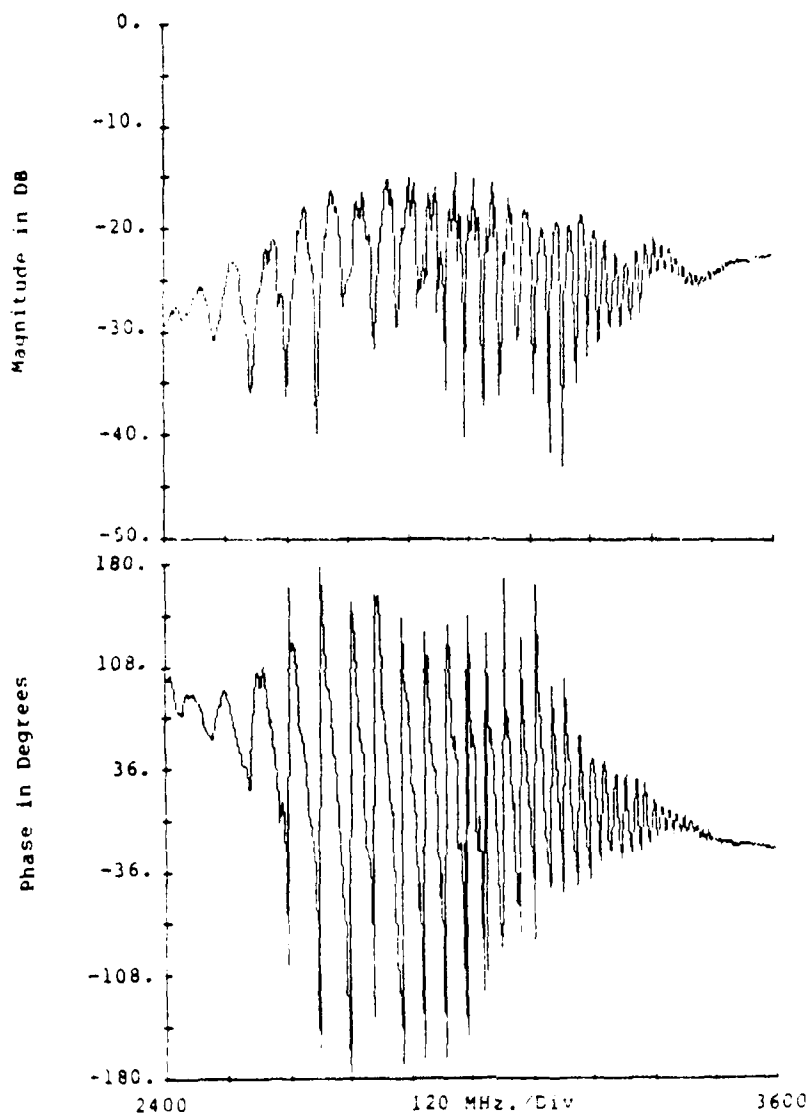
Figure 2.32: Measured S_{12} for 2-Bar 20 μm Transducer

55
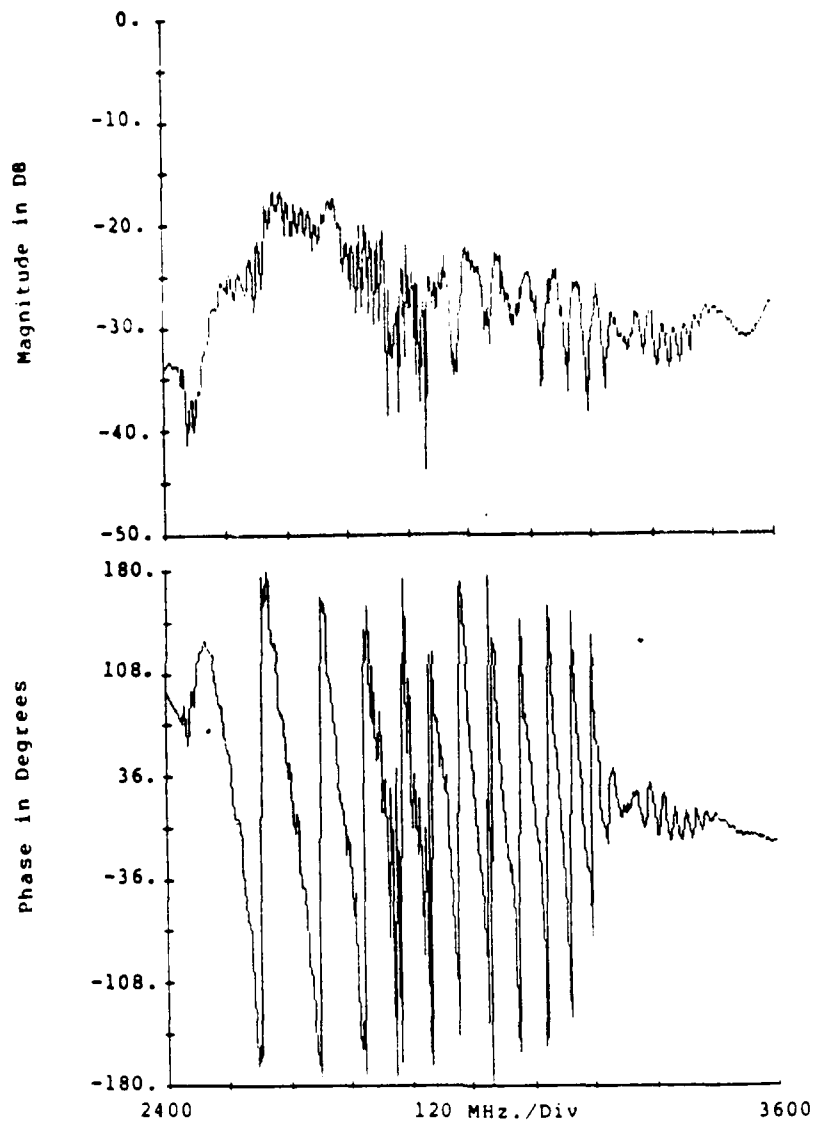
Figure 2.33: Measured S_{13} for 2-Bar 20 um Transducer

56
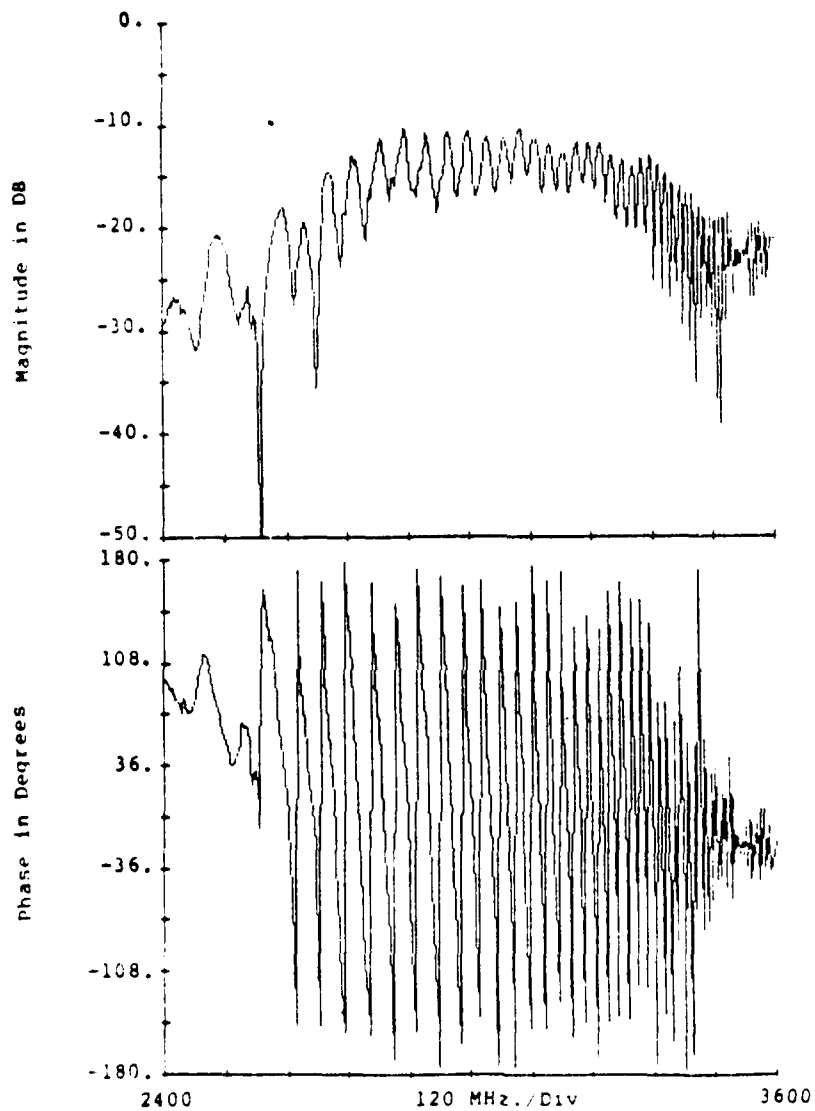
Figure 2.34: Measured S_{21} for 2-Bar 20 um Transducer

57
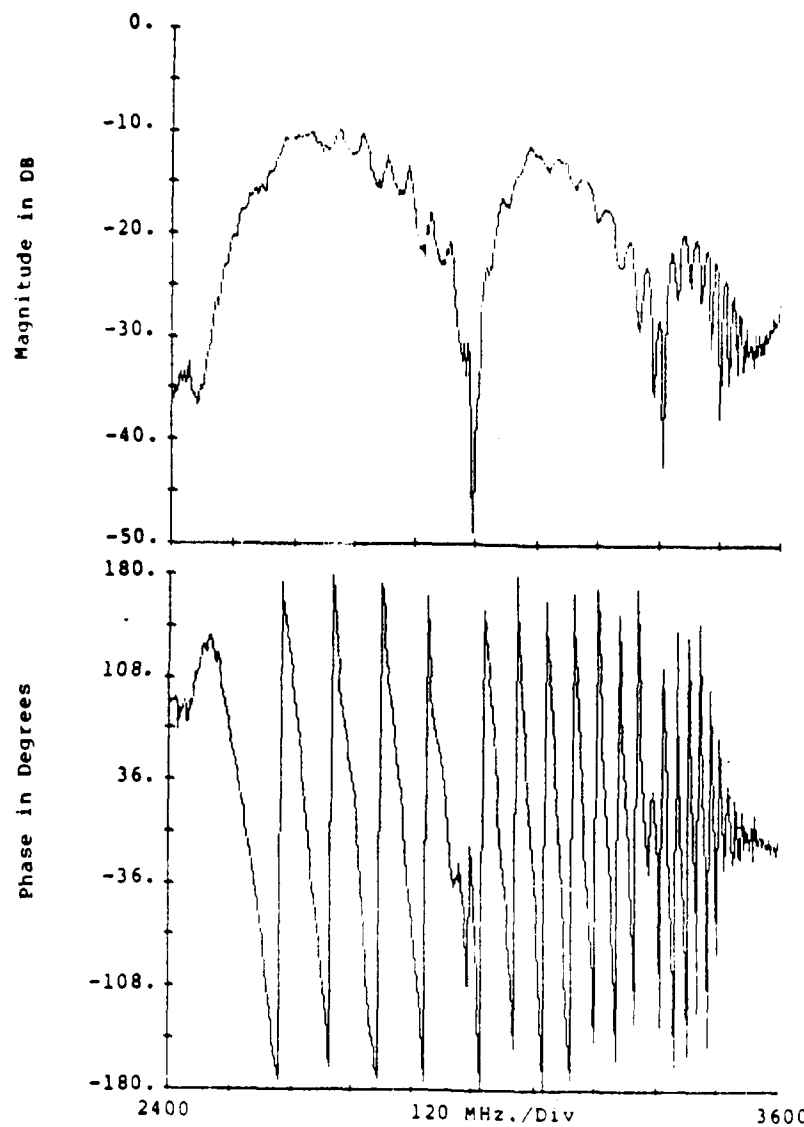
Figure 2.35: Measured S_{23} for 2-Bar 20 um Transducer
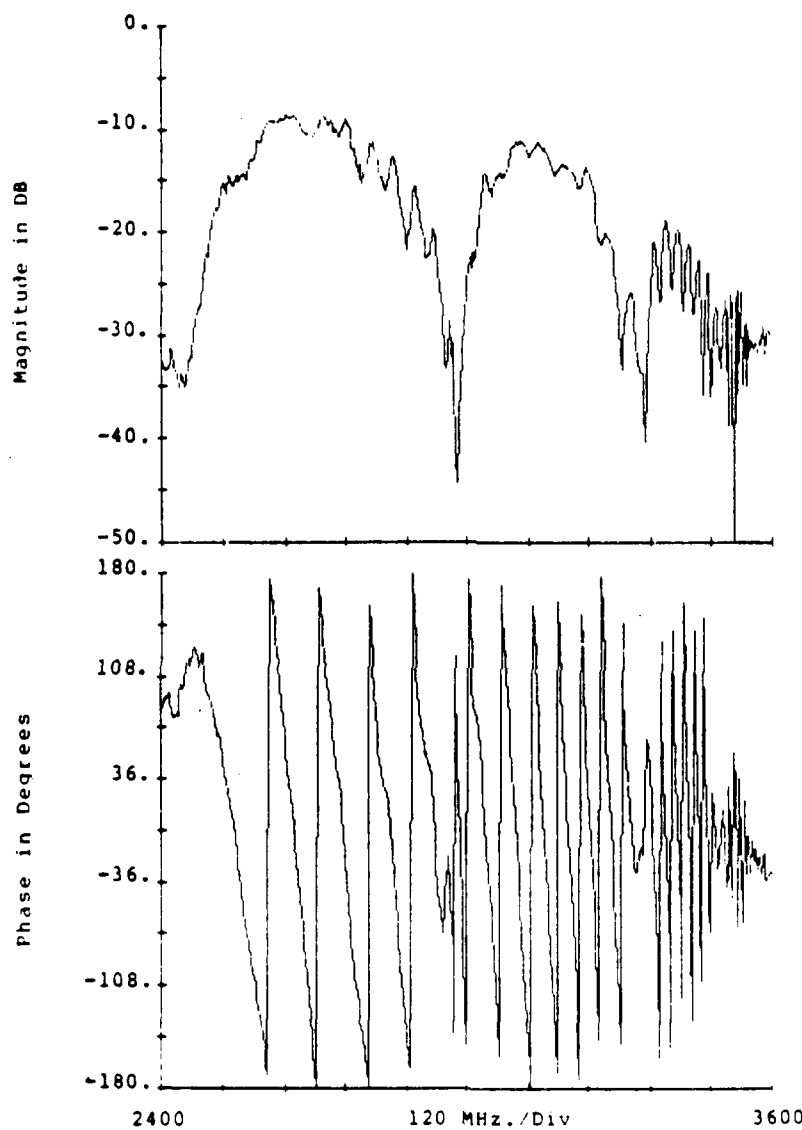
Figure 2.36: Measured S_{31} for 2-Bar 20 um Transducer

59
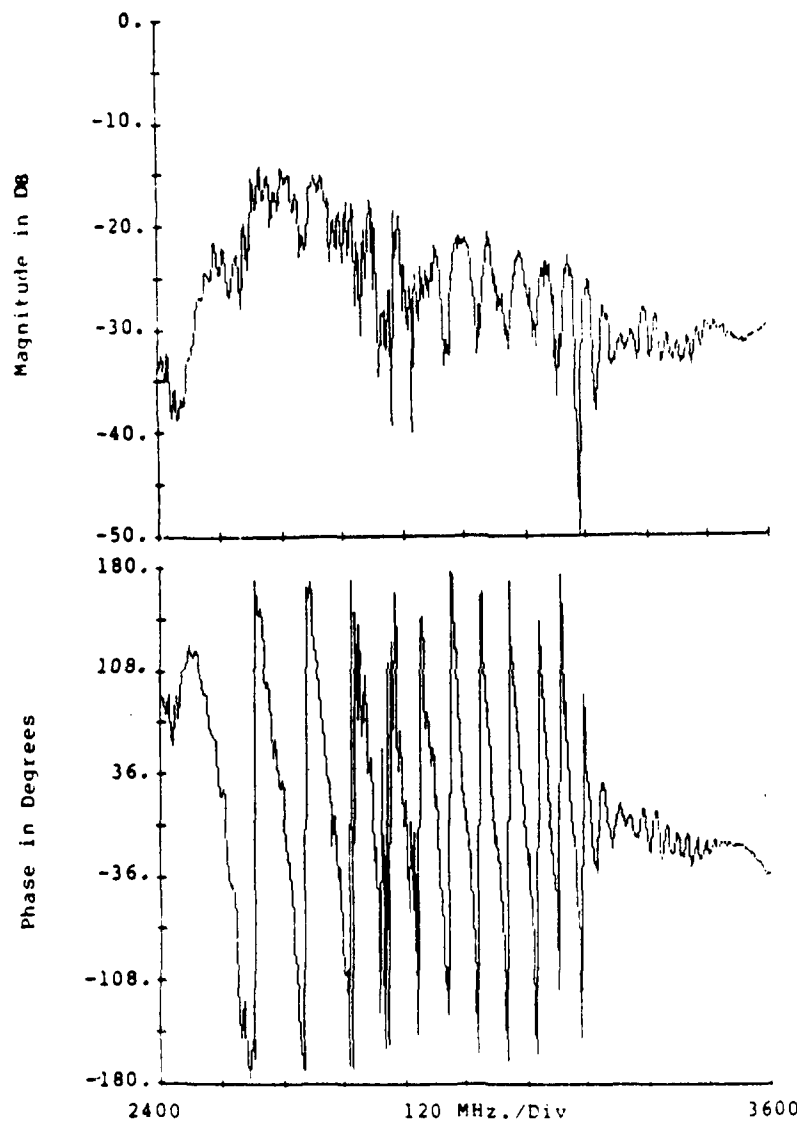
Figure 2.37: Measured S_{32} for 2-Ear 20 um Transducer

60
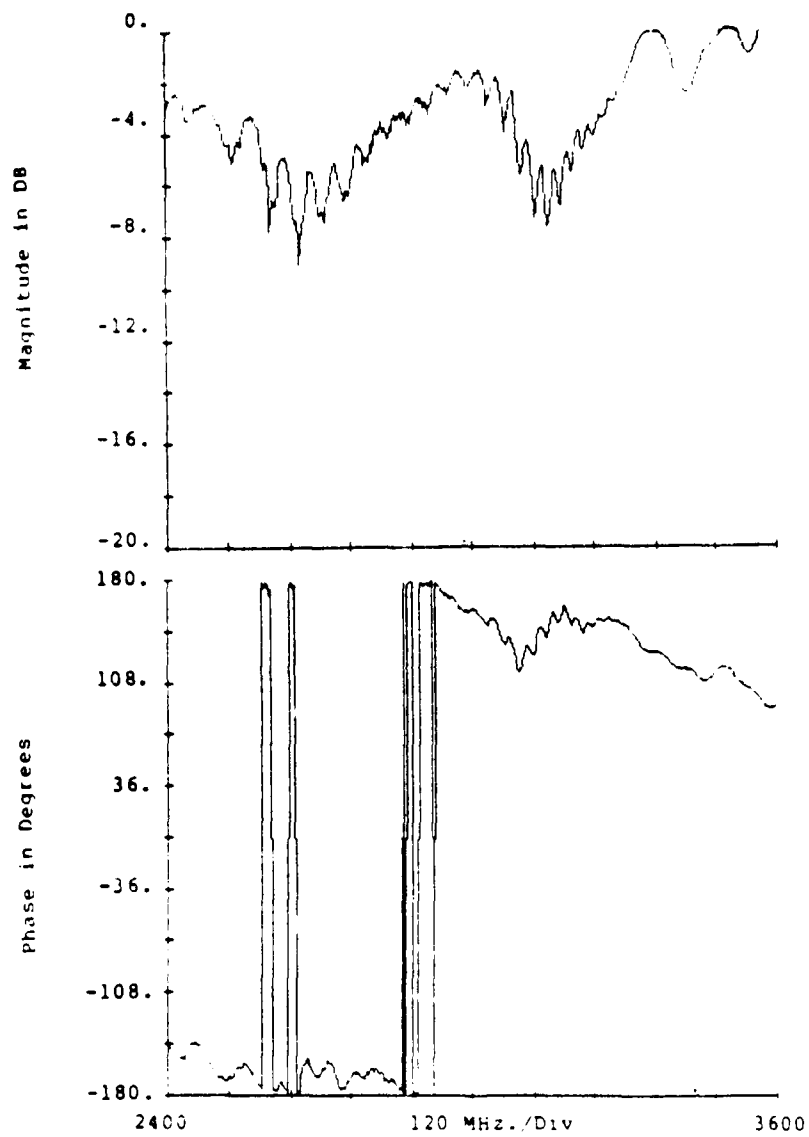
Figure 2.38: Measured S_{33} for 2-Bar 20 um Transducer

61
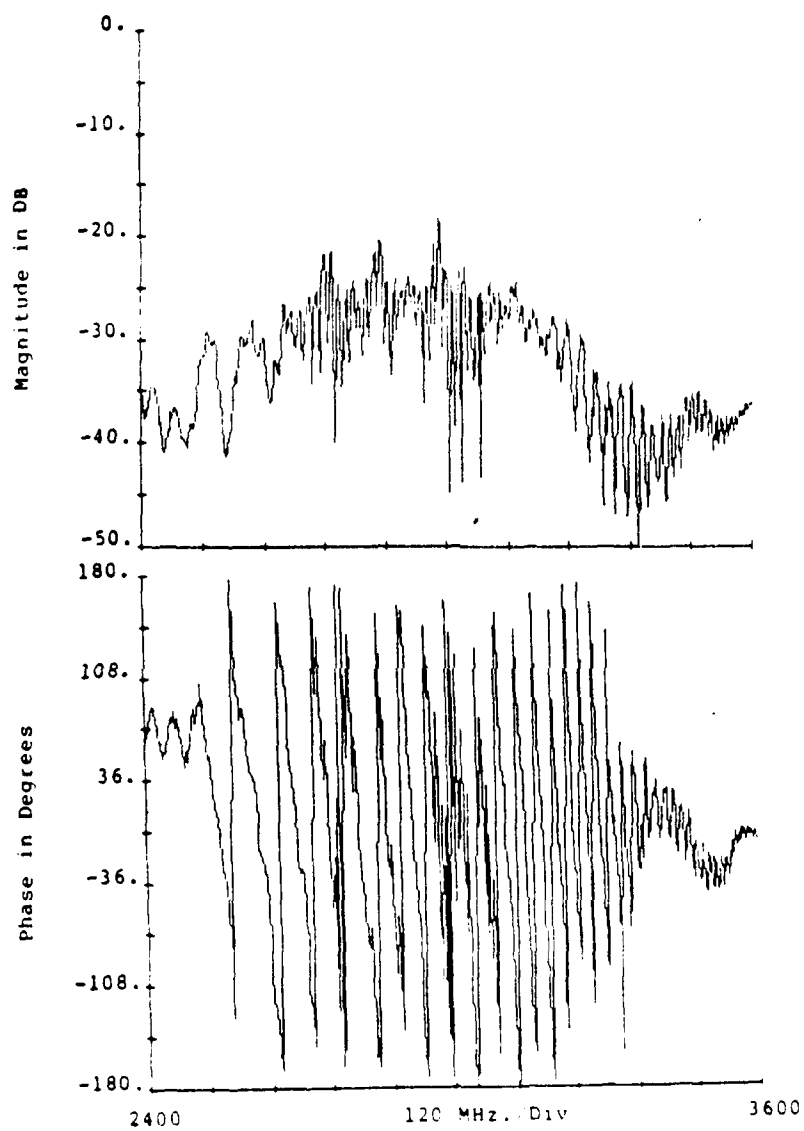
Figure 2.39: Measured S_{11} for 4-Bar 5 um Transducer
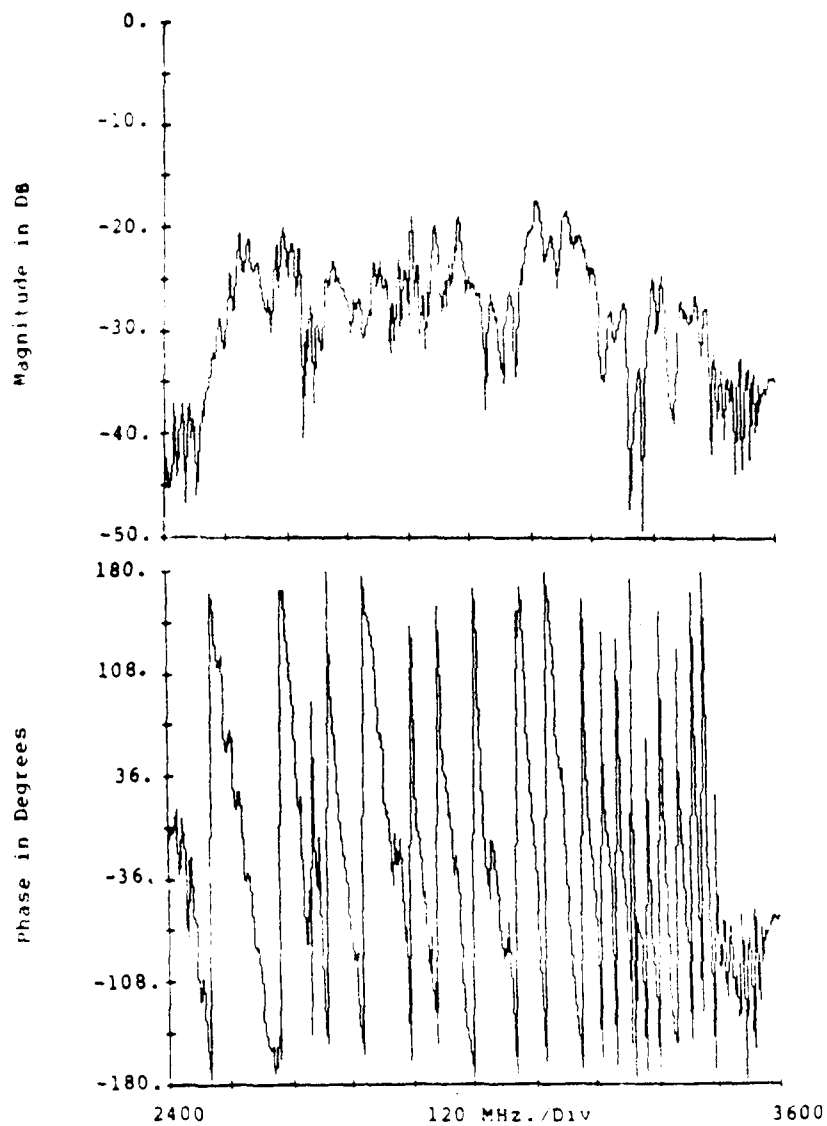
Figure 2.40: Measured S_{13} for 4-Bar 5 μm Transducer
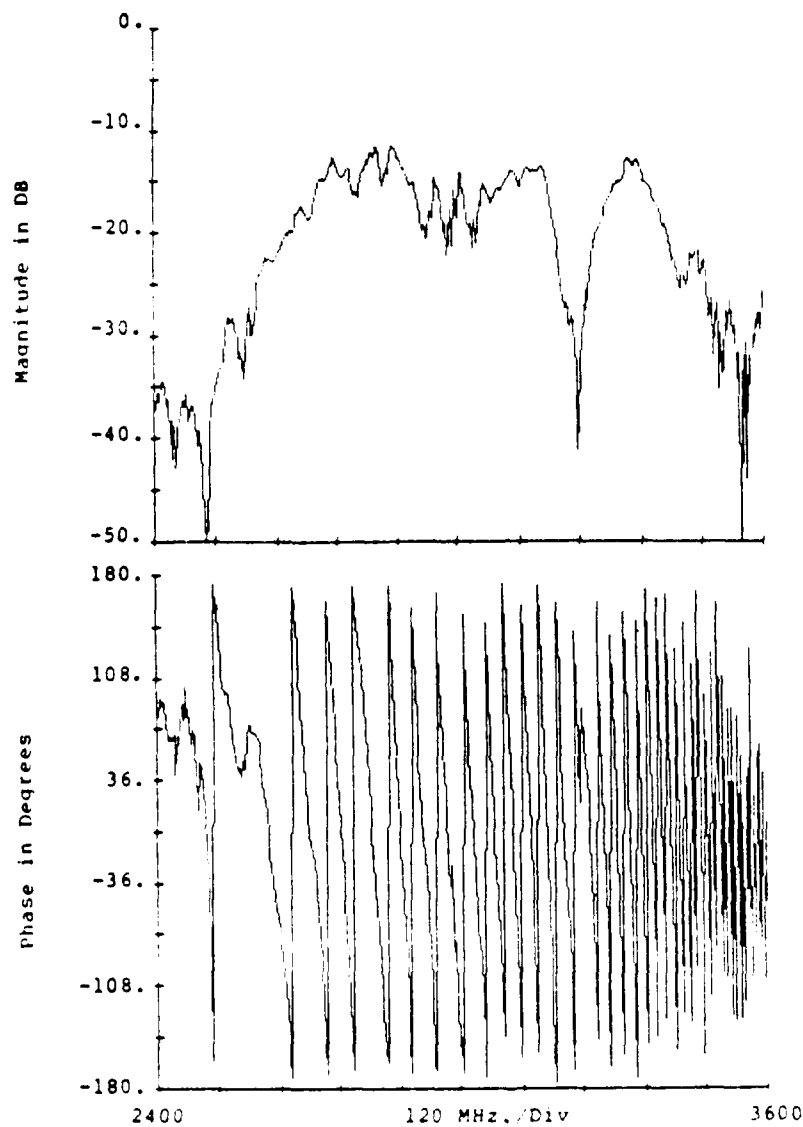
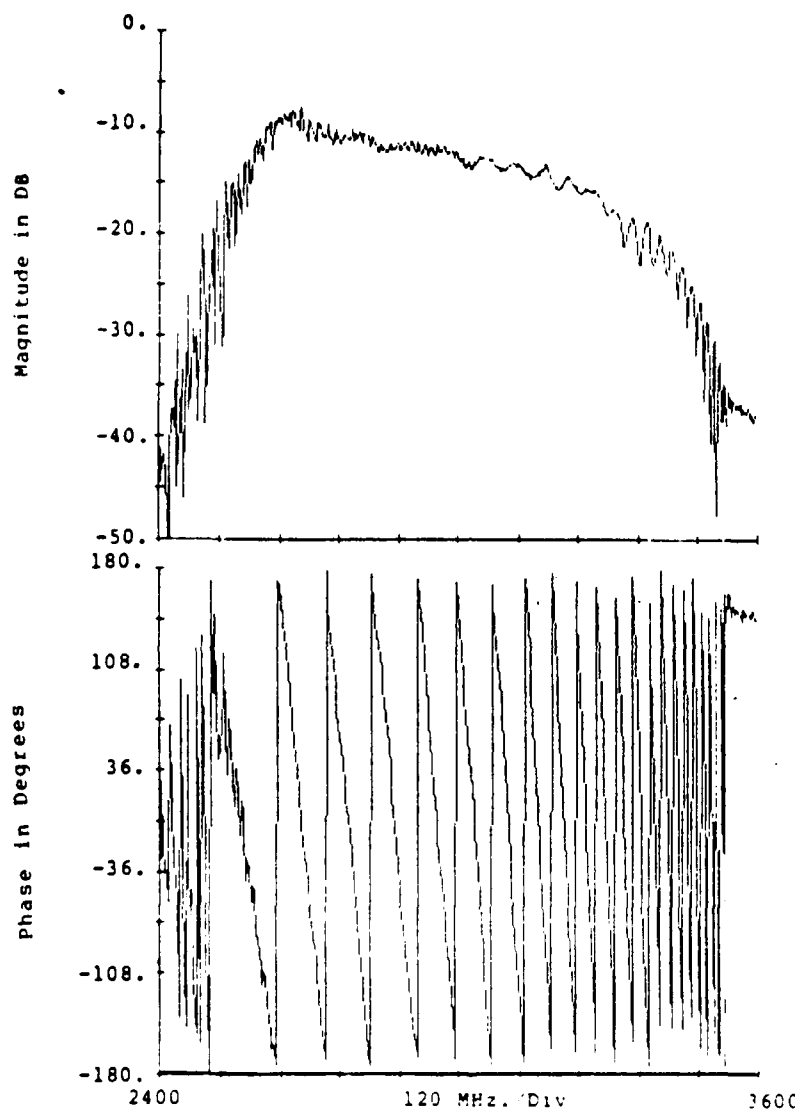Figure 2.41: Measured S_{21} for 4-Bar 5 um Transducer
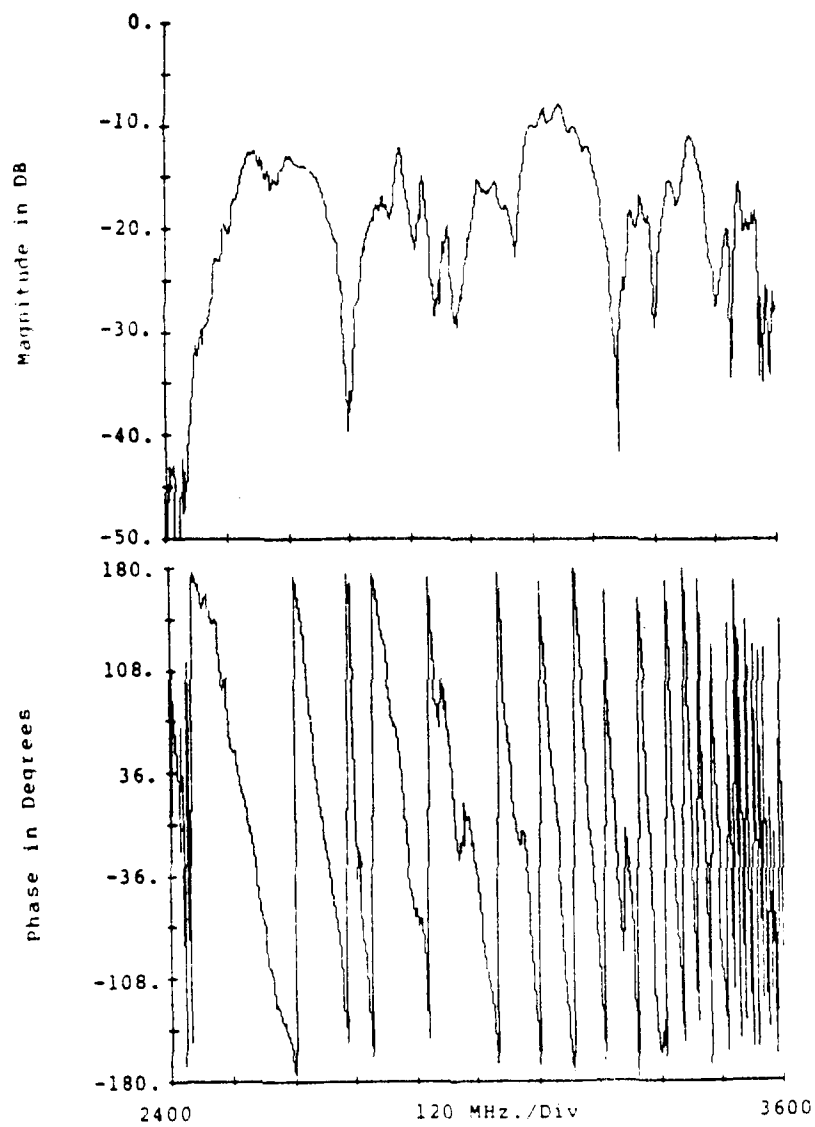
Figure 2.42: Measured S_{23} for 4-Bar 5 um Transducer
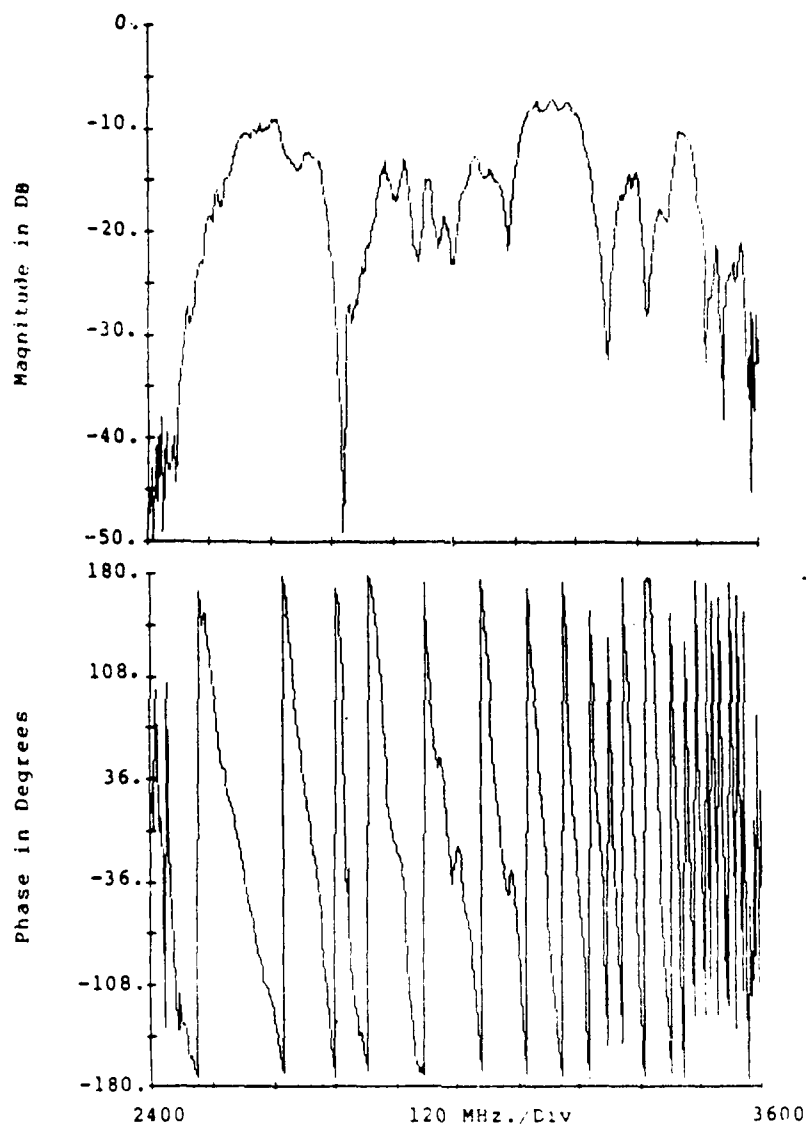
Figure 2.43: Measured S_{31} for 4-Bar 5 um Transducer
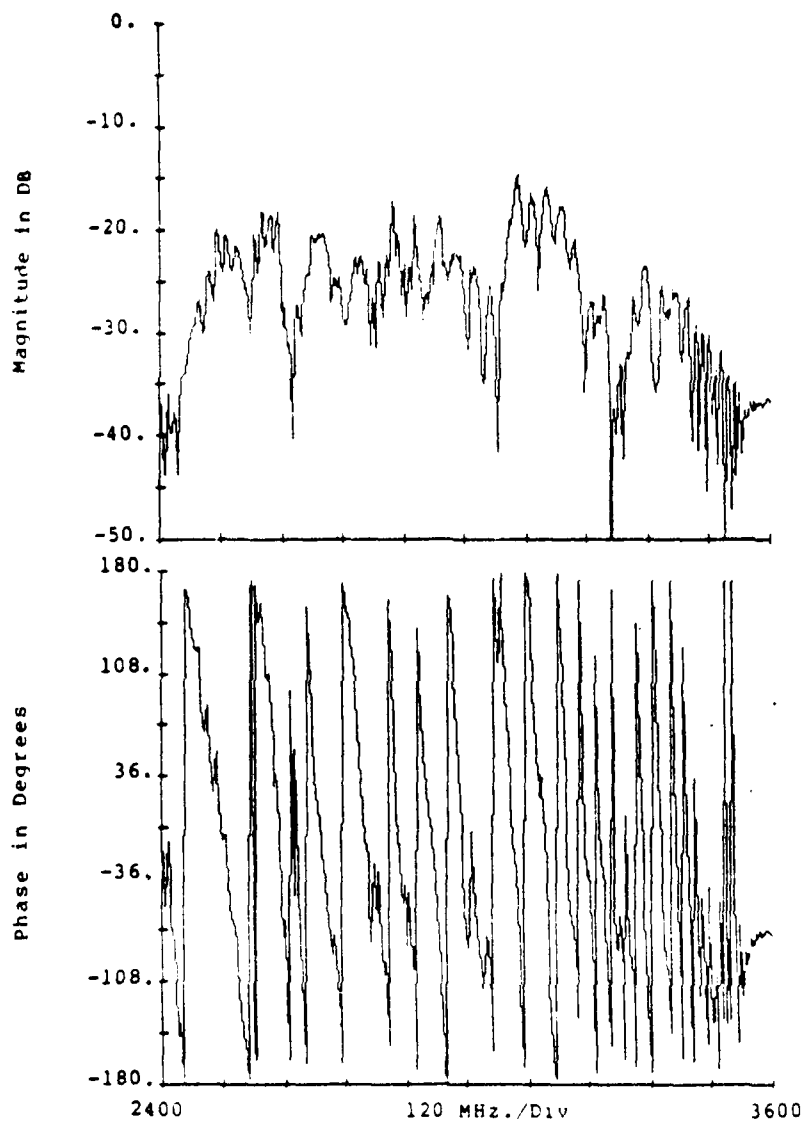
Figure 2.44: Measured S_{32} for 4-Bar 5 um Transducer

67

Magnitude in DB

Phase in Degrees

2400 120 MHz./Div 3600
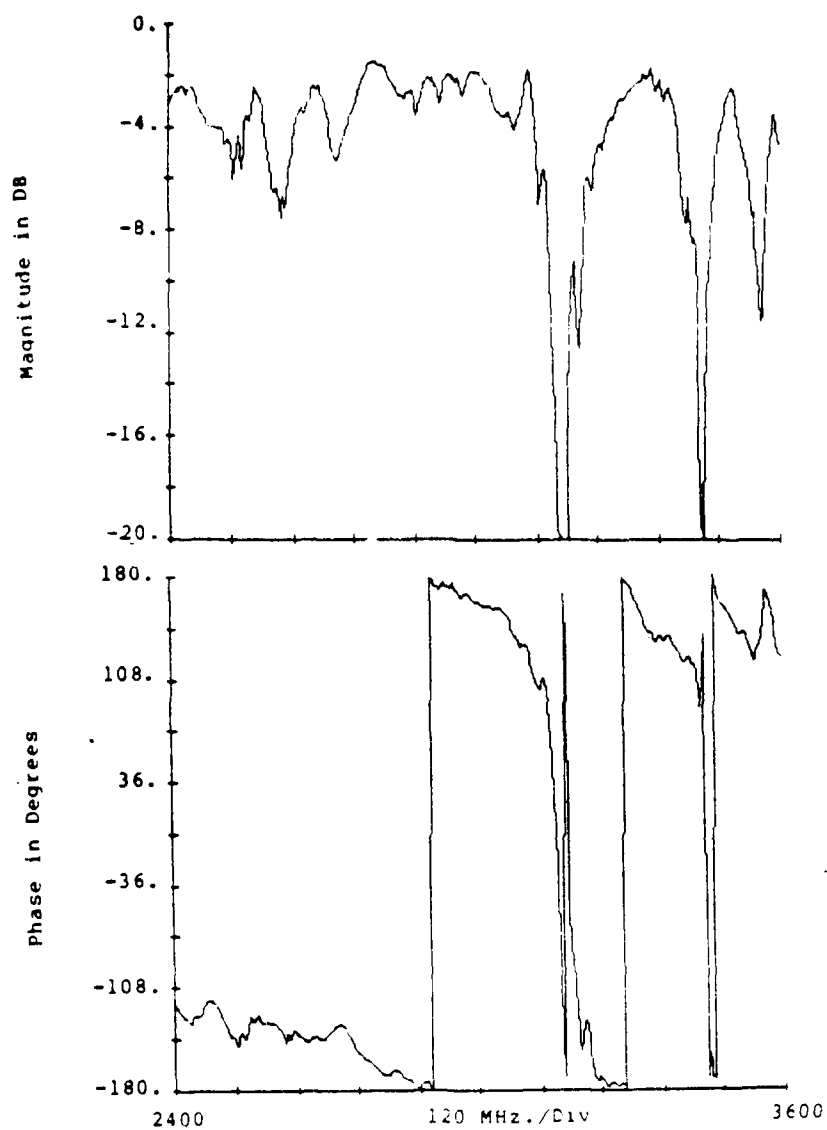
Figure 2.45: Measured S_{11} for 4-Ear 5 um Transducer

68
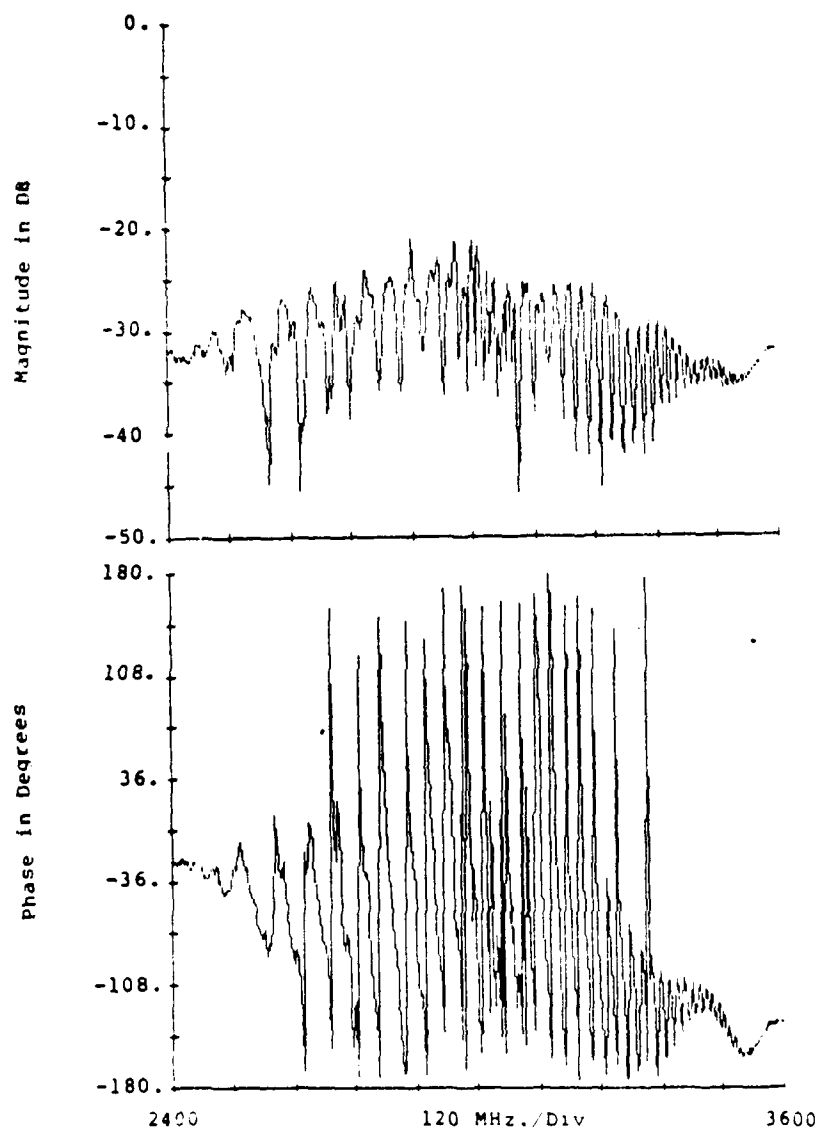
Figure 2.46: Measured S_{12} for 8-Bar 20 um Transducer
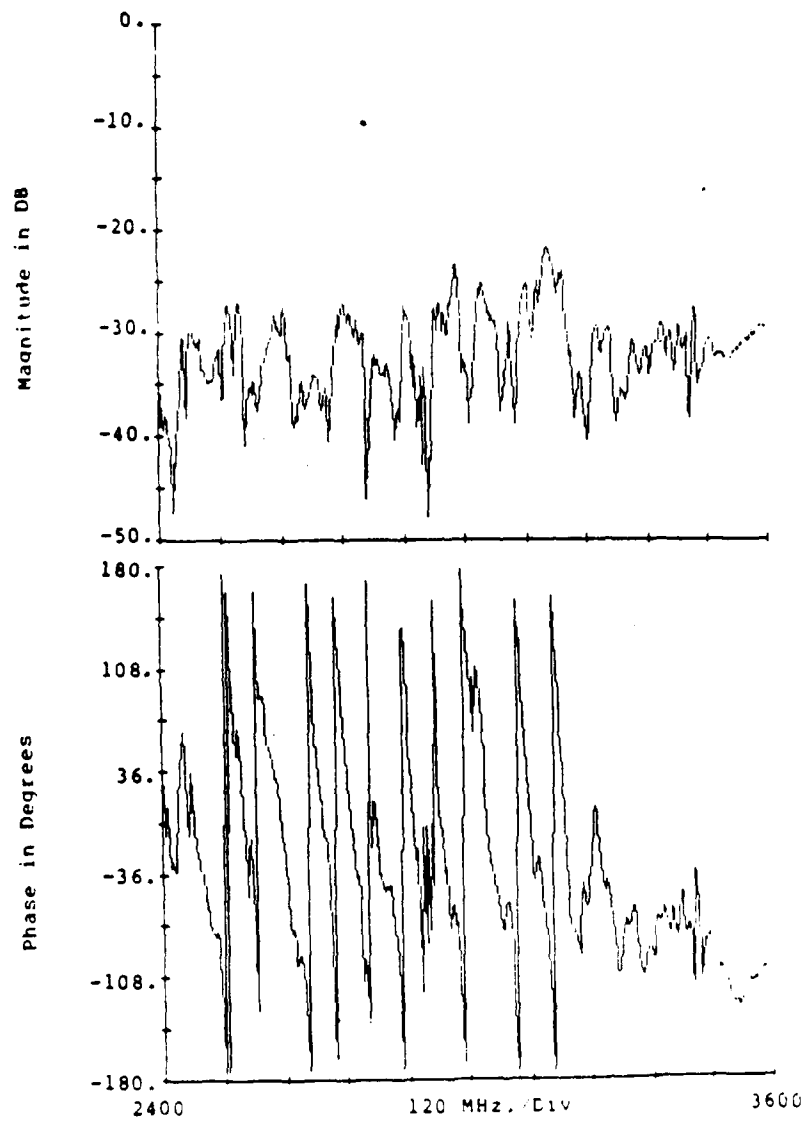
Figure 2.47: Measured S_{13} for 8-Bar 20 um Transducer

70
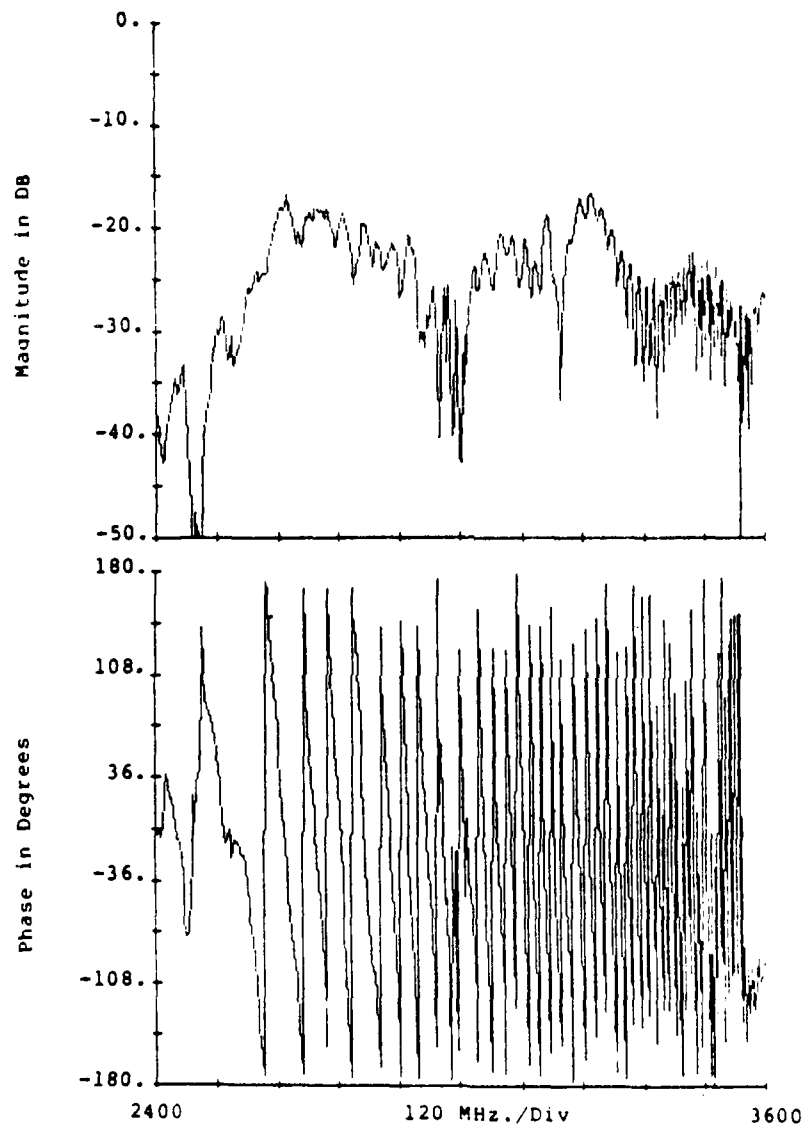
Figure 2.48: Measured S_{21} for E-Bar 20 um Transducer

71
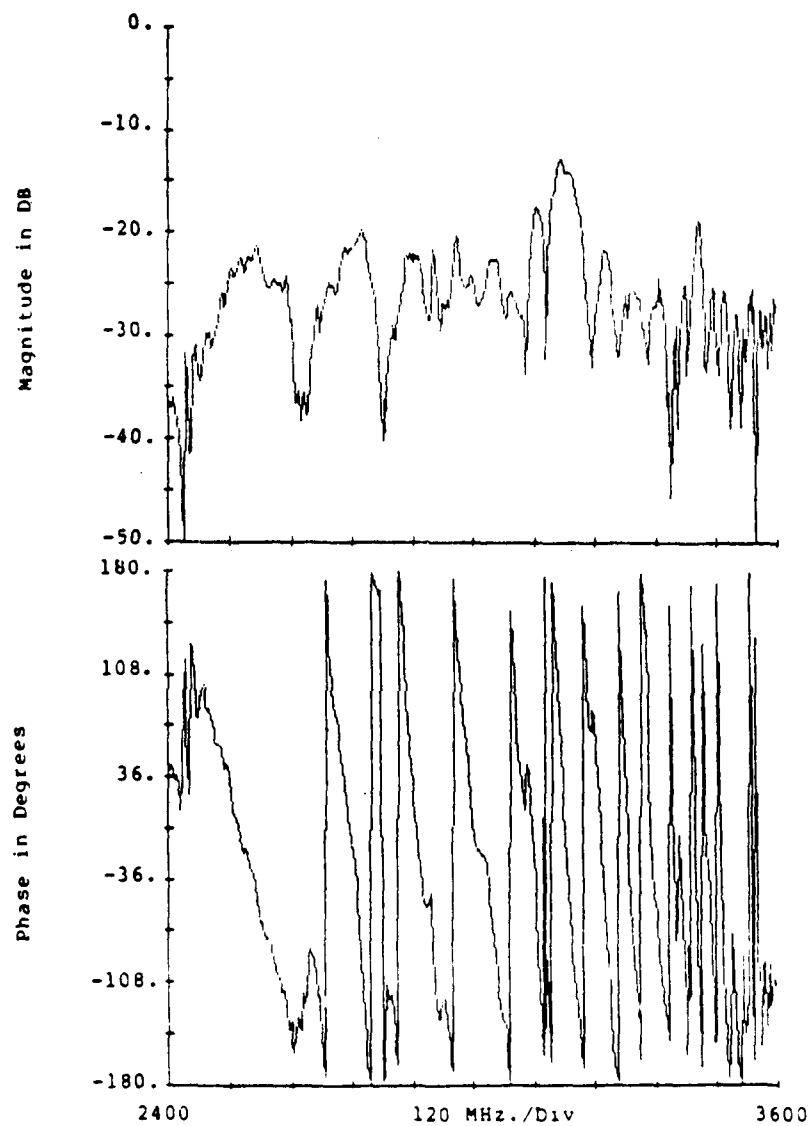
Figure 2.49: Measured S_{23} for 8-Bar 20 um Transducer
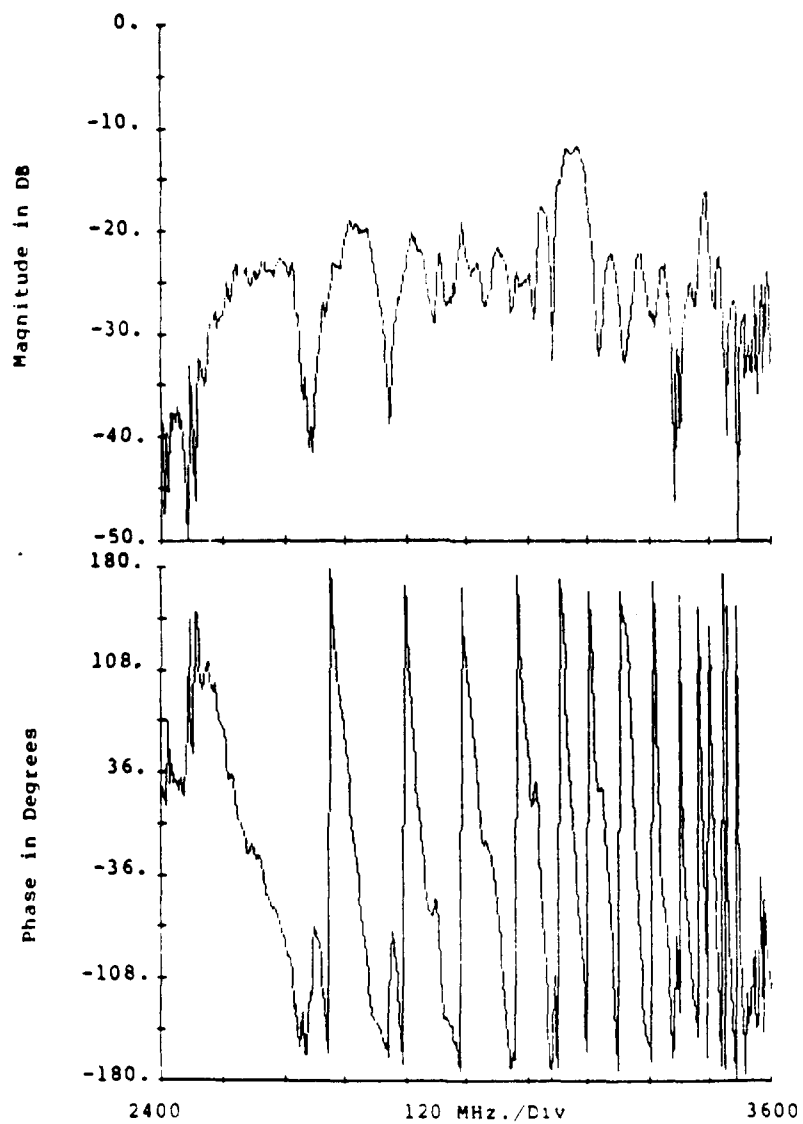
Figure 2.50: Measured S_{31} for 8-Bar 20 um Transducer

73
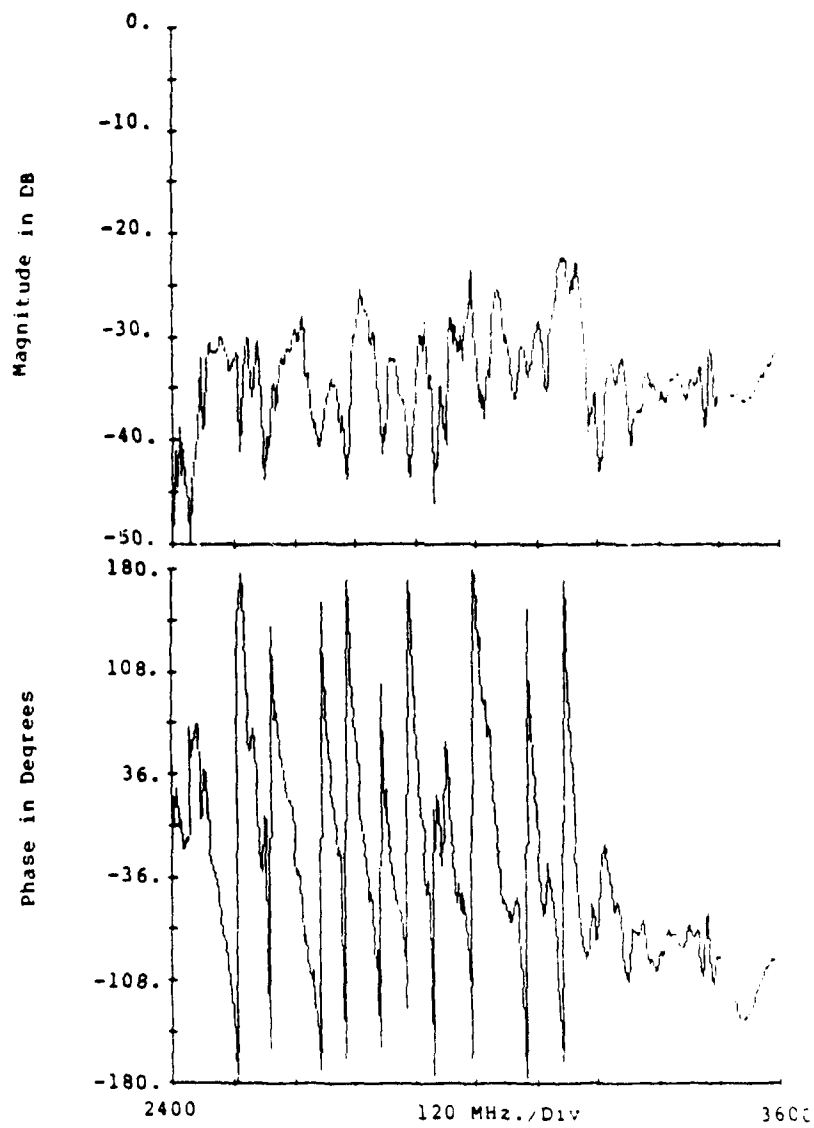
Figure 2.51: Measured S_{32} for 8-Bar 20 μm Transducer

Magnitude in DB

Phase in Degrees

0.

-4.

-8.

-12.

-16.

-20.

180.

108.

36.

-36.

-108.

-180.

2400   120 MHz./Div   3600
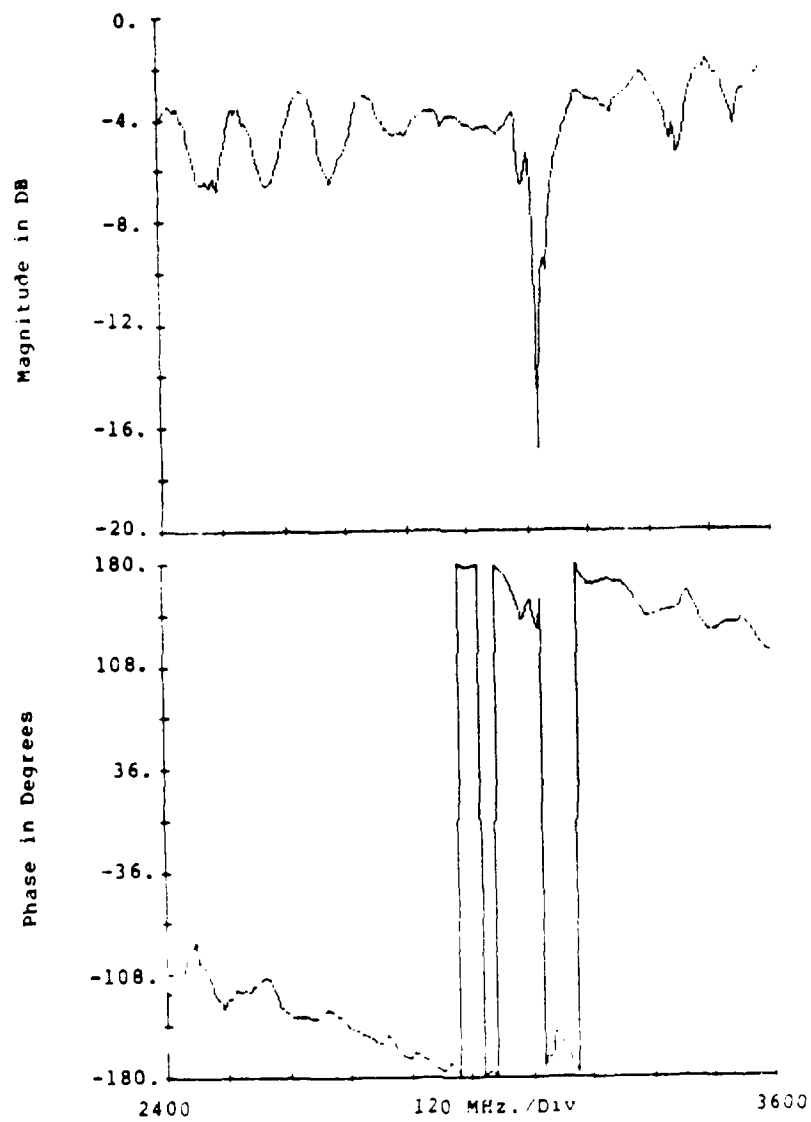
Figure 2.52: Measured S_{33} for 8-Bar 20 um Transducer
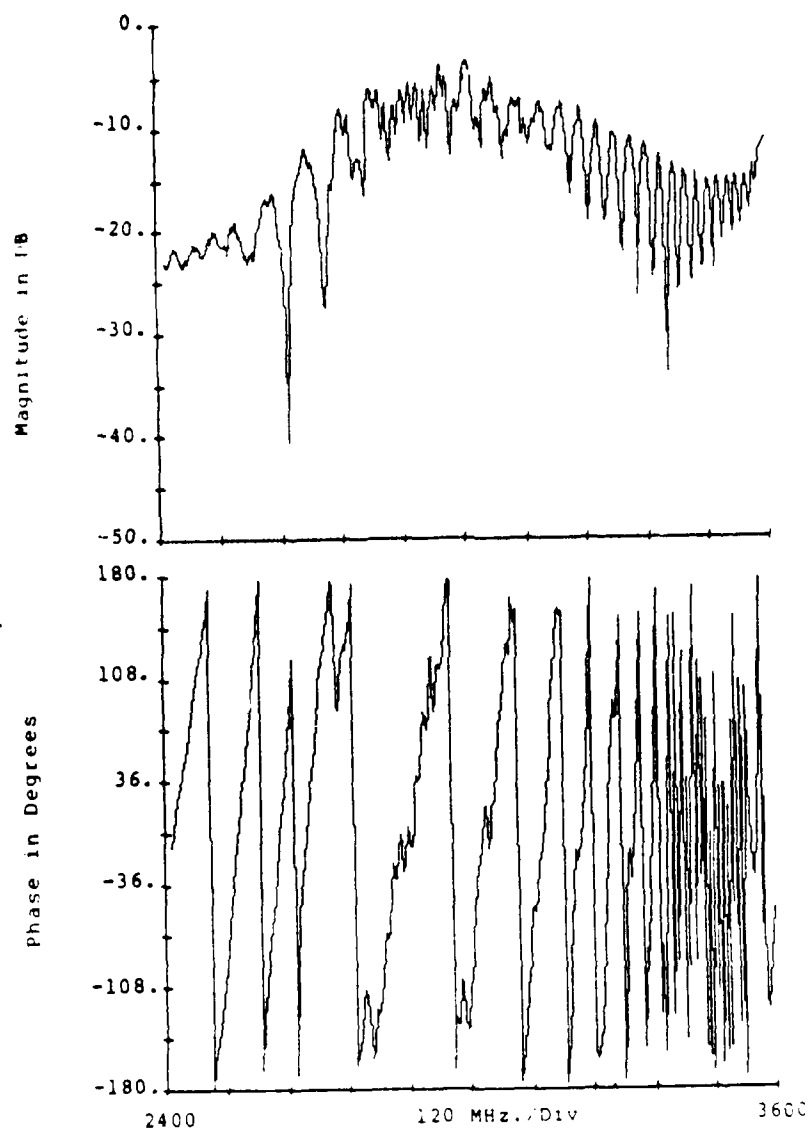
Figure 2.53: Corrected S_{11} for 1-Bar 50 μm Transducer
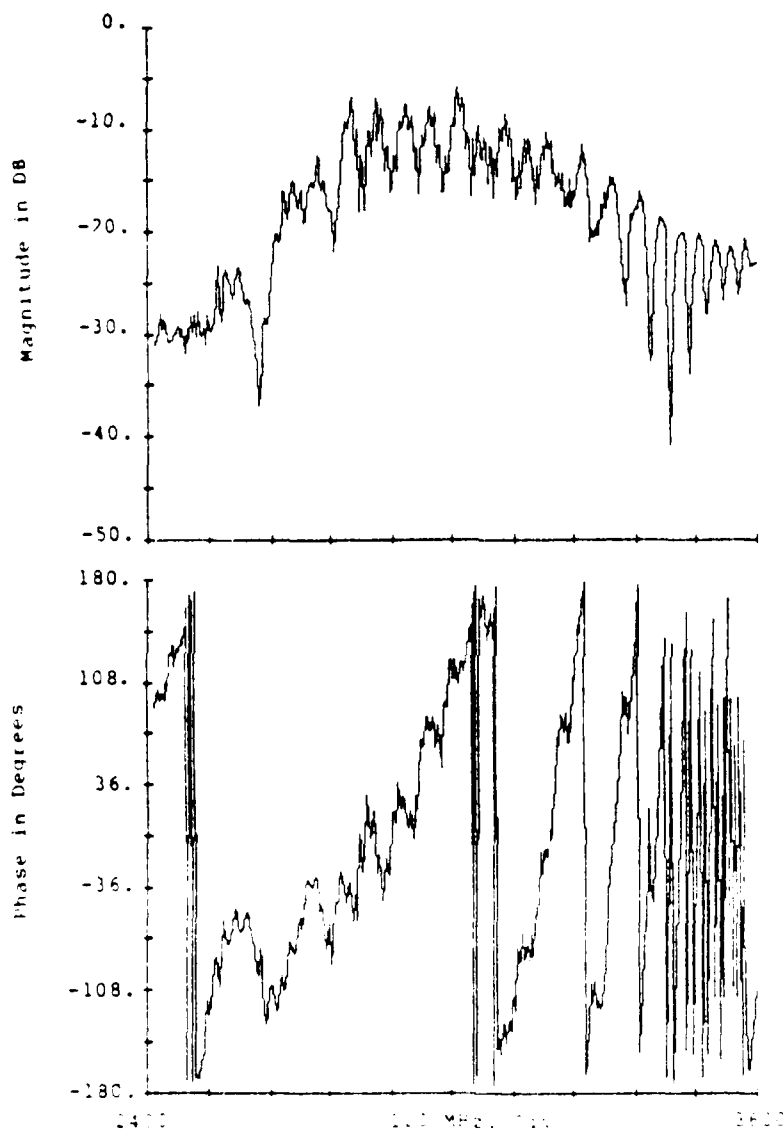
Figure 2.54: Corrected System Impulse Response Characteristics
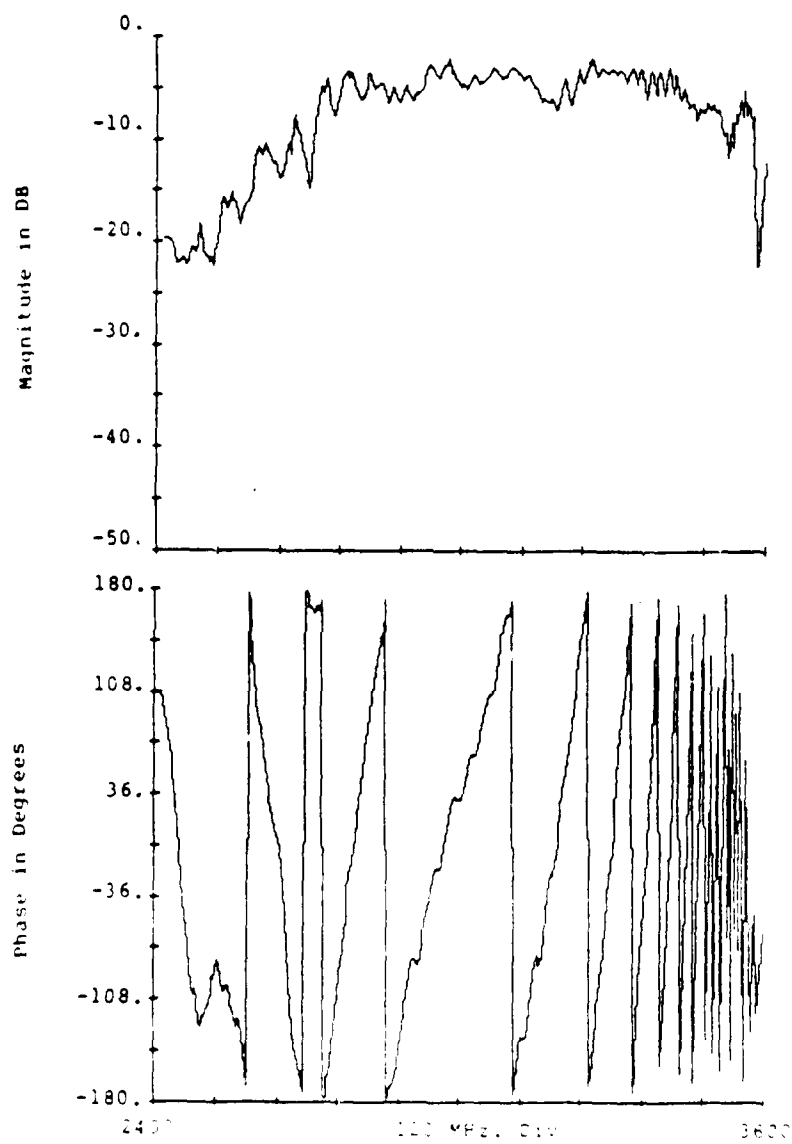
Figure 2.56: Corrected S_{11} for I-Bar 50 µm Transducer
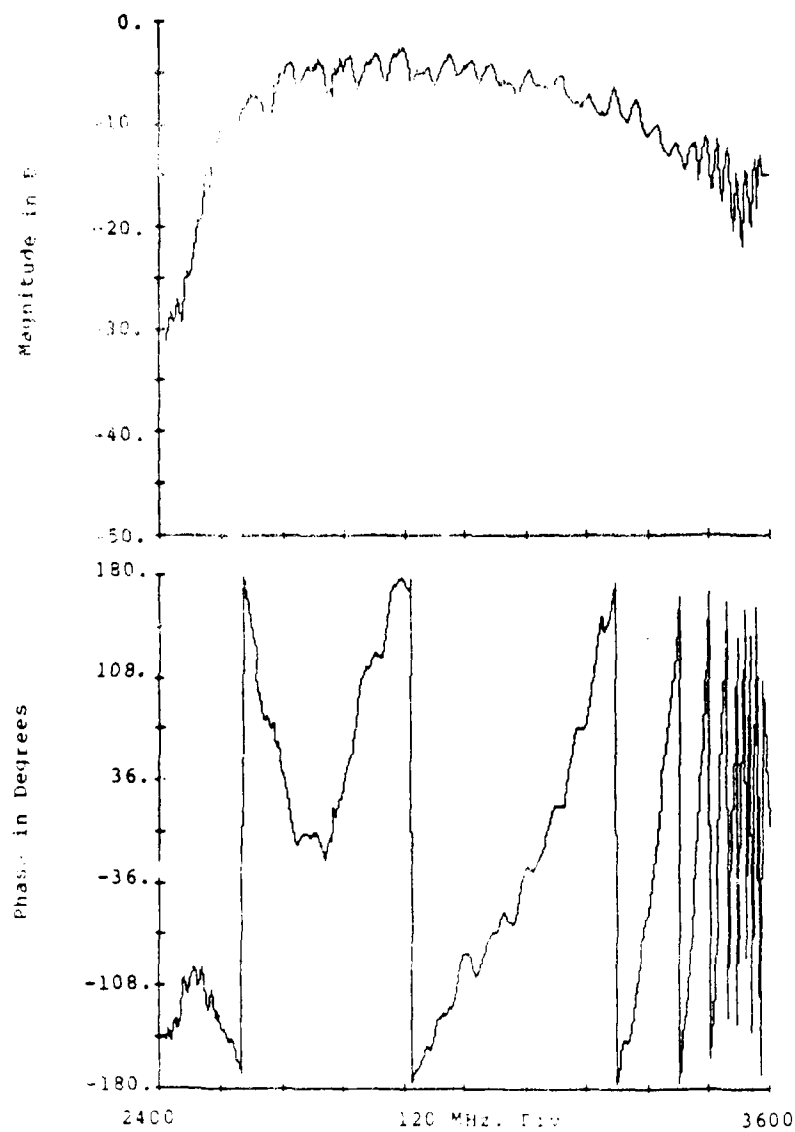
Figure 2.56: Corrected S_{23} for 1-Bar 50 um Transducer

Figure 2:57: Corrected S_{11} for 1-Bar 50 um Transducer
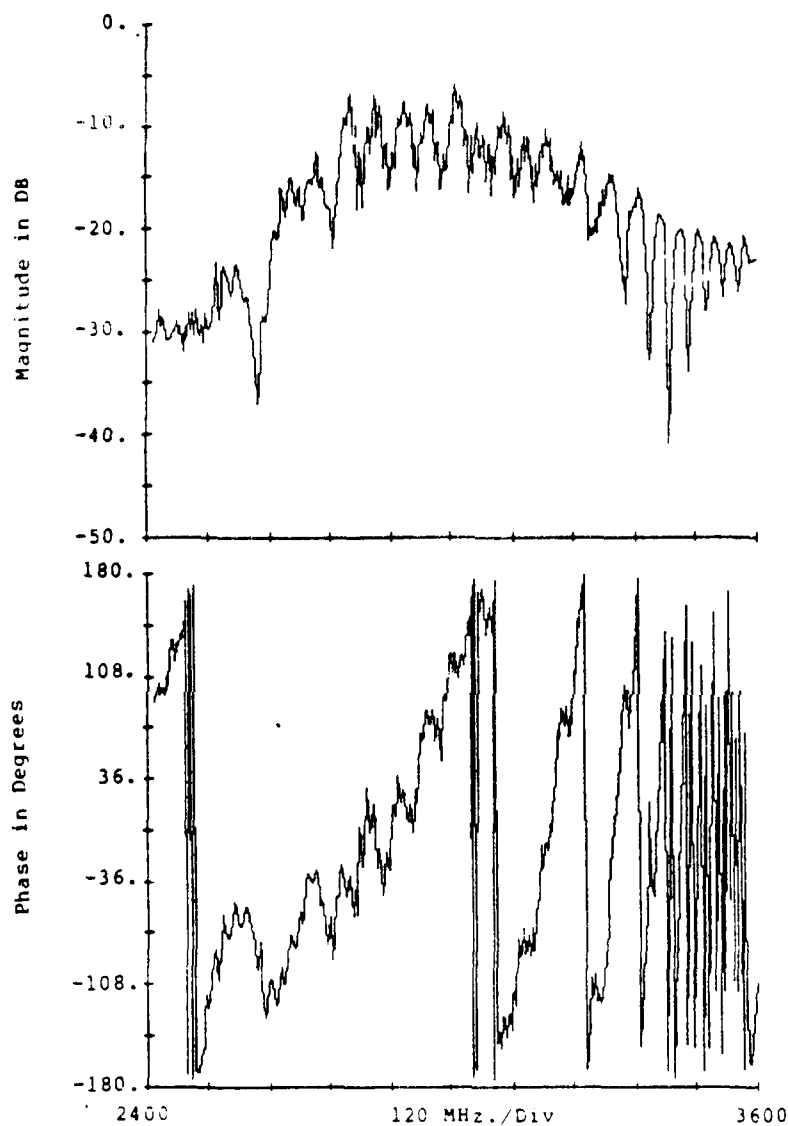
Figure 2.58: Corrected S_{22} for 1-Bar 50 um Transducer
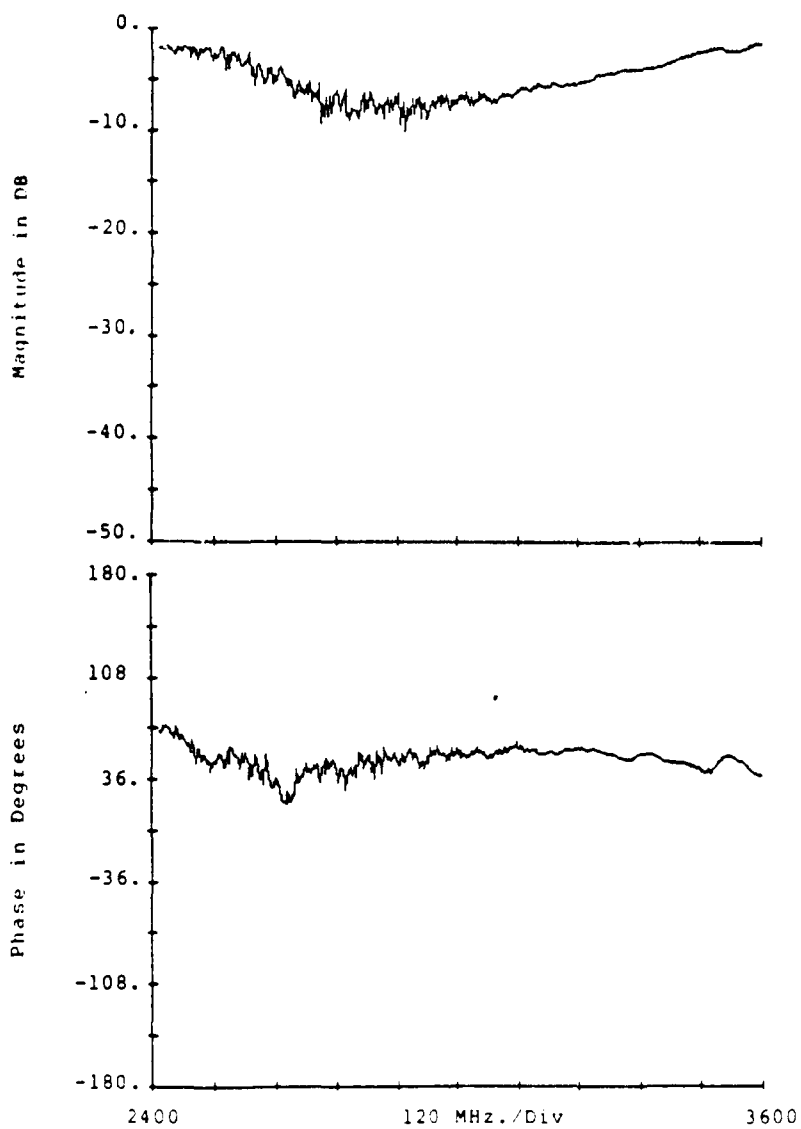
Figure 2.59: Corrected S_{33} for 1-Bar 50 um Transducer

82
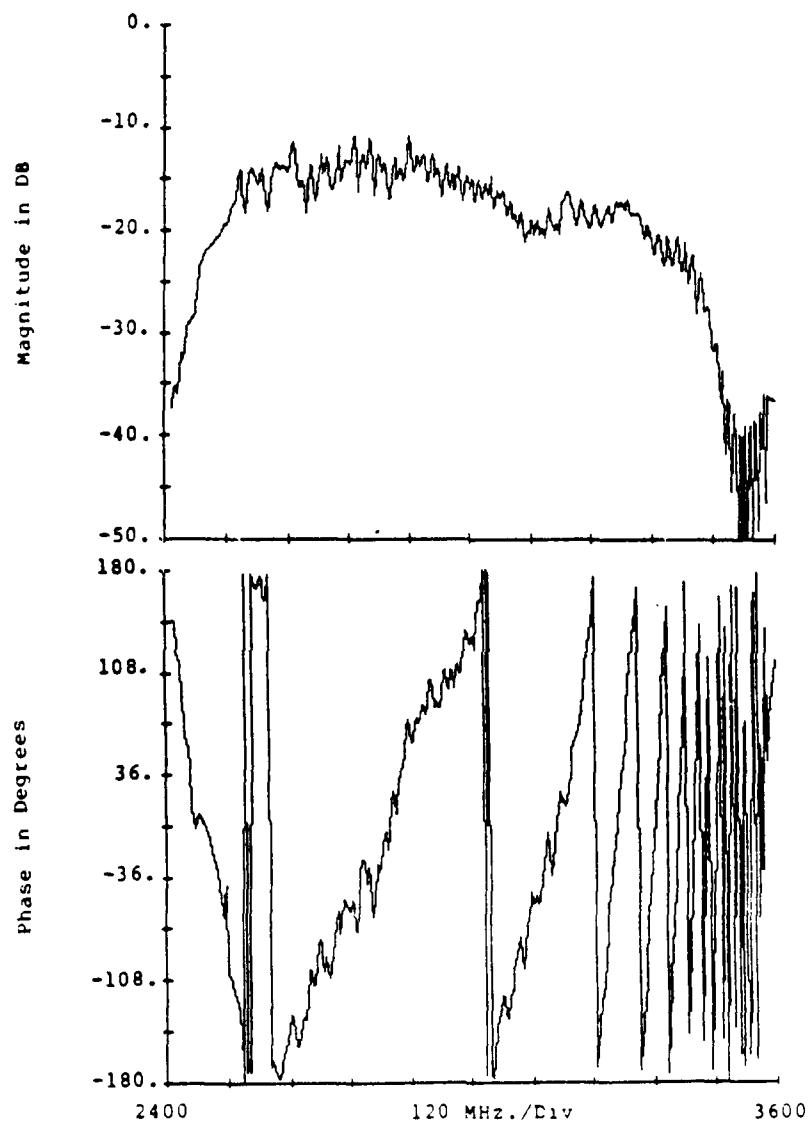
Figure 2.60   Corrected S_{11} for 1-Bar 10 um Transducer
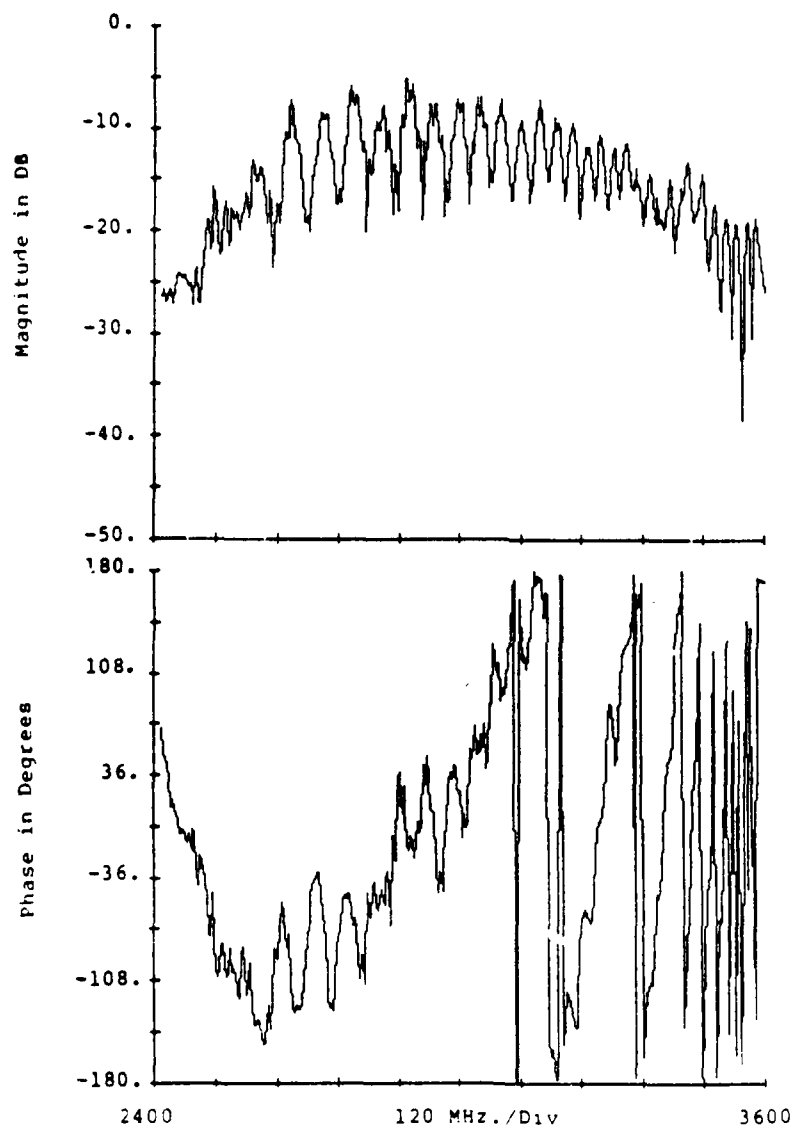
Figure 2.61: Corrected S_{13} for 1-Bar 10 um Transducer

84
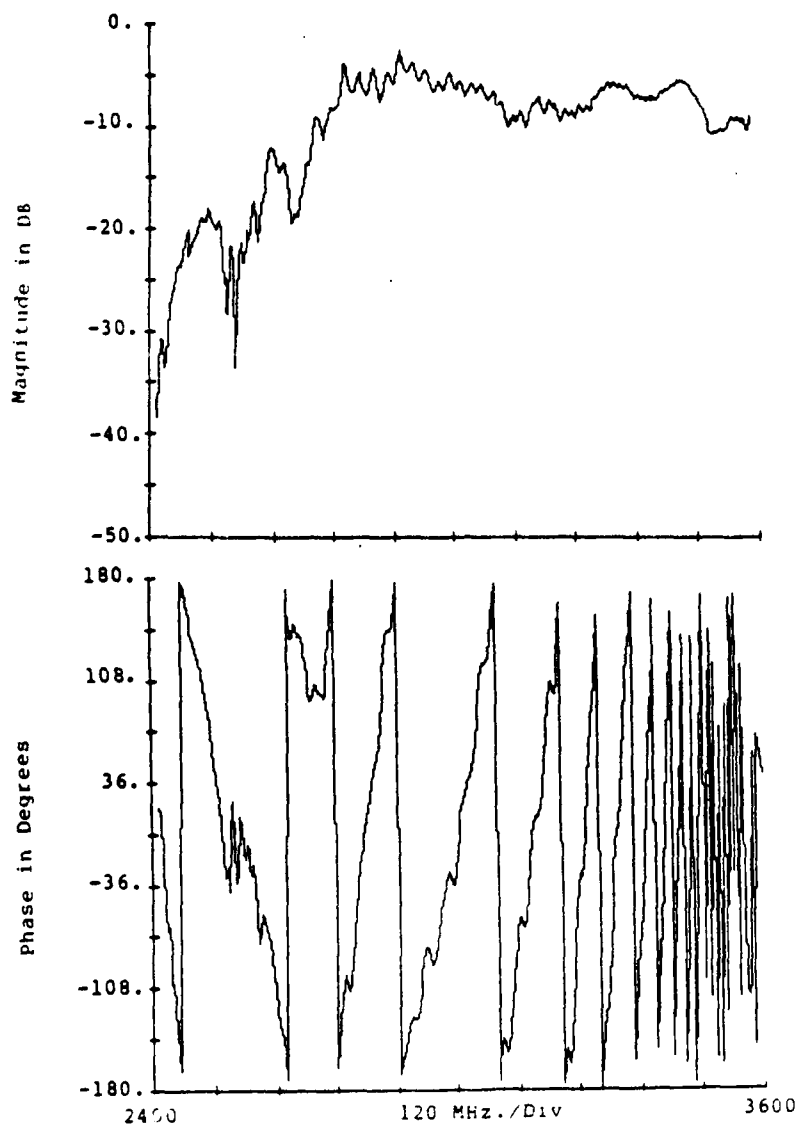
Figure 2.62: Corrected S_{21} for 1-Bar 10 um Transducer

85
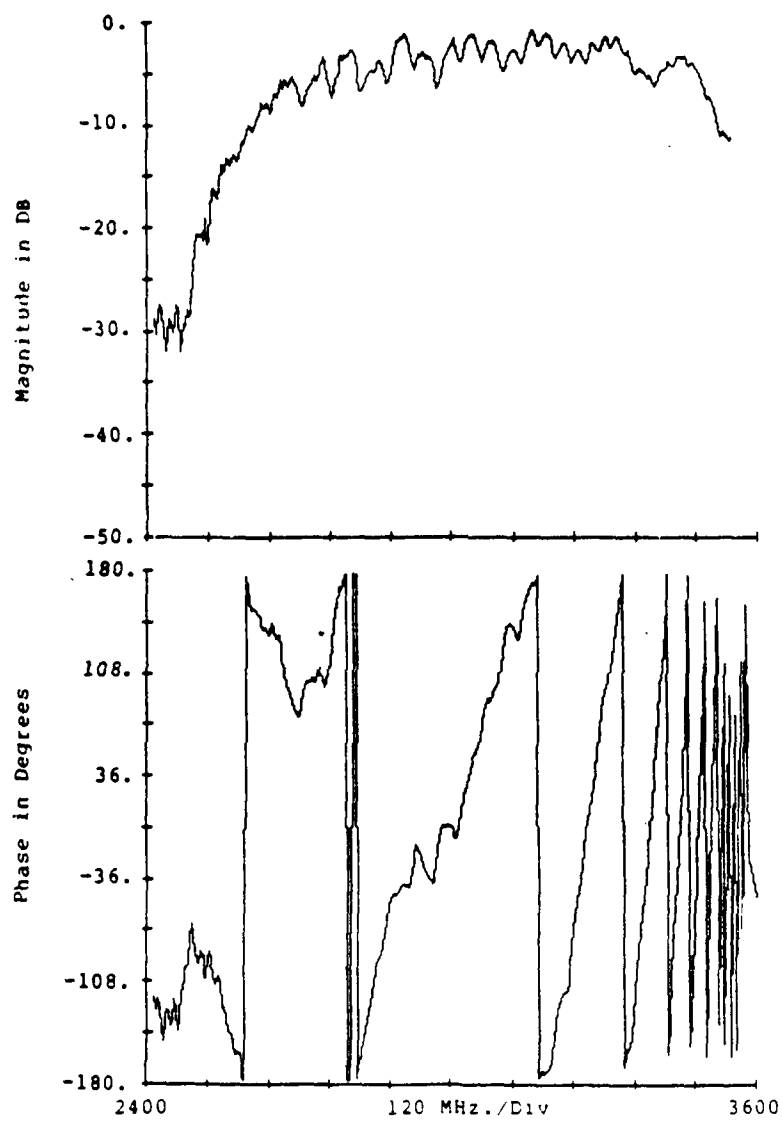
Figure 2.63 Corrected S_{23} for 1-Bar 10 ur Transducer

86
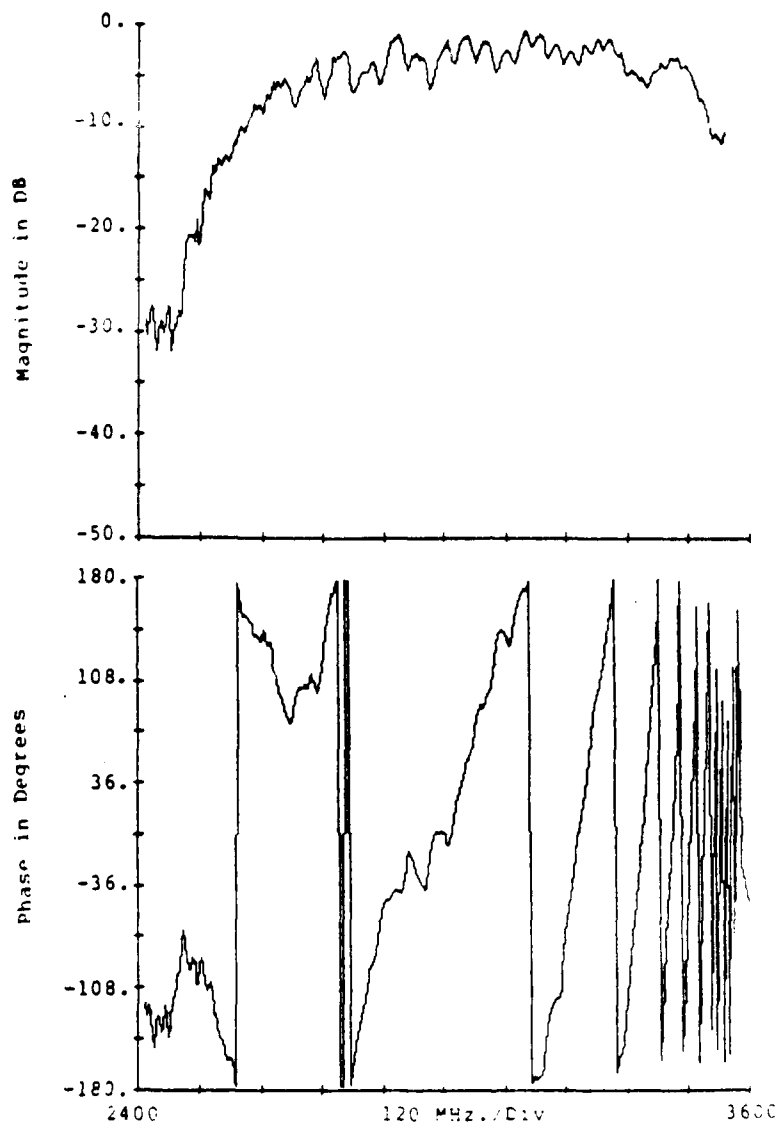
Figure 2.64: Corrected S_{31} for 1-Bar 10 um Transducer

87
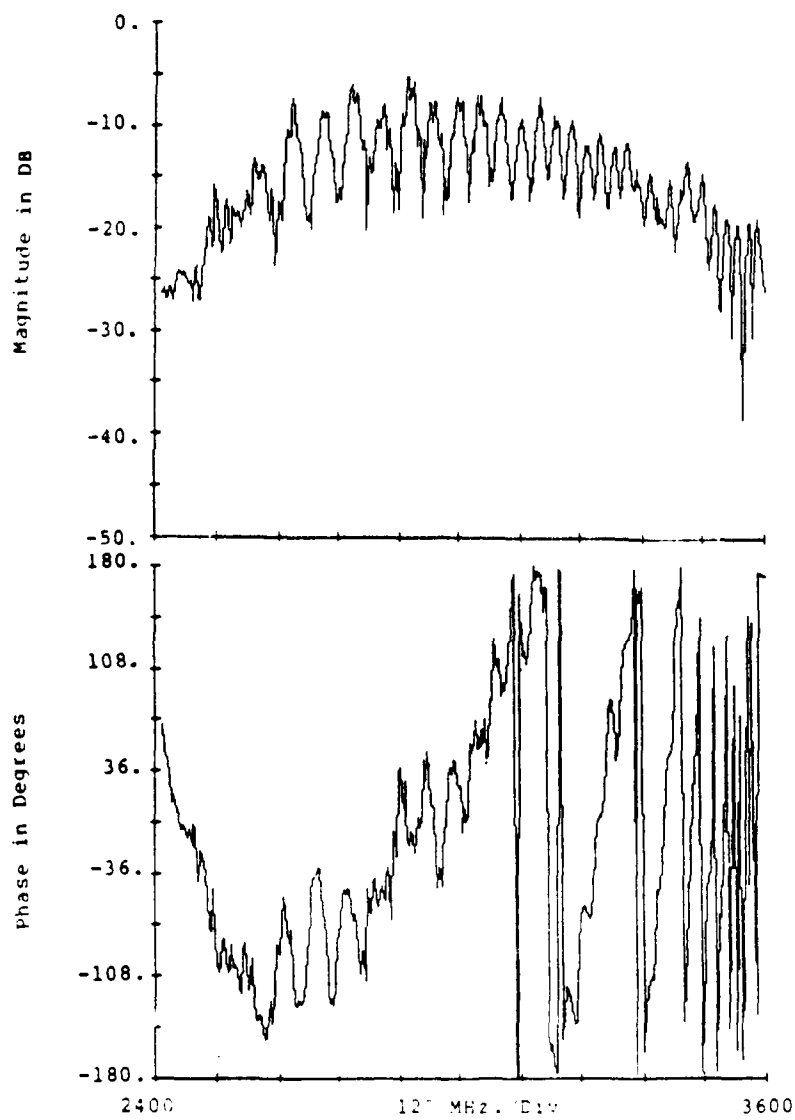
Figure 2.65: Corrected S_{11} for X-Bar 1 um Transducer

88
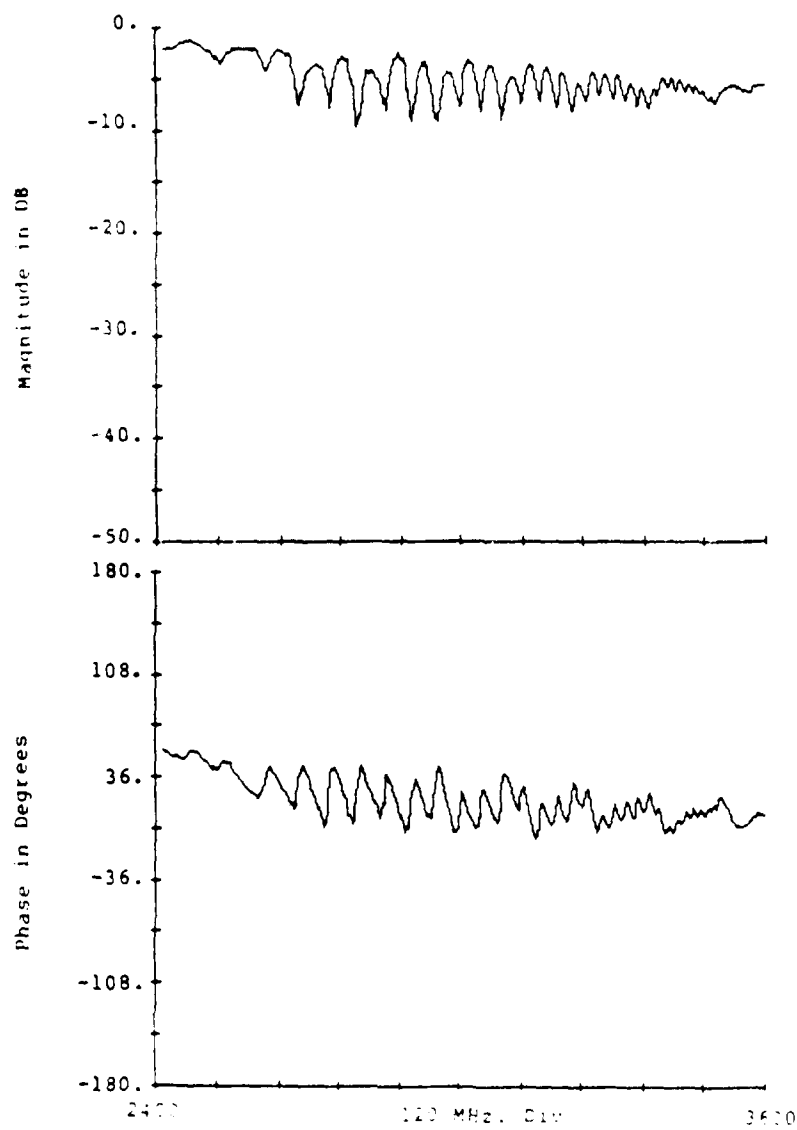
Figure 2.66: Corrected S11 for 1-Bar Mium Transducer

89
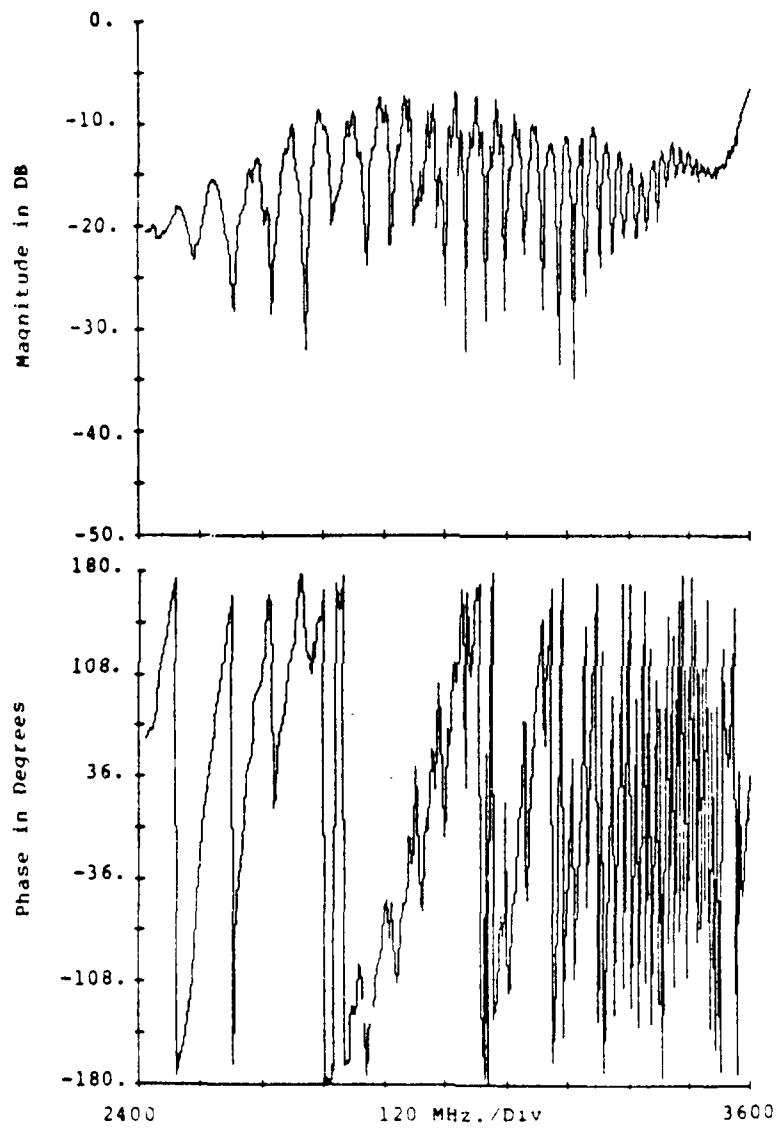
Figure 2.67: Corrected S_{12} for 2-Bar 20 μm Transducer
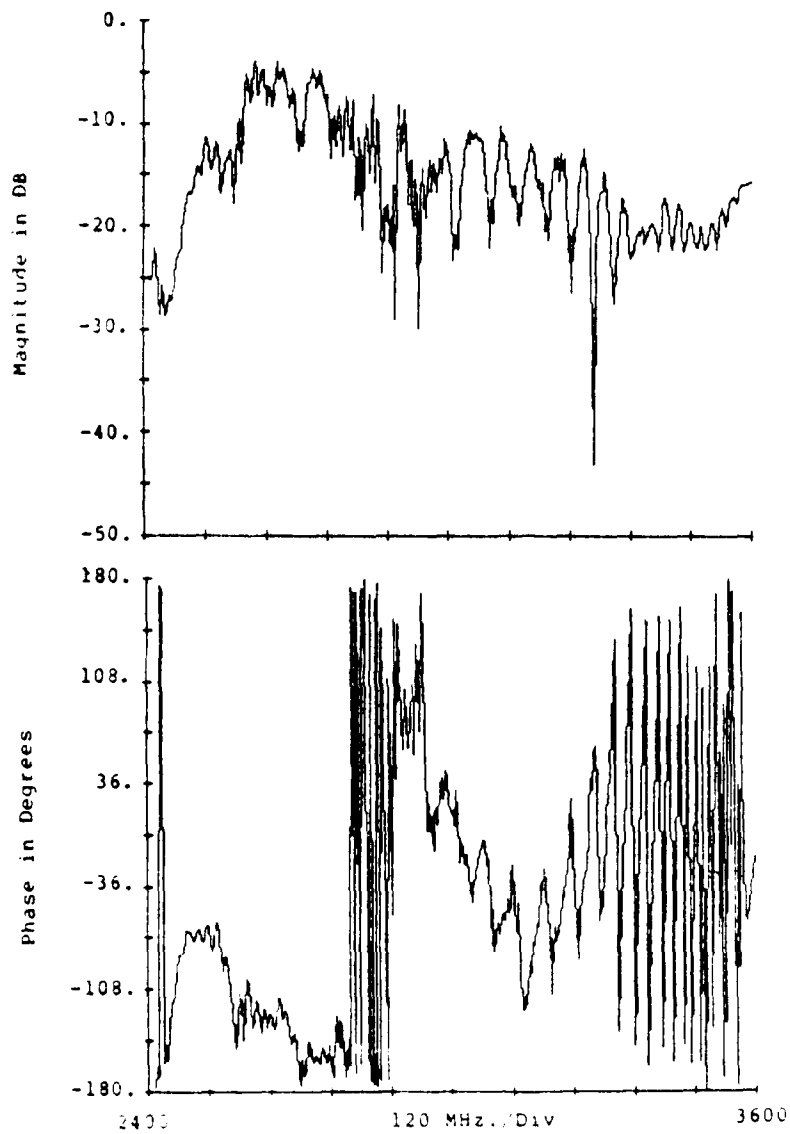
Figure 2.68: Corrected S_{13} for 2-Bar 20 um Transducer

Figure 2.69: Corrected S_{11} for 2-Bar 20 um Transducer

MICROCOPY RESOLUTION TEST CHART

NATIONAL BUREAU OF STANDARDS - 1963 - A

Figure 2.70: Corrected S13 for 2-Bar 20 um Transducer
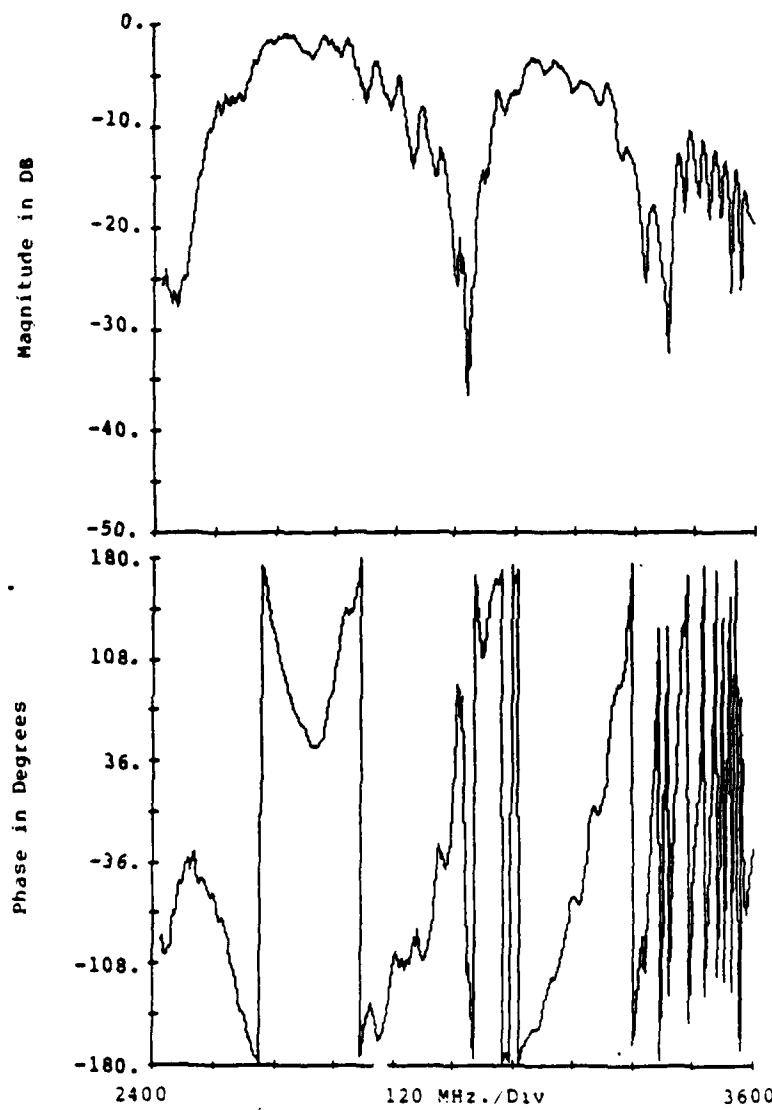
Figure 2.71: Corrected S_{31} for 2-Bar 20 um Transducer
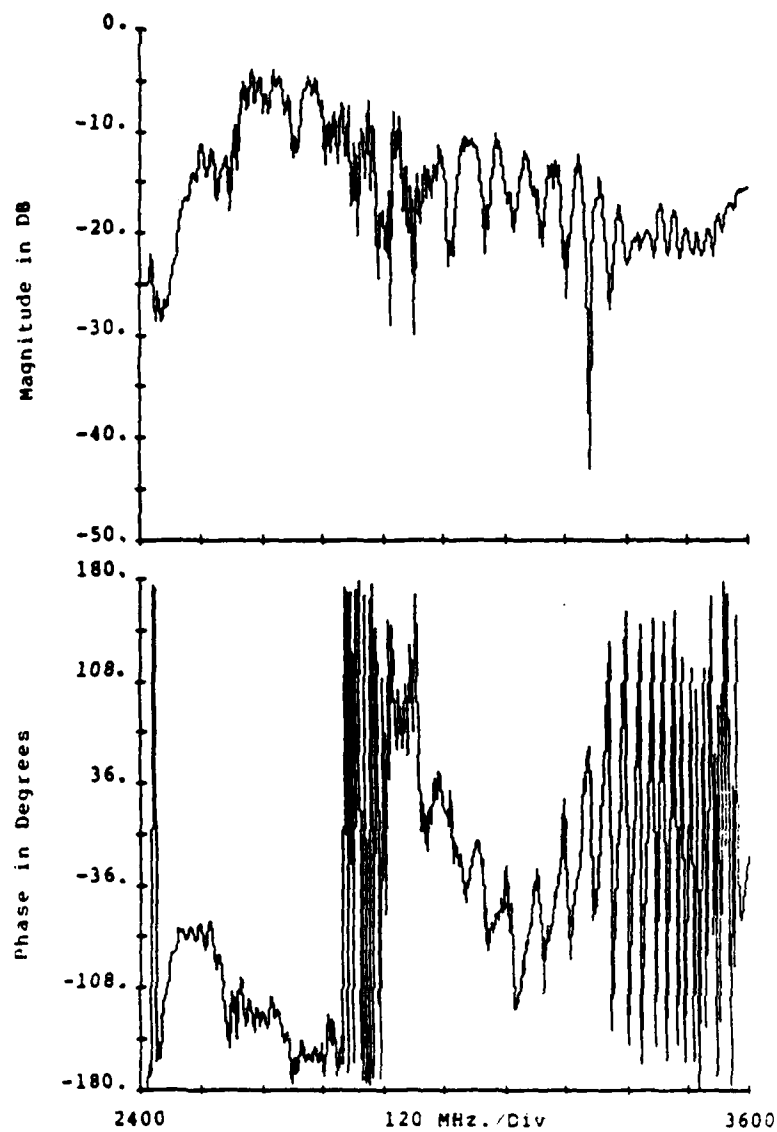
Figure 2.72: Corrected S_{32} for 2-Bar 20 μ- Transducer
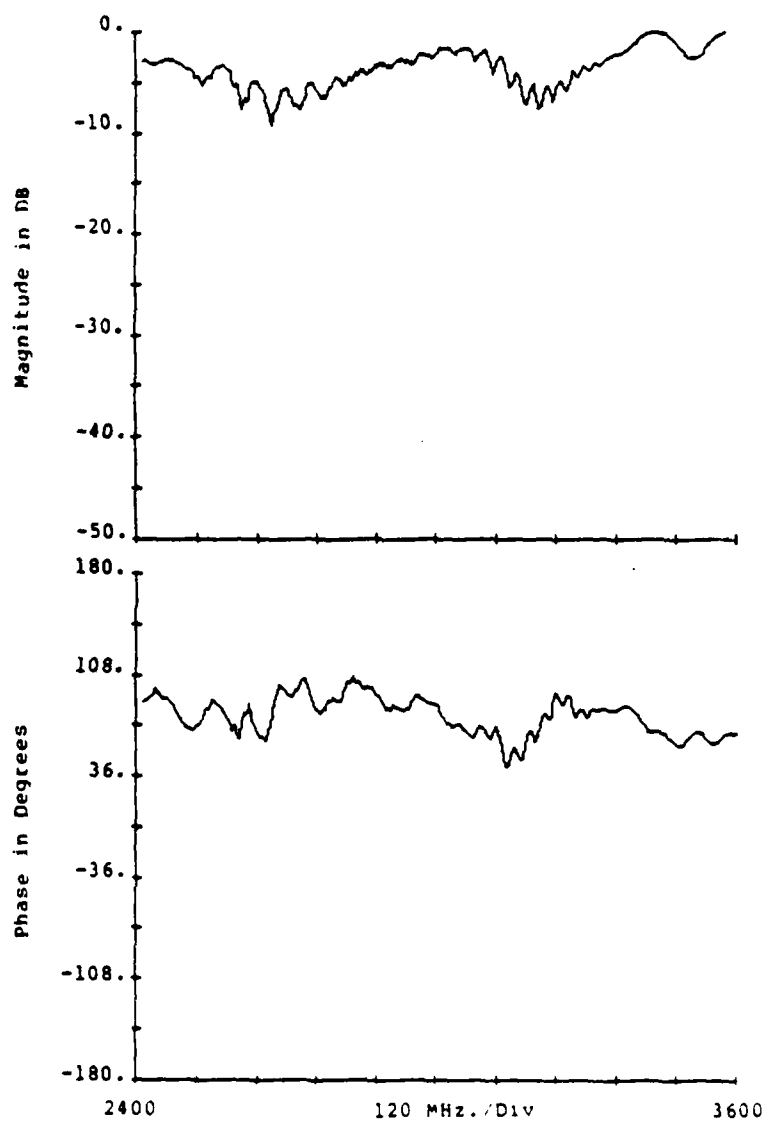
Figure 2.73: Corrected S_{33} for 2-Bar 20 um Transducer

96
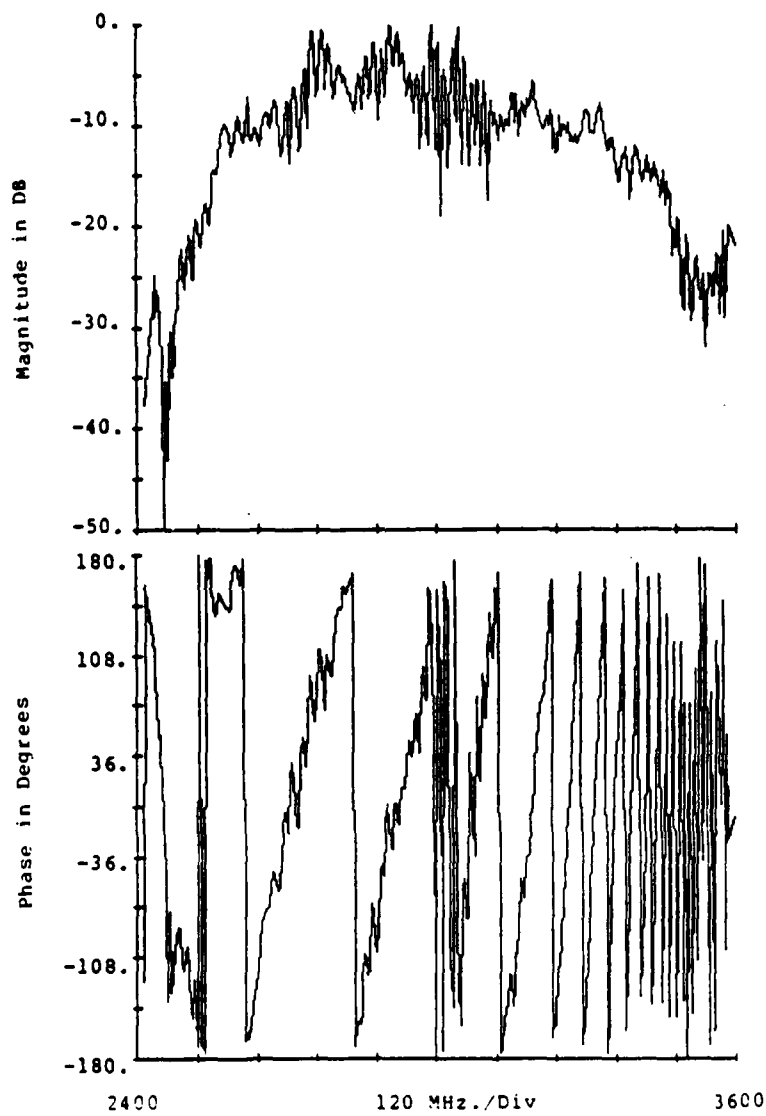
Figure 2.74: Corrected S_{12} for 4-Bar 5 um Transducer

97
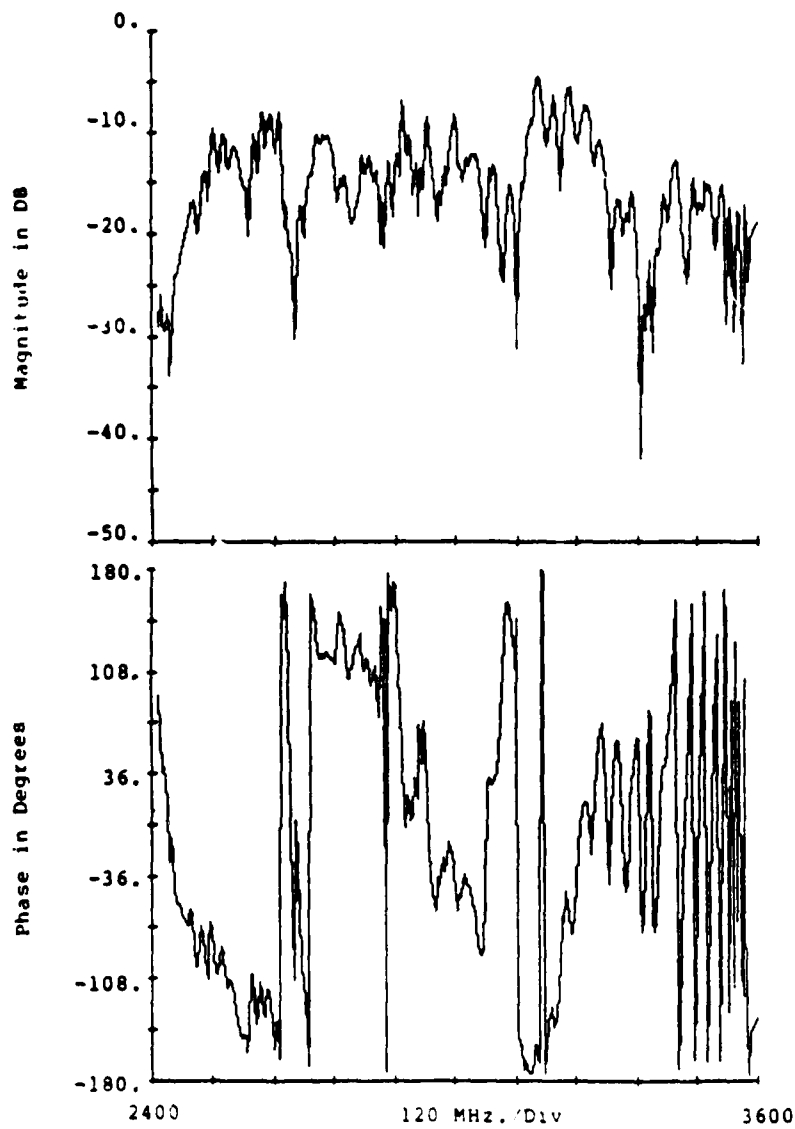
Figure 2.75: Corrected S_{13} for 4-Bar 5 um Transducer
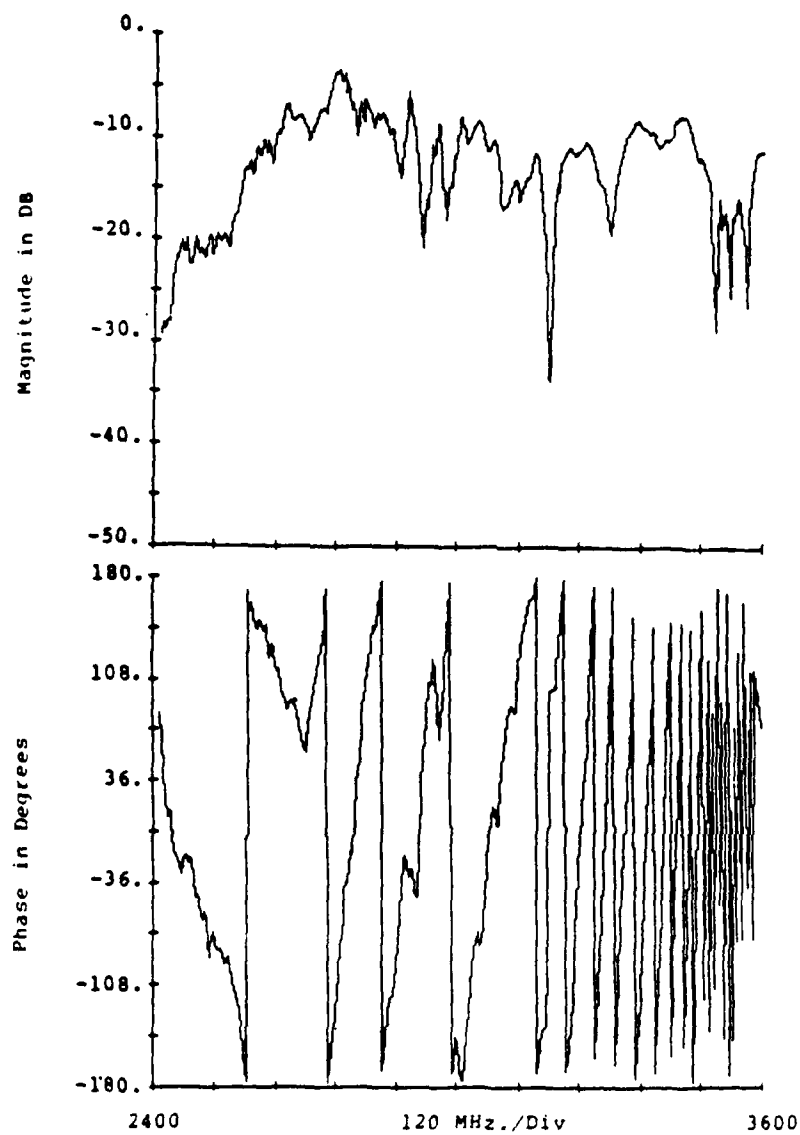
Figure 2.76: Corrected S_{21} for 4-Bar 5 um Transducer

99
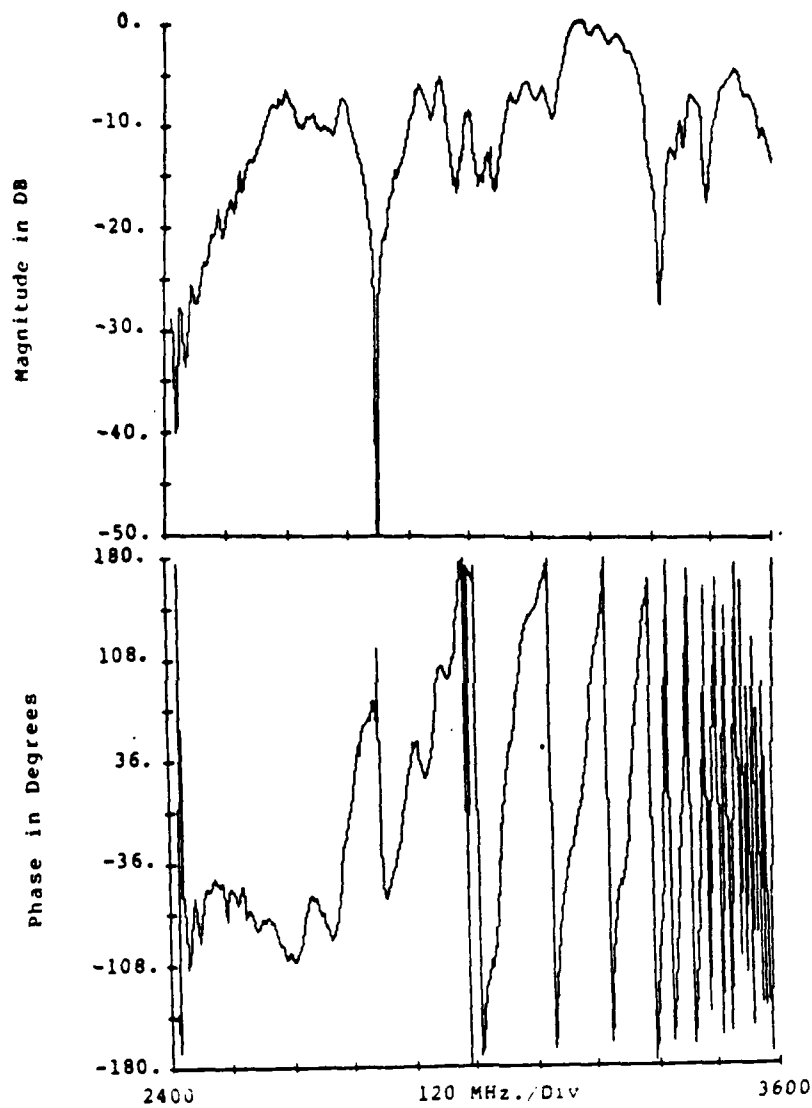
Figure 2.77: Corrected S_{23} for 4-Bar 5 um Transducer

100
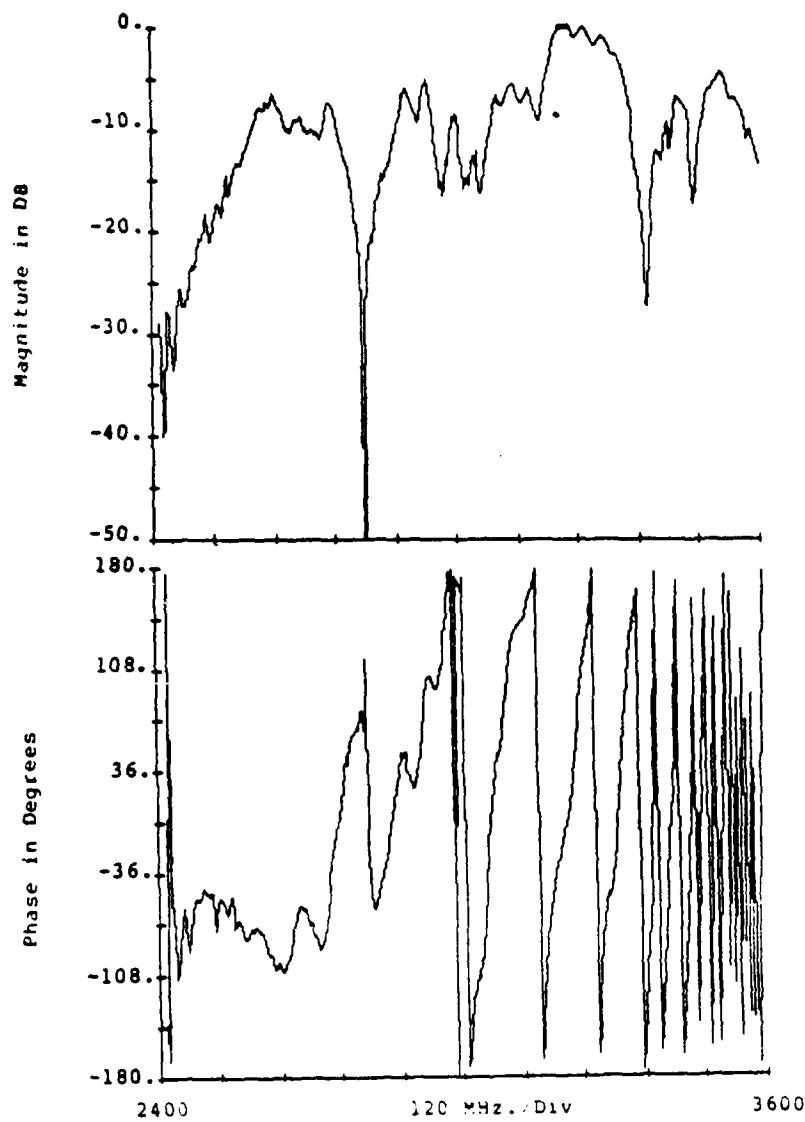
Figure 2.78: Corrected S_{11} for 4-Bar 5 um Transducer
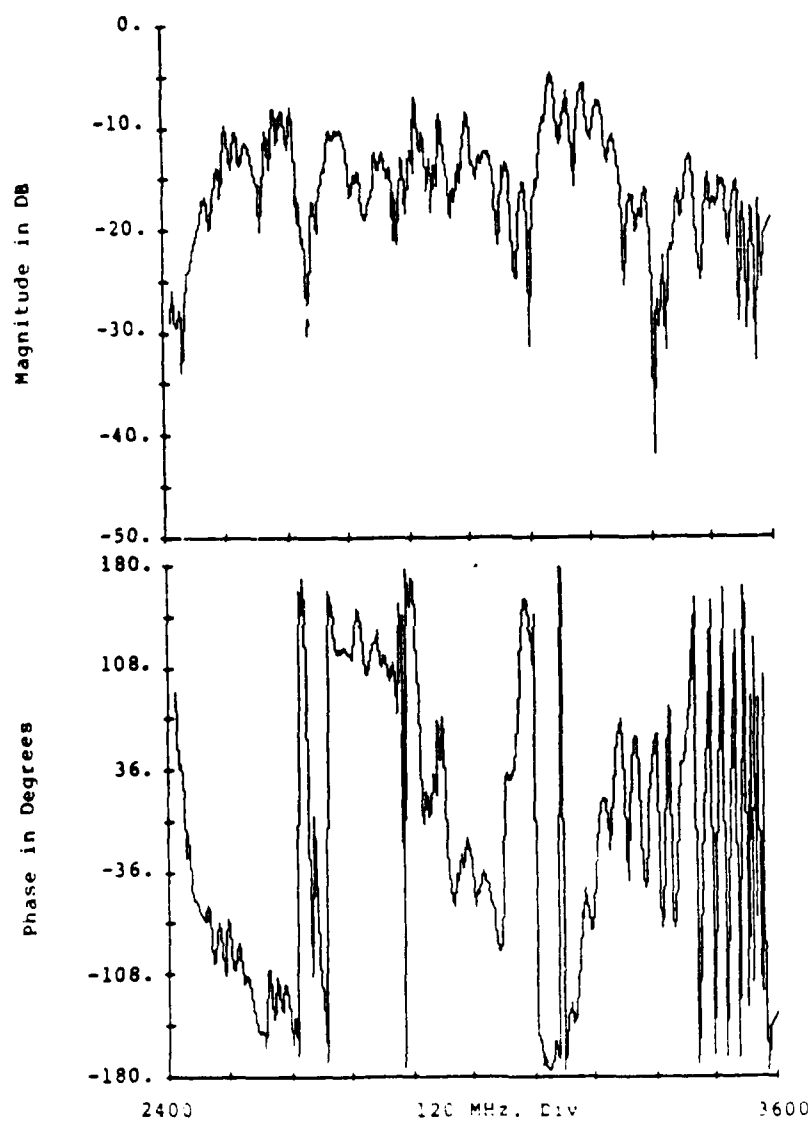
Figure 2.79: Corrected S_{21} for 4-Bar 5 μm Transducer

102
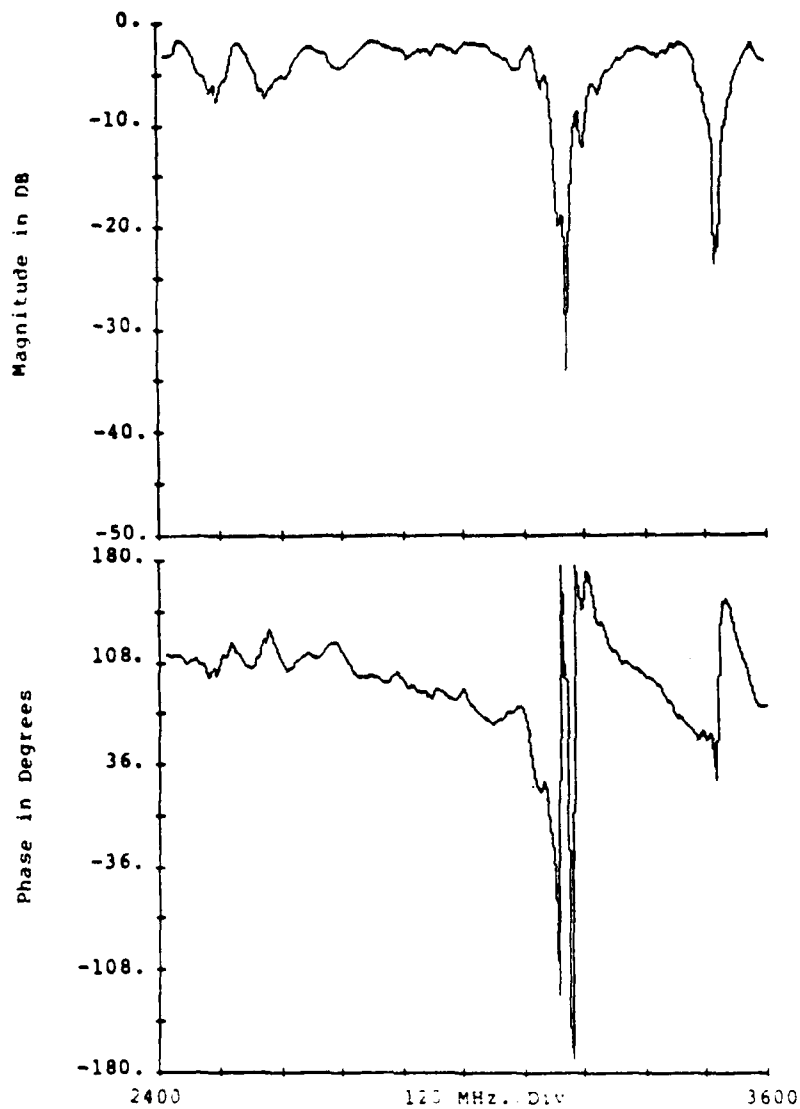
Figure 2.80: Corrected S_{33} for 4-Bar 5 μm Transducer

103
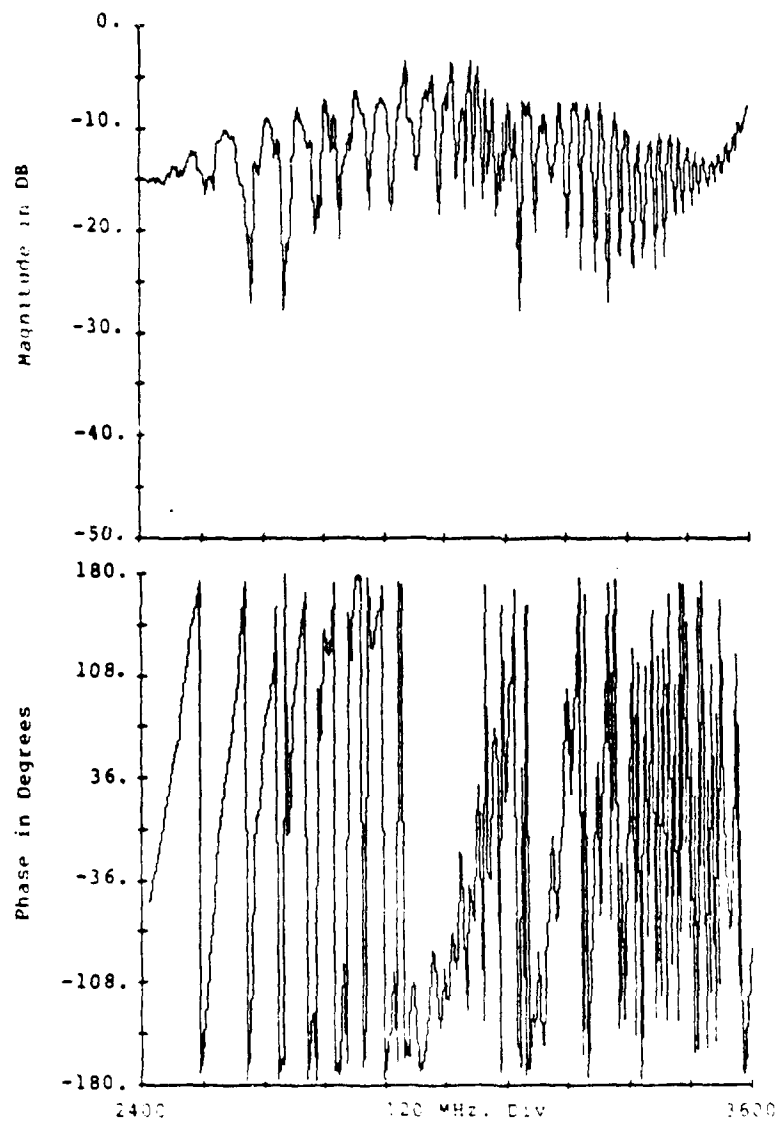
Figure 2.81: Corrected S_{11} for p-Bar 1 in Transducer
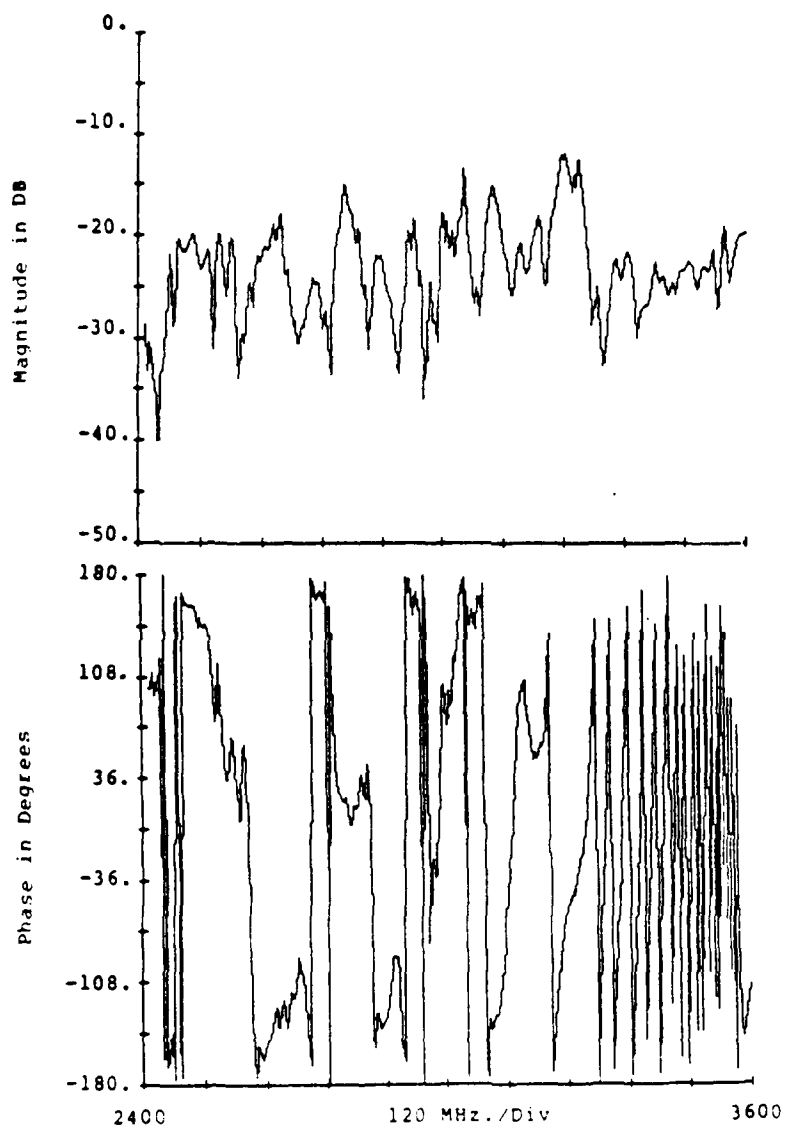
Figure 2.82: Corrected S_{11} for 8-Bar 20 um Transducer
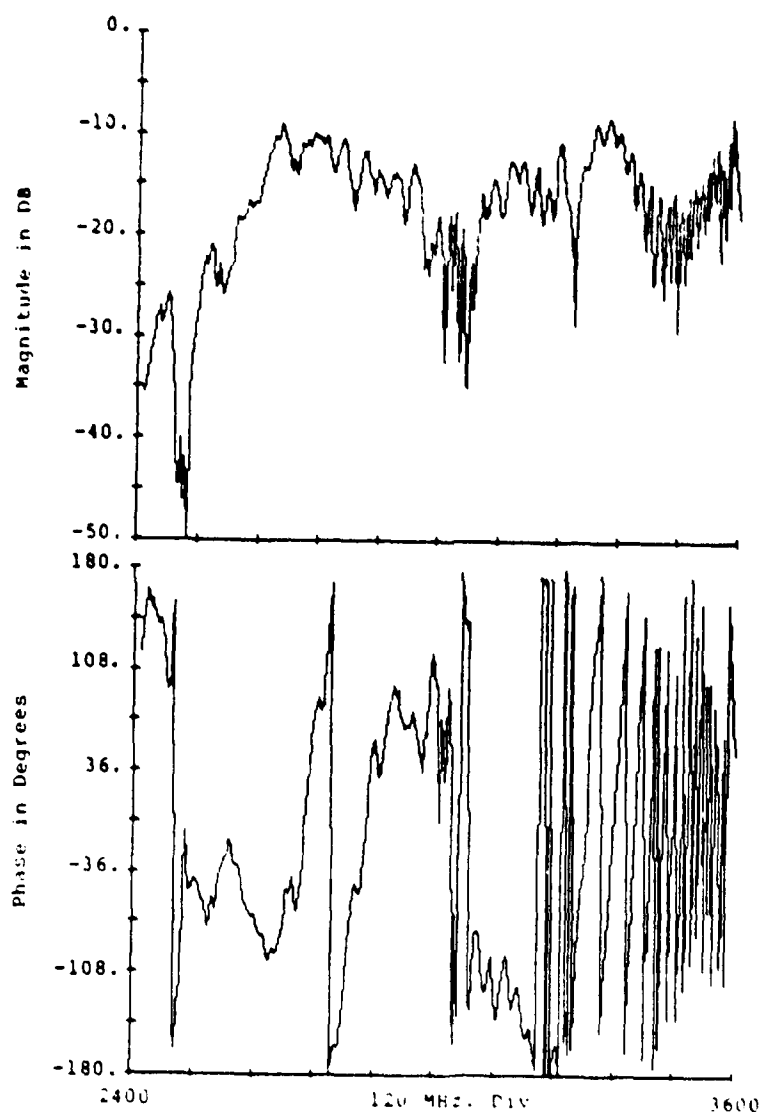
Figure 2.83: Corrected S_{11} for S-Bar 20 um Transducer
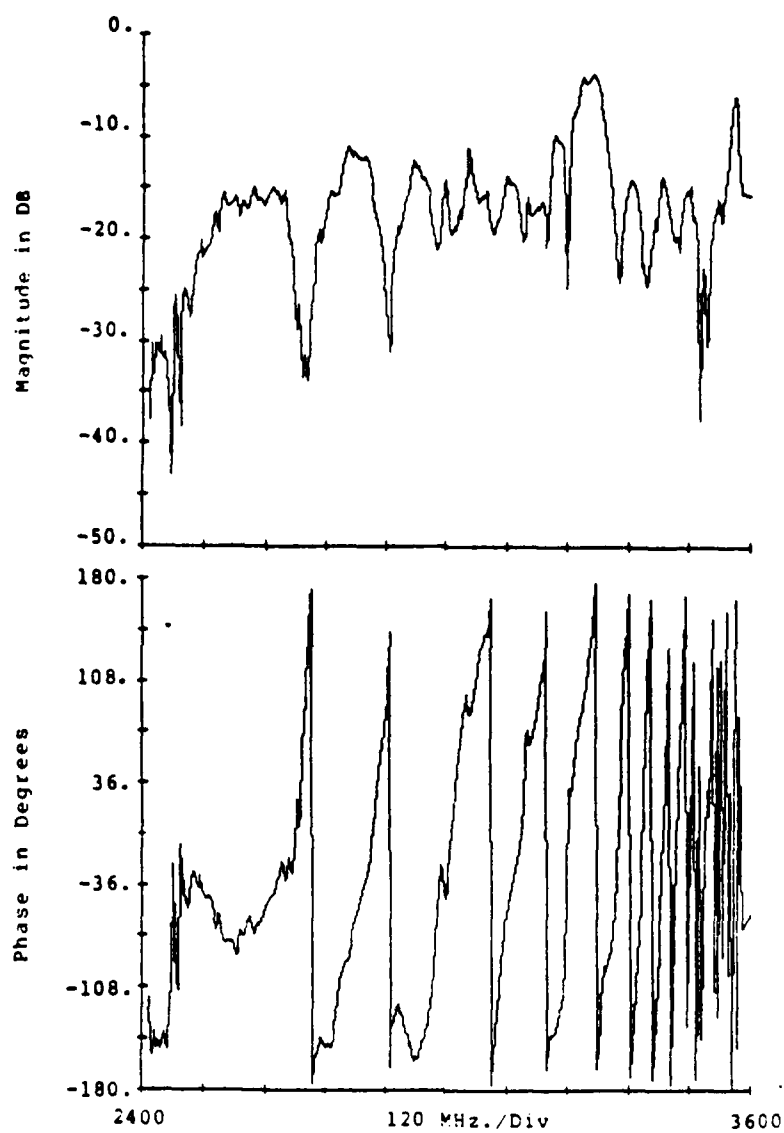
Figure 2.84: Corrected S_{11} for 8-Bar 20 um Transducer

108
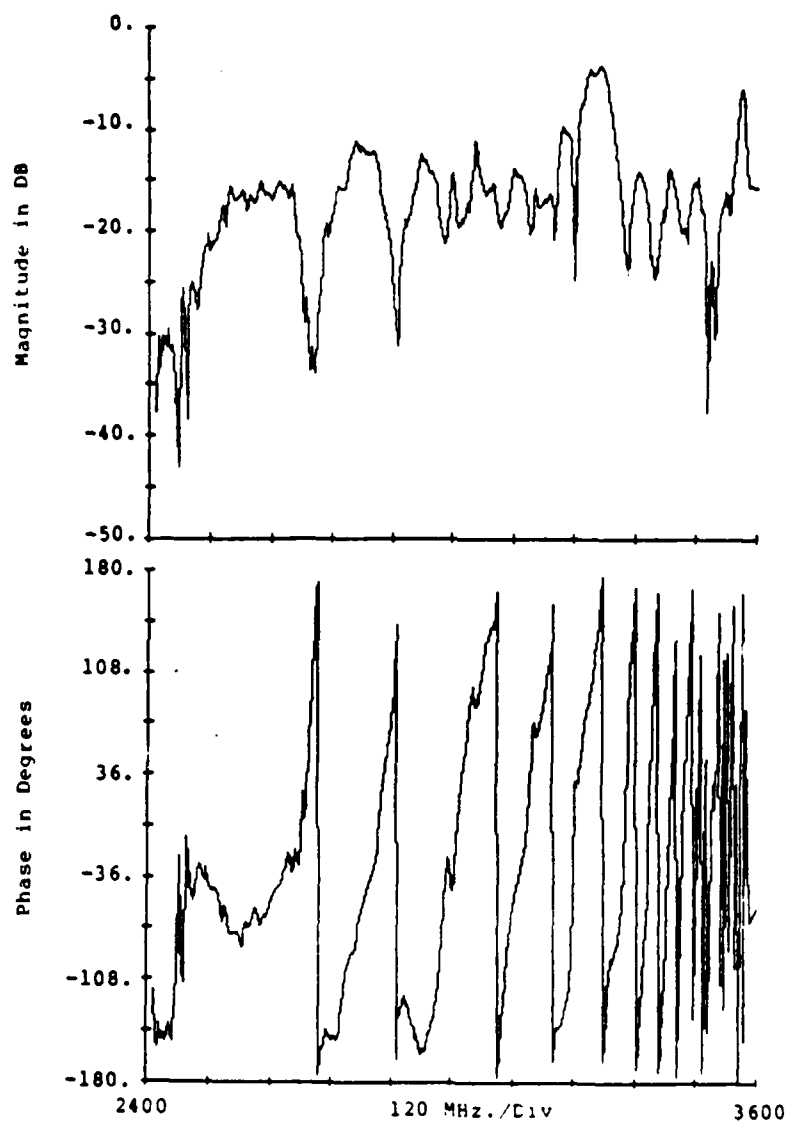
Figure 2.85: Corrected S_{31} for 8-Bar 20 um Transducer
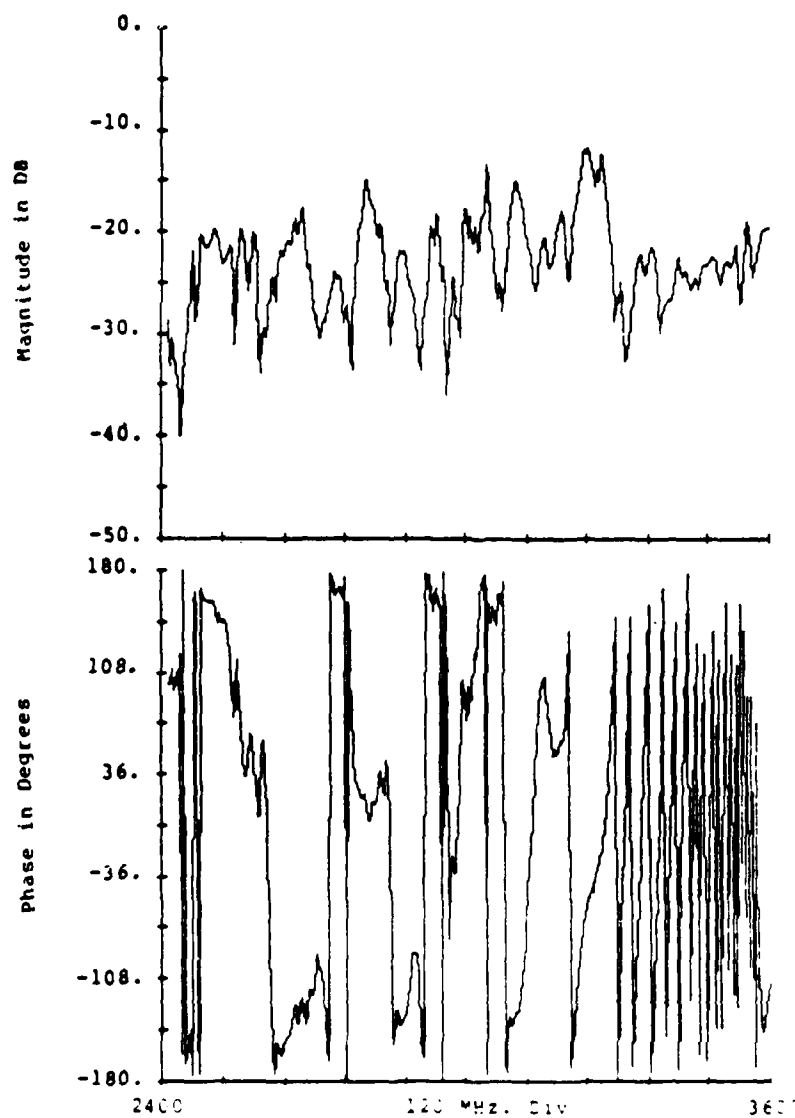
Figure 2.86.   Corrected S_{11} for H-Bar 20 μm Transducer
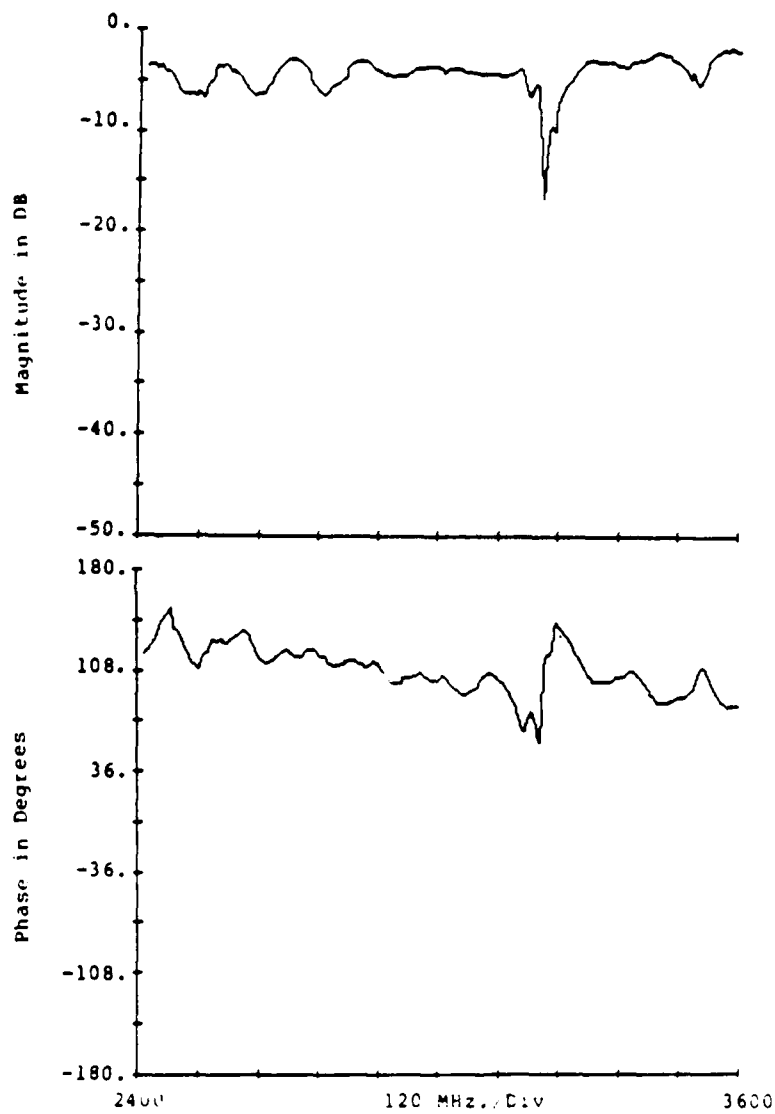
Figure 2.87:   Corrected S_{22} for H-Bar 20 µm Transducer

111

be detected is that it is shifted up has not changed but
has only shifted up.

2.3.5 Empirical Model Results

Figures 2.18 thru 2.52 show the frequency response
calculated by substituting the corrected S-parameters for
the theoretical S-parameters in the computer program of
Appendix 1. This leads to an empirical model. When these
results are compared with previous experimental data
(Figures 2.93 thru 2.97 there is not much difference in
the resonance notch structures or the insertion loss.
This indicates that the model is good at least to the
first order. To exploit the model more fully, one must
try to calculate multiple bar responses. Figures 2.98 and
2.99 show the results of using the single bar 50um data to
predict the frequency response of two and four bar arrays.
The calculated two bar frequency response when compared to
the experimental two bar frequency response of Figure 2.100
looks good; however, the calculated four bar frequency
response does not match the experimental four bar
frequency response of Figure 2.101. The difference is in
the resonance notch structure and in the insertion loss.
The resonance structure of the 2-bar array looks very
close. The only problem is in the roll off rates of each
lobe. This indicates that the phase change associated
with the resonances is not sharp enough. The problem may
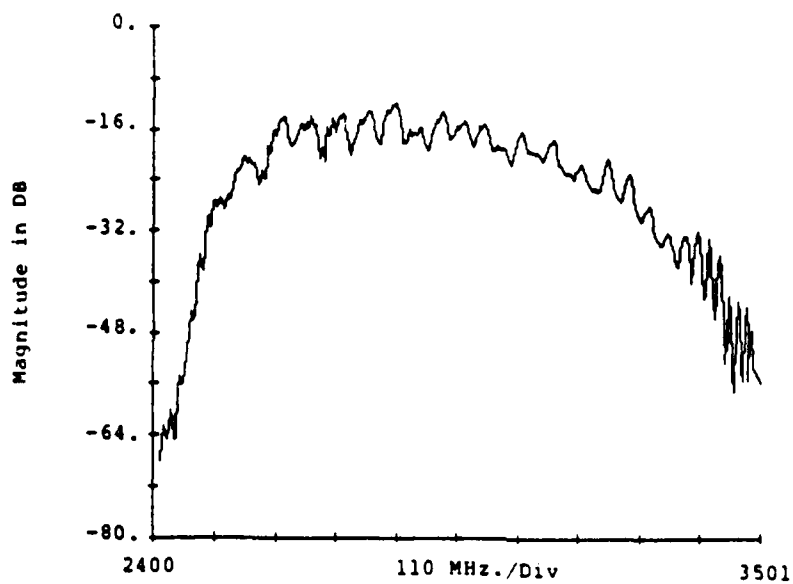
Figure 2.88: Empirical Model Results of 1-Bar 50 um
Transducer
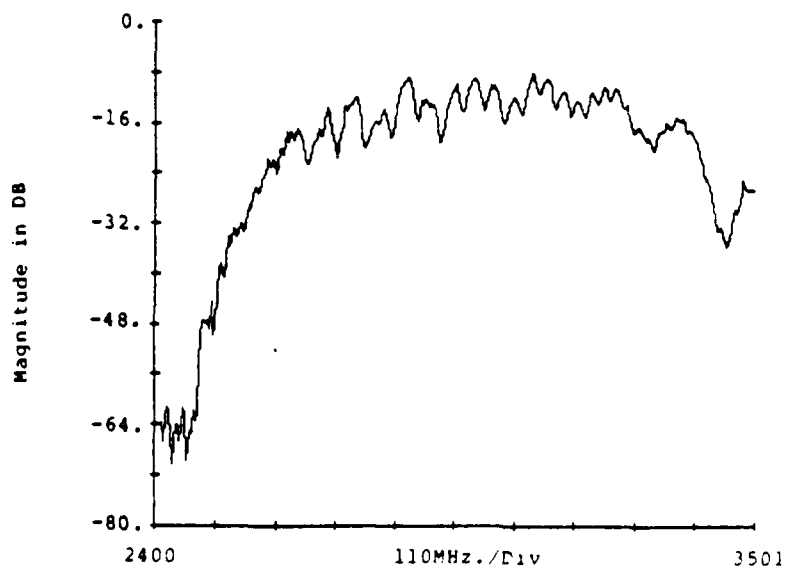
Figure 2.89: Empirical Model Results of 1-Bar 10 um
Transducer

113
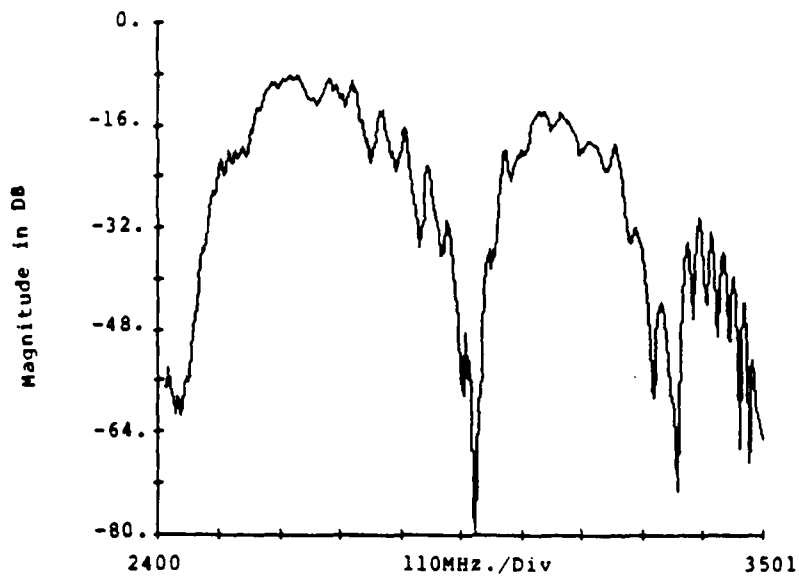
Figure 2.90: Empirical Model Results of 2-Bar 20 um
Transducer
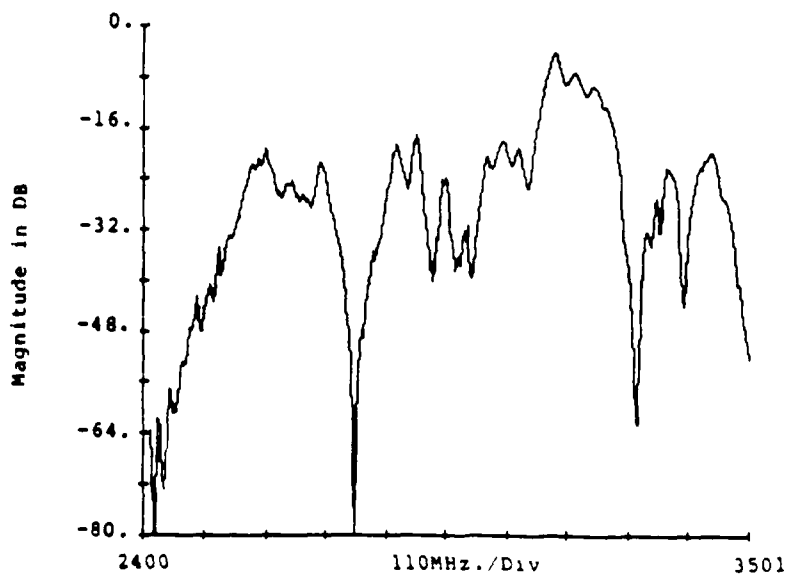
Figure 2.91: Empirical Model Results of 4-Bar 5 um
Transducer

114
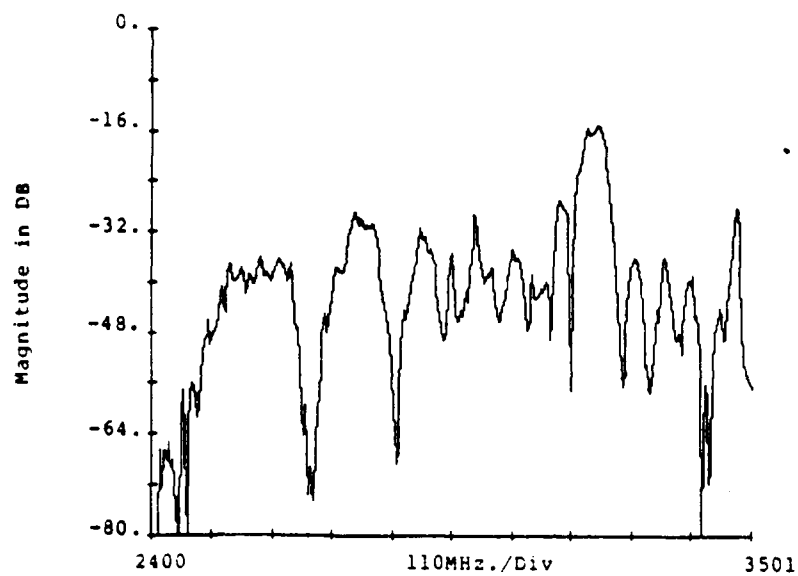
Figure 2.92: Empirical Model Results of 8-Bar 20 um Transducer

Figure 2.93: Experimental Frequency Response for 1-Bar 50um Transducer
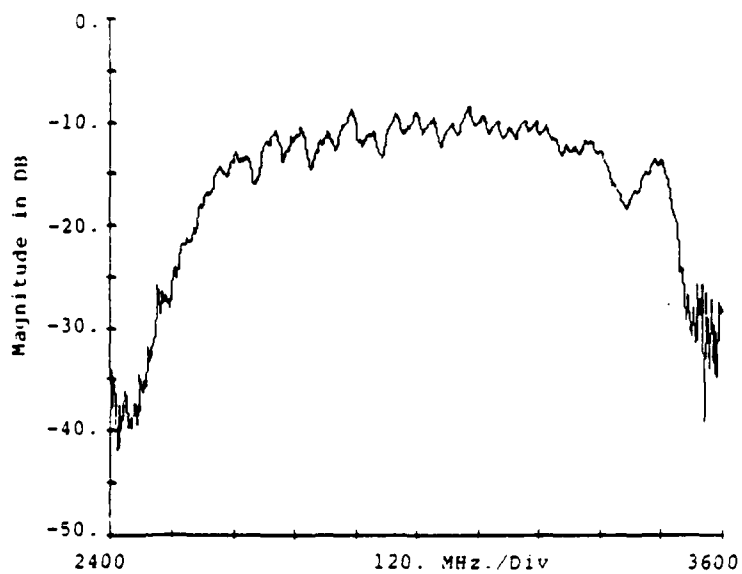
Figure 2.94: Experimental Frequency Response for 1-Bar 10um Transducer
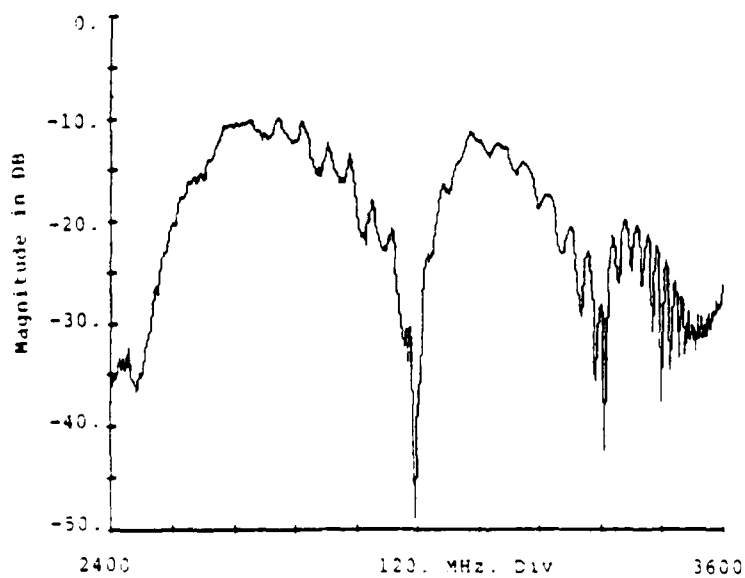
Figure 2.95: Experimental Frequency Response for 2-Bar 20um Transducer
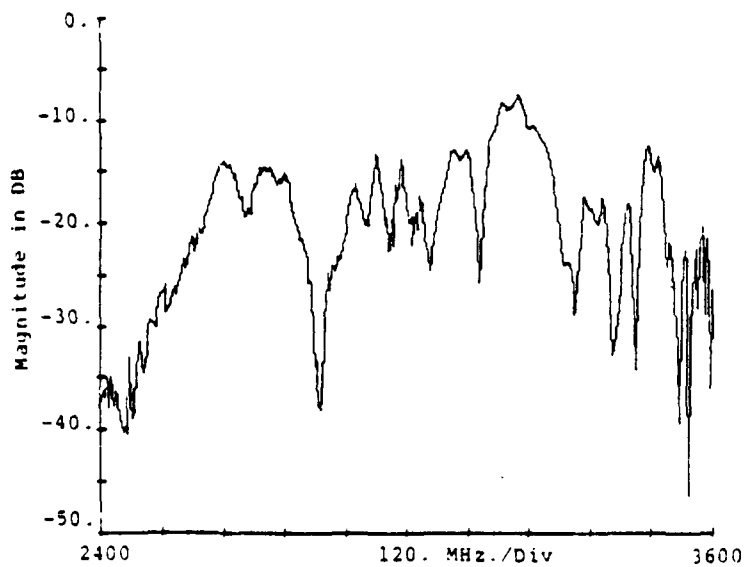
Figure 2.96: Experimental Frequency Response for 4-Bar 5um Transducer
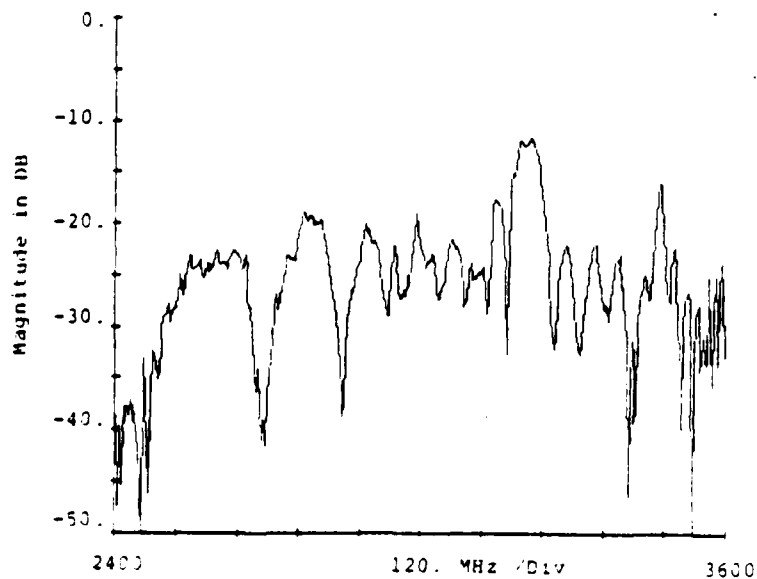
Figure 2.97: Experimental Frequency Response for 9-Bar 20um Transducer

117
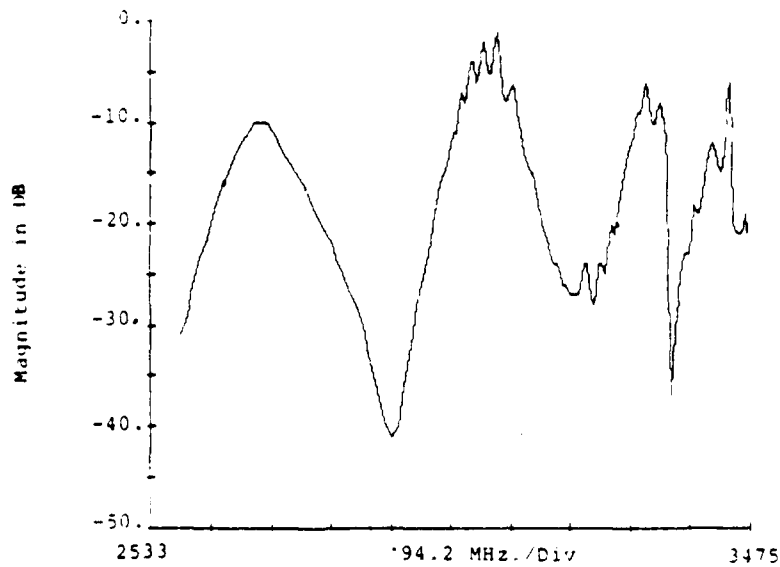
Figure 2.98: Calculated 2-Bar Response Using Corrected Data
Data from Single Bar 50um Transducer
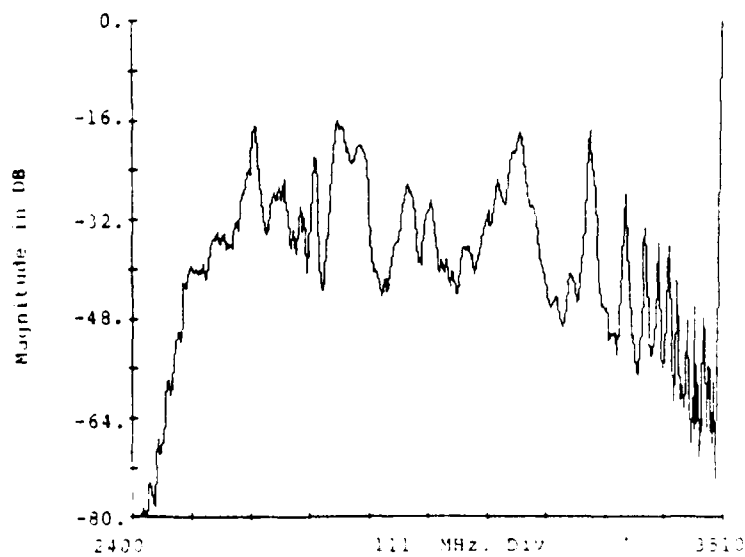
Figure 2.99: Calculated 4-Bar Response Using Corrected Data
Data from Single Bar 50um Transducer

118
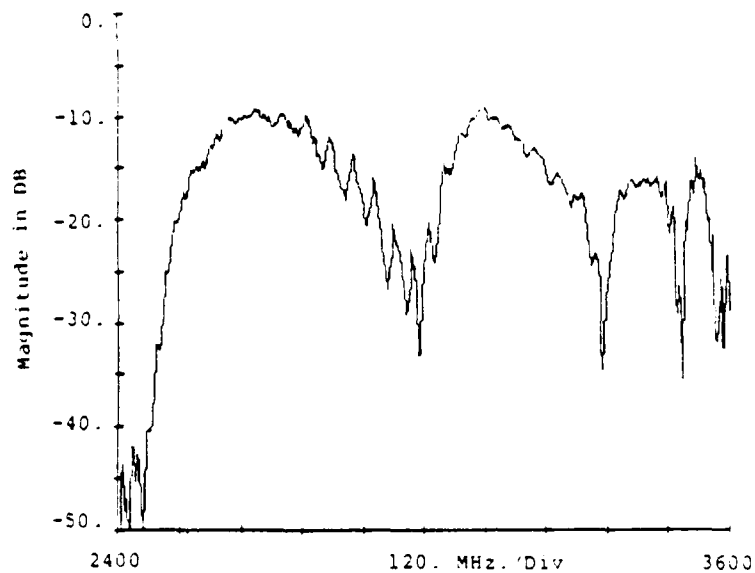
Figure 2.100: Experimental Frequency Response for 2-Bar
50um Transducer
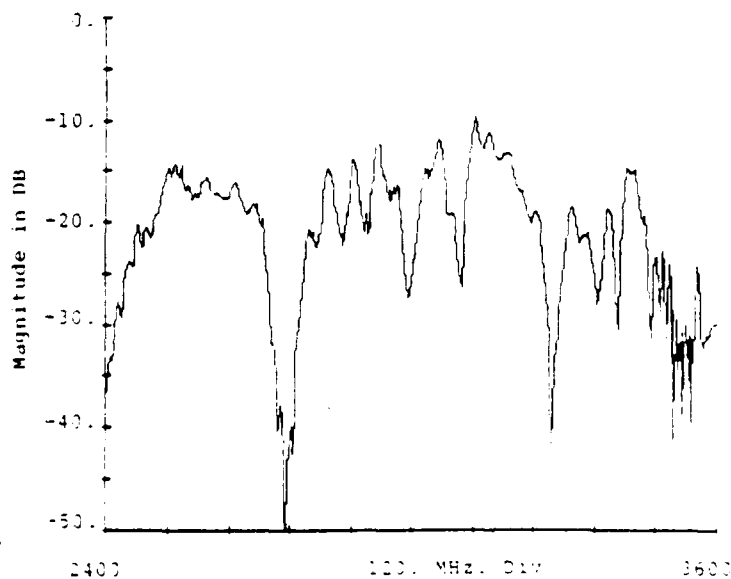
Figure 2.101:Experimental Frequency Response for 4-Bar
50um Transducer

119

be helped by more accurate phase combining of the data. There seems to be many small problems associated with the empirical model. The most pronounced problem is probably measurement errors arising from misalignment of the different measurements on each device and the inherent accuracy *of the network analyzer*. *Another error occurs* from the fact that this is primarily a superposition model and that there is no accounting for mutual coupling between the microstrips. These errors as well as a few other problems will be examined in the concluding chapter.

CHAPTER V

2.4   CONCLUSION

2.4.1 Introduction

In this chapter, a final look will be taken at each model and their results. The good points as well as the weak points will be examined for both models. Finally, recommendations for futher study will be made.

2.4.2 The Theoretical Model

The theoretical model of Chapter 2 is a good model for simple MSSW structures. Problems arise, however, when the structures become more complex. This break down is simply due to the assumptions of $S_{23}=S_{31}$, $S_{13}=S_{32}$, and that the transmission line model can be used to find the wave port parameters directly. These assumptions are necessary due to the very complex nature of MSSW and its' nonreciprocal properties. The model approach of using scattering parameters is very good and is probably the easiest way to go as can be seen from the empirical model.

2.4.3 The Empirical Model

The empirical model of Chapter 4 is an excellent model for MSSW. This model uses the same principles as

the theoretical model. The only difference is that the empirical model uses measured S-parameters, where the theoretical model uses mathematically derived parameters. The empirical model is not without its' problems. S_{11} and S_{22} are assumed to be zero because they could not be measured. This may be nearly true for single microstrip transducers, but, since the transducer arrays have interference and resonators can be construced, the condition of $S_{11}=S_{22}=0$ cannot be absolutely true. Most of the other measured S-parameters are as expected except for the appearance that $S_{13}=S_{32}$ and $S_{31}=S_{23}$. All the devices measured (see Figures 4.1 thru 4.5) display these characteristics. The reason the meaurements show this is because of inadequate error correcting. The coupling loss added by the measuring transducers can be accounted for, but there is no possible way to separate the phase change that takes place in going from electromagnetic waves to magnetostatic waves and from magnetostatic waves to electromagnetic waves. The five micrometer transducers hopefully are decoupled, but there will still be some phase change. Another error in this model is that it does not account for mutual interaction and coupling between the microstrips in each array. Although this model does have some problems, it is still able to yield the correct response (see Figures 2.88 thru 2.92). Difficulties do

arise in trying to cascade the single microstrip 50 micrometer results as can be seen in Figures 2.98 and 2.99. The two bar results are not bad, but the four bar results are. The reason is that there are many errors including alignment of the different measurements on each device, and in the accuracy of the automatic network analyzer. The automatic network analyzer is a good accurate system but it is not perfect. The errors that do occur are propagated and greatly magnified when the microstrips are cascaded.

2.4.4 Recommendations for Further Study

For the empirical model, there is probably no way to improve on the measured data unless a more accurate measurement system is found. However, study of the measurement techniques and development of new techniques might possibly yield better results. The real solution is to address the theoretical model and the problems associated with it.

REFERENCES

1. B. A. Auld, "Walker Modes in Large Ferrite Samples," J. Appl. Phys. 31, 1642 (1960).

2. R. W. Damon and J. R. Eshbach, "Magnetostatic Modes of a Ferromagnetic Slab", J. Phys. Chem. Solids 19, 308, (1961).

3. W. L. Bongianni, "Magnetostatic Propagation in a Dielectric Layered Structure", J. Appl. Phys. 43, 2541 (1972).

4. J. D. Adams et al, "Electromagnetic Matching Considerations for YIG Delay Lines", Proc. IEEE 56, 1373, (1968).

5. H. J. Wu, "Magnetostatic Wave Transducers", PhD Dissertation, EE Department, University of Texas at Arlington, Dec. (1978).

6. G. Hasnain, "Magnetostatic Wave Transducer Array Filters", Masters Thesis, EE Department, University of Texas at Arlington, August (1980).

7. H. J. Carlin, "The Scattering Matrix in Network Theory", IRE Transactions on Circuit Theory, June (1956).

8. W. R. Smith, "Analysis of Interdigital Surface Wave Transducers by Use of an Equivalent Circuit Model", IEEE TRANS. on Microwave Theory and Techniques, Vol. MTT-17 No. 11, Nov. (1969).

9. E. P. Snapka, "Two-port Magnetostatic Surface Wave Resonators", Master Thesis, EE Department, University of Texas at Arlington, May (1978).

10. W. R. Brinlee, "MSSW Two-port Metal Strip Array Resonators", Masters Thesis, EE Department, University of Texas at Arlington, May (1981).

APPENDIX I

CCCCCCCCCCCCCCCCCCCCCCCCCCCCCCCCCCCCCCCCCCCCCCCCCCCCCCCCCC

        COMPUTER PROGRAM FOR CALCULATING THE THREE PORT
    S-PARAMETERS FOR MSSW TRANDUCERS.   THIS PROGRAMS
    USE THE DISPERSION PROGRAM OF BRINLEE AND THE
    RADIATION IMPEDANCE CALCULATED FROM WU'S MODEL.

CCCCCCCCCCCCCCCCCCCCCCCCCCCCCCCCCCCCCCCCCCCCCCCCCCCCCCCCCC


```
      DIMENSION FRQ(152),WAV(152),PLOSS(152),RGF1(152),
     $AGF1(152)
      DIMENSION E1(5),E2(5),D1(5),D2(5),SC1(5),SC2(5)
      DIMENSION S1(25),S2(25),AGF2(152),AGR2(152)
      DIMENSION RGF2(152),RGR2(152),RGR1(152),AGR1(152)
      DIMENSION RMF(152),XMF(152),RMR(152),XMR(152)
      COMPLEX*8 ARR1(3,3),ARR2(3,3),A1(3,3),A2(3,3),
     $R1(3,3),R2(3,3)
     1,PP(3,3),YSB(3,3),Z,VF1,VR1,TZ1,PPP(3,3)
      COMPLEX*8 ZIN,CSINH,CCOSH,CTANH,JJ,TZ2
      COMPLEX*8 ZF2,ZR2,ZF1,SSB(3,3),ZR1
     2,AM,BM,CM,DM,GAMMA,KF1,KR1,KF2,KR2,W0
      COMPLEX*8 GF1(152),GR1(152),GF2(152),GR2(152),
     $U1,U2,GAMMAF,GAMMAR
C                       INITIALIZATION OF VARIBLES
      DATA P,KT,KAT,LL,M/1.0E-05,1,0,0,59/
      DATA E1(1),E1(2),E1(3),E1(4),E1(5)/10.0,1.0,1.0,
     $16.0,16.0/
      DATA E2(1),E2(2),E2(3),E2(4),E2(5)/0.0,0.0,0.0,
     $0.0,0.0/
      DATA SC2(1),SC2(2),SC2(3),SC2(4),SC2(5)/0.0,0.0,
     $0.0,0.0,0.0/
      DATA IF,IFF,MIFF,IHEAD/0,1,0,0/
      CSINH(Z)=(CEXP(Z)-CEXP(-Z))/2.
      CCOSH(Z)=(CEXP(Z)-CEXP(-Z))/2.
      CTANH(Z)=CSINH(Z)/CCOSH(Z)
      DATA EPS,NSIG,KN,NGS,N,ITMAX/1.E-5,5,0,1,1,50/
      DATA ZC,RS,DIFP/90.,50.,0./
C
```

```fortran
      PI=ACOS(-1.)
      U0=PI*4.E-7
      GYRO=2.8
      JJ=(0.0,1.0)
      READ(5,*) D0,TU,T0,H0,SM,DHM,NSAMP
      READ(5,*) T,B0,RLGH DIST,N1,N2
      READ(5,*)(S1(I),I=  N1)
      READ(5,*)(S2(I),I=1,N2)
      READ (5,*)(D1(I),I=1,5)
      READ(5,*) (SC1(I),I=1,5)
      DO 101 I=1,5
101   D2(I)=D1(I)
      T1=B0
      DO 18 MM=1,N1
18    T1=T1+S1(MM)
      T2=B0
      DO 28 MM=1,N2
28    T2=T2+S2(MM)
      A0=DIST*1.E3-(T1+T2)/2.
      WRITE(6,66) D0,TU,T0,H0,SM,DHM
      WRITE(6,67) T,B0,RLGH,A0
      WRITE(6,68) N1,(S1(I),I=1,N1)
      WRITE(6,69) N2,(S2(I),I=1,N2)
      KF2=CMPLX(0.393423885E-05,0.125572526E-03)
      KR2=CMPLX(0.961030200E-05,0.307895565E-03)
C                         COMPUTE PASSBAND
      FPM=1760.
      HI=375.
       GA=2.8
       GM=GA*FPM
      OH=HI/FPM
       FRQ3=SQRT(OH*(OH+1.))*GM
       FRQ4=(OH+0.5)*GM
       FRQ1=FRQ3*1.01
       FRQ2=FRQ4*0.99
      QF=0.5*(FRQ2+FRQ1)
      DF=(QF-FRQ1)/100.0
C     FREQUENCY SAMPLING 152 POINTS FOR DISPERSION RELATION
      FRQ(1)=FRQ3+0.75*(FRQ1-FRQ3)
      FRQ(2)=FRQ1+0.5*DF
      DO 102 I=1,49
      RI=I
      J=I+2
  102 FRQ(J)=FRQ(2)+RI*DF*2.0
      FRQ(52)=QF+DF*0.25
      DO 103 I=1,99
      RI=I
```

126

```fortran
        J=52+I
  103 FRQ(J)=FRQ(52)+RI*DF
      FRQ(152)=FRQ2+0.25*(FRQ4-FRQ2)
  731   FORMAT(' FRQ', E16.8)
      WM=GYRO*SM
      GH=GYRO*H0
  4   DHM2=DHM/2.0
      STARTF=FRQ(1)/1000.0
      STOPF=FRQ(152)/1000.0
      UM=PI*4.0E-09
  C            BEGIN FREQUENCY SCAN
      NSAMP=NSAMP-1
      DO 10 M=1,NSAMP
      F=FRQ(M)
      PRSNTF=F/1000.0
      DH=DHM2*(3000.0/F+F/3000.0)
      W0=CMPLX(GH,(GYRO*DH/2.0))
      U1=1.0+W0*WM/(W0**2-F**2)
      U2=WM*F/(W0**2-F**2)
      KF1=JJ*CLOG(((U1-U2-1.0)*(U1+U2))/((U1+U2+1.0)*(
     $U1-U2)))/2.0/D1(4)
      KF1=CMPLX((3.0*REAL(KF1)),AIMAG(KF1))
      KR1=JJ*CLOG(((U1+U2-1.0)*(U1-U2))/((U1-U2+1.0)*(
     $U1+U2)))/2.0/D1(4)
      KR1=CMPLX((2.0*REAL(KR1)),AIMAG(KR1))
      CALL DSPRSN(F,U1,U2,E1,D1,SC1,EPS,GAMMAR,GAMMAF,
     $KF1,KR1)
      IF (ABS(REAL(GAMMAF)).GE.ABS(AIMAG(GAMMAF)))
     $GAMMAF=KR1
      IF (ABS(REAL(GAMMAR)).GE.ABS(AIMAG(GAMMAR)))
     $GAMMAR=KF1
      GF1(M)=KF1*1.0E+04
      GR1(M)=-KR1*1.0E+04
      CALL DSPRSN(F,U1,U2,E2,D2,SC2,EPS,GAMMAR,GAMMAF,KR2,KF2)
      KF2=GAMMAF
      KR2=GAMMAR
      GF2(M)=GAMMAF*1.0E+04
      GR2(M)=-GAMMAR*1.0E+04
  10    CONTINUE
      DO 11 M=1,NSAMP
      F=FRQ(M)
      FQ=F*1.0E6
      W=FQ
      ZF1=JJ*UM*W/GF1(M)
      ZR1=-JJ*UM*W/GR1(M)
      ZF2=JJ*UM*W/GF2(M)
      ZR2=-JJ*UM*W/GR2(M)
```

```
          RM=(RMF(M)+RMR(M))
          XM=(XMF(M)+XMR(M))
         ALPH=6.32E-7*SQRT(FQ)/(B0*1.0E-06*ZC)+0.5*RM/ZC
         BETA=3.6361E-8*FQ+0.5*XM/ZC
         AR1=0.5*RMF(M)/ZC
         AR2=0.5*RMR(M)/ZC
         GAMMA=CMPLX(ALPH,BETA)
         ZIN=ZC*CTANH(GAMMA*RLGH*1.0E-03)
         RIN=REAL(ZIN)
         RM1=RIN*AR1/ALPH
         RM2=RIN*AR2/ALPH
         VF1=CEXP(-GF1(M)*B0*1.0E-04)
         VR1=CEXP(-GR1(M)*B0*1.0E-04)
         TZ1=(ZF1+ZR1)
         TZ2=ZF2+ZR2
C    FIND T MATRIX FOR METALIZED SECTION
         AM=(ZF1*VF1+ZR1*VR1)/TZ1
         BM=(ZF1*ZR1*(VF1-VR1))/TZ1
         CM=(VF1-VR1)/TZ1
         DM=(ZF1*VR1+ZR1*VF1)/TZ1
C    FIND S-PARAMETERS
30       CALL SE(ZIN,RS,ZF2,ZR2,RM2,RM1,SSB)
         CALL SW(ZF2,ZR2,AM,BM,CM,DM,SSB)
         CALL PATH(ZF2,ZR2,TZ2,GF2(M),A0,GR2(M),PP)
         CALL PATH(ZF2,ZR2,TZ2,GF2(M),S1(1),GR2(M),PPP)
         .CALL CASCAD(YSB,PPP,YSB,ARR1,F)
          CALL CASCAD(YSB,PPP,YSB,ARR2,F)
33       CALL FQRP(ARR1,PP,ARR2,RS,ZR2,ZF2,PLOSS,M)
         WAV(M)=2.*PI/AIMAG(GF2(M))
11       CONTINUE
         WRITE(6,87)
87       FORMAT('1',10X,'FRQ,WAV,PLOSS,TDY'//)
         DO 88 I=1,NSAMP
88       WRITE(6,*)I,FRQ(I),WAV(I),PLOSS(I)
         P=0
         CALL PLOT80(FRQ,PLOSS,WAV,-80.,0.,NSAMP)
66       FORMAT(25X,'MATERIAL PARAMETERS'//' YIG THICKNESS
        $=',F5.1,
        3' UM'/' AIR-GAP =',F5.1,' UM'/' ALUMINA =',F7.1,' UM'/
        1' MAGNETIC BIAS FIELD =',F7.2,' OERSTEDS'/' MAGNE
        $TIC SATURATION'
        2,F7.1,' OERSTEDS'/' MINIMUM LINEWIDTH =',F5.2,'
        $OERSTEDS'/)
67       FORMAT(25X,'TRANSDUCER PARAMETERS'//' THICKNESS
        $=',F5.2,'UM'/
        3' WIDTH =',F5.1,' UM'/' LENGTH =',F4.1,' MM'/'
```

128

```
         $SEPERATION ='
         4,F7.1,' UM'/)
68       FORMAT(' INPUT TRANSDUCER:',I5,' BARS; SPACING
         $IN UM:'/15F8.1/)
69       FORMAT(' OUTPUT TRANSDUCER:',I5,' BARS; SPACING
         $IN UM:'/15F8.1/)
61       FORMAT(//25X,'A SAMPLE OF VALUES'//' NO.',I5/'
         $FREQUENCY =',
         1F8.2/' FREE-YIG GAMMA =',2E16.5/' METALLIZED
         $GAMMA =',2E16.5/
         2' RADIATION RESISTANCE =',E16.5/' RADIATION
         $REACTANCE   ='
         3,E16.5/' INPUT IMPEDANCE =',2F14.5/' LUMPED
         $RAD. RES. =',F9.4/)
78       FORMAT(//3(1X,2F14.5,3X))
         STOP
         END
C
C
         SUBROUTINE DSPRSN(F,U1,U2,E,D,S,EPS,GAMMAF,
         $GAMMAR,GF,GR)
         DIMENSION D(5),E(5),S(5),K(5),KP(5)
         COMPLEX*8 J,U1,U2,K,G,K12,K32,K132,G34,G54,C1,
         $C2,CX2,CX4,CT3,CT1,K132P,G34P,G45P,C1P,C2P,GR,
         1CT5,TANH13,FG,GMA,DIF,GN,FGMA,KP,K12P,K32P,
         2,CX2P,CX4P,CT3P,CT1P,CT5P,TNH13P,GAMMAF,GAMMAR
         $FGDG,FGP,W0,GF
         DATA E0,U0,PY,GYRO/8.8419E-18,1.256637E-12,
         $3.141592654,2.8/
         J=CMPLX(0.0,1.0)
         W=2.0*PY*F*1.0E+06
         GMA=GF
4        DO 5 M=1,700
         CALL FUNCTN(U0,E0,W,D,E,S,J,PY,GMA,U1,U2,K,K12,
         $K32,K132,G34,G54,C1
         1,C2,CX2,CX4,CT3,CT1,CT5,TANH13)
         FGMA=CX4*(G54*C2+CT5)*(G34*C1+TANH13)-(G54*C1-
         $CT5)*(G34*C2-TANH13)
         IF(CABS(FGMA).LE.EPS) GO TO 13
         GN=GMA
         GMA=CSQRT((J*CLOG((G54*C1-CT5)*(G34*C2-TANH13)/
         $((G54*C2+CT5)*(G34*
         1C1+TANH13)))/(2.0*D(4)))**2-W*U0*(W*E0*E(4)-J*
         $S(4))*(U1**2-U2**2)/
         2U1)
         DIF=GN-GMA
         IF(CABS(DIF).LT.(1.0E-05*CABS(GN))) GO TO 13
```

```fortran
       IF(M.LE.10) GO TO 5
       GMA=(GMA+GN)/2.0
5      CONTINUE
       WRITE(6,103)M,GN,FGMA,DIF,GMA
103    FORMAT(10X,'THERE IS NO CONVERGENCE IN ',I3,'
      $ITERATIONS: FINAL VAL
      $UES WERE:'/25X,'GN=',2(E15.8,1X),5X,'FGMA=',
      $2(E15.8,1X)/25X,'DIF='
      $,2(E15.8,1X),5X,'GMA=',2(E15.8,1X))
       STOP
13     GAMMAF=GMA
14     WAVF=2.0*PY/CABS(GAMMAF)
15     GMA=GR
18     DO 19 M=1,700
       CALL FUNCTN(U0,E0,W,D,E,S,J,PY,GMA,U1,U2,K,K12,
      $K32,K132,G34,G54,C1
      1,C2,CX2,CX4,CT3,CT1,CT5,TANH13)
       FGMA=CX4*(G54*C1+CT5)*(G34*C2+TANH13)-(G54*C2-
      $CT5)*(G34*C1-TANH13)
       IF(CABS(FGMA).LE.EPS) GO TO 27
       GN=GMA
       GMA=CSQRT((J*CLOG((G54*C2-CT5)*(G34*C1-TANH13)/
      $((G54*C1+CT5)*(G34*
      1C2+TANH13)))/(2.0*D(4)))**2-W*U0*(W*E0*E(4)-J*
      $S(4))*(U1**2-U2**2)/
      2U1)
       DIF=GN-GMA
       IF(CABS(DIF).LT.(1.0E-05*CABS(GN))) GO TO 27
       IF(M.LE.10) GO TO 19
       GMA=(GMA+GN)/2.0
19     CONTINUE
       WRITE(6,103)M,GN,FGMA,DIF,GMA
       STOP
27     GAMMAR=GMA
28     WAVR=2.0*PY/CABS(GAMMAR)
       RETURN
       END
       SUBROUTINE FUNCTN(U0,E0,W,D,E,S,J,PI,GAM,U1,U2,
      $K,K12,K32,K132,G34,
      1G54,C1,C2,CX2,CX4,CT3,CT1,CT5,TANH13)
       DIMENSION D(5),E(5),S(5),K(5)
       COMPLEX*8 X,CSINH,CCOSH,CTANH,CCOTH,CCSCH,CSECH,
      $J,GAM,U1,U2,K,K12
      1,K32,K132,G34,G54,C1,C2,CX2,CX4,CT3,CT1,CT5,TANH13
       CSINH(X)=0.5*(CEXP(X)-CEXP(-X))
       CCOSH(X)=0.5*(CEXP(X)+CEXP(-X))
       CTANH(X)=CSINH(X)/CCOSH(X)
```

```fortran
      CCOTH(X)=CCOSH(X)/CSINH(X)
      CCSCH(X)=2.0/(CEXP(X)-CEXP(-X))
      CSECH(X)=2.0/(CEXP(X)+CEXP(-X))
      K(2)=-J*CSQRT(GAM**2+W*U0*(W*E0*E(2)-J*S(2)))
      K(4)=-J*CSQRT(GAM**2+W*U0*(W*E0*E(4)-J*S(4))*(
     $U1**2-U2**2)/U1)
      DO 1 I=1,5,2
1     K(I)=-J*CSQRT(GAM**2+W*U0*(W*E0*E(I)-J*S(I)))
      K12=K(1)/K(2)
      K32=K(3)/K(2)
      K132=K12*K32
      G34=-K(3)/(GAM**2+W*U0*U1*(W*E0*E(4)-J*S(4)))
      G54=-K(5)/(GAM**2+W*U0*U1*(W*E0*E(4)-J*S(4)))
      C1=U1*K(4)+J*GAM*U2
      C2=U1*K(4)-J*GAM*U2
      CX2=CEXP(2.0*K(2)*D(2))
      CX4=CEXP(2.0*K(4)*D(4))
      CT3=CTANH(K(3)*D(3))
      IF(D(1).EQ.1.0E+06) GO TO 2
      IF(D(5).EQ.1.0E+06) GO TO 5
      CT1=CTANH(K(1)*D(1))
      CT5=CTANH(K(5)*D(5))
      GO TO 6
2     IF(D(5).EQ.1.0E+06) GO TO 3
      GO TO 4
3     CT1=CMPLX(1.0,0.0)
      CT5=CT1
      GO TO 6
4     CT1=CMPLX(1.0,0.0)
      CT5=CTANH(K(5)*D(5))
      GO TO 6
5     CT1=CTANH(K(1)*D(1))
      CT5=CMPLX(1.0,0.0)
6     TANH13=((1.0-CX2)*(CT1*CT3+K132)-(1.0+CX2)*(K32*
     $CT1+K12*CT3))/((1.
     10-CX2)*(CT1+K132*CT3)-(1.0+CX2)*(K12+K32*CT1*CT3))
      RETURN
      END
         SUBROUTINE PLOT80 (X,Y,Z,Y1,Y2,M)
         DIMENSION X(M),Y(M),Z(M),G(80),H(9)
         DATA BL,ST,DA,VT,R1,R2/1H ,'*','-','¶','L','G'/
         N=80
         DY=(Y2-Y1)/8
         H(1)=Y1
         DO 12 K=1,8
12       H(K+1)=H(K)+DY
         WRITE(6,29)(H(L),L=1,9)
```

131

```
          DO 17 I=1,M
          NY=IFIX(N*(Y(I)-Y1)/(Y2-Y1)+0.5)
          DI=FLOAT(I)/5.-FLOAT(I/5)
          DO 20 J=1,N
          DJ=FLOAT(J)/10.-FLOAT(J/10)
          IF(DI.EQ.0.0)GO TO 25
          G(J)=BL
          GO TO 20
25        G(J)=DA
          IF(DJ.EQ.0.0)G(J)=VT
20        CONTINUE
          IF(NY.GT.N)GO TO 15
          IF(NY.LT.1)GO TO 16
          G(NY)=ST
          GO TO 17
15        G(N)=R2
          GO TO 17
16        G(1)=R1
17        WRITE(6,30)X(I),VT,(G(L),L=1,N),Y(I),Z(I)
30        FORMAT(1X,F7.1,2X,A1,80A1,2F12.4)
29        FORMAT('1',20X,'PLOT OF Y VERSUS X AND Z'///3X,
         $9(F10.2)/
     1    10X,'¶',8(9('-'),'¶'))
          RETURN
          END
C     SUBROUTINE TO COMPUTE FREQUENCY RESPONSE
C
          SUBROUTINE FQRP(Y1,PP,Y2,RS,ZR1,ZF1,ZIL,M)
          COMPLEX*8 Y1(3,3),PP(3,3),Y2(3,3),ZR1,ZF1,W1,W2,
         $W3,W4,W5,W6
          COMPLEX*8 A,B,C,D,E,NUM,VLS
          DIMENSION ZIL(152)
          GS=1./RS
C
          W1=Y1(2,2)-PP(1,1)
          W2=Y1(1,1)+1.0/ZR1
          W3=Y1(3,3)+GS
          W4=-PP(2,2)+Y2(1,1)
          W5=Y2(2,2)+1.0/ZF1
          W6=Y2(3,3)+GS
          NUM=((W2*Y1(2,3)-Y1(2,1)*Y1(1,3))*(Y2(2,1)*Y2(3,2
         $)-Y2(3,1)*W5))
          A=W2*W1*W3+Y1(1,2)*Y1(2,3)*Y1(3,1)+Y1(1,3)*Y1(2,1
         $)*Y1(3,2)
          B=Y1(1,3)*Y1(3,1)*W1+Y1(1,2)*Y1(2,1)*W3+Y1(2,3)*
         $Y1(3,2)*W2
          C=W4*W5*W6+Y2(1,2)*Y2(2,3)*Y2(3,1)+Y2(1,3)*Y2(2,1
```

132

```fortran
     $)*Y2(3,2)
      D=Y2(1,3)*Y2(3,1)*W5+Y2(1,2)*Y2(2,1)*W6+Y2(2,3)*
     $Y2(3,2)*W4
      E=PP(1,2)*PP(2,1)*(Y1(1,3)*Y1(3,1)-W3*W2)*(W5*W6
     $-Y2(2,3)*Y2(3,2))
      VLS=-GS*PP(2,1)*NUM/((A-B)*(C-D)+E)
      ZIL(M)=20.*ALOG10(CABS(VLS))
      RETURN
      END
C     SUBROUTINE TO CONVERT S-PARAMETERS TO Y-PARAMETERS
      SUBROUTINE STOY(S,ZF2,ZR2,RS,Y)
      COMPLEX*8 S(3,3),S1,S2,S3,A11,A12,A13,A21,A22,A23
      COMPLEX*8 A31,A32,A33,DET1,DET1P,DET1N,DET2,DET2N
     $,DET2P,DET3
      COMPLEX*8 DET3P,DET3N,DEN1,DEN2,DEN3,Y(3,3),ZF2,
     $ZR2,ZR,ZF,Z1,Z2
      ZR=CSQRT(ZR2)
      ZF=CSQRT(ZF2)
      Z1=ZR/ZF
      Z2=ZF/ZR
      S1=S(1,1)+Z2
      S2=S(2,2)+Z1
      S3=S(3,3)+1.0
      DET1P=S(1,1)*S2*S3+S(1,2)*S(2,3)*S(3,1)+S(1,3)*
     $S(2,1)*S(3,2)
      DET1N=S3*S(2,1)*S(1,2)+S2*S(3,1)*S(1,3)+S(1,1)*
     $S(3,2)*S(2,3)
      DET1=DET1P-DET1N
      DET2P=S1*S(2,2)*S3+S(1,2)*S(2,3)*S(3,1)+S(1,3)*
     $S(2,1)*S(3,2)
      DET2N=S3*S(2,1)*S(1,2)+S(3,1)*S(2,2)*S(1,3)+
     $S(3,2)*S(2,3)*S1
      DET2=DET2P-DET2N
      DET3P=S1*S2*S(3,3)+S(1,2)*S(2,3)*S(3,1)+S(1,3)*
     $S(2,1)*S(3,2)
      DET3N=S(1,2)*S(2,1)*S(3,3)+S(2,3)*S(3,2)*S1+
     $S(3,1)*S(1,3)*S2
      DET3=DET3P-DET3N
      A11=(S2*S3-S(2,3)*S(3,2))/DET1
      A21=(S(2,3)*S(3,1)-S3*S(2,1))/DET1
      A31=(S(2,1)*S(3,2)-S(3,1)*S2)/DET1
      A12=(S(1,3)*S(3,2)-S3*S(1,2))/DET2
      A22=(S1*S3-S(3,1)*S(1,3))/DET2
      A32=(S(1,2)*S(3,1)-S1*S(3,2))/DET2
      A13=(S(1,2)*S(2,3)-S2*S(1,3))/DET3
      A23=(S(1,3)*S(2,1)-S(2,3)*S1)/DET3
      A33=(S1*S2-S(1,2)*S(2,1))/DET3
```

```
        RSS=SQRT(RS)
        DEN1=ZF*All+ZR
        DEN2=ZR*A22+ZF
        DEN3=RSS*(A33+1.0)
        Y(1,1)=(All/ZF-1.0/ZR)/DEN1
        Y(2,1)= (A21*(1.0/ZR+Z1/ZF))/DEN1
        Y(3,1)=2.0*A31/(RSS*DEN1)
        Y(1,2)=A12*(1.0/ZF+Z2/ZR)/DEN2
        Y(2,2)= (A22/ZR-1.0/ZF)/DEN2
        Y(3,2)=A32*2.0/(RSS*DEN2)
        Y(1,3)=A13*(1.0/ZF+Z2/ZR)/DEN3
        Y(2,3)= A23*(Z1/ZF+1.0/ZR)/DEN3
        Y(3,3)=(A33-1.0)/(RSS*DEN3)
        RETURN
        END
C       SUBROUTINE TO CALCULATE THE WAVE PORT PARAMETERS
C
        SUBROUTINE SW(ZF1,ZR1,A,B,C,D,SS)
        COMPLEX*8 ZF1,ZR1,A,B,C,D,SS(3,3)
        COMPLEX*8 S11NUM,S11DEN,DETN,S21NUM,S21DEN
        COMPLEX*8 S22NUM,S22DEN,S12NUM,S12DEN,JJ
        JJ=CMPLX(0.0,1.0)
        S11NUM=-C*ZF1-D+A+B/ZF1
        S11DEN=-A*ZR1-D*ZF1+B+C*ZF1*ZR1
        SS(1,1)=S11NUM/S11DEN*ZR1
        DETN=B*C-A*D
        S21NUM=DETN*(ZF1+ZR1)
        S21DEN=ZF1*(C*ZR1-D)-(A*ZR1-B)
        SS(2,1)=S21NUM/S21DEN
        S22DEN=C*ZR1*ZF1-A*ZR1-D*ZF1+B
        S22NUM=D+B/ZR1-C*ZR1-A
        SS(2,2)=S22NUM/S22DEN*ZF1
        S12NUM=-(ZF1+ZR1)
        S12DEN=ZR1*(C*ZF1-A)-(ZF1*D-B)
        SS(1,2)=S12NUM/S12DEN
        RETURN
        END
C       SUBROUTINE TO CALCULATE THE THIRD PORT PARAMETERS
C
        SUBROUTINE SE(ZIN,RS,ZF2,ZR2,RM2,RM1,SS)
        COMPLEX*8 ZIN,ZF2,ZR2,SS(3,3),JJ,A,B,C
        JJ=CMPLX(0.0,1.0)
        SS(3,3)=(ZIN-RS)/(ZIN+RS)
         THETA1=AIMAG(RM1/ZIN)/REAL(RM1/ZIN)
         THETA2=AIMAG(RM2/ZIN)/REAL(RM2/ZIN)
         TA1=ATAN(THETA1)
         TA2=ATAN(THETA2)
```

```
            C=2.0*ZIN/(ZIN+RS)
            A=(RS/ZF2)
            B=(RS/ZR2)
            SS(1,3)=C*CEXP(JJ*TA2)*CABS(ZR2/ZIN)*SQRT(RM2/
      $ABS(REAL(ZR2)))
            SS(2,3)=-C*CEXP(JJ*TA1)*CABS(ZF2/ZIN)*SQRT(RM1/
      $ABS(REAL(ZF2)))
            SS(3,1)=A*SS(2,3)
            SS(3,2)=B*SS(1,3)
            RETURN
            END
C          SUBROUTINE  TO CASCADE ZMICROSTRIPS
C       G IS THE FIRST BOX AND H IS THE SECOND
C
            SUBROUTINE CASCAD(A,B,C,Y,F)
            COMPLEX*8 ABC,CAB,AB,BA,Y(3,3),B(3,3),C(3,3),
      $A(3,3),ZM,BZMA
            BZMA=B(1,1)-A(2,2)
            BA=B(1,2)*A(1,2)
            AB=B(2,1)*A(2,1)
            ZM=C(1,1)-B(2,2)+B(2,1)*B(1,2)/BZMA
            ABC=(B(2,1)*A(2,3)/BZMA-C(1,3))/ZM
            CAB=(C(3,1)-A(3,2)*B(1,2)/BZMA)/ZM
            Y(1,1)=A(1,1)+A(2,1)*A(1,2)/BZMA-BA*AB/(BZMA*BZMA*ZM)
            Y(1,2)=B(1,2)*C(1,2)*A(1,2)/(BZMA*ZM)
            Y(1,3)=A(1,3)+A(1,2)*A(2,3)/BZMA-BA/BZMA*ABC
            Y(2,1)= B(2,1)*C(2,1)*A(2,1)/(BZMA*ZM)
            Y(2,2)=(C(2,2)-C(2,1)*C(1,2)/ZM)
            Y(2,3)=(C(2,3)+C(2,1)*ABC)
            Y(3,1)=A(3,1)+A(3,2)*A(2,1)/BZMA+AB*CAB/BZMA
            Y(3,2)=C(3,2)-C(1,2)*CAB
            Y(3,3)=C(3,3)+A(3,3)+A(3,2)*A(2,3)/BZMA+ZM*CAB*ABC
C          WRITE(6,34)
34          FORMAT(' MIN')
C          WRITE(6,*)F,Y
            RETURN
            END
C   SUBROUTINE TO FIND Y-PARAMETERS OF LAND REGION
            SUBROUTINE PATH(ZF2,ZR2,TZ2,GF2,A0,GR2,PP)
            COMPLEX*8 ZF2,ZR2,TZ2,GF2,GR2,PP(3,3),WF,WR,AP,
      $BP,CP,DP
38          WF=CEXP(-GF2*A0*1.0E-04)
            WR=CEXP(-GR2*A0*1.0E-04)
            AP=(ZF2*WF+ZR2*WR)/TZ2
            BP=(ZF2*ZR2*(WF-WR))/TZ2
            CP=(WF-WR)/TZ2
            DP=(ZF2*WR+ZR2*WF)/TZ2
```

```
PP(1,1)= AP/BP
PP(1,2)=-1.0/BP
PP(2,1)=-(AP*DP-BP*CP)/BP
PP(2,2)= DP/BP
RETURN
END
```

3.1 Linearly Dispersive Time-Delay Control Of Magnetostatic Surface Wave By Variable Ground Plane Spacing

3.1.1 Introduction

The propagation characteristics of magnetostatic waves in expitaxial yttrium garnet (YIG) films have been extensively investigated both experimentally and theoretically for a number of years (1-4). These studies have shown that the delay versus frequency characteristics of MSSW delay lines of a YIG film spaced from a ground plane are function of the saturation magnetization, bias field, YIG film thickness, and ground plane spacing. A study of how different parameters affect the delay characteristics of surface waves indicated that dispersion control by ground plane spacing is most effective (4). This chapter described the theoretical and experimental results on the theoretical simulation and experimental evaluation of a magnetostatic surface wave variable ground plane spacing delay line with linear group delay.

3.1.2 Theoretical Simulation

Fig. 3.1 shows the variation of the group delay with frequency for MSSW delay lines with ground plane spacing (Ti) and propagation length (Li) as adjusting parameters. The YIG film thickness used in these calculations is 30 uM. Examination of this figure indicates that it is possible to achieve a linear variation of delay by adjusting the length of the short section (Li) of the step ground plane as shown in Fig. 3.2. A nine step ground plane structure is selected,
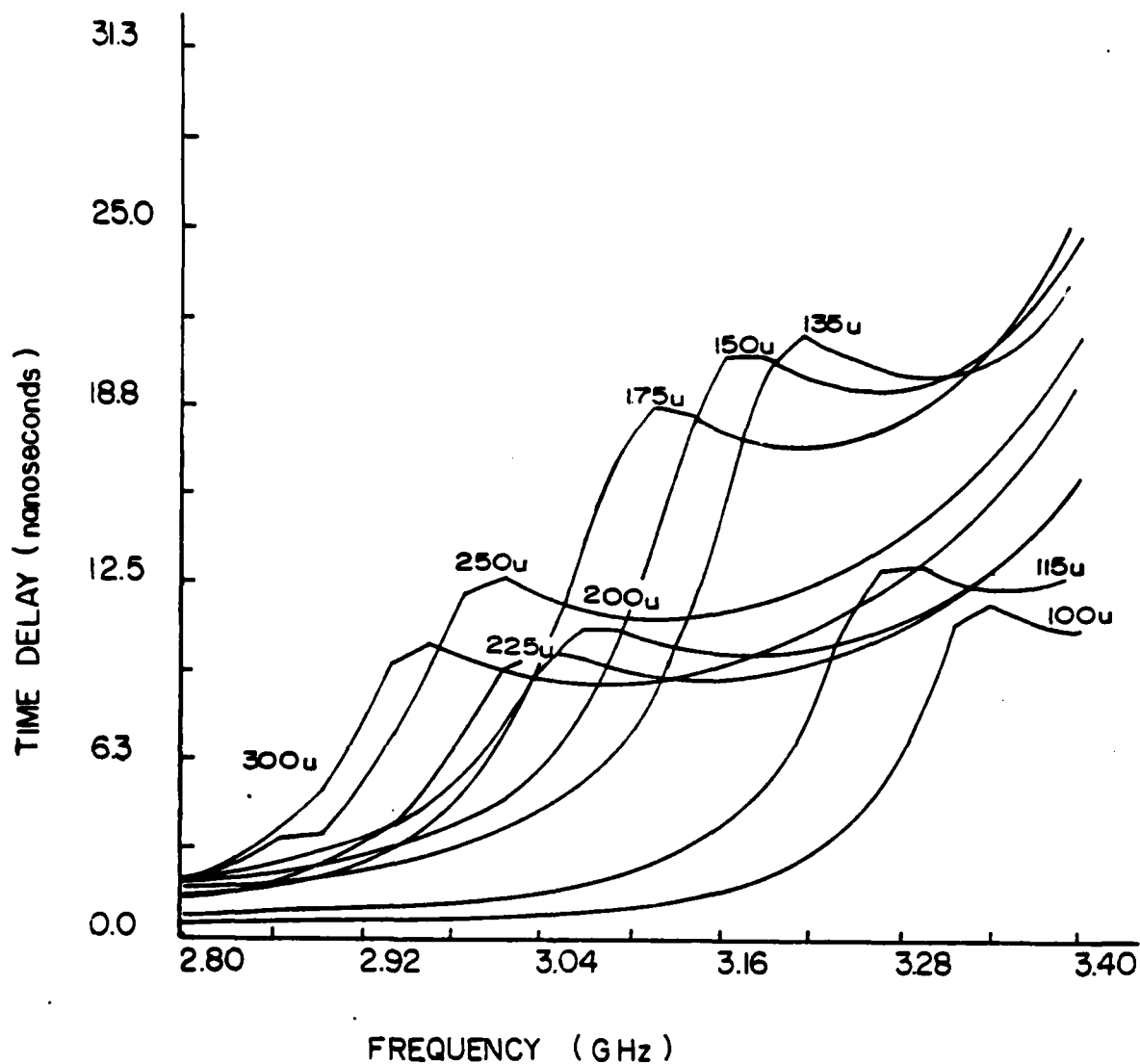
Fig. 3.1 Variation of group delay with frequency for MSSW delay lines with ground plane spacing (Ti) and propagation distance (Li) as adjusting parameters.

138
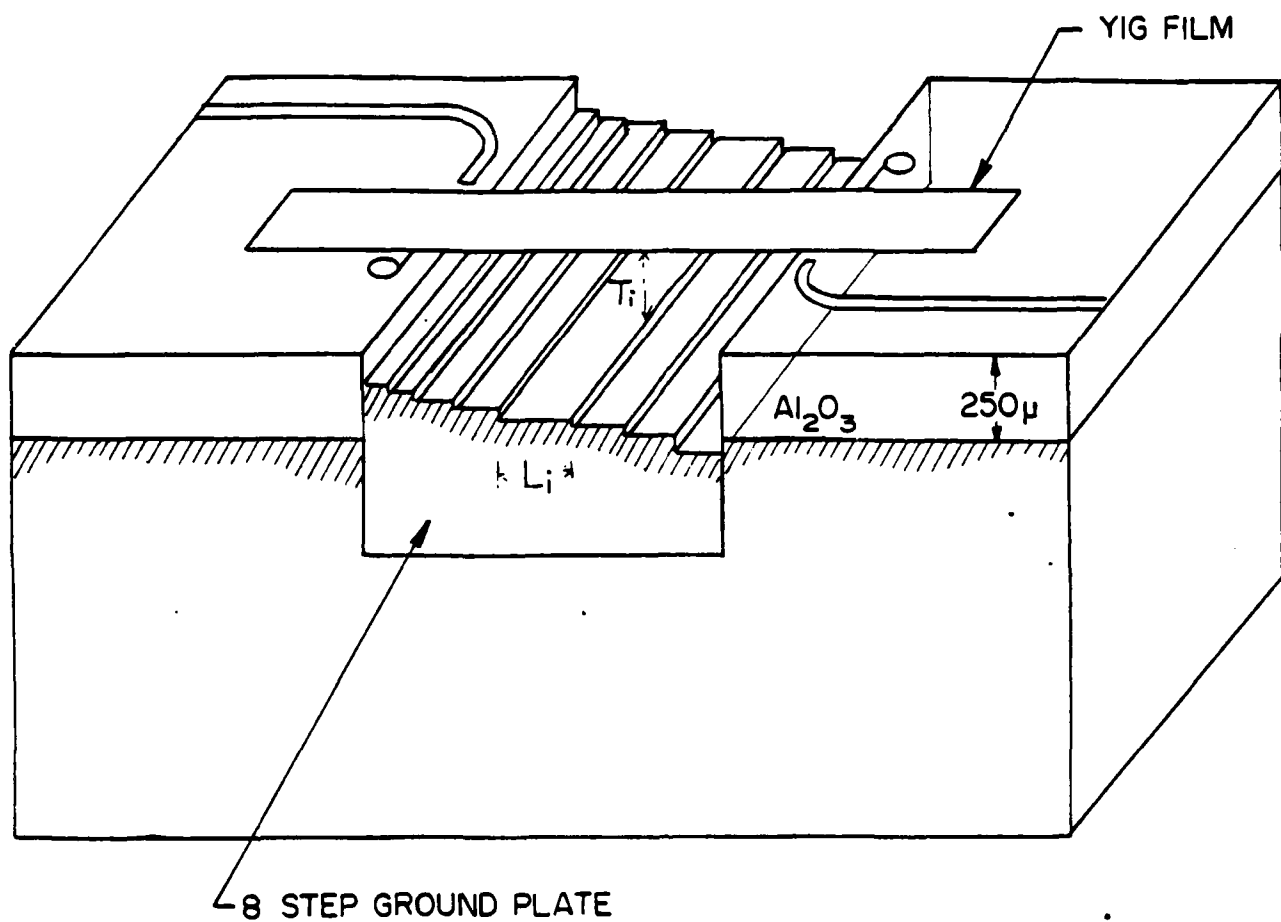
Fig. 3.2   MSSW Delay line with stepped ground plane

139

with a eight steps ground plane in the middle of this MSSW steped ground plane delay line. The separation of this eight steps ground to the YIG film can be adjusted by a pair of set screw . The nineth step in this MSSW delay is fixed by the substrate thickness which is 250 uM with propagation length can be adjusted by changing the single bar transducer separation to the edge of the substrate photographically. The length of each section is then optimized to provide a minimun deviation from quadratic phase over the linearized delay bandwidth. The linear time delay characteristic which is obtained by summing the individual time delay corresponding to each section of the MSSW 9 stepped ground plane structure, is shown in Fig. 3.3 A linear regression fit is also shown in this figure which indicated a linear delay region between 2.89 to 3.33 GHz with a positive slope of 26.6 nsec/100 MHz for the nine stepped ground plane structure shown in Table 3.1. The calculated phase error in degrees from a quadratic phase of this linear delay region between 2.89 to 3.33 is shown in Fig. 3.4. The R.M.S. deviation from quadratic phase over this 440 MHz bandwidth is 8 degrees. The corresponding time bandwidth product (TBP) is near 120 for this nine stepped ground plane MSSW theoretical simulated linear delay line.

3.1.3 Experimental Evaluation

Due to difficulty and long waiting period for the fabrication of the eight stepped centre ground plane, a continuously variable ground plane is used to provide the

140
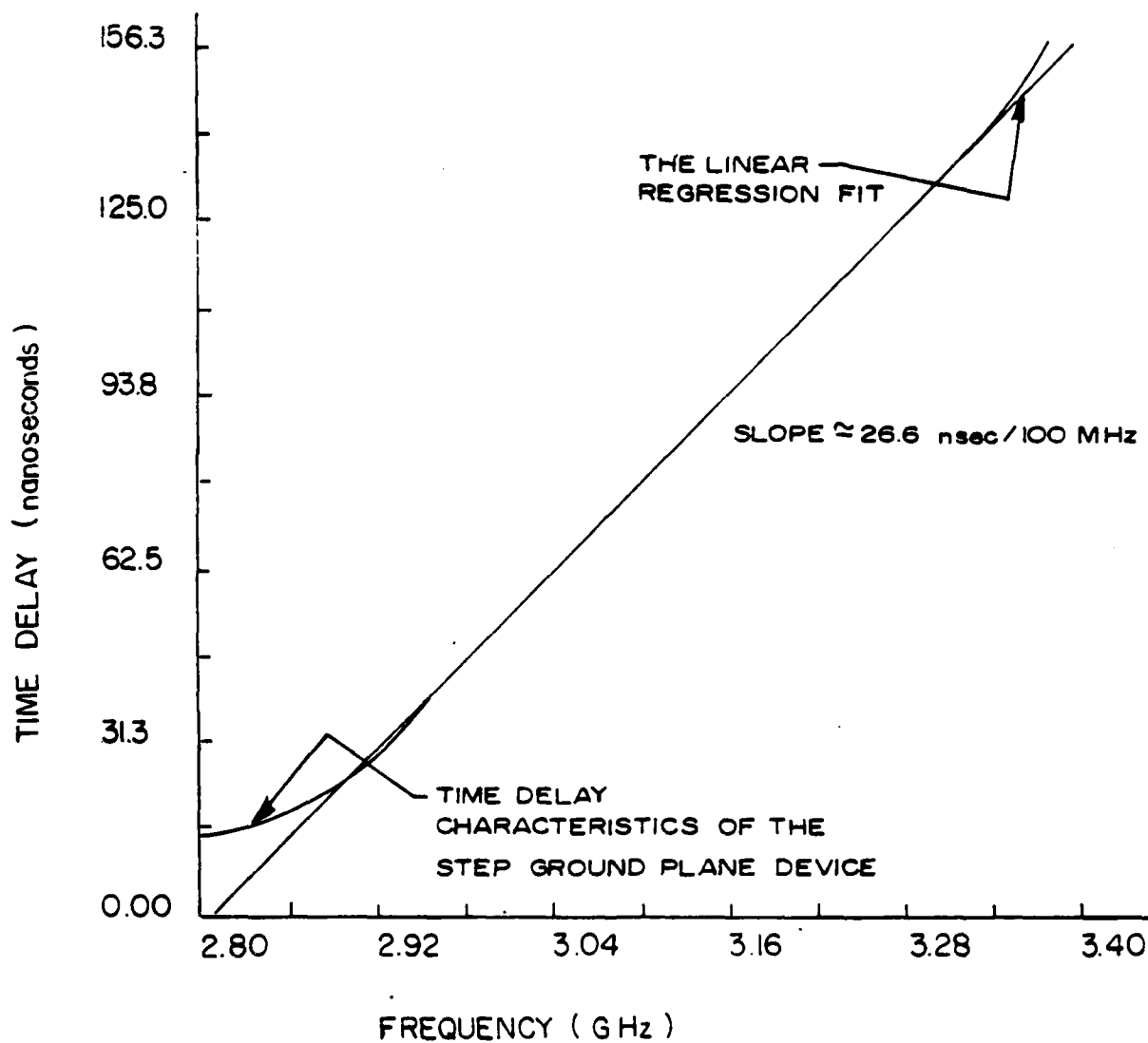
Fig. 3.3 The summation of the individual time delay section in the 9-step ground plane structure, with dimension shown in table 2.1, results a linear time delay characteristic between 2.89 to 3.33 GHz. Thickness of YIG is 30 uM.

141

Ti(uM)	Li(cm)
300	.18
250	.20
225	.15
200	.15
175	.23
150	.22
135	.20
115	.10
100	.07

Table 2.1   Ground plane spacings and lengths for a nine-
              section delay line
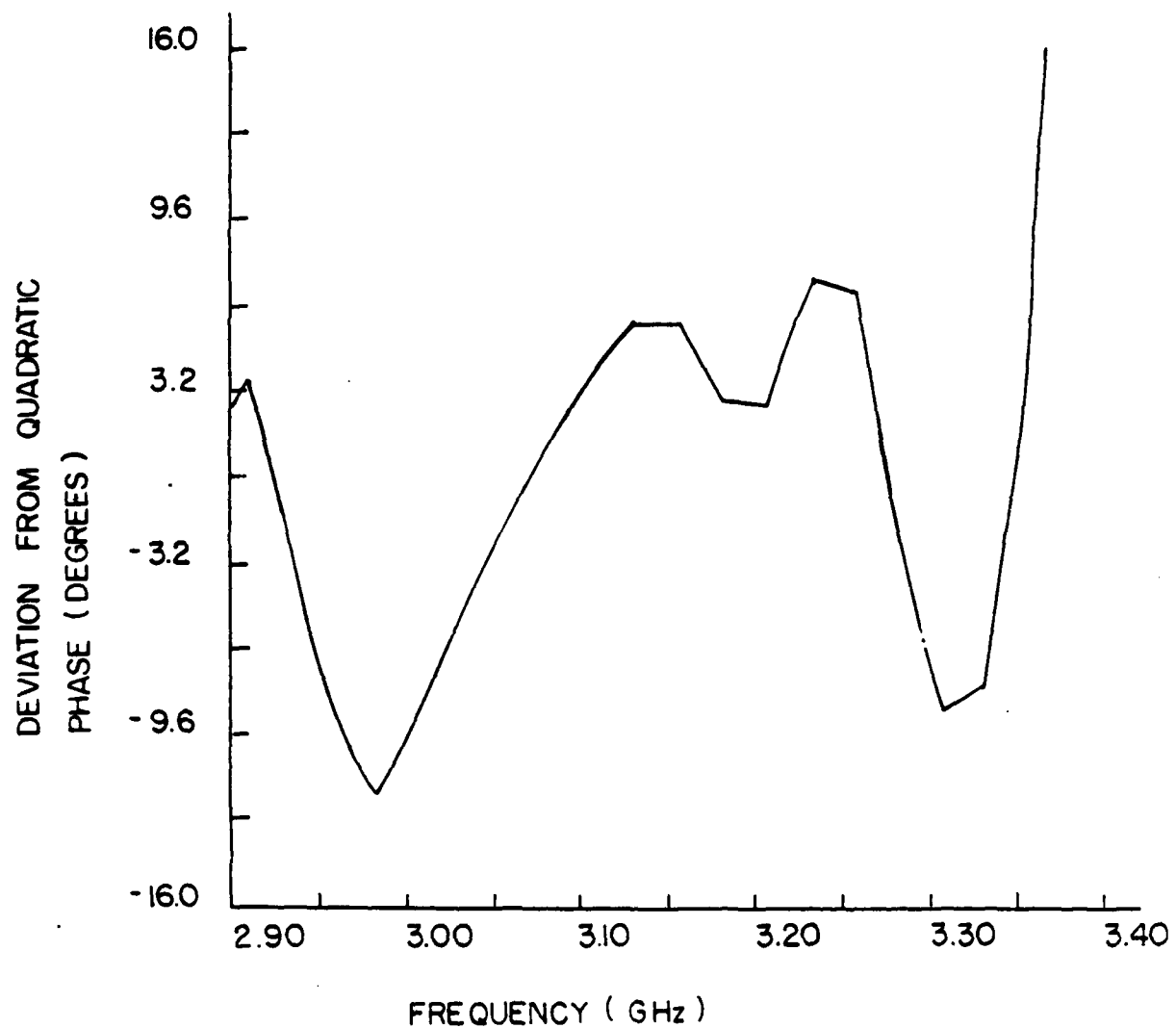
Fig. 3.4   The quadratic phase error of the linear delay
region of the 9-step ground plane structure
The R.M.S. deviation from quadratic phase in this
bandwidth is 8 degrees.

143

continuous variation of ground plane spacing to the YIG film along the propagation direction of the MSSW delay line. The separation of this continuously variable ground plane to the YIG film can be adjusted by changing structure of the ground plane and varying the distance of this ground to the film by a pair of set screw.

Fig. 3.5 shows a sketch of the MSSW variable ground plane delay line. The device is in a "flipped" configuration with the YIG film flipped over the single bar microstrip transducer. A pair shorted-circuited 50 uM-wide, 3 mm-long, and 3 uM-thick microstrip couplers are used for the lunching and receiving of the microwave energy for MSSW propagation along the YIG film. A 25 uM-thick 3 mm-wide and 15 mm-long YIG film grown by liquid phase epitaxy on a 500 uM-thick gadolinium gallium garnet (GGG) substrate was used for the delay measurement. The HP 8409B automatic network analyzer was used to measure the reflection and transmission parameters of the device under test.

The group delay was then obtained from the S12 phase data by calculation of phase slope. Since this is a differentiation process, the resolution is determined both by the frequency aperture (f) and the phase detector resolution of the network analyzer. By increasing the frequency aperture and the corresponding phase different, an averaging effect is performed to reduce the time delay ripples. A 30 MHz frequency aperture is chosen in order ot optimize the calculated time dealy obtained from the automatic network analyzer phase measurement. A modification of the control

144

MICROSTRIP TRANSDUCER

GGG

YIG

Al_2O_3

Al_2O_3

T_i

L_i
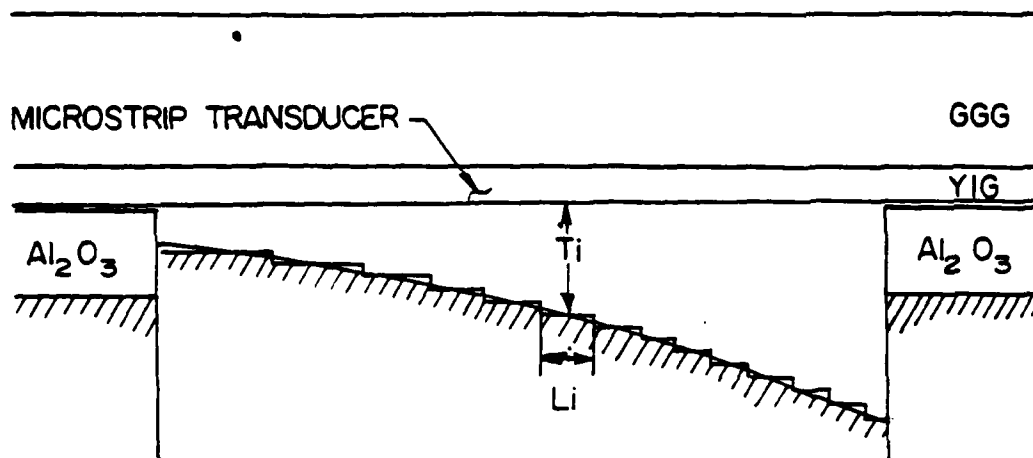
A 15 STEP GROUND PLANE MODEL IS USED TO
OBTAIN THE THEORETICAL CASCADED DELAY
CHARACTERISTIC

i	T_i (μm)	L_i (cm)
1	800	.0516
2	750	.0253
3	700	.0303
4	650	.0303
5	600	.0357
6	550	.0506
7	500	.0648
8	450	.0901
9	400	.0972
10	350	.1245
11	300	.2000
12	250	.1708
13	200	.2260
14	150	.1190
15	140	.1300

Fig. 3.5 Sketch of continuously variable ground-plane MSSW
delay line

program of the automatic network analyzer is performed to computed the absolute phase change as a function of frequency over the frequency bandwidth of interest. For a linear delay bandwidth, the corresponding absolute phase function is a quadratic function of frequency (For a constant delay bandwidth, the corresponding absolute phase fuction is a linear function of frequency). A root mean square fit is then performed for this experimental determined phase data. The deviation from quadratic phase defined as the difference between the quadratic fit phase function to the experimental phase data is then used as the parameters to determine the deviation from linear delay (quadratic phase) over the bandwidth of interest of the device under test.

By carefully adjusting the separation of the continuously variable ground plane to the YIG film , linear delay of bandwidth up to 500 MHz can be experimental obtained with phase error less than 20 degrees. The slope of the linear region can also be adjusted by changing the structure of the continuously variable ground plane. Fig. 3.6 shows the experimental delay measurement of one of the device under test. A linear delay of 500 MHz bandwidth (between 2.62 to 3.12 GHz) with a slope of 15.3 nsec/100 MHz was observed. Fig. 3.7 shows the quadratic phase error of this device in the linear delay region. The corresponding R.M.S. phase error is 13 degrees. The insertion loss over the linear region is between 15 to 20 dB (unmatched). The separation of
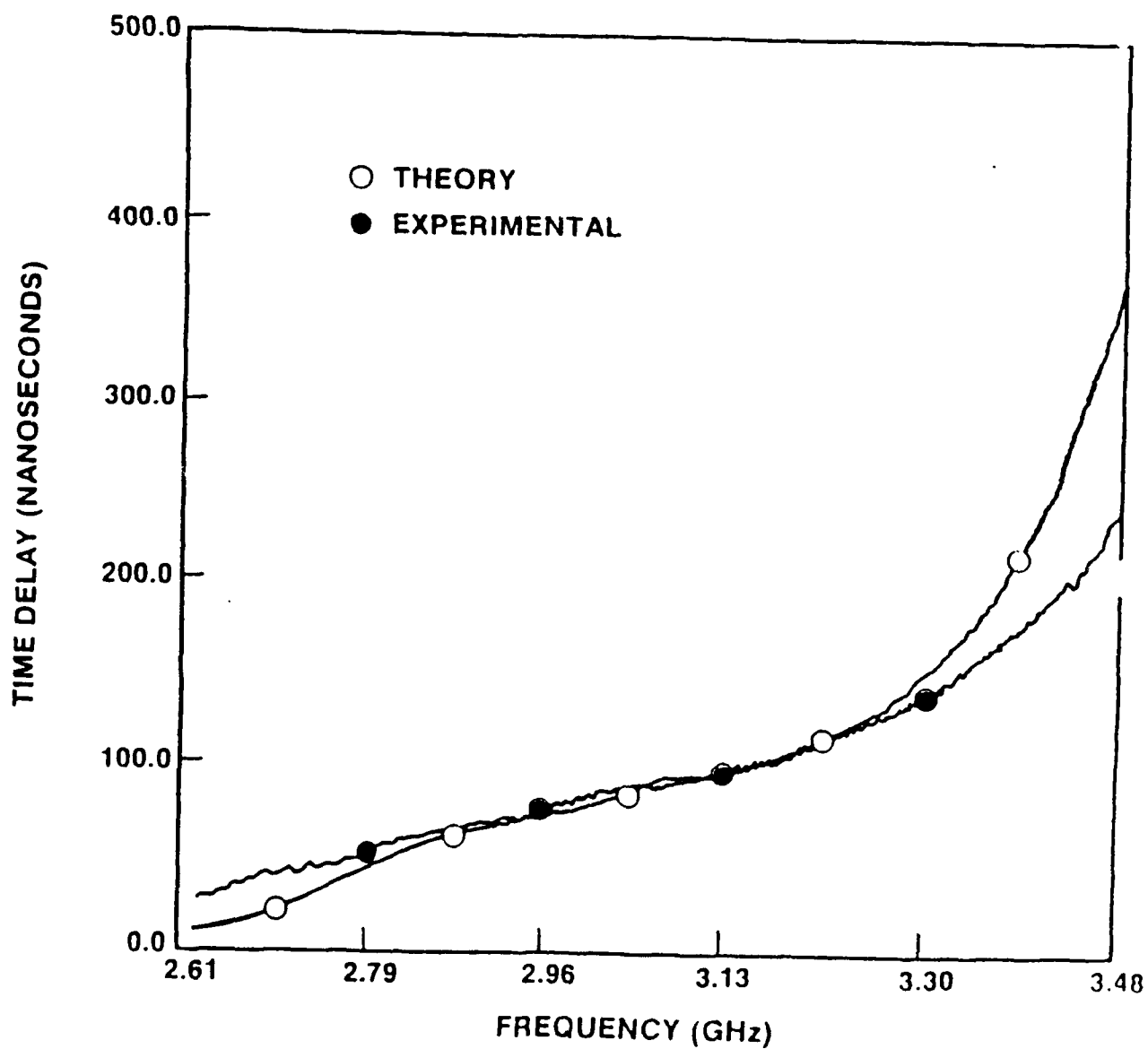
Fig. 3.6   Experimental dispersion curve for a variable
ground plane MSSW delay line. The theoretical
curve was calculated for a 15 step model.
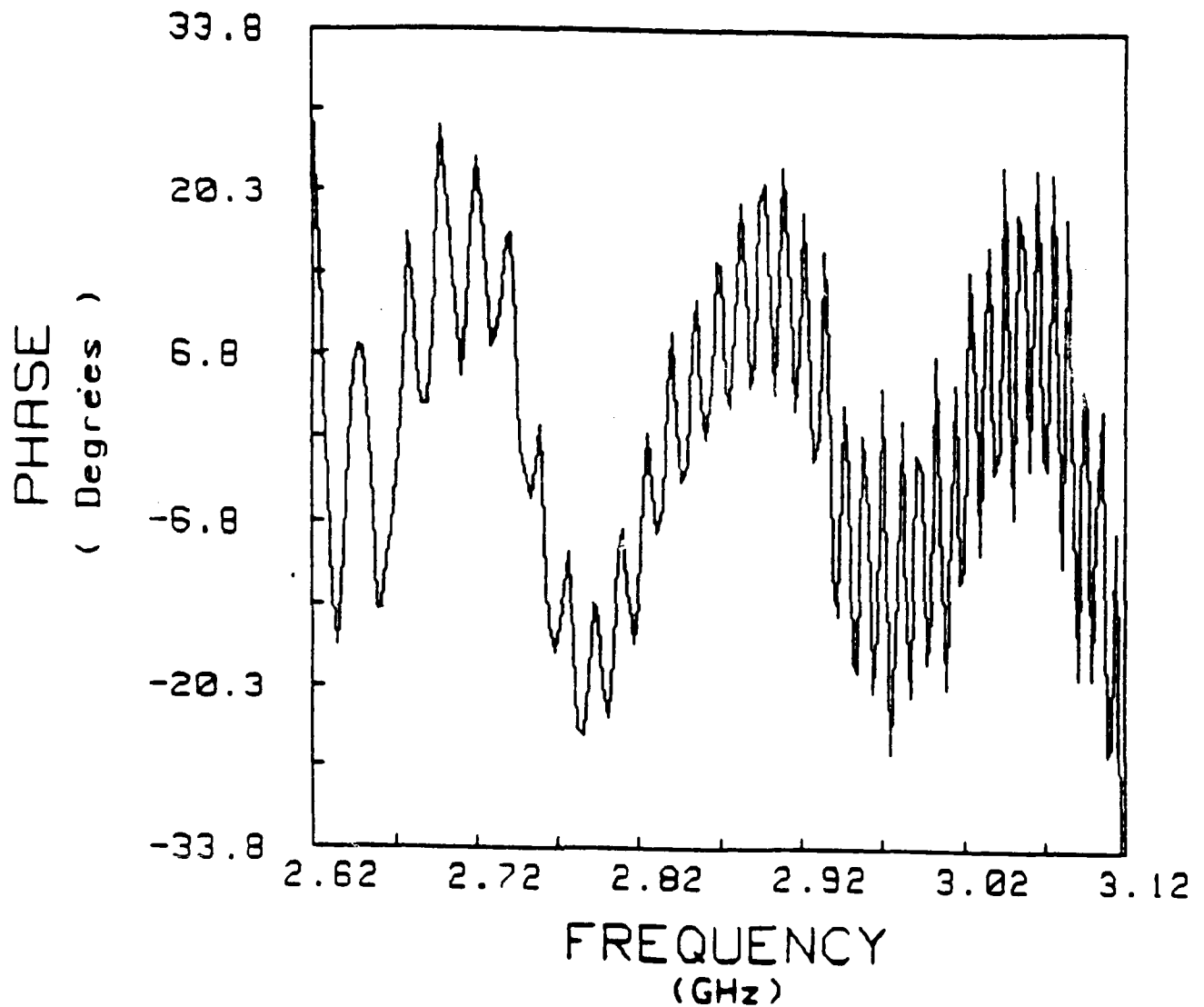
Fig. 3.7 The quadratic phase error of the continuously variable ground plane MSSW delay line
The R.M.S. phase error is 13 degrees over the linear delay bandwidth.

148

this continuously variable ground plane to the YIG is roughly determined by removing the "flipped" over YIG film and measuring the profile of the MSSW delay line along the direction of propagation. A 50 uM air gap was added to the measuring data to represent the air gap which is unavoidable in the flipped configuration. A 15-step ground plane structure ,with dimensions given is Fig. 3.5, was then used to approximate the continuously variable ground plane structure measured. The computing delay characteristic of this 15-step model is also in Fig. 3.6. The difference between this computing delay characteristic to the expertimental linear delay characterictic is quite large. This large discrepancy is due to the error associated with the measurement of the bias field strength, YIG thickness,and separation of the ground plane to the YIG film.

Applications of these MSSW linear delay devices include pulse compression system (5,6), compressive receivers and variable time delay devices utilizing a cascade configuration with a linearized backward volume wave device (7,8).

3.2 Electronically Variable Time Delays Using Cascaded Magnetostatic Wave Delay Lines

3.2.1 Introduction

Two features which make magnetostatic wave (MSW) devices attractive are (a) an operating frequency range above one GHz and (b) electronic tunability. Both of these features are required for electronically variable time delay components used in phased array radar and communication systems. The basic architecture for variable time delay device based on MSW technology was described originally by Setheres, Owens and Smith (7). A Schematic of their approach is illustrated in Figure 3.8. Briefly, two MSW delay lines, one biased to operate in the backward volume wave (MSBVW) mode and the other biased to operate in the surface wave (MSSW) mode, are cascaded together. The dispersion (i.e., the delay vs. frequency) of the MSSW device has a positive slope, while the slope of the MSBVW dispersion is negative. If the absolute magnitudes of these two slopes are identical , and if the dispersions are linear, then the net dispersion of the cascaded device will be zero over a common frequency band. If the frequency domain of one delay line is shifted by changing the strength of its applied biasing field, then the absolute delay of the cascaded device will also be shifted. Thus, different values of constant delay can be obtained by simply changing the strength of the bias by a small amount. One impediment to the realization of a device of this with large bandwidth is the fact that in

150
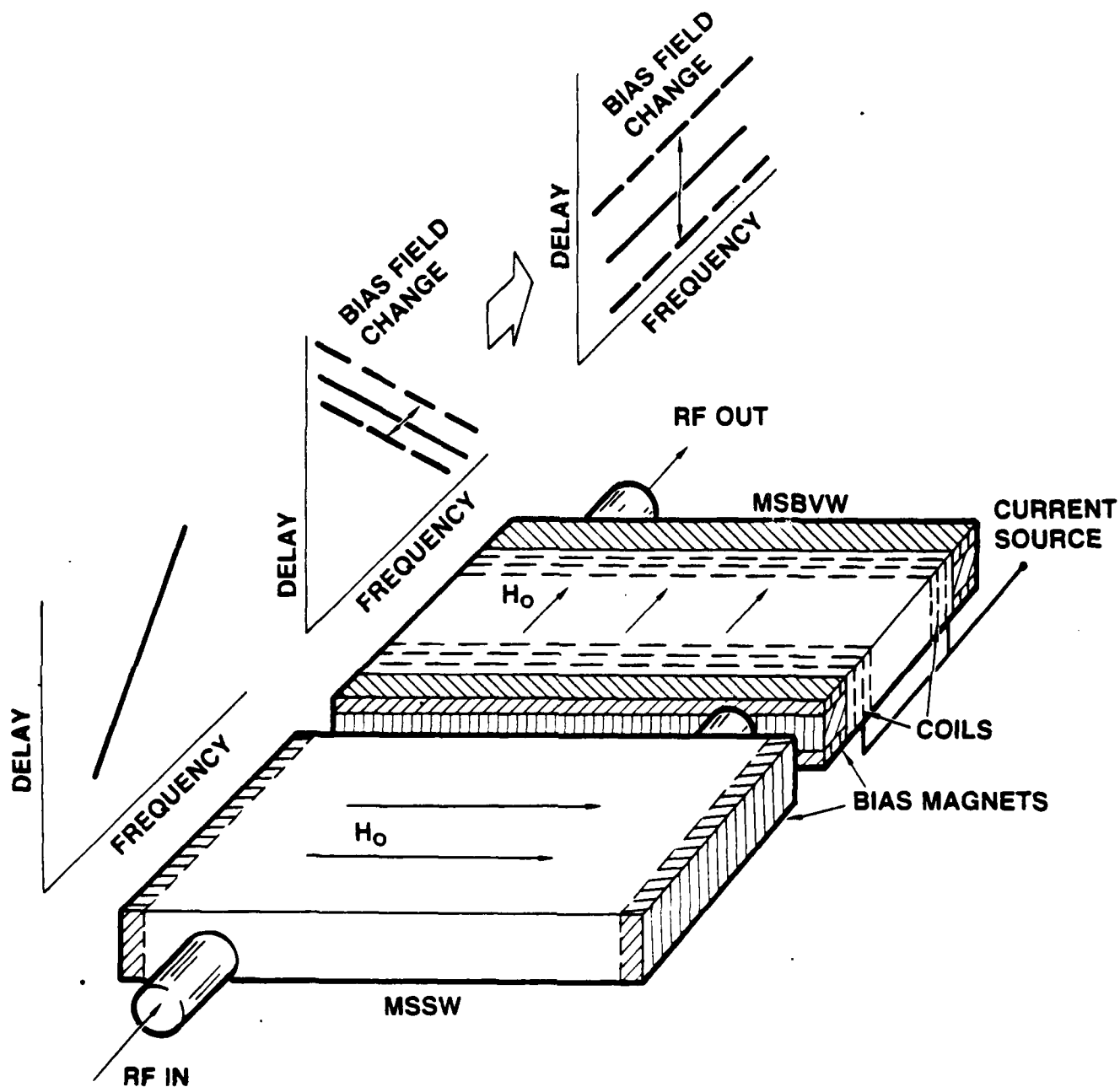
Fig 3.8   Schematic of the MSW variable time dlay device

general the dispersion of typical MSW devices is non-linear. In the original experiments no attempt was made to linearize the individual dispersions. Even so the results were generally encouraging. In this chapter an improved version the the original device in which care has been taken to linearize the dispersion for both the surface and backward modes is reported.

3.2.2 Theory

From the study of the dispersive characteristics for MSSW and MSBVW delay line, it is found that the shape of the dispersion curve is strongly dependent on the thickness of the film and the spacing above the ground plane. It has been demonstrated (9) that the linearity of the dispersion can be substationally improved by carefully adjusting the spacing between the ground plane and the YIG film. Thus, the ground spacing technique was incorporated into the design of the delay line components of the cascaded device.

A linear MSBVW dispersion curve can be obtained in a straight forward manner by using a 35 uM thick layer of YIG spaced 250 uM above the ground plane. This spacing is very close to the standard for MSW delay lines and no special fabrication techniques are required, other than some polishing of the dielectric spacer. It requires a much closer ground plane spacing to achieve the same results with the MSSW mode and past experience has shown that ground current losses increase as the spacing decreases.

To circumvent this problem a variable ground plane structure

of the type reported in section by Chang, Owens and Carter (10) was selected for the MSSW device. The essence of this approach is that the YIG delay line is held above a ground plane whose distance from the YIG film is a function of the path length. A schematic of the technique is shown in Fig. 3.5. The advantage of this approach is that in principle optimum dispersion control can be achieved and the minimum spacing required is greater than in the uniform spacing case.

For both modes of propagation the figure of merit is defined in terms of the phase deviation from the appropriate theoretical phase vs. frequency curve. If the delay time is a linear function of the frequency then, the phase dependence on frequency is quadratic. On the other hand, if the delay time is constant over the frequency band, then the phase is a linear function of frequency. In principle, it is possible to achieve close to zero deviation from quadratic phase over a bandwidth of 500 MHz centered at 3 GHz using the ground plane spacing techniques described in chapter 2.

3.2.3 Experimental Results

A cascaded device was prepared using a MSSW delay line with a variable ground plane and a MSBVW delay line with a YIG film thickness 35 microns and ground plane spacing of 254 microns. The characteristic of the MSBVW delay line is shown in Fig. 3.9. The variable ground plane was prepared by polishing a ground plane into a smooth curve. The ground plane curve was optimized by alternating vs. frequency measurements with block sanding until the desired dispersion
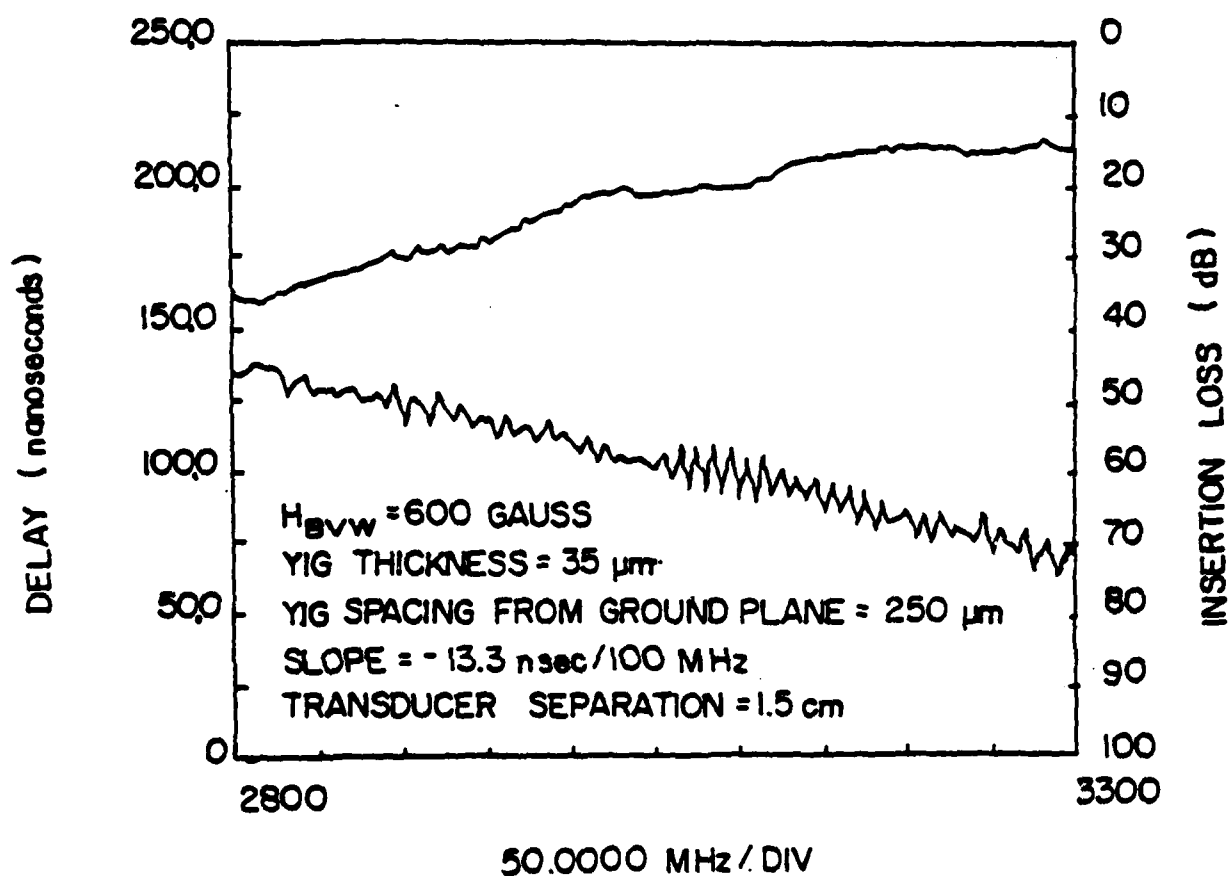
Upper curve: Transmission loss for the MSBVW
              delay line.
Lower curve: Delay versus freauency with arrows
              defining a band of linear delay.

Fig. 3.9   The characteristic of the MSBVW delay line

154

curve was obtained.

The delay line material was prepared by growing YIG films on one inch diameter gallium gadolinium garnet (GGG) wafers using the liquid phase epitaxy (LPE) method. The YIG thickness for the MSSW delay line was 25 microns, while the thickness of the MSBVW delay line YIG was 35 microns. The wafers were cut into bars for delay line use, and the ends of these bars were beveled to reduce reflections.

The individual delay lines were experimentally evaluated with an automatic network analyzer. Large laboratory electromagnets were used to supply the necessary d.c. bias. In the final configuration both the MSSW delay line and the MSBVW delay line exhibited R.M.S. phase deviation from quadratic of about 13 degree over approximately 500 MHz bandwidth centered at 3 GHz. Experimental plots from the network analyzer of delay time vs. frequency for both MSSW and MSBVW devices are given in Figure 3.10. The slopes of these curves are 9.6 nsec/100 MHz and -9.7 nsec/100 MHz, respectively.

It is found that by adjusting the d.c. bias field of the virable ground plane MSSW delay line, the dispersion characteristic of the linear delay bandwidth becomes nonlinear. In order the deviation from quadratic phase over the frequency band of interest increases substantially by changing the bias field. For the backward volume wave delay line although the linear bandwidth is changed by adjusting the bias field but the dispersion characteristic over the bandwidth of interest remains linear with a slightly
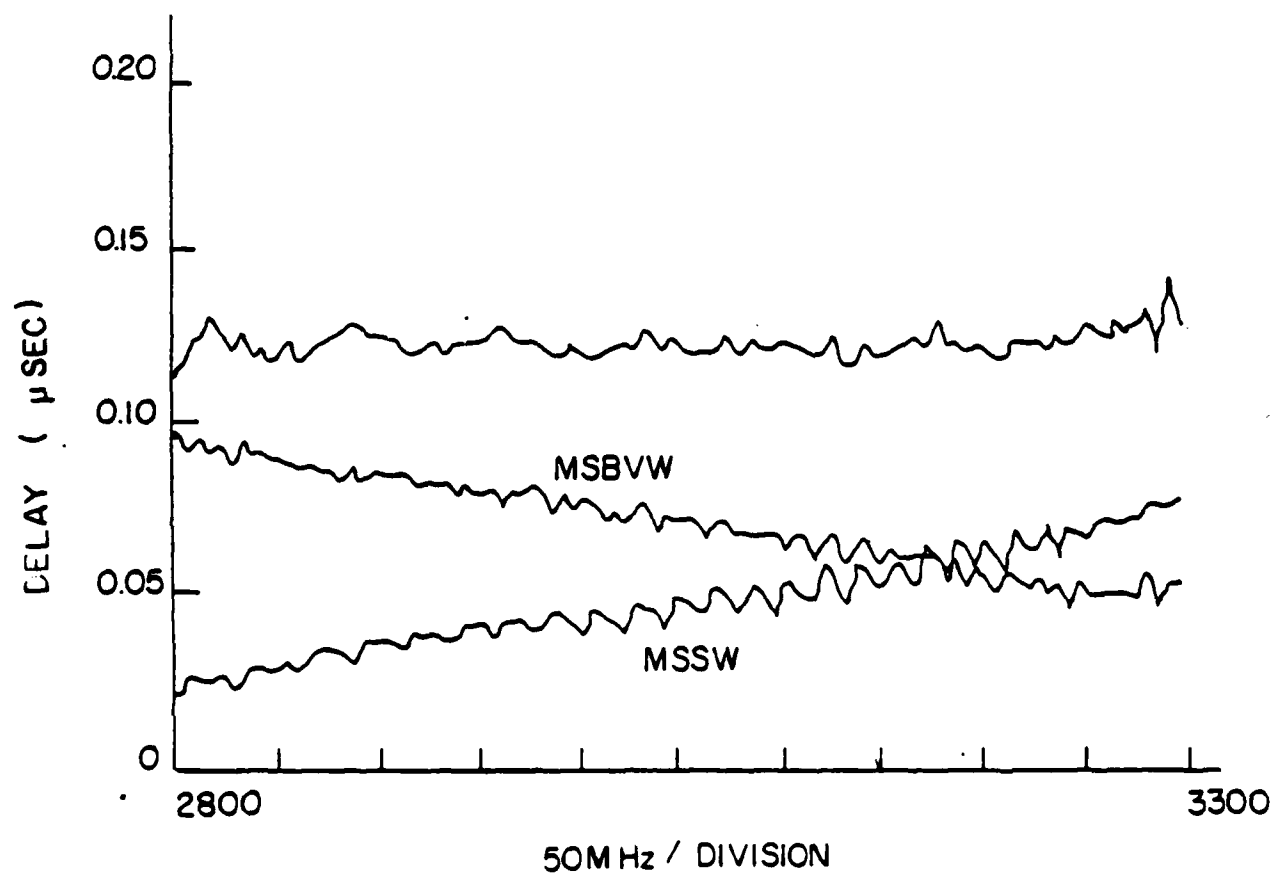
Fig. 3.10 MSSW and MSBVW dispersion curve and their sum

156

adjustment in the slope . Table 3.2 given the effect of changing the d.c. bias of the MSBVW delay line on the slopes of the linearized frequency band. Because of these experimental results, the bias field for the MSSW linear delay line in fixed at the same value whereas the bias field of the MSBVW linear delay line can be changed to provide the adjustment for the time delay in the cascaded device.This two MSW delay line is then cascaded together to performed the variable time delays experiments.

Delay vs. frequency curves experimentally obtained from the cascaded MSSW and MSBVW device are shown in Fig. 3.11. To obtain these curves the bias on the MSSW delay line was held constant at 410 Gauss while the bias applied to the MSBVW delay line was varied from 540 to 650 Gauss. The data obtained are summerized in Table 3.3. The maximum delay differential obtained was 42 nsec with an applied bias differential of 110 Gauss. The bandwidth of this variable is between 2.9 to 3.15 GHz , and the R.M.S. phase deviation from linearity ranged from 6.4 degrees to 12.9 degrees. These values are quite acceptable for a number of phased array radar/communicatins applications and represent a significant advancement in the state of the art for MSW devices.

There is one problem with the cascaded device as it stands now. The insertion loss is high, approximately 35 db across the band. This high value is due in large part to the fact that the device was not tuned, and the loss should be reduced consederably with proper matching of the

157

H(BVW)	Slope(nsec/100MHz)	R.M.S. PH. ERROR
550	-14.0	8.9
575	-12.5	7.7
600	-12.6	7.3
625	-13.6	7.9
650	-14.1	11.0

Transducer separation: 1.5 cm
YIG Thickness: 35uM
Ground spacing: 250uM
Bandwidth: 2.8 to 3.15 GHz

Table 3.2   The effect on changing the slopes of the MSBVW
linear delay line by adjusting the bias field
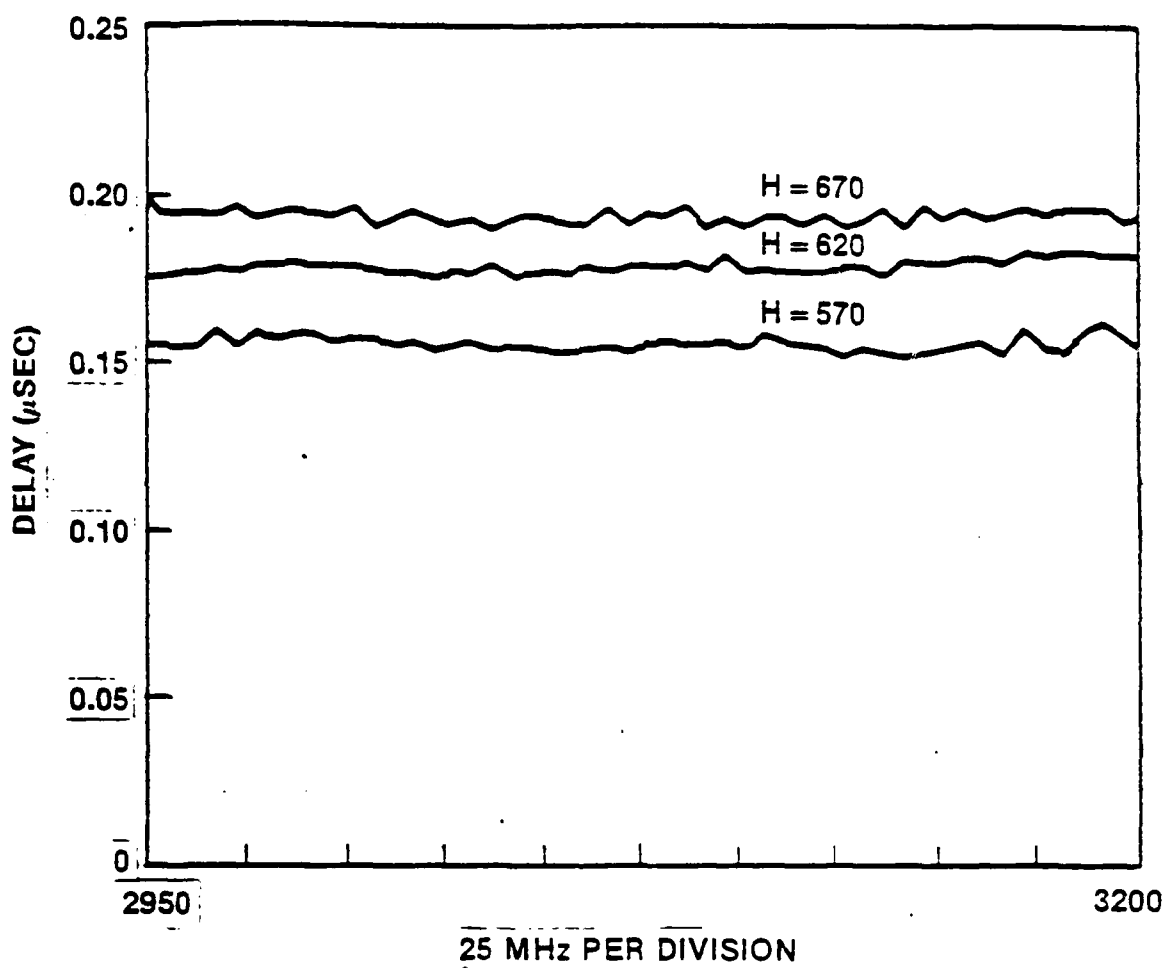
Fig. 3.11 Dispersion curves for cascad delay line as a
function of bias field

159

Experimental results for the MSW Variable Time delay lines

H_{BVW}(Gauss)	T(nsec)	R.M.S. (degrees)
540.0	149.6	9.75
550.0	154.7	12.90
562.5	159.7	11.10
575.0	164.7	10.60
587.5	169.3	9.50
600.0	173.8	9.10
612.5	178.0	6.40
625.0	182.4	6.80
637.5	186.7	6.40
650.0	191.4	12.20

Bandwidth: 2.9 TO 3.15 GHz

Table 3.3 Experimental results for the MSW Variable Time delay lines

transducers.

3.2.4 Summary

An electronically variable time delay device comprised of two cascaded MSW delay lines has been fabricated and evaluated, and the operating characteristics are substationally better than previously reported embodiments of this device. The improvements are due mainly to the linearization of the two component dispersions. With a reduction in insertion loss and compact packaging a device of this type will be ready for service in phased array systems.

4.0   3-6 GHz Tunable MSSW Resonator

Magnetostatic wave propagation in EPI YIG films satisfy the equation
$\nabla \times h = 0$ or $h = \nabla\psi$.

The wave can propagate in three modes such as Surface, Forward volume
wave and Backward volume wave (Fig. 4.2)

The surface wave mode is excited when the bias field lies on the surface
of the YIG films such that the field direction is normal to the wave
propagation direction.

For Backward volume wave, the field is in the direction of the wave
propagation and for forward volume wave, the field is perpendicular to
the YIG surface.

4.1   INTRODUCTION

Magnetostatic wave (MSW) devices form the basis of a new emergence of
microwave analog signal processing. Among these devices, MSW resonators
offer over surface acoustic wave (SAW) resonators simple transducers not
needing narrow-line-width photolithography and broad frequency tunability
by an externally applied magnetic field. Over yttrium iron garnet (YIG)
sphere resonators which operate well at microwave frequencies, but which
require tedious and expensive fabrication procedures, MSW techniques
provide means of obtaining high Q resonators allowing MSW oscillator and
complex filter functions.

MSSW are predominantly magnetic, slow, dispersive electromagnetic waves
(with dispersion shown above) that propagate with the field maxima at the
ferrite surfaces. For the forward propagation mode, if the wave energy
is confined to the top surface of the YIG then for the reverse
propagation mode, the energy is confined to the bottom surface of the
YIG.

The basic element of a MSSW Resonator is a periodic grating on the YIG
surface which reflects MSSW at specific wavelength determined by the
period of the grating.

A schematic of a two-port MSSW resonator is shown in figure 4.6 The
two-port resonator consists of a pair of distributed mirrors separated by
a propagating spacing. The input and output loop transducers are usually
placed within the spacing between the two arrays with the structure (a)
on top of the structure (b) in flipped configuration. The structure
provides an easy isolation between the input and the output port.
Efficient distributed reflectors are formed by several types of
discontinuities (1) chemically or ion beam milled etched groove arrays or
(2) metal dot arrays. In this work, the grooves are plasma etched, and
theresonators were designed to operate at $\lambda = 300$ μm.

In this work, we have attempted on the improvement of the following
characteristics of a MSSW resonator.

162

Bias Field Orientation	Dispersion relation	Dispersion Diagram
	(MSSW) Surface Wave :	

(MSSW) **Surface Wave :**

Unmetallised

$$\exp 2ks = \frac{(2\pi M)^2}{(H_1+2\pi M)^2-(\frac{\omega}{\gamma})^2}$$

$\frac{\omega}{\gamma}=H_1+4\pi M$

$\frac{\omega}{\gamma}=H_1+2\pi M$

One surface Metallised

$$\exp 2ks = \frac{2\pi M(H_1+4\pi M\mp\frac{\omega}{\gamma})}{(H_1+4\overset{-}{\underset{-}{}}M\pm\frac{\omega}{\gamma})(H_1+2M\mp\frac{\omega}{\gamma})}$$

$(\frac{\omega}{\gamma})^2=H_1(H_1+4\pi M)$

(MSBVW) **Backward Volume Wave :**

$$2\cot\alpha ks = \alpha-\alpha^{-1}$$

$$\alpha = \frac{(\frac{\omega}{\gamma})^2-(H_1)^2}{H_1(H_1+4\pi M)-(\frac{\omega}{\gamma})^2}$$

$(\frac{\omega}{\gamma})^2=H_1(H_1+4\pi M)$

$\frac{\omega}{\gamma}=H_1$

(MSFVW) **Forward Volume Wave :**

$$\tan(ks/2\alpha) = \alpha$$

$$\alpha = \frac{(\frac{\omega}{\gamma})^2-(H_1)^2}{H_1(H_1+4\pi M)-(\frac{\omega}{\gamma})^2}$$

$(\frac{\omega}{\gamma})^2=H_1(H_1+4\pi M)$

$\frac{\omega}{\gamma}=H_1$

Figure 4.2 Dispersion relations of magnetostatic waves in YIG plates
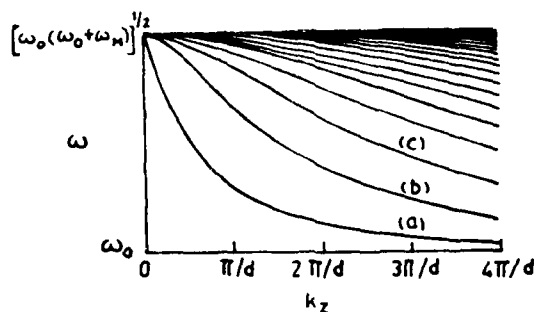
Figure 4.3   Dispersion curves for the case of magnetostatic wave
propagation along the biasing field.   The curves designated
by(a),(b),(c), etc., correspond to n=0,1,2, etc.   The slope of
ω vs k curves is negative throughout the frequency range for all
mode orders.   Thus the modes are backward waves for which the
directions of energy flow and phase propagation are mutually
opposite (after Damon and Eshback, 1961).
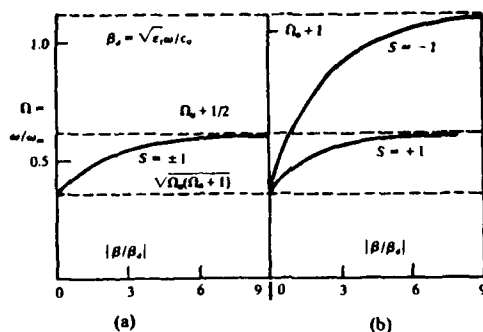
Figure 4.4   Magnetostatic dispersion curves for (a) free ferrimagnetic
slab, and (b) metal-backed ferrimagnetic slab.   In (b) S=±1
corresponds to propagation along the ±y-direction.   The introduction
of the metal plate thus removes the degeneracy and renders the
propagation characteristics nonreciprocal (after Seshadri, (1970).
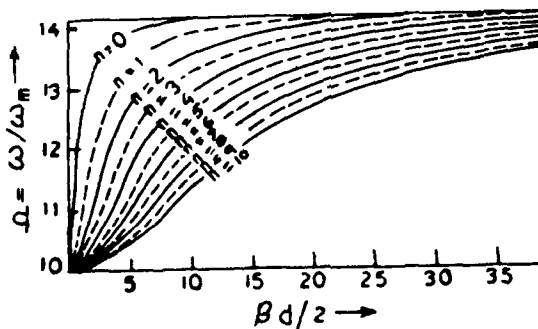
Figure 4.5   Magnetostatic mode spectrum for a normally magnetized slab.
The phase velocity is smaller for the higher-order modes
(after Damon and van de Vaart, 1965).

164

(a) Uniform Array Geometry

(b) Non-Uniform Array Geometry
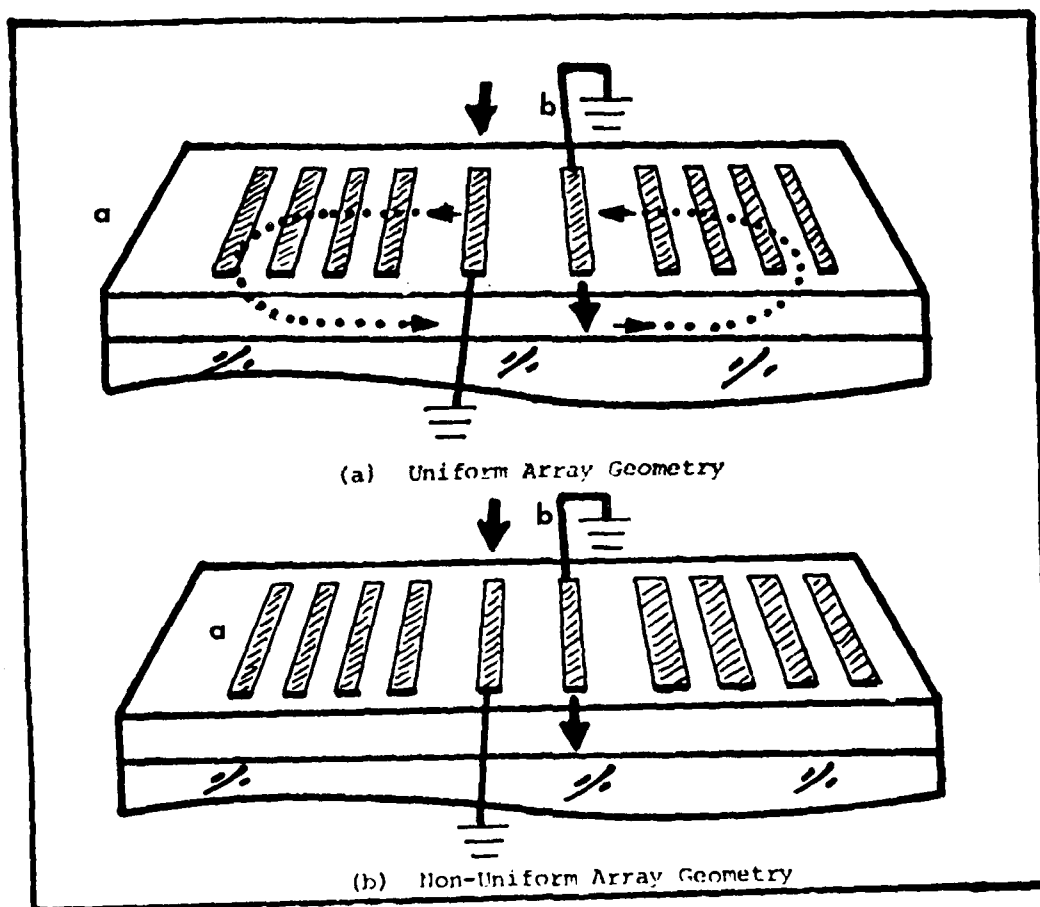
Figure 4.6 Schematic sketch of a resonator and transducer
combination
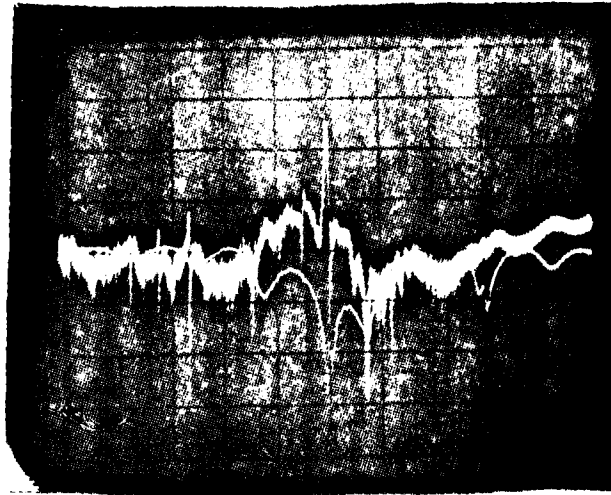
Figure 4.7 Resonator (# K2) response at 6 GHz with the matched 1 mm
transducer. The bottom trace correspond to S_{11}. The dip
near resonance shows matching. The insertion loss at
resonance is 14 dB. It can be seen that the insertion
loss can be further improved if the resonance is placed
at the center (top) of the transducer passband. This will
increase the out of resonance rejection.
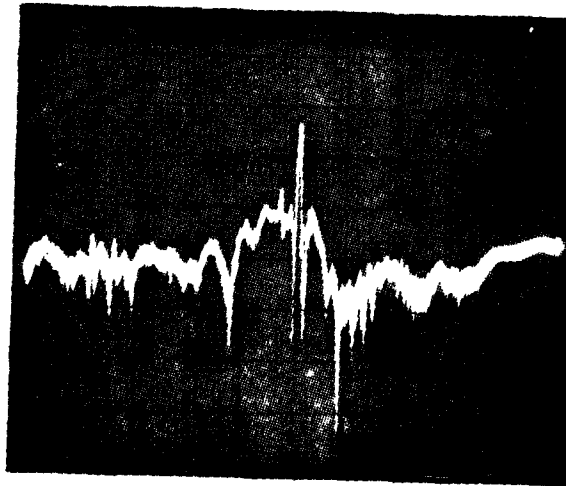
Figure 4.8 Resonator response (# K2´) showing 13 dB insertion loss at 6
GHz. 1 mm matched transducer is used.

1) Smooth tunability of resonance over 3-6 GHz
2) High loaded quality factor Q without the necessity of insertion of any dielectric decoupler between the YIG and the transducer as it increases the insertion loss.
3) Insertion loss lower than those obtained so far in literature (CASTERA et al)
4) High off resonance rejection and single mode operation

4.1.1   EXPERIMENTAL RESULTS

Our works show that it is possible to meet all the above four criteria in 1 mm wide resonators built with EPI YIG (YIG thickness d 14 μm, etch depth h/d = 2.5% # bars = 65, array separation 2.4 mm, L = 75 μm, GGG thickness = 500 μm) and using matched loop transducer with 1 mm long. microstrip built on gold plated quartz substrates of thickness 250 μm (50 μm strip width).

The measured loaded Q lies between 600-2000 over 3-6 GHz with insertion loss 8-14 dB (13 dB IL at 6 GHz has also been obtained for one resonator Fig. 4.7 The off resonance rejection is 10-14dB, higher at high frequencies. The saturation power is 4 dBm at 3 GHz and increases with frequency. The resonators are tunable over 3-6 GHz (see the attached figures).

As is apparent from the trace (Figure 4.9) that sidelobe rejection might possibly be increased to 20 dB or better by carefully adjusting the separation of the two bars of a loop transducer. This will change the wavelength of the launched wave, which can shift the resonance peak exactly on top of the transducer response. This later improvement is being attempted.

3 mm wide and 1.5 mm wide resonators were also fabricated along with 3 mm long and 1.5 mm long loop transducer.

Loaded quality factor Q in the range 800-2800 over 3-6 GHz was obtained with 3 mm resonator. (The separation between the two arrays @1.5 mm.) The corresponding insertion loss was 15-34 dB. The off resonance rejection is found to be only 6 dB. However, the resonators in general are not usable beyond 4.5 GHz because of the appearance of the uniform resonance mode higher than the MSSW resonance, (at low frequency side of the MSSW resonance) Q in general increases at higher frequencies so does the insertion loss. (A typical 3 mm resonator response is shown in Fig. 4.11)

Using 1.5 mm wide MSSW resonators and 1.5 mm long transducer, we found that MSSW resonance is tunable over 3-6 GHz, however the insertion loss 16-29 dB was still considered to be high. The corresponding Q was found to be lower than 3 mm resonator (namely 650-2400).

In order to reduce the insertion loss further 1 mm wide resonators were made along with 1 mm gold transducers on quartz substrates, though this reduced Q slightly (600-2000 over 3-6 GHz), the insertion loss was reduced appreciably to 8-20 dB.
After it is found that using narrow (1 mm wide) resonator and narrow transducer strip (1 mm long microstrip) the insertion loss was reduced to

8-20 dB, it was decided to match the transducer to 50 ohm input output load. S_{11} parameters (both magnitude and phase) were determined at resonance over 3-6 GHz. To measure S_{11} calibration was done over 3-6 GHz with the corresponding transducer short i.e., by shorting the 1 mm transducer feeder line at the input of the loop microstrips.

S_{11} parameters were plotted on Smith Chart and primary matching design principles were followed as provided by Hewlett Packard. (Application note 154). As Matching over an octave band 3-6 GHz is difficult, we tried to optimize the matching through COMPACT (computer optimization of microwave passive and active circuits). The measured S_{11} parameters over 3-6 GHz are shown in Smith Chart polt A. The circuit which optimized the matching is shown below: (To be built on 250 μm quartz substrates $\varepsilon_r = 3.8$.)
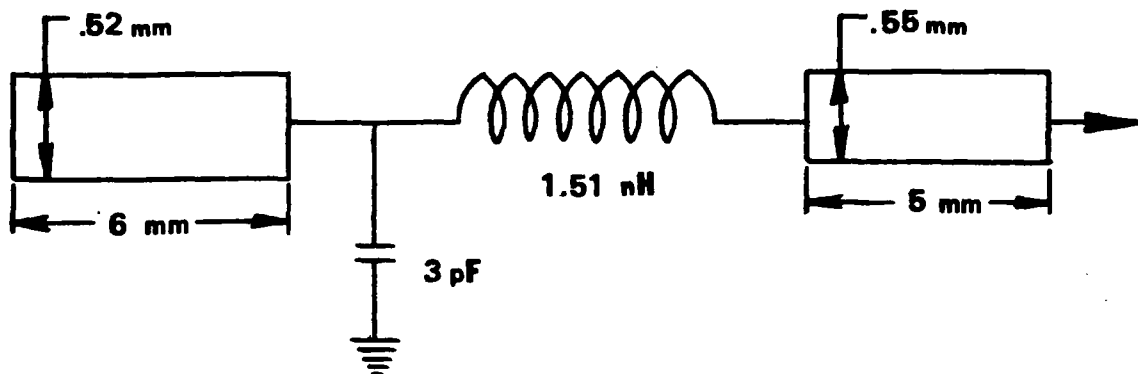
This circuit is found to reduce the S_{11} parameters within 4000-5850 mHz as shown in Smith Chart plot B which shows the computer optimized S_{11} parameters. We were not much concerned about optimization in the range 3-4 GHz, because the insertion loss at resonance was within 8-12 dB even with an unmatched 1 mm transducer.

Microstrip Matched Circuit:

Inductance and capacitance of the computer optimized circuits were realized through the following circuit equations

1) High Impedance Microstrip Lines
   Impedance around 100 ohm were used. (ZoL = 100Ω)
   Required length of the microstrip line for the inductance (1.5 nH) was determined as described below

2) Discontinuity and inductance were utilized in the circuit as shown in Fig. 4.12
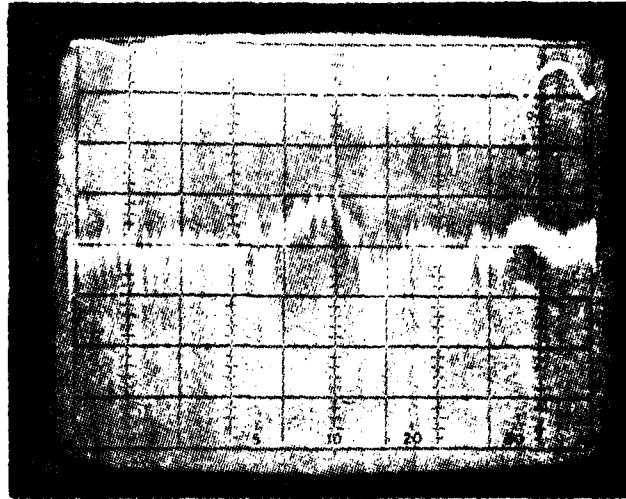
Figure 4.9 MSSW resonator with 1 mm unmatched transducer at 6 GHz.
The resonator is designed to operate at 300 micron
wavelength. The insertion loss is 20 dB with Q at resonance
2000. The upper trace corresponds to S_{11}. It is seen that
at the resonance point there is not a significant dip in S_{11}.
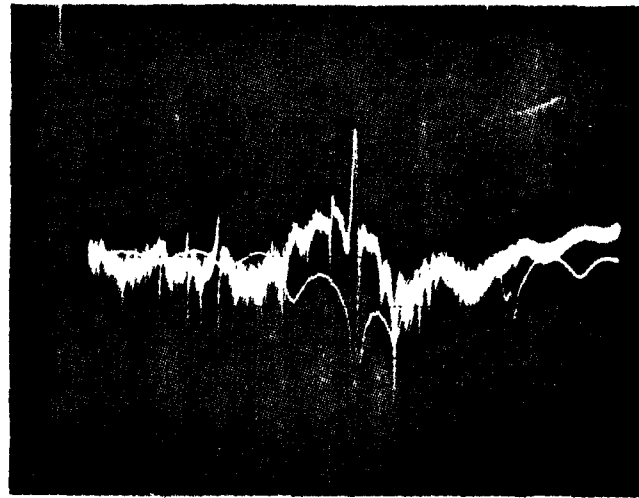
Figure 4.10 MSSW resonator response with 1 mm matched transducer at
6 GHz. The insertion loss at resonance is 14 dB with the
same resonator as above. The bottom trace corresponds to
S_{11}. It is seen that there is a significant dip in S_{11} at
resonance. The S_{11} at resonance is 0.15. The resonator
identification number is K2.
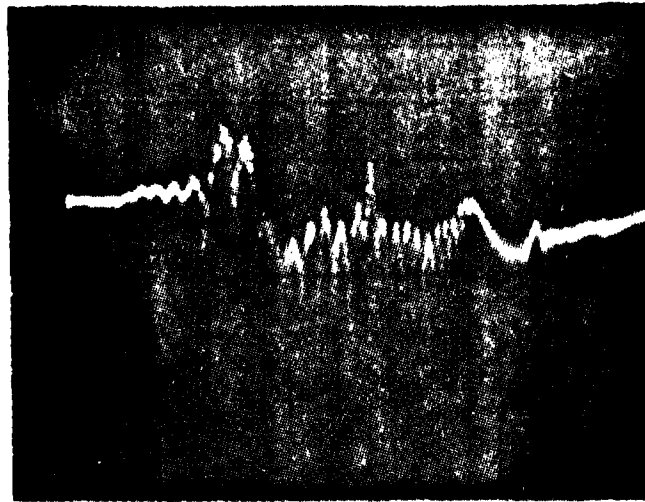
Figure 4.11 A typical 3 mm wide resonator response with 3 mm transducer at 5.5 GHz.

Resonator identification #6
f = 5.5 GHz
Δf = 1 GHz
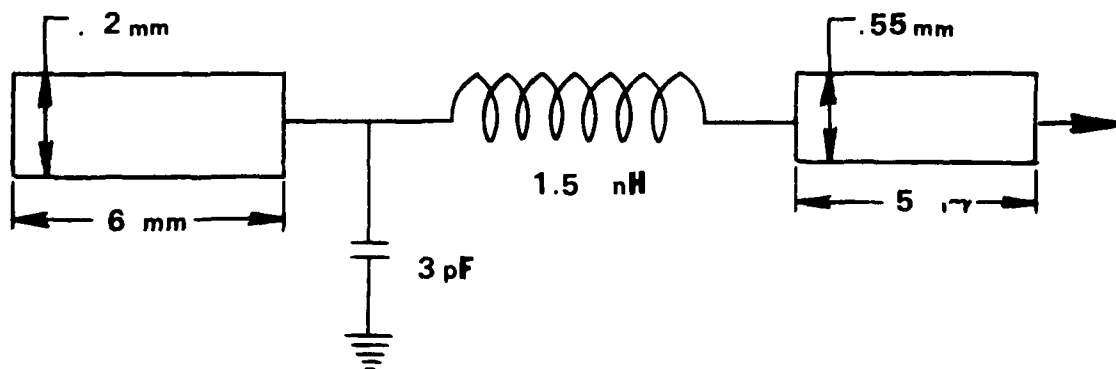
Figure 4.12 Matched input transducer circuit as obtained through compact

Input Transducer

Equivalent Circuits

to 50 Ω

.52 mm

6 mm

I_L (2) (1)

.55 mm

5 mm

(3)

Between A and B

L_1 C L_2

$$L_1 = \frac{c Z_{oc}}{2f \lambda_{gc}} \qquad L_1 \approx L_2$$

$$C = \frac{I_c}{f \lambda_{gc} Z_{oc}}$$

Between B and C

L_3 C_L C_L

three discontinuities (1), (2), and (3)

$$2L_1 + L_3 = 1.51 nH$$

$$C + 2C_L = 0.3 pF$$
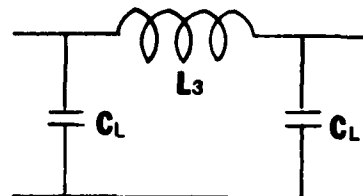
$$I_L = \frac{\lambda_{gL}}{2\pi} \sin^{-1}\left(\frac{\omega L}{Z_{oL}}\right)$$

$$C_L \approx \frac{I_L}{2f_{oL} \lambda_{gL}}$$

Figure 4.13 The matched input transducer circuit after utilizing the inductance and capacitance through microstrips see pages 173 and 174.

171

The frequency in the following equations were chosen to be the center of the band (3-6 GHz).

$$\varepsilon_{eff}^{(f)} = \varepsilon_r - \frac{\varepsilon_r - \varepsilon_{eff}}{1 + (\frac{h}{Z_o})^{1.33}(0.43\ f^2 - 0.009\ f^3)} \qquad (1)$$

ε_{eff} obtained from

$$eff = \frac{\varepsilon_r}{0.96\ \varepsilon_r + (0.109 - 0.004\ \varepsilon_r)\{log(10 + Z_o) - 1\}} \qquad (2)$$

$$\text{For } Z_o > 50\ \Omega \qquad (3)$$

$$\varepsilon_{eff} = \frac{\varepsilon_r + 1}{2}\{1 + \frac{29.98}{Z_o}(\frac{2}{\varepsilon_r + 1})^{\frac{1}{2}}(\frac{\varepsilon_r - 1}{\varepsilon_r + 1})(\ell n\ \frac{\pi}{2} + \frac{1}{\varepsilon_r}\ \ell n\ \frac{4}{\pi})^2\}$$

$$\text{For } Z_o > 50\ \Omega \qquad (3)$$

ε_r for quartz = 3.8

ε_{eff} for inductor microstrip AB (Zo1 = 100 Ω) can be obtained from equation (3).

ε_{eff} for capacitance microstrip can be determined by first finding out Z_{oc} corresponding to the microstrip of width 'w' $\cong$ 0.55 mm from the equations.

$$\frac{w}{h_s} = (\frac{e^{H'}}{8} - \frac{1}{4e^{H'}})^{-1}$$

where

$$H' = \frac{Z_{oc}\sqrt{2(\varepsilon_r + 1)}}{119.9} + \frac{1}{2}(\frac{\varepsilon_r - 1}{\varepsilon_r + 1})(\ell n\ \frac{\pi}{2} + \frac{1}{\varepsilon_r}\ \ell n\ \frac{4}{\pi}) \qquad (4)$$

h_s = 250 μm is the quartz substrate thickness. Z_{oc} is then used in equation (2) to determine ε_{eff}.

Now the frequency dependence of ε_{eff} was taken into consideration.

ε_{eff}(f = 4.5 Ghz) is determined for corresponding Z_{o1}, Z_{oc} from equation (1).

λ_{gc} and λ_{gL} can then be determined from the equation

172

$$\lambda_{gL,C} = \frac{300}{f\sqrt{\varepsilon_{eff}^{L,C}} \ (f=4.5)} \tag{5}$$

using the corresponding ε_{eff} as obtained above.

As applicable to the microstrips and the equivalent circuits (Fig. 4.12) the following equations allow us a unique determination of the required length ℓ_I of the inductor microstrip. It was assumed that

$$L_1 \cong L_2$$

$$2L_1 + L_3 = 1.51 \ \text{nH}$$

$$C + 2C_L = 0.3 \ \text{pF}$$

$$L_1 = \frac{\ell_c Z_{oc}}{2 \ f \ \lambda_{gc}} \tag{6}$$

$$C = \frac{\ell_c}{f \ \lambda_{gc} Z_{oc}}$$

$$C_L = \frac{\ell_I}{2f \ Z_{oL} \ \lambda_{gL}}$$

$$\ell_I = \frac{\lambda_{gL}}{2\pi} \sin^{-1} \left(\frac{\omega L_3}{Z_{oL}}\right)$$

Z_{oc} was used in the above equations (6) as an unknown parameter, rather than the characteristic impedance of the 5 mm microstrip betwewen B & A. (At A & B there are microstrips of different characteristic impedances.) Next the width 'w' of the inductor microstrip was determined from

$$Z_{oL} = \frac{119.9}{\sqrt{2(\varepsilon_r + 1)}} \ \left[\ell n\{4 \ \frac{h_s}{w} + \sqrt{16(\frac{h_s}{w})^2 + 2}\} - \frac{1}{2} \ (\frac{\varepsilon_r-1}{\varepsilon_r+1})(\ell n \frac{\pi}{2} + \frac{1}{\varepsilon_r} \ \ell n\frac{4}{\pi})\right]$$

h_s the substrate thickness is 0.25 mm $\hspace{2cm}$ (7)

Final length 1_I and the width w of the inductor microstrip were calculated to be 1.1 mm and 131 μm. The matched transducer was then fabricated through usual photolithographic technique. The output transducer was a mirror impage of the input transducer shown in Fig. 4.12 After matching the following improvements have been observed

1) It has been possible to reduce the insertion loss by 6 dB more, i.e., the insertion loss at resonance with most of the 1 mm resonators can be kept at 8-14 dB over 3-6 GHz (Fig. 4.16 At 3 GHz, insertion loss as low as 6 dB at resonance has been obtained for some resonators (Fig. 4.14)

2) The out off resonance rejection has been improved by 4 dB i.e., 10-14 dB within 3-6 GHz (Fig. 4.7,4.16,4.17). Before matching it was around 7-10 dB.

3) The matched S_{11} parameters have been found to be quite low (0.15) around 5-6 GHz than compared to those of the computer optimized values. In the 3-5 GHz range measured values were closed to the optimized values.

4) Smith Chart plot C gives the measured values of S_{11} with one of the resonators (identification # K2) using both matched and unmatched 1 mm transducer.

5) Tunability also improved after matching.

With most of the resonators matched transducer did not provide higher Q resonance.

Conclusions:

1. By reducing the width of the resonator and by reducing the length of loop strip of the transducer, the insertion loss at resonance is reduced significantly. This is also reflected in the lower S_{11} parameters (see the Smith chart plot of S_{11}).

2. By matching the transducer the insertion loss has been reduced further by 6 dB. The off resonance rejection has improved by at least 4 dB; Q however did not improve.

3. Q of resonators (as studied in this work) depends mainly on (i) exact reproduction of the mask on YIG i.e., uniform land and Groove spacings throughout the arrays. (ii) large # of bars typically ~ 60 (iii) d/h ≅ 2.5%. Earlier workers (Collins et al, CASTERA used high d/h (as high as 6·4% to 11%) to obtain high Q. Our works show that high d/h basically helps to obtain a single moded resonance with large off resonance rejection. For a given resonator transducer combination, Q at the resonance also depends on the position of the transducers relative to the spacings between the two arrays. By reducing the separation between the two arrays the spurious response or sidelobes can be diminished to a great extent; however the loaded Q is also theoretically predicted to be reduced. Reduction in Q also occurs with the reduction in the width of the resonator. Reduction in Q may be compensated by properly choosing the etch.
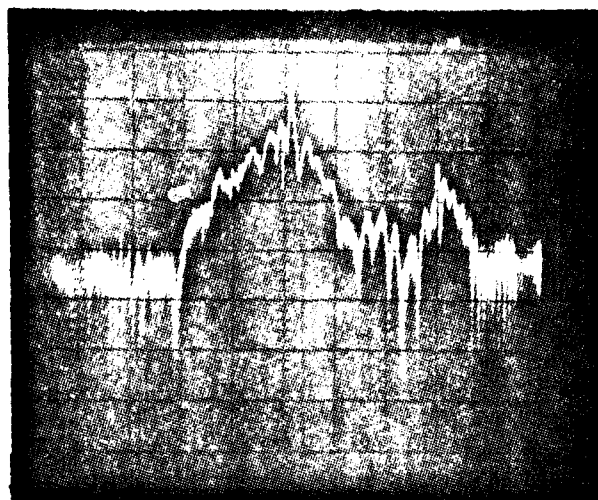
Figure 4.14 This figure shows 6 dB insertion loss at resonance.
f=3.5 GHz; 1.5 mm wide resonator (#K 21)used with 1 mm
matched transducer. The high frequency side resonance
however was not observed with other 1 mm resonators.
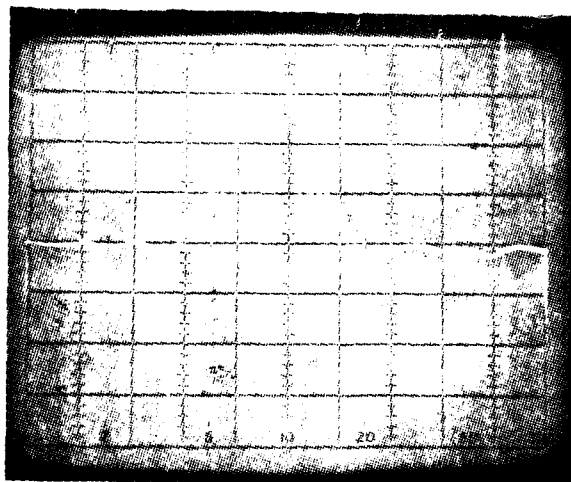
Figure 4.15 1 mm wide NSSW resonator (# K2) response at 3 GHz with 1 mm
matched loop transducer. The insertion loss is 10 dB at
resonance. The bottom trace corresponds to S_{11}. It is

seen that there is not a significant dip at resonance. .
The S_{11} is about 0.4. The Q at resonance is about 600.

For optimum Q we have to sacrifice IL by 2 dB. The
corresponding Q at 6 GHz was 1800 and IL = 16 dB.

depth (d/h ~ 2-3%), land and groove width as well as the position of the transducer with respect to the cavity spacings. Our works show that low array separation (< 2 mm does not provide high off resonance rejection). Higher off resonance rejection (~20 dB) may be possible by carefully choosing the separation of the loop strips. Because of metal loading by the YIG, the effective wavelength λ_{eff} of the wave launched by the transducer differs from that expected on the basis of equation $\lambda o=2s$ where s is the separation between the two microstrips of a loop. If this separation can be chosen carefully, the insertion loss will improve further and will be less than 14 dB at 6 GHz (Fig. 4.7) This is expected to improve the rejection out off resonance, too.

It may be mentioned that at higher bias field (which corresponds to higher resonance frequency, the transducer passband shrinks because of the narrowing down the difference between the upper and lower cut off frequencies in ferrite (see Fig. 4.3,4.4,4.5) for the MSSW wave. Because of this, the matching of wavelength of the wave launched by the transducer with the periodicity of the resonator grating becomes very important. A small mismatch will place the resonance peak at a different position other than the top of the passband and this will add to the insertion loss significantly at high frequency. Change of wavelength because of the metal loading by the YIG needs to be taken into account. These above mentioned problems are found to be very significant for short narrow resonators (8 mm long and 1 mm wide) operating at low wavelength (100 micron). (Fig. 4.20)

Experimentally further improvements may be attempted by giving ± small variations about the length and width of the inductor microstrip (Fig. 4.12) to reduce the S_{11} at high frequencies.

In this work, single modedness of the resonance over 3-6 GHz was determined by finding out the phase shift at the resonance as the resonator is tuned over 3-6 GHz. Only phase shift about 10-12° could be recorded.
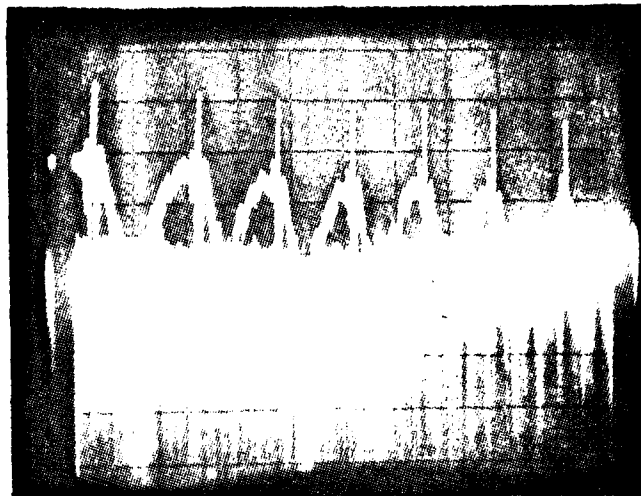
Figure 4.16 1 mm resonator (MSSW) response tunability in the range
2.75-6 GHz with a 1 mm matched loop transducer and resonator
#K2 is used.
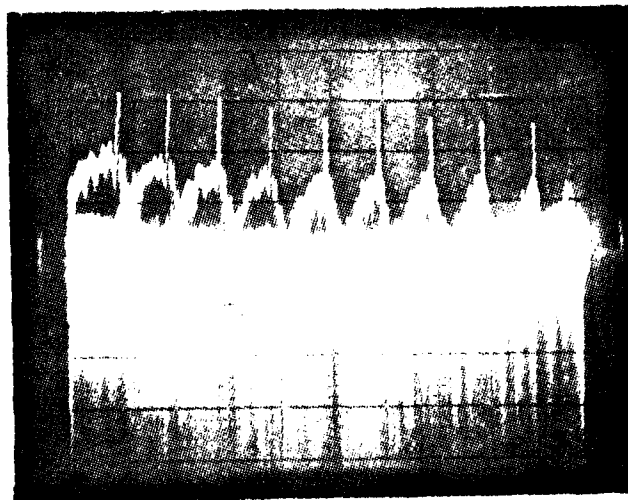
Figure 4.17 Resonance response tunability in the range 2.5 6 GHZ
with a different resonator transducer combination. 1 mm
wide resonator used with 1 mm matched transducer.
Resonator #I is used.
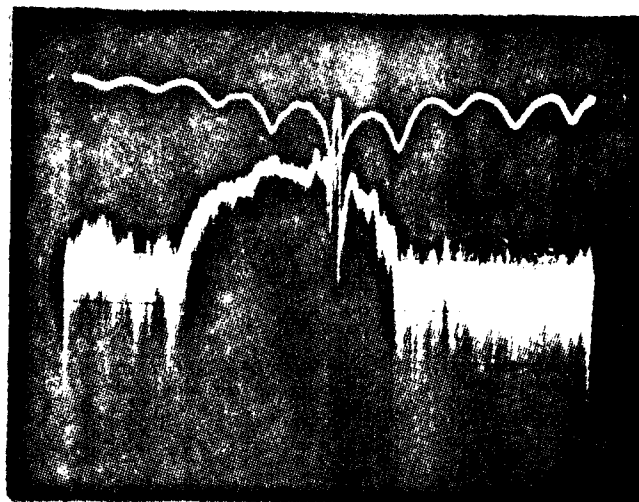
Figure 4.18 1 mm wide resonator response with 1 mm wide matched
transducer. The upper curve corresponds to S_{11} trace.
The bottom trace corresponds to S_{21}. The center
frequency is 3.75 Ghz. Sweep range = 1 GHz. It may be
noted that there is a very significant dip in S_{11}
occurring at the resonance point. This happens only
when the resonator is matched. For unmatched resonator
see figure below.
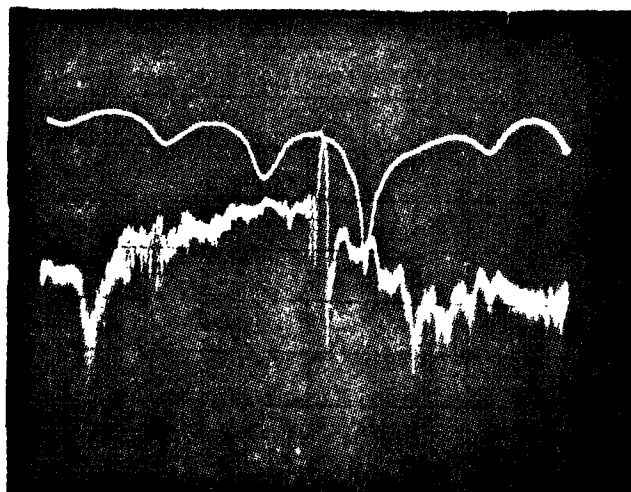
Figure 4.19 1 mm wide resonator (#K2), same as used for the upper
figure) with 1 mm wide unmatched transducer. It may be
noted that the significant dip in S_{11} occurs at

different frequency than the resonance point. Resonator
is used.
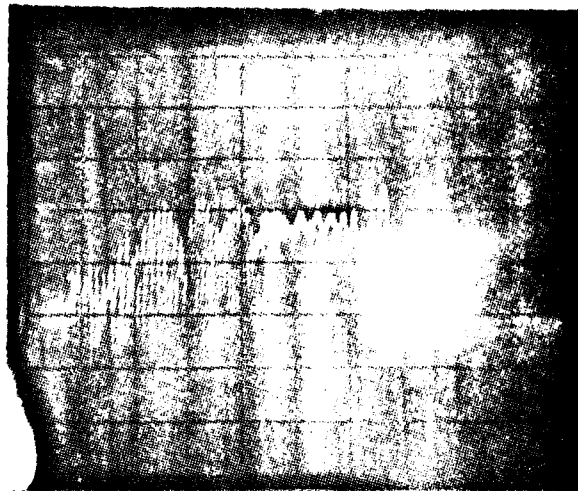
Figure 4.20   1 mm x 8 mm x 13 μm MSSW YIG resonator designed for λ=100 μm
operates at Δf=4.5 GHz. Δ7=1 GHz. The transducer used has a
loop spacing   50 μm corresponding to λ=100 μm and microstrips
are 20 μm wide and 1 mm long. If is seen that the resonance
is shifted away from the center (top) of the transducer passband
significantly.
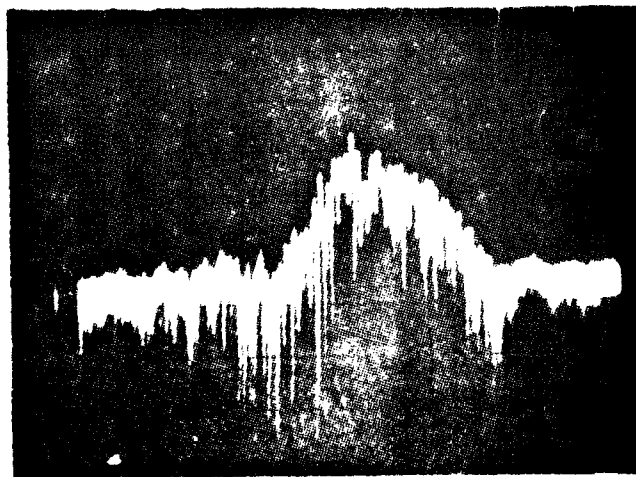
Figure 4.21   1 mm x 8 mm x 13 mm abo   perating at 4.5 GHz.
Δf=1 GHz. The loop transdu   lesigned for λ ≅ 220 μm.
It is seen that unlike that   i0a, the resonance is placed
at the top of the transducer   nd. The transducers
are unmatched. Improvements   ng made on the off
resonance rejection and insertion loss.

4.1.2 Single Mode Character of Resonance

In this work single mode character of the resonance was determined by finding out the phase shift relative to the resonance at 3 GHz as the resonance frequency is varied to 6 GHz at steps of 200 MHz. When corrected for the transmission phase (S_{21}) (of the signal passing through the two matched transducer feeder lines (Fig. 4.12 as obtained from compact (see Fig. 11b) we find that there is only overall phase shift of 10-20° as the resonance is tuned over 3-6 GHz by adjusting the magnetic field. (See Fig. 4.22)

This small phase shift might be due to the fact the compact did not take into account of the frequency dependent electrical characteristics of the microstrips. Further considering the error in the measurement of phase (which is typically around 10°) we can say that the resonance is single moded.

Fig.11a Phase of S_{21} measurements with resonator#K2(1 mm wide) at resonance. 1 mm matched transducer is used.Calibration is done with microwave short.

xxx phase at resonance including that of transducer feeder lines.

ooo phase(electrical lenght of two identical cascaded feeder lines.

Figure 4.22 Phase of S_{21} measures with resonator #K2 (1 mm wide) at resonance. 1 mm matched transducer is used. Calibration is done with microwave short.

xxx phase at resonance including that of transducer feeder lines.

ooo phase (electrical length of two identical cascaded feeder lines.

181

Electrical length of the input and output cascaded
Feeder lines of the transducers.

```
@EDIT (FILE) KK2.DAT.3 (OUTPUT AS) KK2.DAT
Edit: KK2.DAT.3
*P
@0100    MET AA ZZ
00200    TRL AA MS .52 5 3.8 .254
00300    CAP BB PA  -.30114
00400    IND CC SE  -1.5096
00500    TRL DD MS .55 6 3.8 .254
00600    CAX AA DD
00700    CAS AA AA
00800    PRI AA S1 50
00900    END
01000    3000 4400 200
01100    4600 4800 5000 5100 5200 5300 5400 5500
01200    5550 5650 5750 5850 5900 5950 6000
01300    END
*I810
00810    PLO AA S1 50
*EU

[KK2.DAT.4]
@COMPACT
```

USE, DUPLICATION OR DISCLOSURE OF THE PROGRAM IS SUBJECT TO RESTRICTIONS
STATED IN LICENSE AGREEMENT L-164 AND/OR PURCHASE ORDER 1-114-12435 WITH
COMPACT ENGINEERING INC.

COMPACT VERSION 5.1 + 58 - IMPLEMENTED 10/09/80
SEE NEWS FOR FIVE NEW FEATURES PLUS LANGE COST SAVING HINTS

FILE NAME, 'TRXINFO', 'TRLINES', 'LANGE', 'NEWS' OR 'QUIT'?KK2
AN(1), SENS(2), OPT(3), SW(4), MAP(5), VAR(6), MC(7), 1+3(13), RND(44)?1
EDIT YOUR INPUT FILE (Y/N)?N

POLAR S-PARAMETERS IN   50.0 OHM SYSTEM

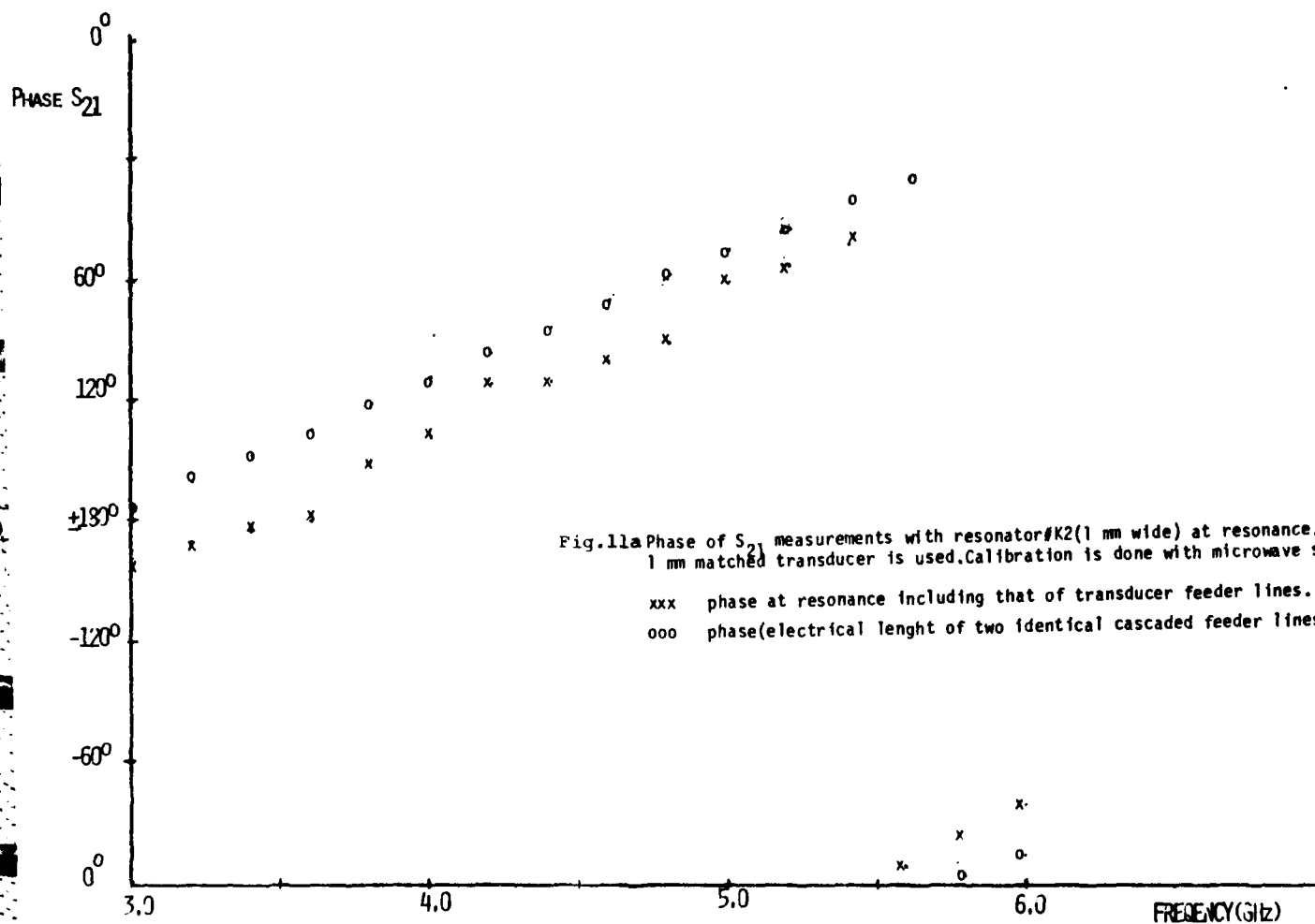| FREQ.	S11 (MAGN<ANGL)		S21 (MAGN<ANGL)		S12 (MAGN<ANGL)		S22 (MAGN<ANGL)		S21 DB	K FACT.
3000.00	0.02<	66	1.00<	173.3	1.000<	173.3	0.02<	101	-0.00	
3200.00	0.06<	51	1.00<	160.4	0.998<	160.4	0.06<	89	-0.01	
3400.00	0.10<	37	0.99<	147.3	0.995<	147.3	0.10<	77	-0.05	
3600.00	0.15<	23	0.99<	134.2	0.989<	134.2	0.15<	65	-0.10	
3800.00	0.20<	9	0.98<	121.0	0.979<	121.0	0.20<	53	-0.18	
4000.00	0.26<	-6	0.97<	107.8	0.966<	107.8	0.26<	41	-0.30	
4200.00	0.31<	-20	0.95<	94.7	0.950<	94.7	0.31<	29	-0.44	
4400.00	0.37<	-34	0.93<	81.6	0.931<	81.6	0.37<	17	-0.62	
4600.00	0.42<	-48	0.91<	68.7	0.909<	68.7	0.42<	5	-0.83	
4800.00	0.47<	-62	0.88<	56.0	0.885<	56.0	0.47<	-6	-1.06	
5000.00	0.51<	-75	0.86<	43.5	0.860<	43.5	0.51<	-18	-1.31	
5100.00	0.53<	-82	0.85<	37.4	0.848<	37.4	0.53<	-23	-1.44	
5200.00	0.55<	-88	0.84<	31.3	0.835<	31.3	0.55<	-29	-1.56	
5300.00	0.57<	-95	0.82<	25.3	0.823<	25.3	0.57<	-34	-1.69	
5400.00	0.58<	-101	0.81<	19.4	0.811<	19.4	0.58<	-40	-1.82	
5500.00	0.60<	-108	0.80<	13.5	0.800<	13.5	0.60<	-45	-1.94	
5550.00	0.61<	-111	0.79<	10.6	0.794<	10.6	0.61<	-48	-2.00	
5650.00	0.62<	-117	0.78<	4.8	0.784<	4.8	0.62<	-53	-2.11	
5750.00	0.63<	-123	0.77<	-0.9	0.774<	-0.9	0.63<	-59	-2.22	
5850.00	0.64<	-129	0.77<	-6.6	0.765<	-6.6	0.64<	-64	-2.33	
5900.00	0.65<	-132	0.76<	-9.4	0.761<	-9.4	0.65<	-66	-2.37	
5950.00	0.65<	-135	0.76<	-12.2	0.757<	-12.2	0.65<	-69	-2.42	
6000.00	0.66<	-138	0.75<	-14.9	0.753<	-14.9	0.66<	-72	-2.46	

```
SMITH CHART, RECTANGULAR PLOT OR QUIT (S/R/Q)?S
WHICH PLOT: S11(1), S22(2), OR QUIT(0)?3
WHICH PLOT: S11(1), S22(2), OR QUIT(0)?1
WHAT IS YOUR TERMINAL LINES PER INCH(25.4MM), 6 LIN/IN (6), OR 7 LIN/IN (7)?7
```

Figure 4.23   Magnitude and phase angle of S_{21} for the two cascaded
feeder lines of the 1 matched transducer (see fig. 4.12
page 170)

COMPACT matched S$_{\text{II}}$ parameters for 1mm resonator#I studied with
1 mm X ducer

```
@EDIT (FILE) DILIP5.DAT.32
Edit: DILIP5.DAT.32
*P
00100MET AA ZZ
00200TRL AA MS .52 6 3.8 .254
00300CAP BB PA -.30334
00400IND CC SE -1.5096
00500TRL DD MS .55 5 3.8 .254
006000NE EE IR 50
00700CAX AA EE
00800PRI AA IR 50 .1E+06
00900END
010003000 4400 200
011004600 4800 5000 5100 5200 5300 5400 5500
012005550 5650 5750 5850 5900 5950 6000
01300END
01400.4 100
01500.4 90
01600.22 95
*RUNN\U\R\EU

[DILIP5.DAT.33]
@RUN COMPACT

USE, DUPLICATION OR DISCLOSURE OF THE PROGRAM IS SUBJECT TO RESTRICTION
STATED IN LICENSE AGREEMENT ! 164 AND/OR PURCHASE ORDER 1-114-12435 WI
COMPACT ENGINEERING INC.

COMPACT VERSION 5.1 : 58 - IMPLEMENTED 19/09/30
SEE NEWS FOR FIVE NEW FEATURES PLUS LARGE COST SAVING HINTS

FILE NAME, 'TRXINFO', 'TRLINES', 'LANGE', 'NEWS' OR 'QUIT'?DILIP5.DA)

%FRSAPR Integer overflow?C- 205?

. %FRSAPR Integer overflow?C- 205?
AN(1), SENS(2), OPT(3), SW(4), MAP(5), VAR(6), ME(7), 1+3(13), RND(44)?
AN(1), SENS(2), OPT(3), SW(4), MAP(5), VAR(6), ME(7), 1+3(13), RND(44)?
EDIT YOUR INPUT FILE (Y/N)?
EDIT YOUR INPUT FILE (Y/N)?N
```

INPUT REFL. COEF. AND VSWR IN 50. OHM SYSTEM WITH V******* OHM LOAD

F(MHZ)	RHO(MAGN. ANGLE)		VSWR	RET LZC (DB)	Z(R+JX)OHM	
3000.000	0.490	69.6	2.92:1	-6.19	42.26	51.1
3200.000	0.422	-87.2	2.82:1	-6.44	32.71	-40.3
3400.000	0.330	-85.2	1.98:1	-9.64	42.32	-31.2
3600.000	0.287	109.3	1.80:1	-10.85	38.74	-23.8
3800.000	0.202	-58.9	1.51:1	-13.88	54.63	-20.8
4000.000	0.241	-122.1	1.63:1	12.37	35.84	-15.5
4200.000	0.216	137.9	1.55:1	-13.32	34.89	-10.5
4400.000	0.224	145.1	1.79:1	-11.23	30.31	10.29
4600.000	0.390	29.2	1.98:1	-8.19	42.18	49.09
4800.000	0.186	21.3	1.46:1	14.61	69.59	10.9
5000.000	0.133	22.3	1.31:1	17.50	63.67	6.5
5100.000	0.081	67.8	1.18:1	-21.82	52.55	7.9
5200.000	0.202	143.2	1.51:1	-13.89	35.14	8.8
5300.000	0.231	126.3	1.60:1	-12.72	35.66	14.0
5400.000	0.363	103.4	1.13:1	8.80	28.34	19.7
5500.000	0.371	83.4	1.18:1	-8.62	41.01	35.03
5550.000	0.354	52.1	1.10:1	-9.01	53.99	-40.1
5650.000	0.142	32.5	1.33:1	-16.24	62.79	-9.7
5750.000	0.249	67.8	1.66:1	-12.09	53.66	-26.3
5850.000	0.314	-14.5	1.92:1	10.05	91.90	-16.1
5900.000	0.231	-95.8	2.13:1	-2.72	13.84	-43.20
5950.000	0.465	65.0	2.74:1	-6.65	47.62	-51.2
6000.000	0.738	90.6	2.42:1	1.24	14.62	-47.31

```
FILE NAME, 'TRXINF  , 'TRLINES', 'LANGE', 'NEWS' OR 'QUIT'?DILIP..\5.DC
AN(1), SENS(2), O   3), SW(1), MAP(5), VAR(6), ME(7), 1+3(13), RND(14)
```

Smith Chart plot of S_{11} measured over 3-6 GHz at 500 MHz steps. 3 mm wide resonator # x 1 was used with 3 mm unmatched transducer. Corresponding transducer short was used for calibration.

IMPEDANCE OR ADMITTANCE COORDINATES

RADIALLY SCALED PARAMETERS
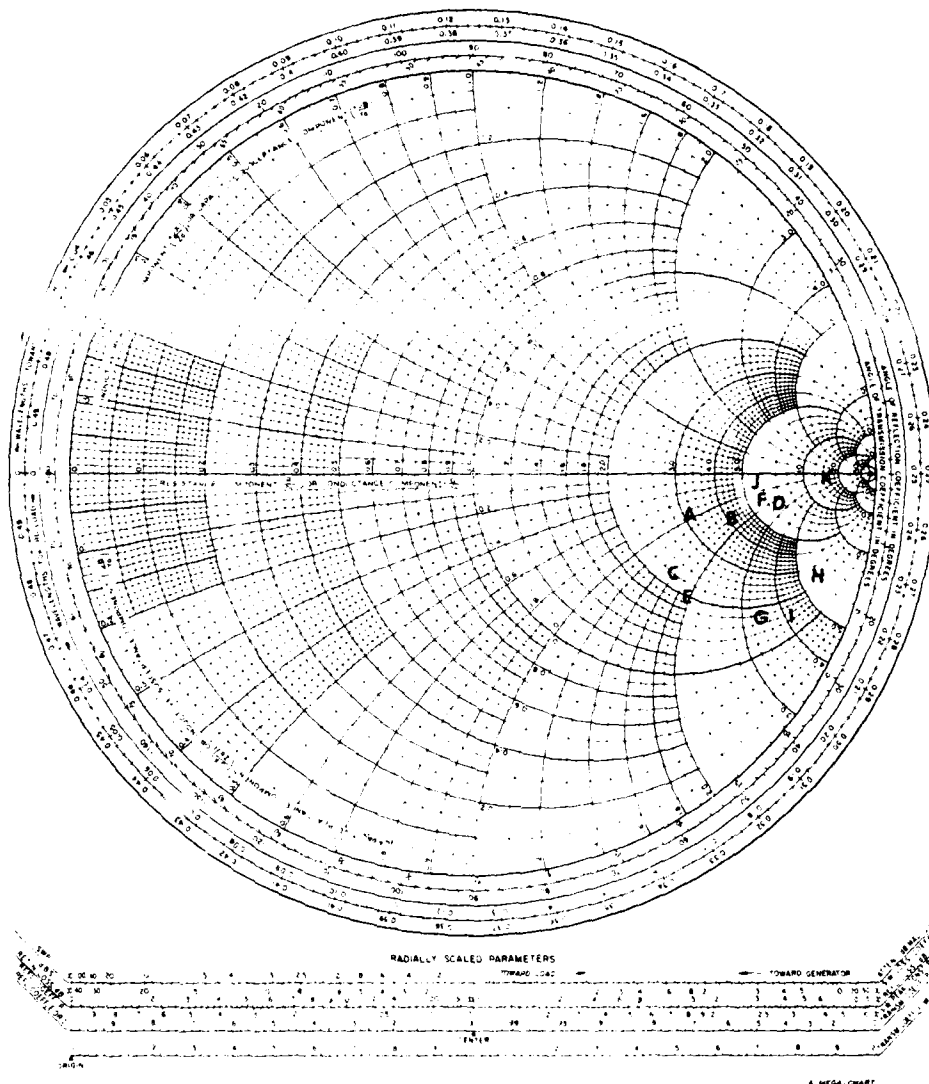
Smith Chart plot of S_{11} measured at resonance over 3-5 GHz at 200 MHz steps. 3 mm wide resonator #X3 was used with 3 mm unmatched transducer.
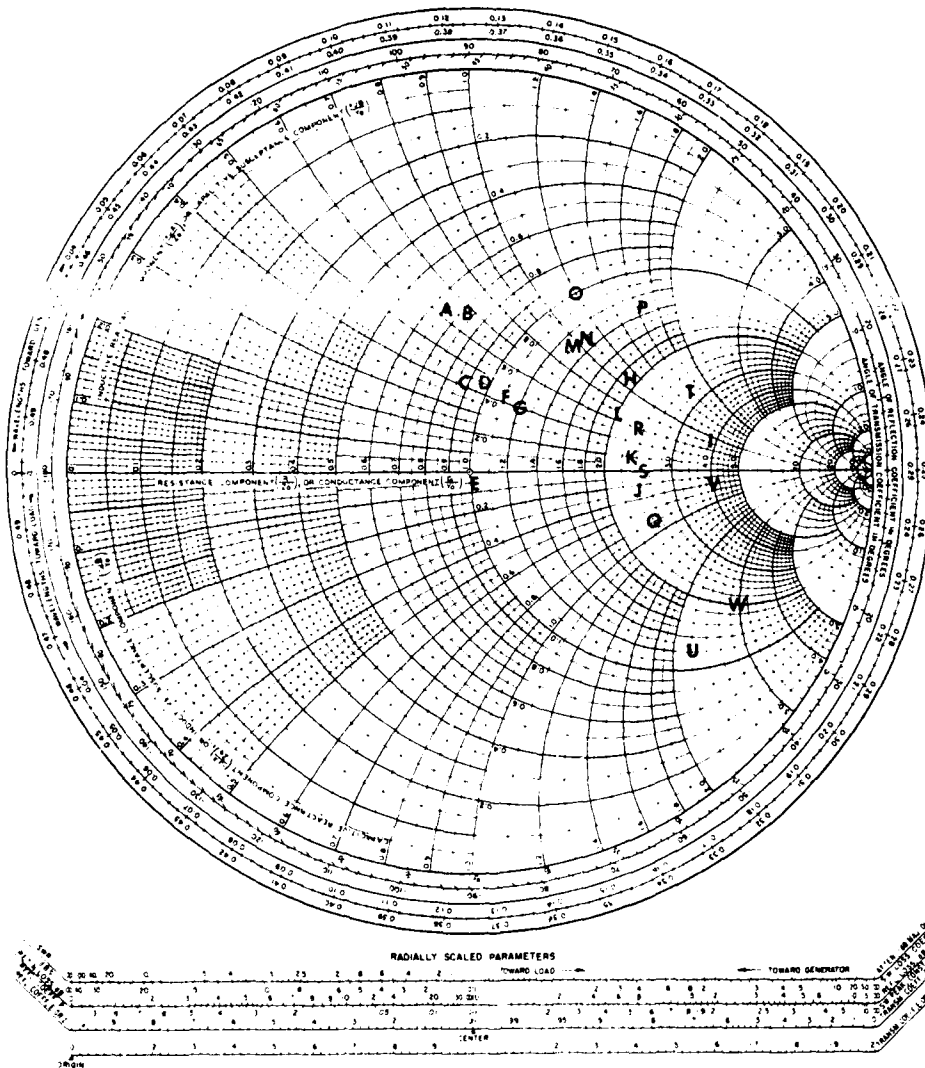
Smith Chart plot of S_{11} measured at resonance point over 3-6 GHz. 1 mm resonator #I was used with 1 mm unmatched loop transducer. Matching through COMPACT was done on these parameters. Frequency increases alphabetically. (See page 190) Corresponding transducer short was used for calibration.

IMPEDANCE OR ADMITTANCE COORDINATES

RADIALLY SCALED PARAMETERS
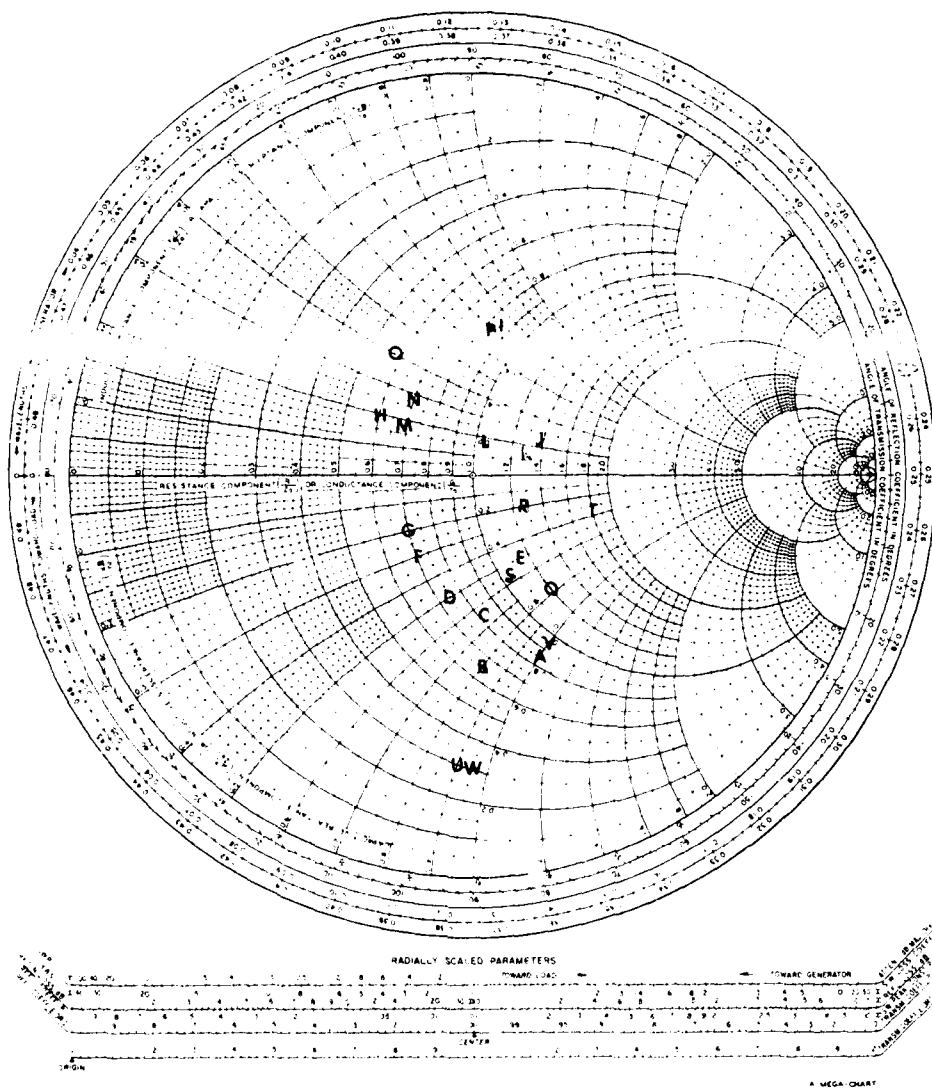
COMPACT matched reflection co-efficients with microstrips as defined in the text. Frequency range 3-6 GHz(see page 190 for frequency interval)
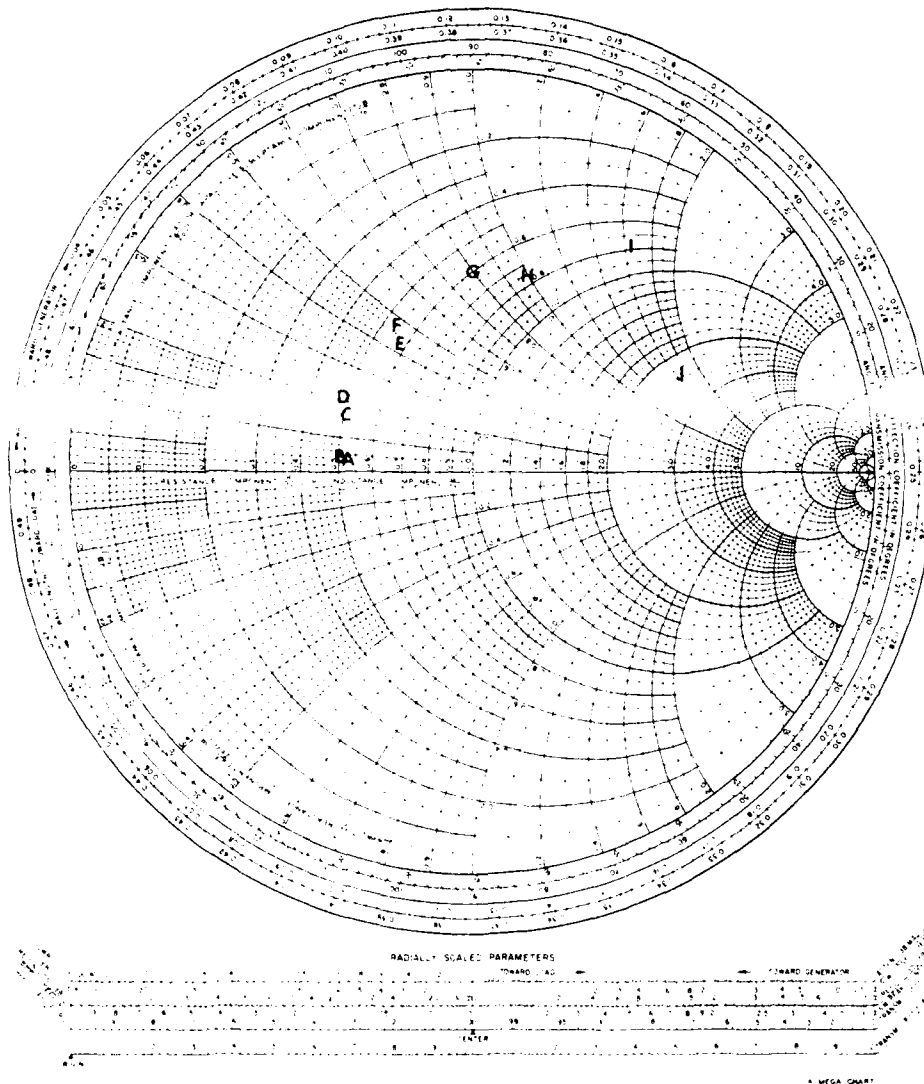
Smith Chart plot of S_{11} measured at resonance over 3-5 GHz at 200 MHz steps. 1.5 mm wide resonator #X1 is used with 1.5 mm unmatched transducer.

IMPEDANCE OR ADMITTANCE COORDINATES

S_{11} measured with one of the resonators #K2 with matched transducer #K2 with matched transducer used at resonance point with respect to microwave short.

END

FILMED

DTIC
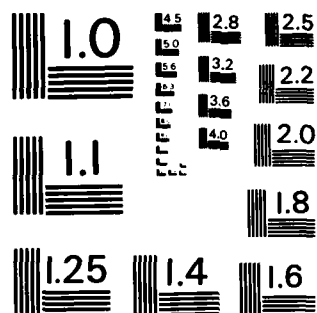
MICROCOPY RESOLUTION TEST CHART

NATIONAL BUREAU OF STANDARDS-1963-A

Measured reflection coefficients with resonator #1 and 1 mm x ducer.
Matching was done on this set of data.

Freq. (MHz)	$|S_{11}|$	S_{11}
3000	0.444	100
3200	0.4	90
3400	0.22	95
3600	0.2	80
3800	0.03	-90
4000	0.19	65
4200	0.21	55
4400	0.44	30
4600	0.59	7
4800	0.41	5
5000	0.39	5
5100	0.37	20
5200	0.37	50
5300	0.425	50
5400	0.52	60
5500	0.6	45
5550	0.46	-15
5650	0.41	15
5750	0.4	0
5850	0.58	20
5900	0.7	-40
5950	0.6	-3
6000	0.74	-27

4.1.3 Resonator Delay

It may be mentioned that we have carried out time delay measurements at resonance by finding out the phase shift $\Delta\phi$ when the frequency is changed by Δf (= 5 MHz) about the resonance point. The delay is measured through the equation

$$\tau = \frac{1}{2\pi L} \quad \frac{\Delta\phi}{\Delta f}$$

where L is the spacing between the input and output transducers. The measured time delay over the frequency range 3-6 GHz is shown in Fig. for the resonator #I and a matched transducer (1 mm microstrip). THe resonator transducer combination was set for Q = 550 - 1700 in the range 3-6 GHz with corresponding insertion loss 8-16 dB. Increase of insertion loss by 2 dB (higher than 14 dB obtained for fresh transducer) is possibly due to the deterioration of the transducer microstrip and the OSM connectors.

It is found that the delay varies linearly (Fig. 4.24 with resonance frequency in the range 3-6 GHz. It should be noted that the different delay times corresponds to different bias fields.
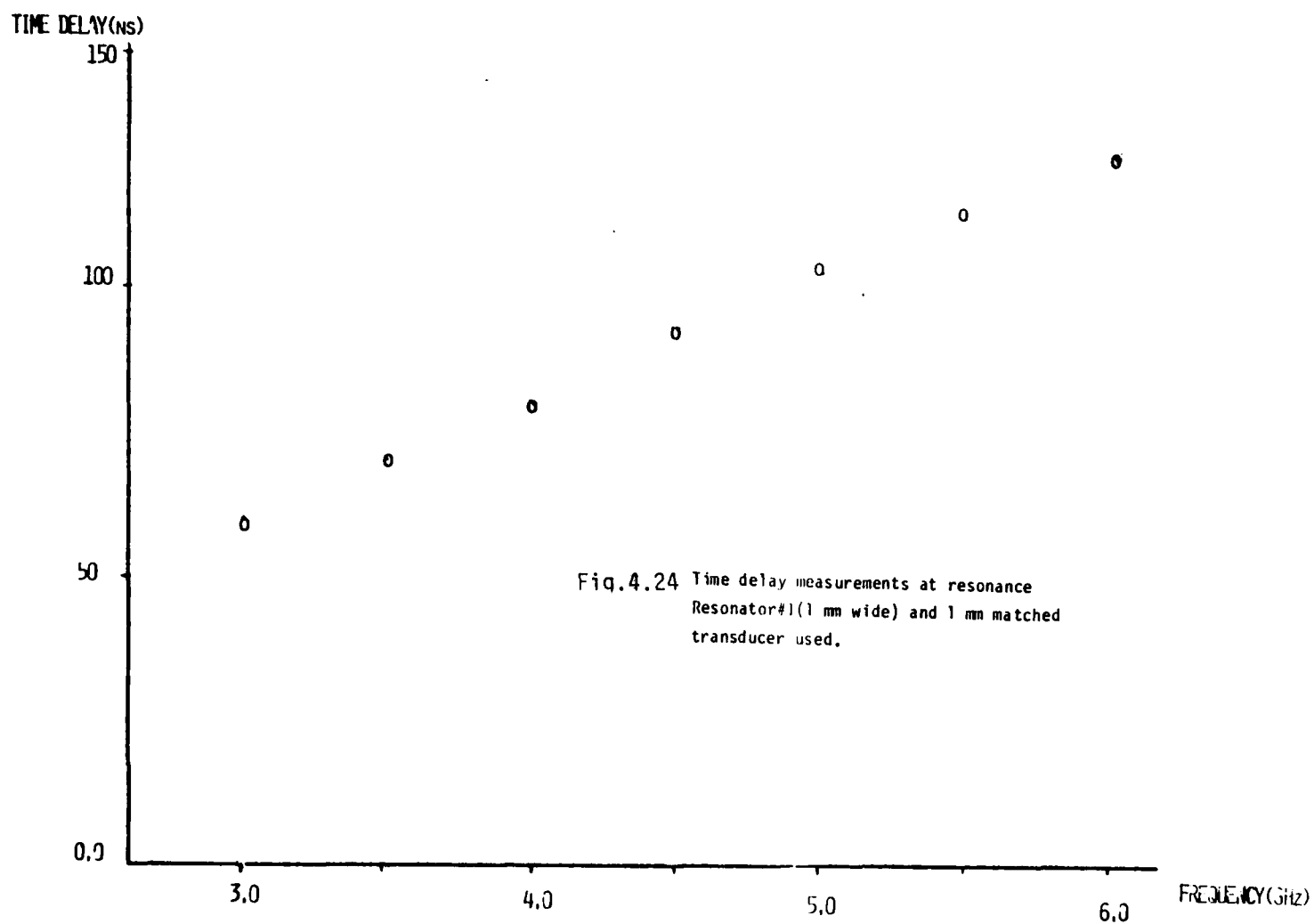
Fig. 4.24 Time delay measurements at resonance; Resonator #I (1mm wide) and 1 mm matched transducer used.

192

4.1.4   Physical Characteristics of the Transducers

1. Resonators with 3 mm aperture are studied with 3 mm long x ducer (i.e., the loop microstrips are 3 mm long). The separation between the input and the output loop strips is 2.4 mm. The microstrip feeder lines are 530 micron wide. The total resistance between input and output OSM connectors was 4.8 ohm.

2. Resonators with 1.5 mm aperture are studied with 1.5 mm long x ducer. The separation between input and output loops strips is 2.1 mm. The total resistance between input and output OSM connectors was 1.6 ohm.

3. The 1 mm wide resonators were studied with 1 mm long x ducers. The separation between the loop strips is 2.4 mm. The total resistance was 0.9 ohm.

   All the x ducers are fabricated on quartz substrates of thickness 0.254 mm and made of gold microstrips.

Physical Characteristics of the Resonators

Resonator #	n of Grooves	width of L G (micron) ±6		s Separation betn the arrays (mm)	d Etch depth (micron) ±	h YIG Thickness(micron) ±
X1	40	65	80	3	1.1	15.3
X3	60	75	72	1.5	0.32	14.4
X2	60	78	70	1.5	.34	15
X4	60	76	71	2	0.4	16
X6	55			3		16
X11	60	63	81	1.5	0.33	16
K8	70			3.6	0.34	11.9
K2	65	70	76	3.0	0.42	13.9
K2'	=	=	=	=	0.62	=
K10	60	72	72	3.6	0.48	10
I	70	72	72	3.6	0.7	7
X5	60			1.5	0.44	16
K9	65	67	79	3.6	0.62	12.2

Summary of Resonator Response Data

Resonator #	Aperture (mm)	Frequency (GHz)	Insertion Loss (dB) ±1	Optimised Q ±50	Resonance Clearance dB	Operating Range (GHz)	Nature of Tranceducer used
X1	1.5	3	16	400	10	3-6	um 1.5 mm
		5	26	800	11		
		6	32	1050			
X1	1.8	3	8	250	8	3-6	um 1 mm
		5	14	750	10		
		6	19	1100	10		
X1	3	3	16	500	7	3-4.5	um 3 mm
		4.5	26	1100	3		
X2	3	3	16	600	7	3-4.8	um 3 mm
		4.5	27	1250	3		
		5.0	30	1900	1		
X3	1	3	17	650	7	3-6	1 mm
		6	25	2000	6		
X3	2	3	18	400	5	3-5.3	um 1.5 mm
		5.5	33	1350	2		
X4	3	3	21	600	6	3-4.5	um 3 mm
		4.5	25	1050	2		
X5	1.5	3	17	350	9	3-6	um 1.5 mm
		5.5	30	1100	10		
X6	3	3	20	500	7	3-5.2	um 3 mm
		5.5	28	1450	3		
X6	1	3	10	400	9	3-6	um 1 mm
		6	19	1200	10		

Summary of Resonator Response Data (Cont)

Resonator #	Aperture (mm)	Frequency (GHz)	Insertion Loss(dB) ±1	Optimised Q ± 50	Resonance Clearance (dB)	Operating Range(GHz)	Nature of Transducer used
X11	3	3 4.5	22 29	600 900	5 3	3-4.5	
X11	1.5	3 5	19 31	500 1250	6 4	3-6	um 1.5 mm
X11	1	3 6	13 24	400 1250	7 8	3-6	um 1 mm
K8	3	3 5	20 28	750 1650	5 2	3-5	um 3 mm
K8	1.5	3 6	16 36	460 1500	6 5	3-6	um 1.5 mm
K8	1	3 6	13 24	500 1700	8 9	3-6	um 1.0 mm
K8	1	3 6	11 20	500 1700	8 9	3-6	m 1.0 mm
K2	3	3 4.5	17 30	550 1300	6 3	3-4.5	um 3 mm
k2	1.5	3 6	16 28	670 2500	6 6	3-6	um 1.5 mm

Summary of Resonator Response Data

Resonaor #	Aperture (mm)	Frequency (GHz)	Insertion Loss(dB)	Optimised Q ± 50	Resonance Clearance (dB)	Operating Range(GHz)	Nature of Transducer used
K2	1	3 6	12 20	550 1900	8 9	3-6	um 1 mm
K2	1	3 6	10 14	550 1500	9 14	3-6	m 1 mm
K9	1	3 6	11 20	500 1500	6 8	3-6	m 1 mm
K10	1	3 6	14 20	300 1300	5 6	3-6	um 1 mm
I	3	3 5.0 6.0	19 33 34	500 1500 2000	7 2	3-5.3	um 3 mm
I	1.5	3	17 32	500 1600	7 6	3-6	um 1.5 mm
I	1	3 6	8 20	650 2000	8 10	3-6	um 1.0 mm
I	1	3					

Summary of Resonator Response Data (Cont)

Resonator #	Aperture (mm)	Frequency (GHz)	Insertion Loss(dB) ± 1 dB	Optimised Q ± 50	Resonance Clearance dB	Operating Range(GHz)	Nature of Transducer used
K2'	1.5	3					
K2'	1	3 6	7 13	450 1300	9 14	3-6	m 1 mm

4.1.5   ABSTRACT

YIG Oscillators: Is Planar Geometry Better

by

R. L. Carter
J. M. Owens
D. K. De

With the advent of planar magnetostatic wave (MSW) resonators there are
two YIG resonator technologies. The planar technologies will be compared
to the YIG sphere technology with regard to design and fabrication
consideration. New Data on the optimization of (MSW) resonators will be
given.

Broad-band tunable signal sources at microwave frequencies are an important systems requirement. In particular, communications systems require oscillators with high spectral purity and low phase noise. A new planar yttrium iron garnet (YIG) technology has been developed over the last ten years which utilizes the propagation of magnetostatic waves (MSW) in thin expitaxial films of YIG on gadolinium gallium garnet substrates.[2] Recently, we have built resonator structures in the YIG/MSW technolgoy which have been used in oscillators reported to have phase noise characteristics of -100 dB_c at 10 kHz offset from the carrier frequency. Castera,[1] et al. have reported -95 dB_c. Tunable MSW oscillators have been reported form 2 GHZ to 10 GHz with multiple octave tunability. For more than 30 years, YIG based resonators have been used in signal sources utilizing spherical YIG structures. This paper will compare the strengths and weaknesses of the application of planar versus spherical structures in the design and fabrication of micro-wave oscillators.

The consideration of factors of material related parameter il apply similarly to both the planar and sphere geometry. Howev: with regard to phase noise considerations, the variance is apparent, since the structure determines the resonator characteristics. The YIG sph: resonator is responding at the uniform spin precession frequency. The planar YIG/MSW resonator is propagating energy at a MSW mode frequency. As a consequence, the YIG/MSW resonator will always have a higher resonant frequency for a given magnetic field than the YIG sphere resonator. The most crucial difference appears in the phase noise characteristics. For a resonator stabilized oscillator, the phase noise can be modelled by.[3].

$$L(f) = 10 \log \frac{G \, k \, T \, F \, F_0}{Q^2 P_o (f-f_o)^2}$$

where G is the amplifier gain (or IL, the insertion loss of the resonator), kT is -174 dB_m, F is the noise figure of the amplifier, f_o is the resonant frequency, f is the frequency at which the noise power is measured, Q is the resonator quality factor and P_o is the output power level of the amplifier. In comparing two saturated resonator based oscillator technologies, the factor $IL/Q_s^2 P_s$ is the figure of merit, where Q_s is now the saturated resonator quality factor and P_s is the resonator saturation power. Of particular interest is the factor Q_s: The reported saturated quality factor of the planar YIG/MSW resonators exceeds that of YIG spheres by nearly a factor of 10. The paper

PLANAR YIG OSCILLATOR
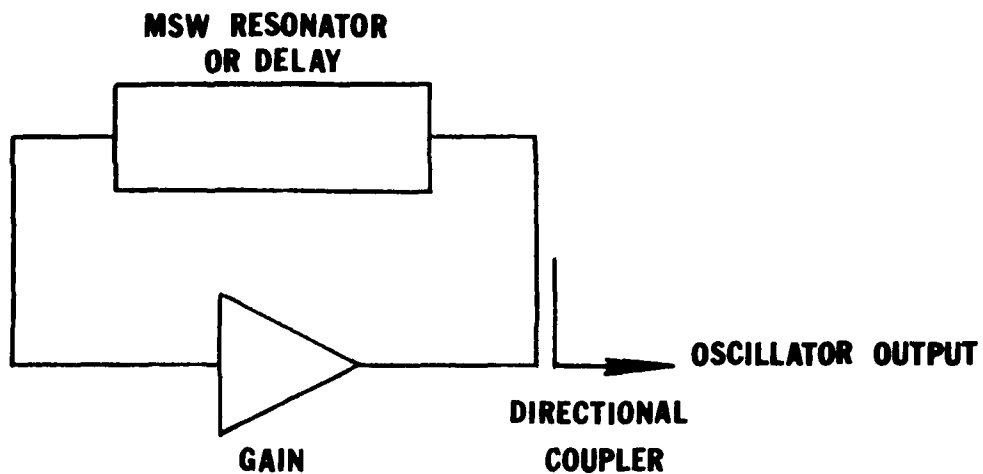
- $Q_{ex}^{MSW} > Q_{ex}^{SPHERE}$
- MIC FABRICATION PROCESS
- LARGER MAGNET STRUCTURE
- TEMPERATURE SENSITIVITY OF $4\pi M_s$

Figure 4.25 Oscillator block diagram

will discuss the limits of each technology with regard to IL, Q_s and P_s, with new data being reported on methods of the optimization of IL and $\hat{Q}$ for YIG/MSW planar resonator.

The fabrication techniques required for an oscillator technology are of considerable importance. The paper will discuss the following factors relating to the planar versus spherical technology.

1. Process Yield
2. Interface to the Oscillator - is integration possible?
3. "Tweaking" processes

Some of the MSSW resonators fabricated in this work were driven by a GaAs FET amplifier to oscillate between 3-5.3 GHz. The hybrid integrated amplifier was fabricated on 10 mℓ alumina substrates with gold metalization. The resonator and hybrid MIC amplifier were assembled into the oscillator configuration of Fig. 4.25 The two stage amplifier had a gain of 18-19 dB in the range 3-5 GHZ.

Phase noise characteristics of some of the oscillations are shown in Fig. 4.26.
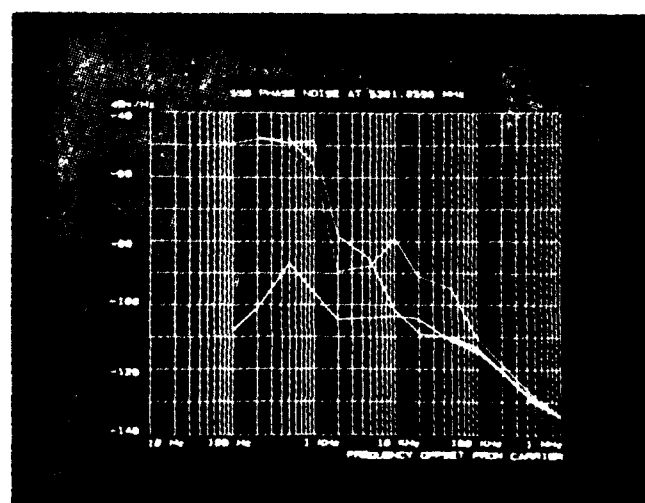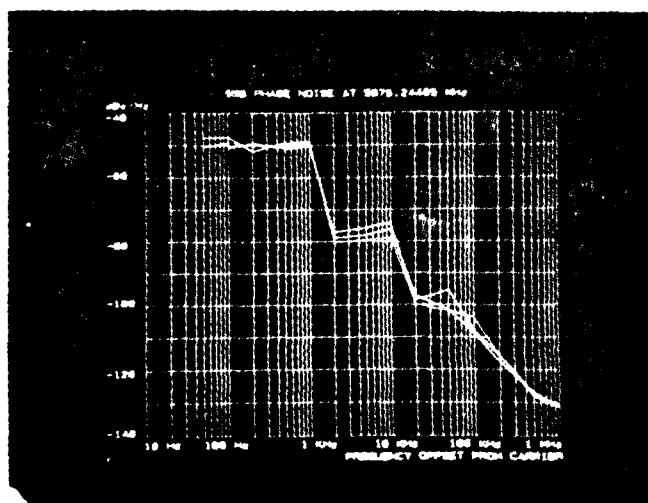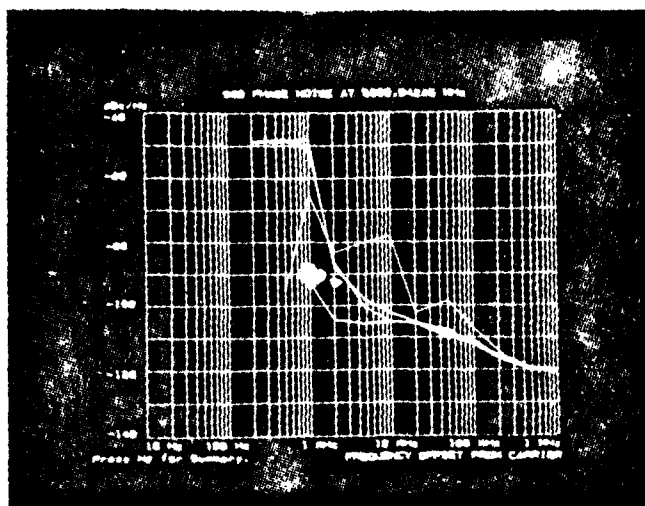
Figure 4.26   The above oscillations were meaasured with a combination
              of RESN #K2 and 1 mm matched Xducer built on quartz
              substrate of thickness 250 micron.   The above
              combination was placed in feed back loop of a two stage
              microwave microstrip amplifier fabricated in this
              laboratory on 250 micron thick alumina substrate.   The
              amplifier has a gain of 18-19 dB in the range of 3-5 GHz.

Figure 4.27 Oscillation photographs (continued).
          The oscillations were measured by hp Spectrum Analyzer Model

5.0 SUMMARY

In summary the primary accomplishments of the third year of this program have been:

1. An Empirical Model has been developed for MSSW Transducers using detailed measurements of MSSW transducers. The theory is still limited by errors in measurement and the inability to measure $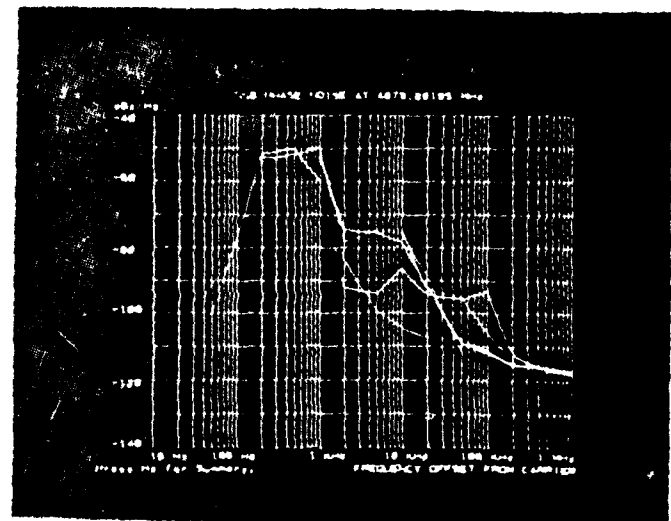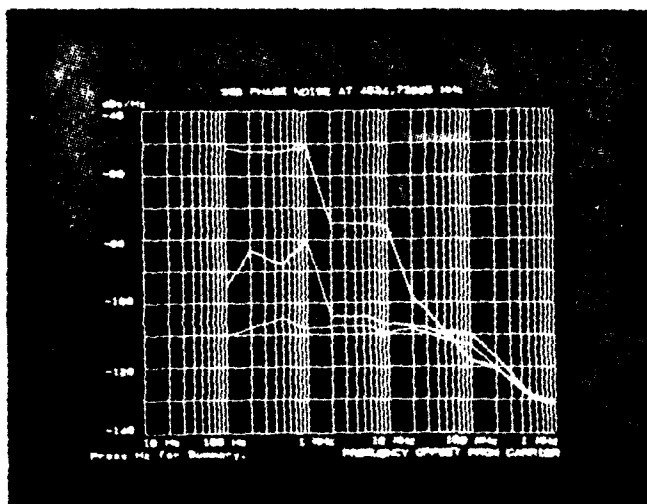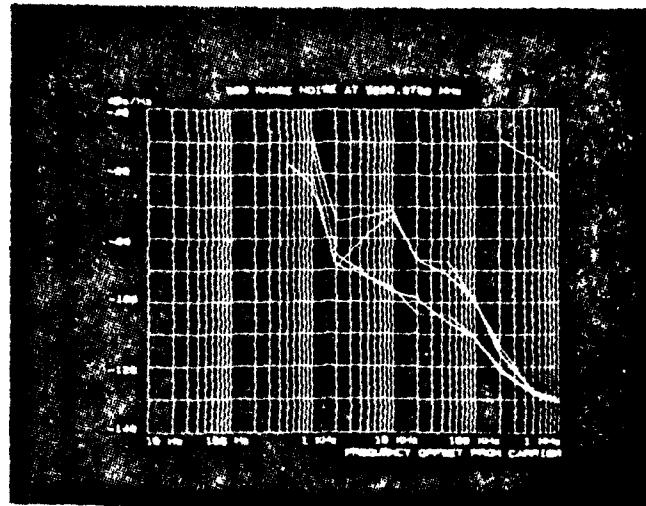S_{11}$ and S_{22} of the magnetostatic ports. Also, errors associated with phase shifts under the transducers, and interaction between the transducer elements are not considered. The solution to the problem lies in either detailed theoretical analysis of the problem (6 region boundary valve problem) or decoupling of the transducer elements to yield a true non-recursive transducer filter.

2. A variable time delay device with an RMS phase error of as low as 6.40° RMS has been built and tested. Time variation of 42 NSEC was achieved. The design procedures for dispersion control utilizing a variable ground plane are well established. The device utilizes a cascaded forward and backward wave delay line with linearized dispersion, and thus matched dispersive line have been developed with significant potential in signal processing applications.

3. Two-port MSSW resonators have been developed with loaded Qs of greater than 2500 at 6 GHz. Oscillators built from these resonators has shown excellent phase noise characteristics with SSB phase noise as low as - 105dBC at 10 KHz offset from carrier and -135dC at 1 MHz offset.

6.0 PUBLICATIONS
FROM AFOSR SUPPORT

1. R. L. Carter, C. V. Smith, Jr., and J. M. Owens, "Magnetostatic Forward Volume Wave-Spin Wave Conversion by Eteched Grating in LPE-YIG," IEEE Trans-Mag, Vol. Mag-16, 5, 1159-1161, September 1980.

2. J. M. Owens, "Magnetostatics Join SAW's" Microwave Systems News, May 1980 v. 10, No. 5, pp. 112-113.

3. C. V. Smith, Jr., J. M. Owens, R. L. Carter and J. H. Collins, "Magnetostatic Waves, Microwave SAW," Ultrasonics Symposium Proceedings, IEEE Cat. No. 80CH1602+2, pp. 506-513, November 1980.

4. J. C. Sethares, J. M. Owens, C. V. Smith, Jr., "MSW Non-dispersive, Electronically Tunable Time Delay Elements," Electronics Letters, Oct. 1980, V. 16, No. 22 pp. 825-826.

5. J. C. Sethares, C. V. Smith, Jr. and J. M. Owens, "MSW Time Delays," Symposium Proceedings, IEEE Cat. No. 80CH1602-2, pp. 518-521, November 1980.

6. J. M. Owens, R. L. Carter, C. V. Smith, Jr., and G. Hasnian, "A 3-Port Model for Magnetostatic Wave Transducers," Symposium Proceedings, IEEE Cat. No. 80CH1602-2, pp. 538-542, November 1980.

7. W. R. Brinlee, J. M. Owens, C. V. Smith, Jr., and R. L. Carter, "Two-port Magnetostatic Wave Resonators Utilizing Periodic Metal Reflective Arrays" J. Appl. Physics, 52, 3, 2276-2278, March 1981.

8. J. M. Owens, C. V. Smith, Jr. and R. L. Carter, "The Status of Magnetostatic Wave Devices," 35th Ann. Freq. Control Symposium USAERADCOM, Ft. Monmouth, N. J. 077030, 358-363 (1981).

9. R. L. Carter, J. M. Owens, W. R. Brinlee, Y. W. Sam and C. V. Smith, Jr. "Tunable Magnetostatic Surface Wave Oscillator at 4 GHz," 1981 IEEE MTT-S Symposium Proceedings, Cat No. 81 Ch 1592-5, pp. 383-385, June 1981.

10. C. V. Smith, Jr., J. M. Owens, N. D. Parikh and R. L. Carter, "Anisotropic Propagation of Magnetostatic Waves in Epitaxial YIG Films," IEEE Trans. Magn., Mag-17, 2967-2969 (1981).

11. R. L. Carter, J. M. Owens, C. V. Smith, Jr., and K. W. Reed, "Ion Implanted Magnetostatic Wave Reflective Array Filter," J. Appl. Phys. 53, 2655-2657 (1982).

12. R. L. Carter, J. M. Owens, C. V. Smith, Jr., and K. W. Reed, "Ion Implanted Oblique Incidence Magnetostatic Wave Reflective Array Filters," 1982 IEEE MTTs Microwave Symposium Digest #82 CH 1705-3, pp. 83-85, June, 1982.

13. G. F. Manes, and J. M. Owens, "Microwave Signal Processing Using Magnetostatic Wave Devices," Alta Frequenza No. 2 VLI, pp. 103-106, (1982).

14. J. M. Owens, C. V. Smith, Jr., and R. L. Carter, "MSW Reflecting Array Filters," Proceedings of the the 1981 RADC Microwave Magnetics Technology Workshop, RADC-TR-83-15, Rome Air Development Center, Griffis Air Force Base, NY 13441, pp. 106-116 (1983).

15. C. V. Smith, Jr., J. M. Owens, R. L. Carter, and K. W. Reed, "Microwave Pulse Compression Loops Using Magnetostatic Wave Delay Lines," Proceedings of the 1981 RADC Microwave Magnetics Technology Workshop, RADC-TR-83-15, Rome Air Development Center, Griffis Air Force Base, NY 13441, pp. 277-289 (1983).

16. J. M. Owens and R. L. Carter, "Magnetostatics Advance: The Shape of Things To Come," Microwave System News, V. 13 No. 3, pp. 103-111 (1983).

17. K. W. Reed, J. M. Owens, R. L. Carter, and C. V. Smith, Jr., "An Oblique Incidence Ion Implanted MSFVW RAF with Linear Group Delay," 1983 IEEE MTT-S International Microwave, IEEE Cat. No. 82CH1871-3 pp. 259-261.

18. J. M. Owens, R. L. Carter, and Y. Y. Sam, "A Hybrid GaAs MIC Oscillator Using a Magnetostatic Wave Resonator," 1983 IEEE MTT-S International Microwave Proceedings. IEEE Cat. No. 82CH1871-3 pp. 323-326.

19. J. M. Owens and R. L. Carter "The Status of Magnetostatic Wave Resonator Oscillators, 1983 Frequency Control Symposium Procceedings, pp. 477-480 IEEE Cat. No. CH1957-0/83/0000.

20. Kok Wai Chang, J. M. Owens, R. L. Carter, "Linearly Dispersive Time-Delay control of Magnetostatic Surface Wave by Variable Ground Plane Spacing" Electronics Letters V. 19 No. 14 (July 7th 1983) pp. 346-347.

21. Kok Wai Chang, L. R. Adkins, R. L. Carter, H. L. Glass, J. M. Owens and F. S. Sterns, "Electronically Variable Time Delays Using Cascaded Magnetostatic Delay Lines," accepted for publication in J. Appl. Phys.

CONFERENCE PRESENTATIONS

1. R. L. Carter, C. V. Smith, Jr. and J. M. Owens, "Magnetostatic Forward Volume Wave - Spin Wave Confersion by Etched Grating in LPE-YIG," presented at 1980 Intermag Conference, April 21-24, Boston, MA.

2. K. W. Reed, J. M. Owens, C. V. Smith, Jr., and R. L. Carter, "Simple Magnetostatic Delay Lines in Microwave Pulse Compression Loops," presented at 1980 IEEE MTT-S International Microwave Symposium, May 28-30, Washington, D.C.

3. C. V. Smith, Jr., J. M. Owens, R. L. Carter and J. H. Collins "Magnetostatic Waves, Microwave SAW?," invited paper presented at 1980 Ultrasonics Symposium, November 5-7, Boston, MA.

4. J. C. Sethares, C. V. Smith, Jr. and J. M. Owens, "MSW Time Delays Presented at the 1980 Ultransonics Symposium. Boston, MA., November 1980.

5. J. M. Owens, R. L. Carter, C. V. Smith, Jr. and G. Hasnian, "A 3-Port Model for Magnetostatic Wave Transducers," Presented at the 1980 Ultrasonics Symposium. Boston, MA, November 1980.

6. W. R. Brinlee, J. M. Owens, C. V. Smith, Jr., and R. L. Carter, "Two-port Magnetostatic Wave Resonators Utilizing Periodic Metal Reflective Arrays," Presented at the 1980 3M Conference Dallas, Texas, November 1980.

7. J. M. Owens, C. V. Smith, Jr. and R. L. Carter, "The Status of Magnetostatic Wave Devices," Presented at the 35th Ann. Freq. Control Symposium, Philadelphia, PA., June 1980.

8. R. L. Carter, J. M. Owens, W. R. Brinlee, Y. W. Sam and C. V. Smith, Jr., "Tunable Magnetostatic Surface Wave Oscillator at 4 GHz," Presented at the 1981 IEEE MTT-S Symposium, Los Angeles, CA, June, 1981.

9. C. V. Smith, Jr., J. M. Owens, N. D. Parikh and R. L. Carter, "Anisotropic Propagation of Magnetostatic Waves in Epitaxial YIG Films", Presented at The 1980 Internal Magnetics Conference, Grenoble, France, May 1980.

10. J. M. Owens, C. V. Smith, Jr. and R. L. Carter, "MSW Reflecting Array Filter," presented at the 1981 Microwave Magnetics Technology Workshop, Electromagnetic Sciences Division IEEAC, Rome Air Development Center, Hanscom AFB, MA, June, 1981.

11. C. V. Smith, Jr., J. M. Owens, R. L. Carter and K. W. Reed, "Microwave Pulse Compression Loops Using Magnetostatic Wave Delay Lines," presented at the 1981 RADC Microwave Magnetics Technology Workshop, Electromagnetic Sciences Division IEEAC, Rome Air, Development Center, Hanscom AFB, MA, June 1981.

12. R. L. Carter, J. M. Owens, C. V. Smith, Jr., K. W. Reed, "Ion Implanted Magnetostatic Wave Reflective Array Filters". Presented at 26th Annual Conference on Magnetism and Magnetic Materials, Atlanta, Nov. 1981.

13. R. L. Carter, J. M. Owens, C. V. Smith, Jr. and K. W. Reed "Ion Implanted Oblique Incidence Magnetostatic Wave Reflective Array Filters, Presented 1982 IEEE MTT-S International Microwave Symposium, Dallas, Texas, June 1982.

14. K. W. Reed, J. M. Owens, R. L. Carter and C. V. Smith, Jr. "An Oblique Incidence Ion Implanted MSFVW RAF with Linear Group Delay, Presented 1982 IEEE MTT-S International Microwave Symposium, Boston, Mass., June 1983.

15. J. M. Owens, R. L. Carter, Y. W. Sam, "A Hybrid GaAs MIC Oscillator Using a Magnetostatic Wave Resonator" presented 1983 IEEE MTT-S International Microwave Symposium, Boston, Mass., June 1983.

16. J. M. Owens, R. L. Carter, "The Status of Magnetostatic Wave Resonator Oscillators" Presented 1983, Frequency Control Symposium, Phiuladelphia, Pa., June 1983.

17. Kok Wai Chang, L. R. Adkins, H. L. Glass, F. S. Stearns, R. L. Carter and J. M. Owens, "Electronically Variable Time Delays Using Cascaded Magnetostatic Delay Lines," the 29th Annual Conference on Magnetism and Magnetic Materials (MMM), Pittsburgh, Pennsylvania, Nov. 1983.

END

FILMED

1-85

DTIC